MODELING OF AN EXTRACTION LENS SYSTEM FOR H^- VOLUME CUSP ION SOURCES USED TO INJECT BEAM INTO COMMERCIAL CYCLOTRONS

by

Karine Marie Gaëlle Le Du

A THESIS SUBMITTED IN PARTIAL FULFILLMENT

OF THE REQUIREMENTS FOR THE DEGREE OF

BACHELOR OF APPLIED SCIENCE

in the School

of

Engineering Science

SIMON FRASER UNIVERSITY

March 2003

APPROVAL

Name: Karine Marie Gaëlle Le Du

Degree: Bachelor of Applied Science

Title of thesis: Modelling of an Extraction Lens System for H^- Volume Cusp Ion Sources Used to Inject Beam into Commercial Cyclotrons

_____
Dr. Mehrdad Saif
Director
School of Engineering Science, SFU

Examining Committee:

Chair and Academic Supervisor:

_____
Dr. John F. Cochran
Professor Emeritus
Department of Physics, SFU

Technical Supervisor:

_____
Dr. Morgan P. Dehnel
President, PEng
Dehnel Consulting Ltd.

Committee Member:

_____
Mr. Steve Whitmore
Senior Lecturer
School of Engineering Science, SFU

Date Approved: _____

Abstract

This thesis examines the effects that the physical parameters of an extraction lens system for H^- volume cusp ion sources used to inject beam into commercial cyclotrons have on the quality of H^- ion beams. The results are intended to assist in optimizing the design of a new extraction lens system. The success of a design is typically judged by how well the system produces a beam of H^- ions that meets certain criteria. In accelerator physics, a high quality beam is one with high brightness and low emittance. But when beam quality is subject to a given application, beam brightness, normalized emittance, and percent of beam transmitted are the key measurements that assess the usefulness of the beam.

The extraction lens system was modelled in SIMION 3D [1]. Five design parameters were identified as variable parameters. These parameters are the separation between adjacent lenses, the aperture diameters of two of the three lenses, and the voltage potential of the second lens. Beam quality was significantly improved when the separation between the first and second lenses was increased and when the voltage potential on the second lens was decreased. Changing the values of the three other parameters showed little effect on beam quality.

Acknowledgments

I would like to express my gratitude to Dr. Morgan Dehnel for his guidance, supervision, patience, and mentorship throughout the evolution of my thesis. Working under his supervision was a confidence-building experience. He gave freely of his time and provided the strategic and knowledgeable support I required to complete this thesis.

I would like to thank Dr. John F. Cochran and Mr. Steve Whitmore, my academic supervisor and committee member, respectively, for their time, effort, and constructive feedback on my work.

I would like to thank my parents, Monique and François Le Du, for their support not only during the completion of my thesis but over the duration of my undergraduate career. I would also like to thank my brother, Yann, for his words of encouragement and guidance over the past five years.

I would also like to thank the Caskeys for their support, especially over the past eight months.

Contents

List of Figures

List of Tables

Chapter 1

Introduction

The use of radioisotopes for the detection of soft tissue damage necessitates hospitals having commercial cyclotrons on site. With a half-life sometimes as short as twenty minutes (depending on the radioisotope), these radioisotopes must be created on site and used immediately. Dehnel Consulting Ltd. (DCL) is an engineering company located in Nelson, BC, Canada, that designs various components of commercial cyclotrons. To expand on the existing expertise of the company, the extraction lens system for a hydride ion (H^-) volume cusp ion source was studied to facilitate future design work of this particular cyclotron component. The purpose of the study was to identify how changes in system parameters, such as physical lens dimensions and voltage potentials, govern the trends of beam characteristic dynamics. The study forms the basis of this thesis.

The current expertise of DCL encompasses designing axial injection systems and complete beamlines for the particle accelerator industry, with expert knowledge of ion sources and inflectors. Chapter 1 includes a brief description of the subsystems that make up the commercial cyclotron, a summary of the fundamentals of accelerator physics pertinent to the work presented in this thesis, and presents the motivation for studying the extraction lens system for an H^- volume cusp ion source.

The topic of Chapter 2 is an explanation of how the study was designed. The design process included defining the scope of the study and developing an appropriate simulation model. The computer simulation tool used to model the extraction lens system was SIMION 3D, Version 7.0, produced by Idaho National Engineering and Environmental Laboratory (INEEL) [1], a software product new to DCL. Much of the

design process involved learning the capabilities of SIMION in order to use this tool to conduct a thorough study. SIMION is discussed briefly in Chapter 2, to introduce SIMION specific terminology and to give a general understanding of the computer simulation tool and how its capabilities affected the simulation model. A brief SIMION user reference guide is included as an appendix, as per DCL's request. It is not intended to replace the software developer's user manual, as it is not nearly as comprehensive as [1]. SIMION is a very powerful tool that simulates both electrostatic, electrodynamic, and magnetostatic devices. Only the program's electrostatic capabilities are discussed herein, as only electrostatic devices are relevant to the study.

The results of this study are presented in Chapter 3 and Chapter 4. The simulation model was based on drawings of an existing extraction lens system licensed by DCL from TRIUMF. The nominal parameter values (physical dimensions and voltage potentials) of the simulation model were obtained from these drawings. To study the effects on the particle beam of changing the dimensions and voltage potentials of the model parameters, all four hundred thirty two possible parameter-value configurations were simulated and the simulation results analysed. In Chapter 3, the beam characteristics of the test configurations that differed from the nominal configuration by one parameter value only are compared to the beam characteristics of the nominal case. In Chapter 4, all of the test cases are compared, and the observed global trends are reported.

Chapter 5 concludes this thesis with a summary of the findings and a brief discussion of possible future work.

1.1 Commercial Cyclotrons and Their Components

Commercial cyclotrons are used in hospitals to produce radioisotopes used to diagnose soft tissue damage. Commercial cyclotrons can essentially be described as having six major components. Each component uses electromagnetic principles to interact with charged particles to prepare a beam of ions for their target in the production of radioisotopes. Electrostatic components are used to accelerate charged particles. Magnetostatic components are used to focus and to steer a beam of charged particles.

Some devices, like the cyclotron itself, use electrostatic, electrodynamic, and magnetostatic components. Figure 1.1 is a block diagram of the cyclotron system in which the major components are labelled.

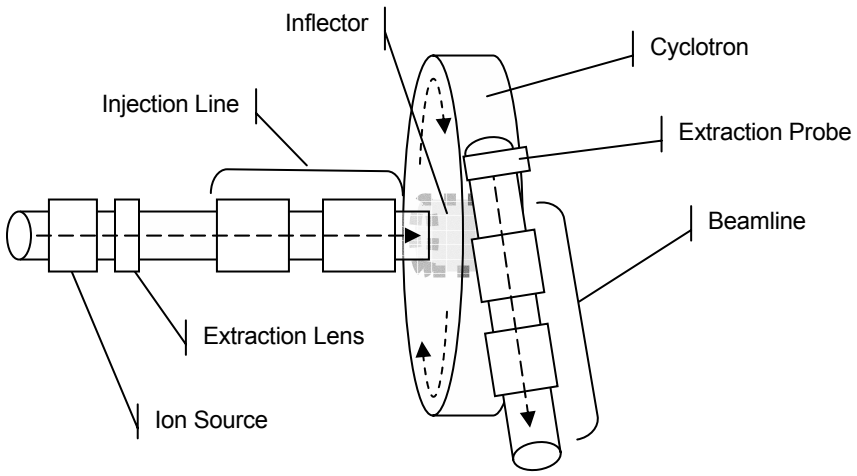

Figure 1.1 Block diagram of the overall particle accelerator system. The dashed arrows show the direction of beam transport through the system. H^- ions are injected into the cyclotron and protons are extracted from it. The extraction lens system adjacent to the ion source is the focus of this project.

1.1.1 Ion Source

Ions, other charged particles, and neutrals are created in the ion source plasma. For the particular application pertinent to this study, H^- ions are the desired particle species.

1.1.2 Extraction Lens System

The extraction lens system for the ion source extracts H^- ions and electrons from the plasma and preferentially accelerates the H^- ions into the axial injection system.

1.1.3 Injection Line

Composed of magnets and electrostatic focussing elements, the injection line focuses and transports the beam of accelerated particles to the cyclotron. The various components along the injection line prepare the beam characteristics for entry into the adjacent system component.

1.1.4 Inflector

The inflector, placed at the end of the injection line, alters the beam's linear trajectory along the cyclotron axis to a spiral trajectory. The beam is bent by 90 degrees from its axial path to match the entrance to the cyclotron and then continues along a spiral orbit inside the cyclotron.

1.1.5 Cyclotron

The purpose of the cyclotron is to accelerate ions along a circular orbit of continually increasing radius. The circular path is maintained by a magnetic field between two large disks. The upper and lower disks contain pie-shaped structures called radio-frequency (RF) dees, which provide the beam ions with acceleration kicks that periodically increase the radius of their circular trajectory. The cyclotron cyclically accelerates the H^- ions until they reach the appropriate kinetic energy, at which point they encounter a graphite foil that strips the electrons from each ion and leaves a proton, which exits the cyclotron.

1.1.6 Beamline

Upon leaving the cyclotron, the ion beam is focussed and steered by means of magnets in various configurations. The ion beam is thereby transported to the targets used for radioisotope production.

1.2 Fundamentals of Accelerator Physics

Electromagnetism is fundamental to the functioning of cyclotrons. In accelerator physics, a particle's kinetic energy is expressed in units of electron-volts (eV). An electron-volt is the energy one electron has when it is accelerated across a potential difference of one volt. In units of Joules, the electron-volt has the following value:

$$1 \text{ eV} = (1.609 \times 10^{-19} \text{ C})(1 \text{ J/C}) = 1.609 \times 10^{-19} \text{ J}. \quad (1.1)$$

Joules, the unit of energy, has dimensions of $(mass)\cdot(length)^2/(time)^2$. Dividing this by the dimensions of velocity, $(length)/(time)$, leaves $(mass)\cdot(length)/(time)$, the dimensions of momentum. Dividing again by the dimensions of velocity leaves $(mass)$. So, by dividing energy in units of eV (or any multiple of eV, such as keV or MeV), by a fundamental constant that has units of velocity, namely c, the speed of light, one can obtain momentum, $p=E/c$. Dividing again by c, one obtains mass, $m=E/c^2$, from which the fundamental equation of relativity is recovered [2]. A useful quantity will be the rest mass of H^-, 1.00837363 amu = 938.2 MeV.

1.2.1 Accelerator Physics

Ions in a beam are described by a six dimensional phase space (x, y, z, p_x, p_y, p_z). (x, y, z) denote the ion's position and (p_x, p_y, p_z) are the components of the ion's momentum. In accelerator physics, it is conventional to use angular divergence (x', y') to describe the orientation of the ion's trajectory with respect to the beam's central axis, which is conventionally assigned to be the z direction. Angular divergence is derived from the ion's momentum vector components and so replaces these without loss of information:

$$x' = dx/dz = p_x/p_z \,, \quad (1.2)$$

$$y' = dy/dz = p_y/p_z \,. \quad (1.3)$$

Angular divergence has units of milliradians. As electrostatic lenses force an ion to accelerate in the z direction, any momentum the ion already had in an off-axis direction

(x and/or y) will cause the ion to follow a trajectory that is not parallel to the z direction. Also, the focusing effect of the lenses will cause ions to converge to or diverge from the z-axis.

The trajectories of ions in a transport beam are tracked using a right-handed, orthogonal coordinate system. The coordinate system's origin moves along the central trajectory of the beam. The coordinate directions are:

$\hat{z}$ is tangential to the central trajectory, in the direction of forward motion.

$\hat{x}$ is a transverse coordinate in the laboratory horizontal plane.

$\hat{y}$ is a transverse coordinate in the laboratory vertical plane.

In particle transport formalism, the four important coordinates that completely describe an ion's trajectory are (x, x', y, y'). These are described as:

x is the horizontal displacement of an arbitrary trajectory with respect to the central trajectory.

x' is the angle between the arbitrary and central trajectories, in the horizontal plane.

y is the vertical displacement of an arbitrary trajectory with respect to the central trajectory.

y' is the angle between the arbitrary and central trajectories, in the vertical plane.

(x, x', y, y') are graphically represented in Figure 1.2. The angular divergences are exaggerated for the sake of clarity.

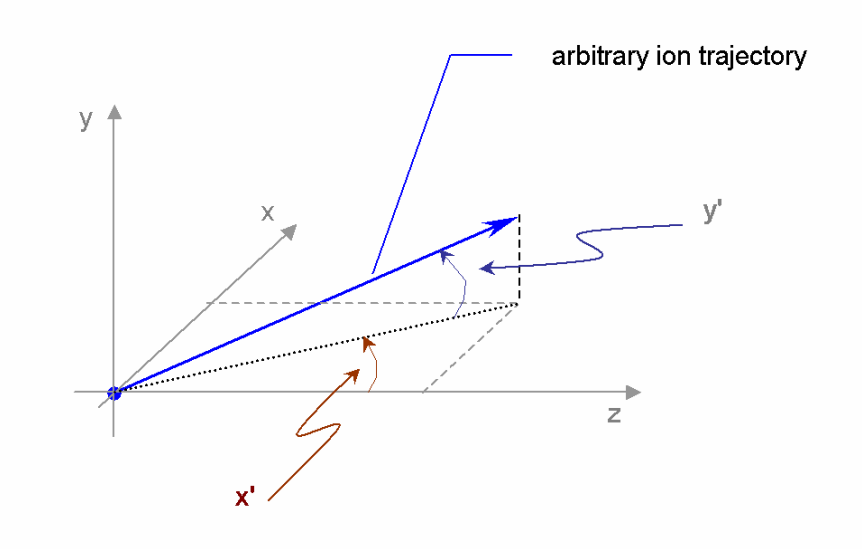

Figure 1.2 Schematic diagram of the four coordinates that completely describe an ion trajectory, where z is the direction of propagation.

1.2.2 Beam Optics

As a whole, the ions injected into a transport system are referred to as a beam. In accelerator physics, a high quality beam is one with high brightness and low emittance. Beam emittance describes the size of the beam in either (x, x') or (y, y') phase space [3]. Since the geometry of the extraction lens system under study is cylindrical, (x, x') and (y, y') can be utilized interchangeably to refer to phase space orientation. Two representative beam ellipses (plots of x versus x') are sketched in Figure 1.3. The upright ellipse on the left is characteristic of the phase space orientation at the beam waist. As the beam drifts in a field free space, the maximum divergence (shown by the dashed horizontal lines) of the beam remains constant while the maximum transverse position increases. The beam ellipse on the right in Figure 1.3 shows how the phase space changes after drifting some amount. Note that the x axis intercepts remain constant in drift space, since particles at positions x along the x axis have no divergence (i.e., they move parallel to the injection line axis and have the same values at all later points when drifting).

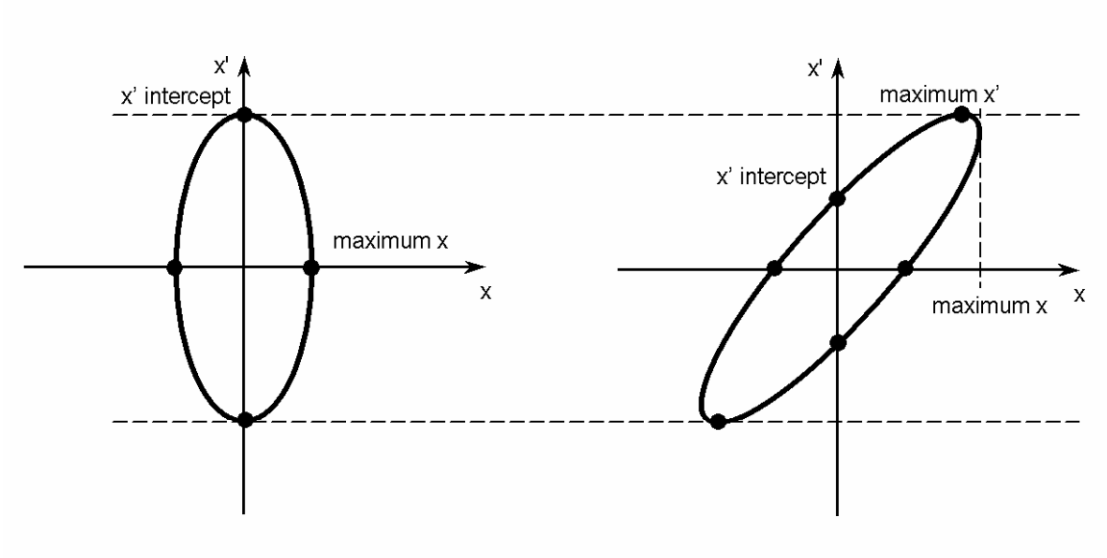

Figure 1.3 Phase space plot (x, x') at the waist (at left) and after drifting through space (at right). The maximum value of x' stays constant over the entire drift space and the emittance also stays constant (area inside the ellipse remains constant).

Beam emittance remains constant in drift space, a result of Liouville's Theorem [4]. The x' intercept decreases such that beam emittance,

$$\varepsilon = x_{\max} \cdot x'_{\text{int}} \ , \tag{1.4}$$

remains constant over the entire drift space. Beam emittance has units of $[\, mm \cdot mrad \,]$. Beam emittance is sometimes defined as the area of the beam ellipse and so is calculated as the product of the semi-major and semi-minor axes times π [5]. The convention adopted here is that the area of the beam ellipse is emittance times π:

$$A = \pi \varepsilon \ . \tag{1.5}$$

To be able to compare the beam emittance of several beams directly, beam emittance must be normalized to take into account the energy of the ions. Equation (1.4) is sometimes referred to as the physical beam emittance, ε_P, to distinguish it from normalized beam emittance, ε_N. Recall, from equation (1.2), that x' is the ratio of momentum in the transverse x direction, p_x, to momentum in the longitudinal z direction,

p_z. Since the beam propagates in the z direction, it is assumed that $p_z >> p_x$, and that the total momentum is approximately $p_{tot} \approx p_z$.

The ions in the beam are travelling at speeds, v, close to the speed of light, c, so relativistic effects must be taken into account [6]. The effective mass of a particle is

$$m = \frac{m_o}{\sqrt{1-\beta^2}}, \tag{1.6}$$

where

$$\beta = v/c \tag{1.7}$$

and m_o is the particle's rest mass. The relativistic momentum of the particle is then

$$p = \frac{m_o v}{\sqrt{1-\beta^2}}. \tag{1.8}$$

The denominator is a common term in relativistic mechanics, often expressed as

$$\gamma = \frac{1}{\sqrt{1-\beta^2}}, \tag{1.9}$$

where γ can also be calculated from the particle's kinetic energy T and its rest mass M

$$\gamma = \frac{T(MeV) + M(MeV)}{M(MeV)}. \tag{1.10}$$

Normalized beam emittance is calculated by multiplying beam emittance by the normalization factor $\beta\gamma$,

$$\beta\gamma = \sqrt{\gamma^2 - 1}. \tag{1.11}$$

Normalized beam emittance is thus

$$\varepsilon_N = \beta\gamma\varepsilon_P , \tag{1.12}$$

and describes the beam size with respect to transverse momentum and transverse beam dimensions regardless of total momentum [3]. The rest mass of an H^- ion, in units of electron volts, as utilized in equation (1.10), is M = 938.2 MeV. At the location where normalized beam emittance was calculated in this study, H^- ion kinetic energy, T, was 25 keV.

Beam brightness, b, is the ratio of beam current, I, to normalized beam emittance squared [5]:

$$b = \frac{I}{\left(\varepsilon_N\right)^2} . \tag{1.13}$$

Brightness has units of $[\,mm \cdot mrad\,]^{-2}$. In this study, beam current is represented by percent of beam transmitted, whereby one hundred percent transmission is the highest beam current achievable by this system. A high quality beam is one with high beam brightness. As equation (1.13) indicates, higher brightness occurs when normalized emittance is low, which is also indicative of a high quality beam, as stated above.

1.3 Purpose of This Study

The extraction lens system for an H^- volume cusp ion source was studied to identify the trends governing the beam characteristics as the various dimensions and voltage potentials of the lenses were changed. Although many intricate phenomena occur throughout the system, only the general trends observed are reported. The results of the study are intended to aid an engineer in optimizing the design of an extraction lens system with regards to such beam characteristics as beam brightness, energy, normalized beam emittance, and beam current, as per the design requirements.

Chapter 2

Study of the Extraction Lens System for an H^- Volume Cusp Ion Source

The extraction lens system for an H^- volume cusp ion source is composed of three electrostatic lenses, electrically isolated from each other. Although the shape and dimensions of each lens are unique, the lenses are cylindrical with axially concentric apertures through which the charged particle beam passes. An assembly drawing on the next page, Figure 2.1, shows the elaborate structure of the extraction lens system with downstream vacuum chamber and beamstop, in cross-sectional view (drawing courtesy of TRIUMF). The bottom frame in the figure zooms in on the three electrostatic lenses that were modeled in this study. The extraction lens system is situated immediately downstream of the ion source.

The first lens in the system is called the plasma lens. This lens is set to a voltage potential of –25 kV. The plasma, in which the H^- ions are created, is at a potential within about 2 V of that of the plasma electrode. The second lens is the extraction lens. Set to –22 kV, the +3 kV potential difference between the plasma and extraction lenses sets up an electric field $\vec{E} = -\nabla V$ that exerts a force $\vec{F}$ on the ions of charge q, in accordance with the Lorentz force equation (2.1).

$$\vec{F} = q \cdot \vec{E} \tag{2.1}$$

The cross product of velocity and magnetic field is omitted from equation (2.1) due to the absence of magnetic fields. The force arising from the electric field extracts the negatively charged ions from the plasma, accelerating them towards the more positive

extraction electrode, in accordance with the Newtonian force equation $\vec{F} = m \cdot \vec{a}$. The third lens, called the shoulder electrode, is electrically grounded (0 V). The effective +22 kV potential difference, combined with the geometry of the lenses, cause the beam of extracted ions to converge to a waist as they are accelerated through the lens system. In doing so, the ions pass through the apertures of the extraction and shoulder lenses without incurring much loss.

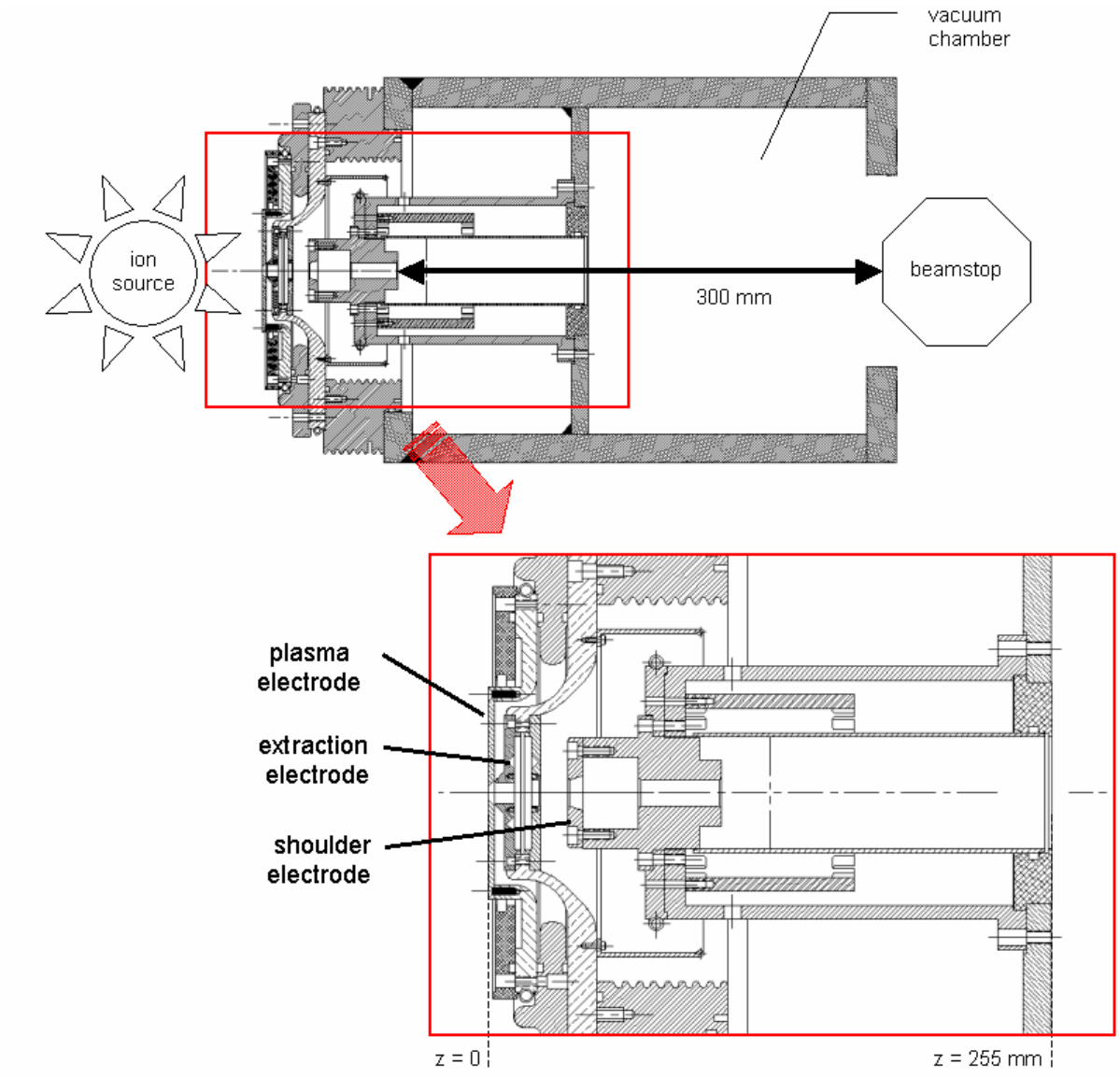

Figure 2.1 Assembly drawing of the extraction lens system, above, with a close-up of the three lenses labelled in the bottom frame. The zero position of the ions is also indicated in the bottom frame. Assembly drawing courtesy of TRIUMF.

The volume subsequent to the shoulder electrode is enclosed in a vacuum chamber whose voltage potential is also 0 V. Thus, ions that exit the shoulder electrode drift without further acceleration until they collide into a beamstop located 300mm downstream from the shoulder electrode (the relative position of the beamstop is also labelled in the top frame of Figure 2.1). Upon reaching the beamstop, the ions have a kinetic energy of approximately 25 keV and zero acceleration.

The beamstop is utilized to measure the H^- beam current during initialization of the ion source. The magnitude of the H^- beam current output from the ion source is linearly related to the arc power supply current setting until saturation is reached. Once the desired H^- beam current is achieved, the beamstop is removed from the beam path to allow the beam to be transported uninterrupted through the injection line, located downstream of the extraction lens system.

2.1 Defining the Scope of the Study

The purpose of studying the extraction lens system for an H^- volume cusp ion source was to identify the trends governing the beam characteristics as various dimensions and voltage potentials of the lenses were changed. The beam characteristics observed were beam brightness (*b*), normalized beam emittance (ε_N), position of beam waist (z), half width (x, y) and half divergence (x', y') at the beam waist, and average kinetic energy of the ions at the beamstop. Specifying half width and half divergence as (x, y) and (x', y') is a generalization of beam optics.

Because the intent of this study was to identify general trends rather than to explore intricate phenomena occurring as system parameters were varied, some assumptions and approximations were made to isolate the key components governing beam characteristics in the extraction lens system. Explanation and justification for the assumptions and approximations made in this study follow.

The plasma at the plasma electrode aperture forms a meniscus, which can be concave, convex, or planar. A concave meniscus is shown in Figure 2.2. Plasmas were not the

focus of this study. In this study, the plasma was not given a meniscus, as this is the neutral state between concave and convex meniscus curvature.

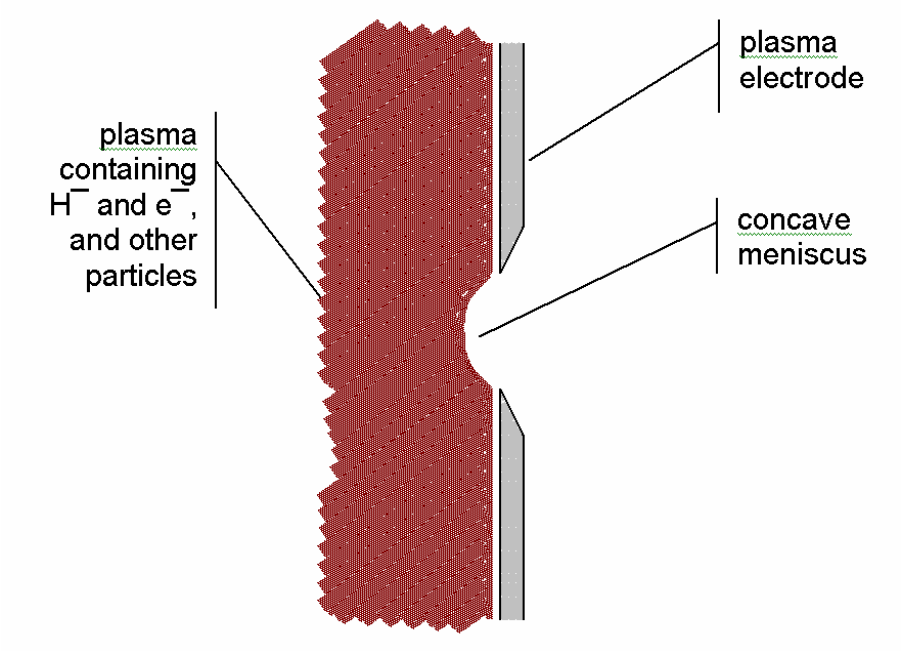

Figure 2.2 Illustration of a concave meniscus formed in the plasma at the aperture of the plasma electrode. The meniscus may also be convex or have no curvature at the aperture. In this study, the plasma is modeled as having no meniscus (i.e., no curvature).

The ion source creates both H^- ions and electrons in the plasma, in addition to neutrals and other charged particles. Having the same electric charge, H^- ions and electrons are both extracted from the plasma by the +3 kV potential difference applied to the first two lenses. However, only H^- ions are desired for acceleration in the cyclotron. The electrons are extracted from the beam by a magnetic filter built into the extraction lens. Four magnetic bars inserted into the extraction electrode set up a magnetic field perpendicular to the charged particles' velocity. Figure 2.3 is a sketch of the region of

the extraction lens in which the magnetic bars are inserted, showing the magnetic field lines and the extraction of electrons.

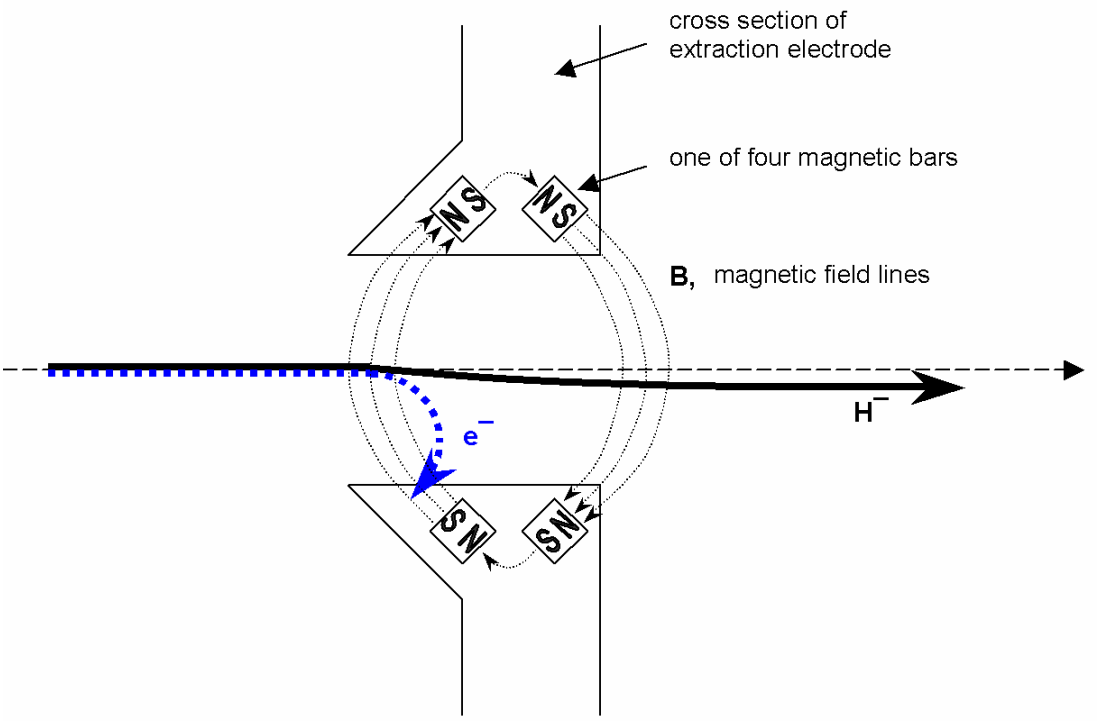

Figure 2.3 Cross-sectional view of the central region of the extraction electrode, showing the four bar magnets inserted into the lens (into the page), transverse to the forward direction of ion velocity (left to right). The centripetal redirection of the electrons, illustrated by the dotted arrow, actually comes out of the page, as per the right hand rule and the Lorentz force equation (2.2).

Application of the right-hand rule and Lorentz force equation (2.2) to charged particles moving with velocity, $\vec{v}$, in a magnetic field, $\vec{B}$,

$$\vec{F} = q\left(\vec{v} \times \vec{B}\right), \tag{2.2}$$

indicate that the ions experience a centripetal force that causes them to travel in a circular path transverse to their forward direction of travel. In the localized region where the

magnetic filter exists, the negative ions do not experience acceleration forces as per equation (2.1). In this region, there is no potential difference and hence no electric field.

Electrons have mass 0.511 MeV and H^- ions have mass 938.2 MeV. From the centripetal force equation (2.3), the radius of curvature of the particles depends on mass as shown in equation (2.4).

$$F = m \cdot \frac{v^2}{r} = qvB \tag{2.3}$$

$$r \propto \sqrt{m} \tag{2.4}$$

H^- ions, being 1836 times more massive than electrons, have a radius of curvature about 43 times larger than that of electrons. As such, the electrons are stripped out of the beam at a much smaller radius of curvature than the H^- ions. The H^- ions also change direction but the magnetic filter is designed such that the net magnetic field is zero so that as the H^- ions pass through the field again, they are forced back to a trajectory parallel to and only slightly translated from the original one, as illustrated by the solid arrow in Figure 2.3. The electrons are no longer in the beam.

Figure 2.3 is drawn in 2D and so does not accurately represent the trajectory of the electrons as they are stripped out of the beam and forced into the electrode. But application of the right-hand rule indicates that the negatively charged particles are forced out of the page, while the particle's velocity and the magnetic field are in the plane of the page. The slight wobble in the H^- ion trajectory is also out of the page as the ions pass by the first pair of magnets and into the page as they pass the next pair. The amount by which the H^- ions are offset from their initial forward trajectory is not precisely known, but steering magnets are installed downstream to ensure that the H^- beam is axially centred in the lens system.

As a result of using the magnetic filter, the H^- ions are preferentially accelerated through the extraction lens system and into the axial injection system. The electrons are stripped out of the beam almost immediately after they are extracted from the ion source plasma (within the first 5 mm of the ~ 400 mm trajectory from plasma electrode to beamstop).

The bulk of charged particle acceleration occurs between the second and third electrodes, where the potential difference is +22 kV and where the beam only consists of H^- ions. Electron stripping and realignment of the H^- ion beam were not modeled in this study, as these processes are secondary to the determination of beam characteristic. The simulated beam contains only H^- ions. Ion repulsion and image forces were not modeled in this study. Although SIMION has the capability to account for such phenomena, doing so was beyond the scope of this thesis.

In the actual system, the electrostatic lenses are mounted on brackets and are separated by spacers and electric insulators (these details are shown in the assembly drawing, Figure 2.1). Only the active regions of the lenses were included in the model because the peripheral assembly components do not act on the beam of ions. The active regions of the lenses include the axially concentric lens apertures, through which the ions travel, and sufficient radial extent in the lenses, to avoid introducing nonlinearities to the electric field intensity in the axial region where the beam is expected to travel. As a rule of thumb, the radial extent of each modeled lens was at least twice the radius of the lens' aperture.

The SIMION model consisted of the three electrostatic electrodes only. Eight extraction lens system design parameters (voltage potentials and lens dimensions) were defined, five of which became the variable test parameters. Their nominal values were obtained from TRIUMF drawings of an existing extraction lens system that DCL has licensed to manufacture. The model designed to simulate the extraction lens system looks like the one in Figure 2.4 below, which is a screen capture from SIMION. A closer look at Figure 2.1 reveals these lens shapes that are isolated in the SIMION model.

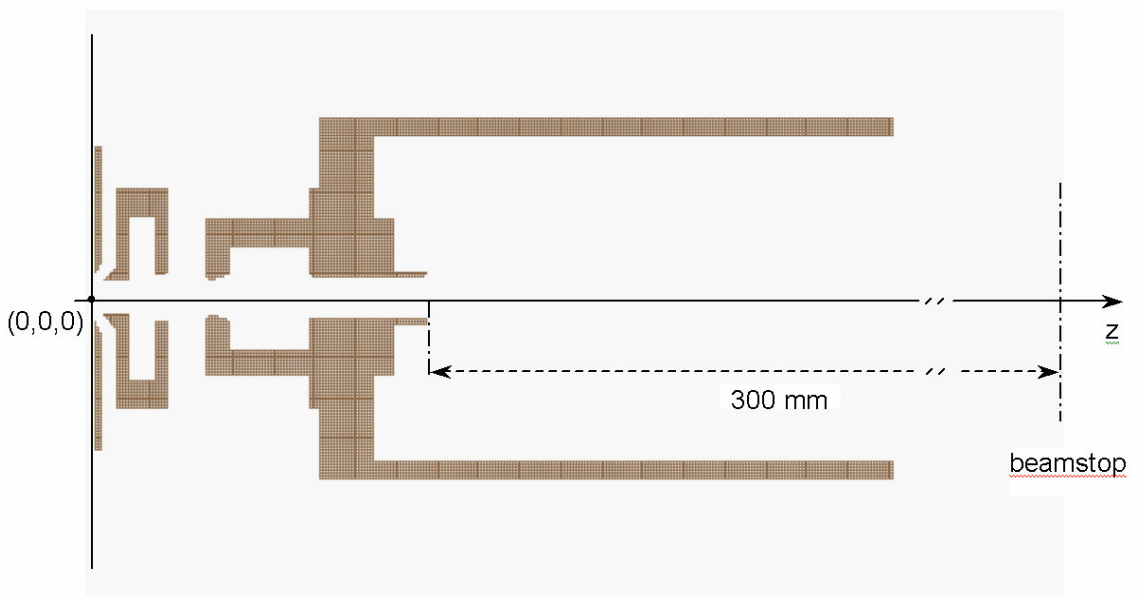

Figure 2.4 Cross-sectional view of the SIMION model of the extraction lens system used in the study. The figure is taken directly from SIMION, as one would view the system during a simulation run (minus the axes, dimensions, and beamstop).

Identification (ID) tags were created to make it easier to refer to the design parameters. They will be used frequently throughout this document. The design parameters, as well as their ID tags and nominal values, are listed in Table 2.1. The system components and design parameters are labelled by their ID tags in Figure 2.5.

Table 2.1 A list of the extraction lens system components and design parameters that served as the variable test parameters in the study, including their nominal values. All parameters were assigned a unique ID tag for ease of reference.

List of design parameters by name	**ID tags & nominal values**
Plasma Electrode	*E1*
Voltage potential	V1 = -25 kV
Aperture diameter	A1 = 13 mm
Extraction Electrode	*E2*
Voltage potential	V2 = -22 kV
Aperture diameter	A2 = 9.5 mm
Shoulder Electrode	*E3*
Voltage potential	V3 = 0 V
Aperture diameter	A3 = 10 mm
Separation between electrodes	
E1 & E2	D12 = 4 mm
E2 & E3	D23 = 12 mm

The values of the test parameters V2, A2, A3, D12, and D23 took on the following test values, in addition to the nominal values listed in Table 2.1:

- V2 = -23 kV, -22.5 kV, -21.5 kV
- A2 = 10.5 mm, 11.5 mm, 12.5 mm
- A3 = 9 mm, 11 mm
- D12 = 7 mm, 10 mm
- D23 = 8 mm, 16 mm

The three other design parameters were held constant at the nominal values: V1 and V3 are fixed in the physical system; A1 was held constant to ensure the beam was the same size at the start of all tests.

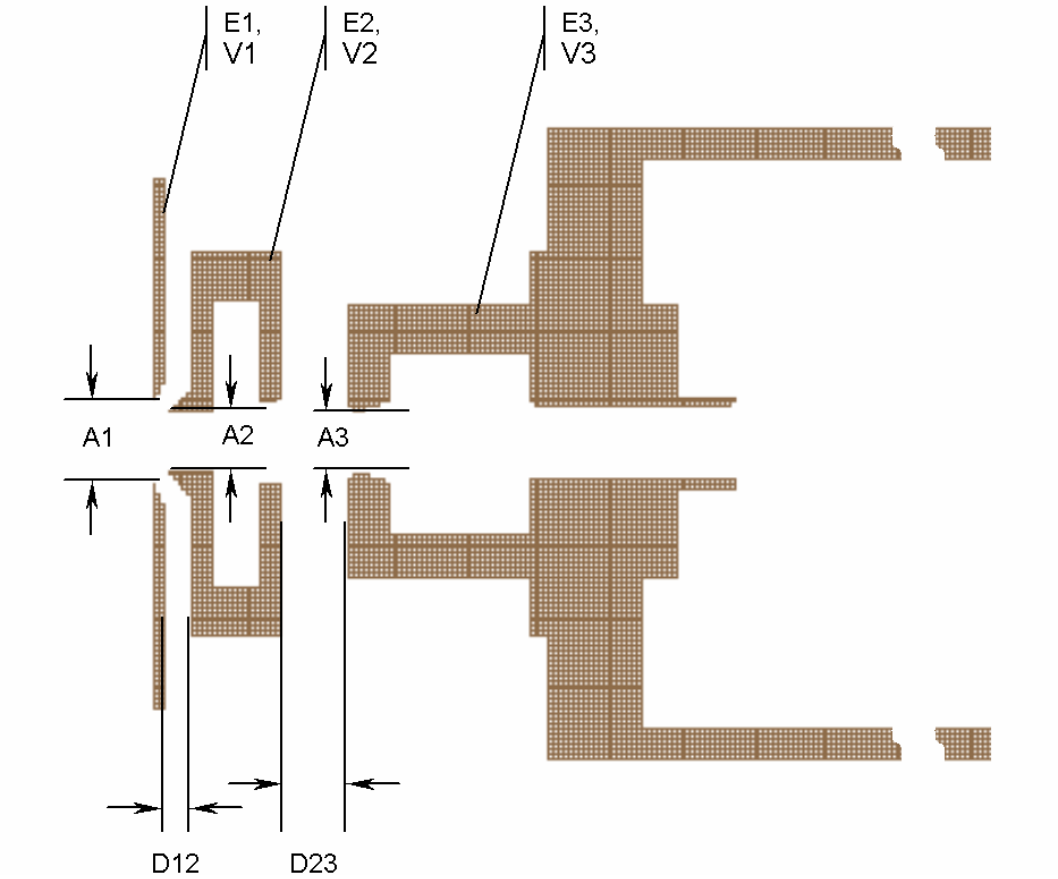

Figure 2.5 The design parameters are labelled here by their ID tags. The ID tags will be used extensively in this document so this figure serves as a practical reminder of what they refer to. Refer to Table 2.1 for the full names of the parameters.

Note that E2 and E3 both have two apertures: one upstream and the other downstream. Only the upstream apertures were varied in the study. It was discovered, during data analysis, that some ions were lost from the beam for larger values of A2 because they

collided into E2 at the downstream aperture (i.e., some ions were located at half widths greater than the radius of the downstream aperture, nominally 7 mm).

Preliminary test results showed that the assumptions made in designing the model were justified. The extraction electrode is known to erode after an extended period of use. The simulations agreeably showed that some ions hit the second electrode, which would indeed lead to erosion. Calculations of normalized beam emittance yielded values within the expected range based on empirical data obtained from experiments using the extraction lens system [7]. Thus, the three-lens model created in SIMION was an adequate representation of the extraction lens system for H^- volume cusp ion sources.

2.2 About the Simulation Tool

Many references will be made to SIMION specific terminology (these will be italicised the first time they are introduced) to describe how the study was designed and how decisions were made in defining the simulation model. Although the details of using SIMION are the topic of Appendix A, this section is intended to briefly explain how SIMION works.

As a general overview, the fundamental steps involved in simulating a model electrostatic system are to define the physical and electrical boundaries of the electrodes, to have SIMION acknowledge and interpret the electrodes, to define the ions that make up the charged particle beam, to select what output data to record, and to simulate ions accelerating through the electrostatic system.

2.2.1 Defining Electrode Geometry

The starting point of all SIMION simulations is a construct called the *potential array*. A potential array is a two- or three-dimensional array of points, in which each point can be assigned a voltage potential. Typically, points in the array will be bound within a geometric shape, and the collective of points will be assigned a voltage potential, in essence, creating an electrode. The group of points that make up the electrode geometry are called *electrode points*. The remaining points are called *non-electrode points*.

Several electrodes can be defined in a single potential array, typically separated by non-electrode points. For example, in this study, the entire three-lens system is defined in a single potential array. Each potential array is saved as a unique file, ending with the extension `.PA#`. The # symbol is how SIMION identifies this particular type of file (refer to Appendix A for more details on this subject).

2.2.2 Refining a Potential Array

Once the electrode geometries are defined in a potential array, SIMION is made to solve the Laplace equation (2.5) to determine the voltage potential at all points between the electrodes.

$$\nabla^2 V = 0 \tag{2.5}$$

This iterative process is called *refining*. Using a finite difference technique, SIMION uses the potentials of electrode points to estimate the potential of non-electrode points. For each non-electrode point, the average voltage potential of its four nearest neighbouring points becomes the estimated value of the potential at that point. The estimates are refined by iteratively estimating potential values for all non-electrode points using the above averaging scheme until further iterations do not significantly change the estimated value obtained. By default, SIMION's stopping criterion is 5×10^{-4}. This criterion means that SIMION stops trying to improve its estimate of the potential at a point when an estimate does not change by more than 5×10^{-4} from one iteration to the next. The more non-electrode points in a potential array, the longer it takes for SIMION to refine the `.PA#` file because it must estimate the potential at each of these points. Having estimated the voltage potential of each non-electrode point, SIMION can now simulate an electric field between the electrodes defined in the potential array by following the potential gradient. The refining process generates one file for each electrode in a potential array, plus an extra file that contains information regarding the entire potential array. These files are identified by the file extensions `.PA0`, `.PA1`, etc.

2.2.3 Defining the Ions

SIMION allows for beams of mixed ions or similar ions. Each ion is defined by all of the following parameters:

- mass, in unified atomic mass units (amu)
- charge, in elementary charge units
- starting kinetic energy, in electron-volts (eV)
- starting location, in millimetres (mm) or grid units (gu)
- starting direction, in degrees (°)
- time of birth, in microseconds (μs)
- colour
- charge weighting factor

Setting the first five parameters is sufficient to define a beam used in a model where delayed ion creation and space charge repulsion are not factors (refer to [1] for details regarding these SIMION capabilities). The number of ions in a beam is also a user-defined parameter.

2.2.4 Selecting What Data to Record

Data recording is an optional feature. If data recording is turned on, the data can be written to a file or simply displayed on the screen for immediate viewing as the simulation runs. SIMION provides pre-defined *data elements* for the user to select what output data to record (refer to Appendix A for a complete list). The list includes such elements as position (x, y, z), acceleration ($|\vec{a}|, a_x, a_y, a_z$), velocity ($|\vec{v}|, v_x, v_y, v_z$), electric field intensity ($|\vec{E}|, E_x, E_y, E_z$), and kinetic energy, which can be measured when a given *event* occurs, or at a specific x, y, or z plane, or at some other pre-defined *trigger*.

Examples of events that trigger data recording are ion creation, hitting an electrode, and being outside the *simulation workbench*. The simulation workbench is a 3D volume that defines the extent of space the simulation is intended to model.

To record data to a file, a file name and extension must be specified. A practical file extension is `.txt`, which can be opened in Microsoft Excel as delimited text such that the data is organized into columns.

2.2.5 Simulating Ion Acceleration

Once the geometries of the electrodes in the electrostatic system are defined in a potential array and the `.PA#` file is refined, an *instance* of the potential array is loaded into the simulation workbench. From within the workbench view, the *ion definition panel* is accessible to define the ions as described in section 2.2.3. From within the ion definition panel, the user can select what data elements to record and can specify a file name to output the data to. Clicking on a button labelled "*Fly'em*" starts the simulation. The cross-sectional view of the system is shown on the screen and the ion trajectories are drawn in as the ions are created and accelerated through the system. Figure 2.6 is a sample ion trajectory after completion of a simulation.

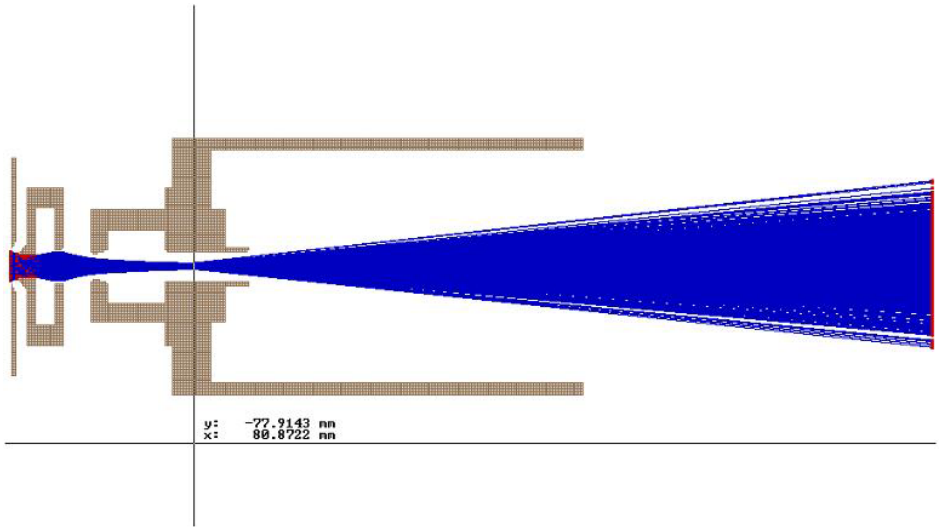

Figure 2.6 Sample ion trajectory.

2.3 Designing the Simulation Model

As with all simulation models, it is of utmost importance to design a model that is a fair representation of the system being studied. Using SIMION as the simulation tool, it was necessary to understand how the program worked, what assumptions the program made, and its limitations as well as its capabilities. How well a model represents reality depends on the amount of care taken to ensure that the simulation tool is actually doing what it is thought to be doing. The assumptions and approximations discussed in section 2.1 will be implied herein without reiteration.

2.3.1 Electrode Geometry

Dimensions of the electrostatic lenses were obtained from manufacturer drawings. The outer diameters, aperture diameters, lens thicknesses, and spacing between lenses were specified on these drawings. Only the active regions of the lenses were included in the potential array geometry definitions, as shown in Figure 2.4. The insulating components, spacers, and mounting brackets that are in the actual system (which can be seen in Figure 2.1) were excluded. In the potential array, the excluded, non-active components were left as non-electrode points for which SIMION estimated the voltage potentials when the `.PA#` file of the simulation model was refined.

Issues that arose during the early stages of designing the simulation model are discussed in the following subsections, as are their solutions. These design issues pertained to defining the geometric and electric boundaries of the electrostatic lenses. Preliminary tests were done to resolve the design issues while the workings of SIMION were still being learned and while details of the study were yet unrefined.

2.3.1.1 Grid Density

Typically, electrode points are assigned voltage potentials and non-electrode points are left unassigned. It is left for SIMION to solve the Laplace equation (2.5) and determine the voltage potential at all non-electrode points. When SIMION solves the Laplace equation, it adheres to the boundary condition that all electric field lines must leave the surface of an electrode perpendicular to its surface.

Much like with the pixelation of a computer monitor, non-orthogonal lines and curved edges in a potential array (PA) appear jagged if the PA contains few points. A jagged edge introduces unwanted distortions in the electric field lines along the surface of the electrode. A curved edge could be drawn more smoothly if the PA had more points. The grid density of a PA refers to the number of grid units that represent one millimeter in the actual system being modeled. The higher the grid density, the more accurately SIMION modeled the physical system. But higher grid density cost more RAM usage (10 bytes per point!), required longer calculations, and made refreshing a view on the screen very slow. A measure of improvement for increasing grid density was the convergence of a simulation output, say electric field intensity, to the expected theoretical value as grid density was increased. Once convergence was achieved, further increasing the grid density did not significantly improve how well SIMION modeled the physical system but instead compromised efficient use of RAM and CPU time.

To determine what grid density to use in defining the extraction lens system, the geometries of the first two lenses were recreated in a series of potential arrays of different grid densities. In addition to a potential array with one-to-one (1:1) scaling, where each grid unit represented one millimeter, the scale factors investigated were two (1:2), four (1:4), eight (1:8), ten (1:10), twelve (1:12), and twenty (1:20) grid units per millimeter. Inspection of the beam trajectory of the (1:1) case revealed that the beam converged to a waist at several positions along its trajectory. By comparing the position of the first waist, and the electric field intensity and voltage potential at the first waist, for each of the different grid densities, the grid density that was sufficient to produce reliable results was determined. The first waist was chosen as a point of measurement because it was a convenient reference point. The results of the grid density test are plotted in Figure 2.7.

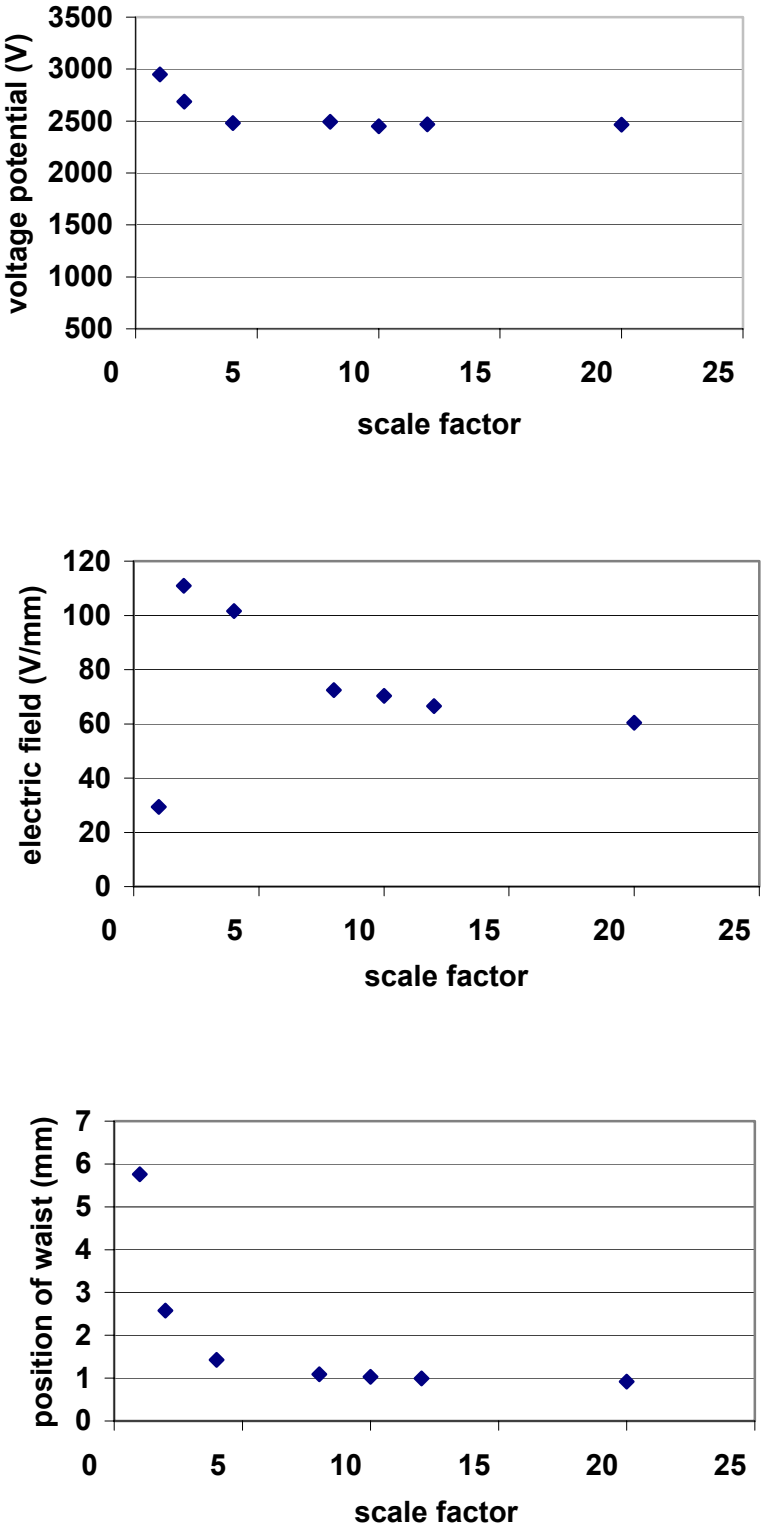

Figure 2.7 The voltage potential (top) and electric field (middle) at the waist, and the waist position relative to z = 0 (bottom) measured for different grid densities, show that a scale factor of eight is optimal.

Referring to the three plots in Figure 2.7, voltage potential (top plot), electric field intensity (middle plot), and position of waist (bottom plot) are each plotted against scale factor. Inspection of the plots in Figure 2.7 indicates that the voltage potential and position of the waist remained reasonably constant for scale factors greater than and including four. The electric field intensity converges reasonably well for scale factors greater than and including eight. To obtain convergence for the three tested parameters, a scale factor of eight was chosen. While a larger scale factor also satisfied the convergence criteria, (1:8) scaling was sufficient to obtain reliable results at the minimum expense of potential array size. With a scale factor of eight, each grid unit represented 0.125mm.

2.3.1.2 Outer Diameter of Lenses

Drawings of the actual extraction lens system (Figure 2.1) show that each lens has a different outer diameter to accommodate assembling the physical system. An effective outer diameter needed to be defined for each lens so that the electrodes drawn in SIMION produced the nominal representative electric field intensities without being so large as to require excessive computational time. The outer diameter of each lens must be sufficiently large that the outer edge field effects do not affect the field intensities at the inner lens apertures (i.e., in the axial region where the beam passes). But if the outer diameters are too large, then the equivalently larger potential array takes up too much RAM, thereby slowing down calculations and other processor intensive tasks.

Five different combinations of outer diameter lens dimensions were tested, with the dimensions progressively decreasing from the nominal value. Outer diameters larger than the nominal values were not tested since the purpose of the test was to reduce potential array size. The variables in this test were the outer diameters of E1 and E2. E3 has the smallest nominal outer diameter and so was left unchanged. The values of the outer diameters of E1 and E2 tested are listed in Table 2.2, along with the measured electric field intensities at a fixed z position for each test case.

Table 2.2 Outer diameter values of E1 and E2 tested to determine how small the outer dimensions could be without introducing nonlinearities to the electric field intensity in the axial region.

	E1 diameter (in grid units)	*E2 diameter (in grid units)*	*electric field intensity (V/mm) at a fixed position, z*
nominal:	766	558	0.0918
	558	558	0.0915
	518	518	0.0869
	478	478	0.0813
	438	438	0.0754

The chosen z position, at which the electric field intensities were measured for the different combinations of outer diameters, was at the downstream waist position, which was about 90mm downstream from z = 0, the starting position of the ions.

The data in Table 2.2 is plotted in Figure 2.8. The data point furthest right is the nominal case, with which only the second test case agrees. The plot clearly shows that the electric field intensity diverges as the outer diameters of E1 and E2 are decreased. Such behaviour is unacceptable: it indicates that the electric field in the axial region where the beam passes differs significantly from the nominal representative electric field intensity.

While reducing the outer diameter of E1 from its nominal value by 208 grid units and keeping the outer diameter of E2 at its nominal value had little effect on the electric field intensity at the fixed z position, there was no appreciable improvement in the time SIMION required to refine the smaller potential array. The nominal values of the outer diameters of E1 and E2 were thus implemented in the simulation model.

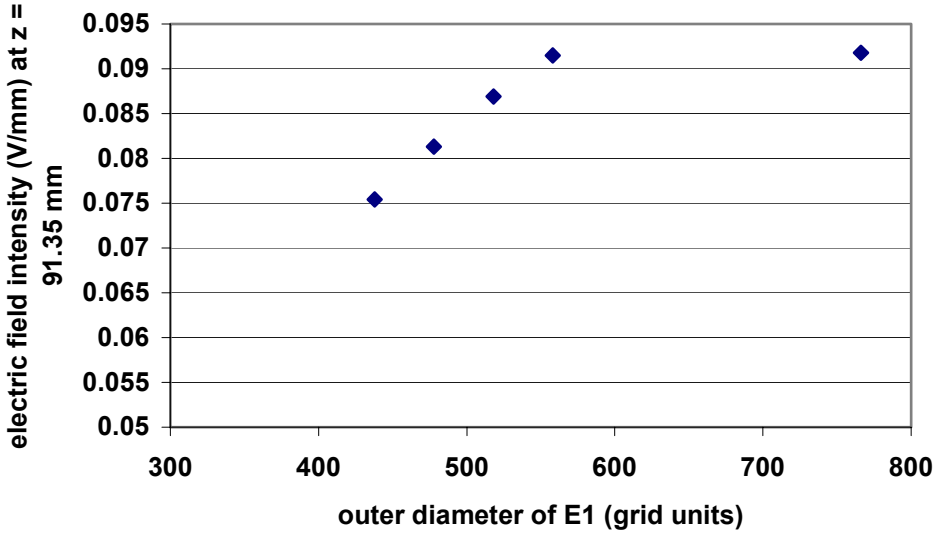

Figure 2.8 Electric field intensity at z = 91.35 mm plotted against the outer diameter value of E1. The rightmost data point is the nominal case. As the outer diameter was decreased, the electric field intensity diverged from the nominal case.

2.3.1.3 Defining the Array Boundary

SIMION handles array boundaries differently depending on whether electrode points extend to the edge of the potential array or not. The refining process uses the average potential of the four nearest neighbouring points to estimate the potential of each non-electrode point. This process works well within the boundaries of the array but not so well at the edges of the array [1]. If the edge of an electrode coincides with the edge of the potential array, SIMION assumes that the electrode shape extends to infinity beyond the boundary. If electrode points do not touch the array's boundary, SIMION uses the averaging scheme to estimate voltage potentials of the non-electrode boundary points to account for field propagation around the nearby electrode. In the extraction lens system for the H^- volume cusp ion source, the ion source plasma is assumed to be within 2 V of the plasma electrode potential of V1 = –25kV.

In the physical system, the plasma immediately precedes the plasma electrode. The potential difference of +3kV between the plasma electrode, E1, and the extraction

electrode, E2, causes the formation of a meniscus in the plasma at the aperture of E1. Assuming a flat meniscus was an approximation made in this study. It was not sufficient to draw the plasma electrode at the edge of the potential array: the array points along the boundary that represent the lens' aperture, A1, were non-electrode points and SIMION used the averaging scheme described above to estimate the potential of each of these points. With this approach to defining the electrode geometries, the potential at the origin of the system was –22.5854584 kV. As such, the ion source plasma effectively differed from V1 by 2.5 kV, rather than 2 V. This inaccurate representation of the physical system was remedied by adding a column of electrode points immediately before the plasma electrode as if the electrode had no aperture. By doing so, the potential at the origin of the system was –24.9999389 kV, less than one thousandth of a percent from the nominal value of –25 kV. This extra column of points laid on the boundary of the array, appropriately being interpreted by SIMION as extending infinitely beyond the array. Adding two columns of electrode points before the plasma electrode did not further improve the averaging estimate of the voltage potential at the system's origin.

2.3.1.4 Grounded Vacuum Chamber

E3, the shoulder electrode, is the third and final electrode in the extraction lens system to act on the H^- ions. Beyond E3, the ions drift through a vacuum chamber towards a beamstop located 300mm downstream of E3. The walls of the vacuum chamber are at the same voltage potential as E3. Without a potential difference between where the ions leave E3 and where they hit the beamstop, no electric force is acting on the particles. As a result, the particles are not accelerated in the vacuum chamber; they drift from E3 to the beamstop.

It was necessary to include a grounded vacuum chamber (otherwise referred to as a ground can) in the potential array to properly define the electrode geometry. Without a confining ground can, the ions leaving E3 experienced non-zero electric fields. A test was conducted to determine what shape and extent of ground can was sufficient to maintain zero electric field between E3 and the beamstop. The actual system has various cylindrical metal structures that are electrically neutral with E3 and that extend beyond the electrode into the vacuum chamber. While redundant concentric cylinders were not

required to ensure zero electric field between E3 and the beamstop, the radial and longitudinal extents of the ground can were important in establishing this. The criterion used to determine the most appropriate ground can was acceleration of the ions at the beamstop. Since the ions are not supposed to be accelerated in the vacuum chamber, it was expected that the ions have zero acceleration at the beamstop.

Of the six test cases created, the following conclusions were made. No ground can, or one that is too short, resulted in the ions still being accelerated as they approached the beamstop. Narrow and long ground cans resulted in loss of beam towards the end of the drift space from E3 to the beamstop. Excessively wide ground cans, requiring larger potential arrays, required too much processing time to be refined and displayed on the screen. The ideal ground can was the one that modeled the actual grounded vacuum chamber most accurately: the ground can in the simulation model had the same outer diameter, thickness, and length as the outermost cylindrical metal structure attached to the shoulder electrode in the actual system.

A note to those who are reading this thesis as a guide to using SIMION, it is recommended that the extent of the potential array in the y direction beyond the radius of the cylindrical system be minimized to avoid unnecessary non-electrode points. If these are not minimized, SIMION will use its averaging method to calculate the electric field at each of these points, which takes much computational time and may introduce fields in areas where they are not intended. For example, excess non-electrode points with a shorter ground can results in non-zero electric field intensity beyond the ground can that act on the ions to accelerate them in the region of the system where they are intended to drift.

2.3.2 Defining the Ion Beam

H^- ions make up the beam of charged particles in this study. H^- has a rest mass of 1.008373630 amu and a charge of –1 elementary charge units. The test beam was populated with 5000 ions. The starting kinetic energy, transverse position, and direction of the 5000 ions used in each simulation run were randomly assigned within ranges specifically chosen for this study. A user-defined program was implemented to create the

5000 ions with these randomly assigned parameter values (refer to Appendix E for the ion creation code).

2.3.2.1 Test Beam

Each test run utilized five thousand ions created at z = 0 mm (longitudinal position), with randomly generated initial (x, y) and (x', y') coordinates. The extent in (x, y) was restricted to a radius of 6.5mm, the half size of A1, since the ions are extracted through the circular aperture of the plasma electrode, E1, which is the only definite constraint on an ion's starting transversal position. The initial divergence (x', y') was not limited, and thus could take on values ranging from –90° to +90°. Since divergence is derived from the ion's momentum, and momentum depends directly on velocity, it was necessary to give the ions initial kinetic energy in order to impart divergence to the charged particles. Without any initial divergence, the initial beam emittance would be zero and would not be observable.

H^- ions in the ion source plasma have kinetic energies of about 1 eV [8]. The exact kinetic energy of the ions is unknown, but in accordance with the observed 2 V difference between the ion source plasma and the plasma electrode [9], the H^- ions were randomly given initial kinetic energies ranging from 0 to 2 eV. The 2 eV initial kinetic energy is negligible compared with the +3 kV potential difference used to extract the ions from the plasma.

SIMION has a built-in random number generator, generating numbers ranging from 0 to 1. The distribution of randomly generated numbers is Gaussian by default. Such a distribution is ideal to populate a beam, as this is the common convention in physics for mathematically representing a beam. A population of 5000 ions in a circular area of radius 6.5 mm ensured that a proper Gaussian distribution was indeed obtained for every simulation test run. By allowing the maximum radial starting position of an ion to be the radius of aperture of the plasma electrode, the model lens system determined its own acceptance.

The alternative to randomly populating the beam was to assign a patterned starting position and direction, which may bias or introduce systematic errors to the observed system acceptance and beam characteristics.

2.3.2.2 Starting z Position

Preliminary test runs showed that the starting z position of the ions affected the position of the beam waist. To account for the column of electrode points that was required to establish the correct electric field at the plasma lens aperture (as explained in section 2.3.1.3), the starting z position was set to z = 0.1251 mm. 0.125 mm is the thickness of the first column of electrode points, taking into account the grid density scale factor of eight grid units per millimeter. Furthermore, the starting position could not be defined inside the electrode, hence 0.0001 mm were added to the 0.125 mm thickness of the first column of electrode points. The 0.0001 mm value was chosen from an example in [1].

2.4 Collecting and Presenting the Data

The dimensions and voltage potentials of the modeled extraction lens system are listed by name and ID tag in Table 2.3. Of the eight design parameters, five became the variable test parameters. The nominal values and variable parameter values tested are also listed in Table 2.3. Refer to Figure 2.5 to locate the design parameters on the simulation model. The three parameters that were left unchanged are A1, V1, and V3. V1 and V3 are set by external power supplies and are fixed at the nominal values during normal operation of the commercial cyclotrons. A1 was held constant to allow for direct comparison of the test results, namely, the beam characteristics, by ensuring that the beam was the same size at the start of every test run.

Four hundred thirty two tests were done to represent all of the possible combinations of design parameters (refer to Appendix B for a detailed listing of all of the tested lens configurations). For each test run, SIMION produced an image on the screen of the ion trajectories as the beam of H^- ions were transported through the simulation model. The half width and the position of the beam's waist were measured on the screen utilizing the cross-hair cursor of the mouse. The ion trajectories could be viewed in the xz plane and

in the yz plane such that four independent measurements of half width and waist position could be made (beam waist dimensions and positions are listed in Appendix C). The output of each test run was a one-megabyte text file containing information about the radial position (x, y), divergence (x', y'), acceleration, and kinetic energy of each ion at its creation and termination, and the voltage potential and electric field intensity at the location of the ion when the data were recorded. Normalized emittance (equation 1.12) at the beam waist and beam brightness (equation 1.13) at the beamstop were calculated from the output data (calculated beam characteristics are listed in Appendix D).

Table 2.3 Nominal and variable test parameter values for the extraction lens system study. The nominal values were obtained from TRIUMF technology drawings. The ID tags are used to reference the variable test parameters more concisely.

List of design parameters by name	**ID tags & nominal values**	**Variable parameter test values**		
Plasma Electrode	*E1*			
Voltage potential	V1 = -25 kV			
Aperture diameter	A1 = 13 mm			
Extraction Electrode	*E2*			
Voltage potential	V2 = -22 kV	-23 kV	-22.5 kV	-21.5 kV
Aperture diameter	A2 = 9.5 mm	10.5 mm	11.5 mm	12.5 mm
Shoulder Electrode	*E3*			
Voltage potential	V3 = 0 V			
Aperture diameter	A3 = 10 mm	9 mm	11 mm	
Separation between electrodes				
E1 & E2	D12 = 4 mm	7 mm	10 mm	
E2 & E3	D23 = 12 mm	8 mm	16 mm	

Of the 5000 H^- ions created in each test run, the number of ions that were transmitted to the beamstop was utilized to calculate the percent of beam transmitted. Loss of beam occurred mostly at A2, as the ions extracted from the ion source plasma were forced along trajectories on a collision course with E2. For certain lens configurations, loss of beam also occurred further downstream of A2, as ions collided into E2 and/or E3.

Beam waist position was measured relative to the beamstop, located 300 mm downstream of the shoulder electrode in each test configuration. Waist positions measured from z = 0 mm, the approximate starting position of the ions, cannot be compared between all the different lens configurations because the different values of D12 and D23 make it such that waist positions measured from z = 0 mm are dependent on D12 and D23. By measuring the waist positions relative to the beamstop, which is at a fixed position located 300 mm downstream of E3 and independent of the values of D12 and D23, the measurements can be directly compared between all test configurations.

The manner in which the data is presented in this thesis is intended to assist in optimizing the design of a new extraction lens system. The success of a design is typically judged by how well the system produces a beam of H^- ions that meets certain criteria. In accelerator physics, a high quality beam is one with high brightness and low emittance. But when beam quality is subject to a given application, beam brightness, normalized emittance, and percent of beam transmitted are the key measurements that assess the usefulness of the beam. In this study, beam current is represented by percent of beam transmitted, whereby one hundred percent transmission is the highest beam current achievable by this system.

Extraction lens systems for H^- volume cusp ion sources are suited to two major types of applications, distinguished as low and high current applications. The Positron Emission Tomography (PET) cyclotron is an example of an application in which a beam of relatively low current and reasonably high brightness is acceptable. High beam currents damage the targets of PET cyclotrons. For a low current beam, high brightness can be achieved at the expense of beam transmission, given a small emittance (as per the equation for beam brightness (1.13)). A brighter beam increases efficiency because it

generally requires less manipulation (i.e., focusing) because the beam typically already has low emittance. For cyclotrons that use high currents, beam brightness and normalized emittance may be compromised to achieve high currents, although it would be best to have high current and high brightness. Magnets are typically implemented downstream of an extraction lens system to focus a high current beam to a smaller spot size.

2.4.1 More Discussion of Beam Characteristics

Small emittance typifies a beam that will not diverge excessively as it drifts through empty space between active devices. A beam that is too divergent can still be used, although it typically will require focussing to match the acceptance of a downstream device. Another criterion to consider regarding drift spaces is the position of the beam waist. The closer the waist is to the beamstop or an adjacent downstream device, the less it will diverge by the time it gets there. A beam waist closer to an adjacent downstream device compensates for a beam with greater divergence.

Beam emittance, ε, is the product of maximum half width (x_{max}) and half divergence at the half width intercept (x'_{int}) at a given longitudinal position (z). Beam emittance can be calculated at any longitudinal position along the beam's trajectory but is easiest to calculate at the waist. Recall from Figure 1.3, the half divergence intercept is maximal at the waist because, at this position, the beam ellipse is upright. (x, x') at the waist were easy to measure from the ion trajectories SIMION produced for each test run.

While beam emittance is the quantity sought to determine beam quality, half width and half divergence at the waist were also noted, since these are intrinsically related to beam emittance. This data is useful for determining which of the two dimensions contributes most significantly to the calculated emittance. Low beam emittance may arise from having a small x_{max} value and a relatively large x'_{int} value, or vice versa.

In order to use beam emittance comparatively to assess beam quality, the calculated beam emittance must be normalized. Normalizing beam emittance accounts for ion energy at

the longitudinal position where the emittance is calculated. A less energetic beam has a lower normalized emittance than a beam with equivalent emittance but higher energy.

Another measure of beam quality, which also accounts for percent transmission of ions, is brightness. For a given emittance, a beam with a higher transmission percentage will result in a brighter, higher quality beam. Lower emittance, which is *a priori* a measure of high beam quality, also contributes to higher brightness due to the inverse relation between brightness and emittance. The percent transmission of ions is also called the beam current. Low beam current occurred when many of the ions hit an electrode rather than passing through each aperture.

The kinetic energy of the ions at the beamstop is a useful quantity because downstream devices are designed to accept ions at a specific energy.

Following is a summary of the beam characteristics that are typically favoured from a beam optics perspective, listed in order of importance:

1) Higher brightness
2) Lower normalized beam emittance
3) Higher/lower beam transmission (depends on application)
4) Smaller beam waist half divergence and half width
5) Beam waist position farther downstream

Chapter 3

Variations on the Nominal System

This chapter addresses the trends observed from the tested lens configurations that differed from the nominal configuration by a single parameter value only. The nominal and variable test parameter values that were listed in Chapter 2 are reiterated in Table 3.1.

Table 3.1 Nominal and variable test parameter values for the extraction lens system study. The nominal values were obtained from TRIUMF technology drawings. The ID tags are used to reference the variable test parameters more concisely.

List of design parameters by name	**ID tags & nominal values**	**Variable parameter test values**		
Plasma Electrode	*E1*			
Voltage potential	V1 = -25 kV			
Aperture diameter	A1 = 13 mm			
Extraction Electrode	*E2*			
Voltage potential	V2 = -22 kV	-23 kV	-22.5 kV	-21.5 kV
Aperture diameter	A2 = 9.5 mm	10.5 mm	11.5 mm	12.5 mm
Shoulder Electrode	*E3*			
Voltage potential	V3 = 0 V			
Aperture diameter	A3 = 10 mm	9 mm	11 mm	
Separation between electrodes				
E1 & E2	D12 = 4 mm	7 mm	10 mm	
E2 & E3	D23 = 12 mm	8 mm	16 mm	

Of the four hundred thirty two tests, whose lens configurations are listed in Appendix B, only a small set were chosen to represent variations on the nominal system (i.e., lens configurations in which only one variable parameter was changed). The test numbers and parameter values representing these tests are listed in Table 3.2. For each test case, the shaded entry indicates the variable that was changed from its nominal value.

Table 3.2 Test numbers and parameter values of the lens configurations that represent variations on the nominal system. The nominal lens configuration is test 1.

test #	V2 (V)	A2 (mm)	A3 (mm)	D12 (mm)	D23 (mm)
test 1	-22000	9.5	10	4	12
test 2	-22000	9.5	10	4	***8***
test 3	-22000	9.5	10	4	***16***
test 4	-22000	9.5	10	***7***	12
test 7	-22000	9.5	10	***10***	12
test 10	-22000	9.5	***9***	4	12
test 19	-22000	9.5	***11***	4	12
test 28	-22000	***10.5***	10	4	12
test 55	-22000	***11.5***	10	4	12
test 82	-22000	***12.5***	10	4	12
test 109	***-23000***	9.5	10	4	12
test 217	***-22500***	9.5	10	4	12
test 325	***-21500***	9.5	10	4	12

To illustrate how the trends of variations on the nominal system were determined, consider the following example. To determine the effects of changing the spacing between the first and second electrode, the data from the three tests 1, 4, and 7 were

compared. Test 1 represents the nominal system, in which all test parameters have the nominal values. Test 4 uses D12 = 7 mm, but all other variables have the nominal values. Similarly, test 7 uses D12 = 10 mm while all other variables have the nominal values. In this manner, each test parameter was isolated and analyzed independently of the other test parameters, treating the nominal values as a test standard.

To reiterate from Chapter 2, following is a summary of the beam characteristics that are typically favoured from a beam optics perspective, listed in order of importance:

1) Higher brightness
2) Lower normalized beam emittance
3) Higher/lower beam transmission (depends on application)
4) Smaller beam waist half divergence and half width
5) Beam waist position farther downstream

The data will be presented herein to reflect how changes in the variable test parameters affected the above beam characteristics. The choice of presentation is intended to facilitate designing an extraction lens system as a function of the above beam characteristics. The terms “decrease” and “increase” are used to describe how to change the values of the test parameters in order to achieve the favoured beam characteristics.

3.1 High Beam Brightness

Beam brightness at the beamstop, located 300 mm downstream of E3, was calculated as per equation (1.13), for each of the test cases listed in Table 3.2. Beam brightness is plotted against the five variable test parameters in the following figures, Figure 3.1 to Figure 3.5. In each plot, the data point corresponding to the nominal values for the variable parameters is enlarged and highlighted. The brightness values are labelled at each data point.

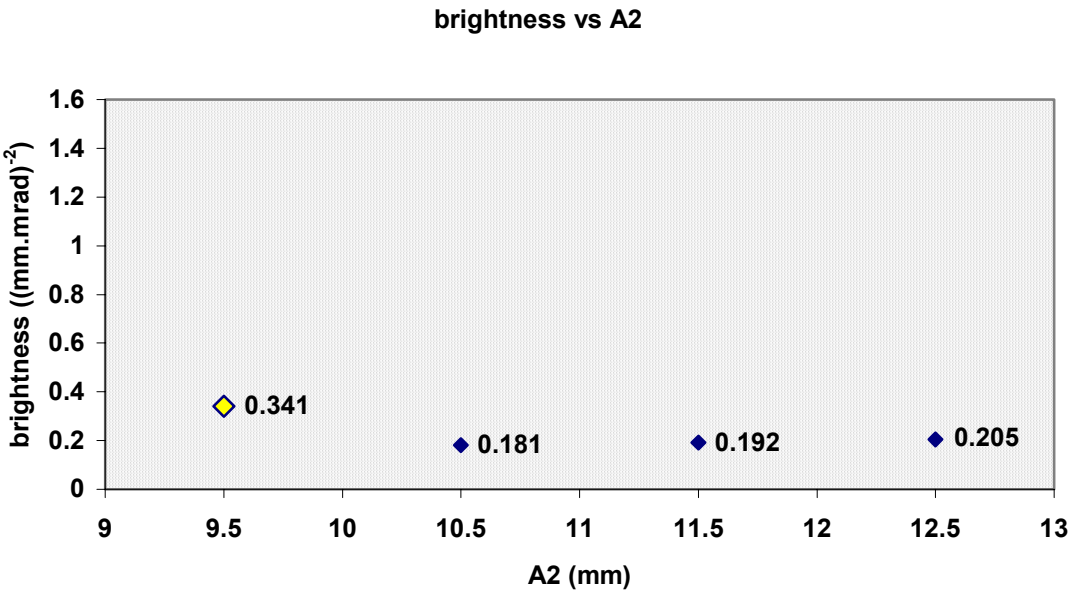

Figure 3.1 Plot of beam brightness versus A2. The trend is flat, suggesting that the values of A2 tested in this study, with the remaining parameter values held at the nominal values shown in Table 3.1, did not have a significant effect on beam brightness.

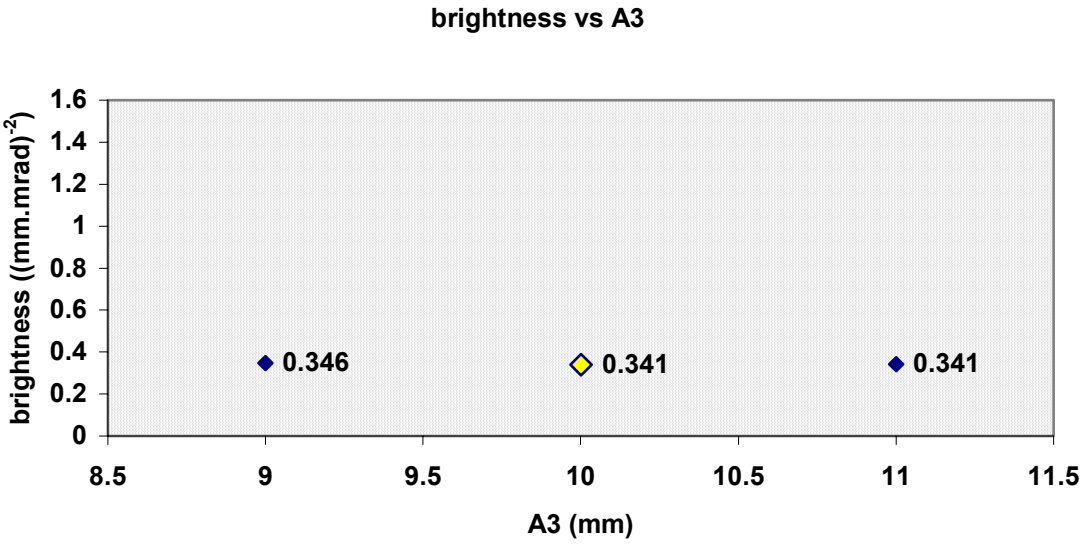

Figure 3.2 Plot of beam brightness versus A3. The trend is flat, suggesting that the values of A3 tested in this study, with the remaining parameter values held at the nominal values shown in Table 3.1, did not have a significant effect on beam brightness.

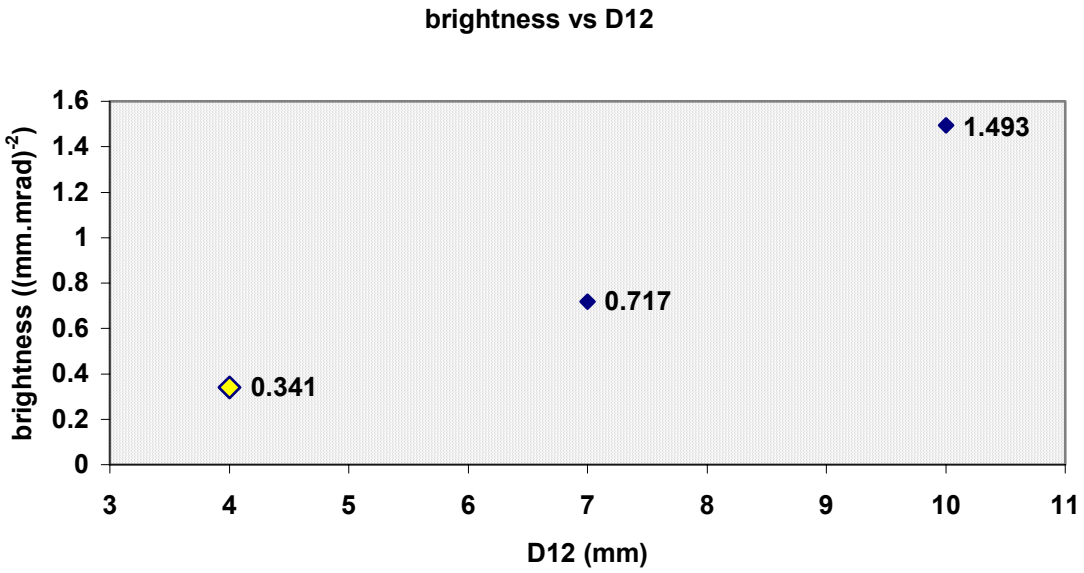

Figure 3.3 Plot of beam brightness versus D12. With all other variables held at the nominal values shown in Table 3.1, the observable trend is that increasing the value of D12 resulted in having a brighter beam at the beamstop.

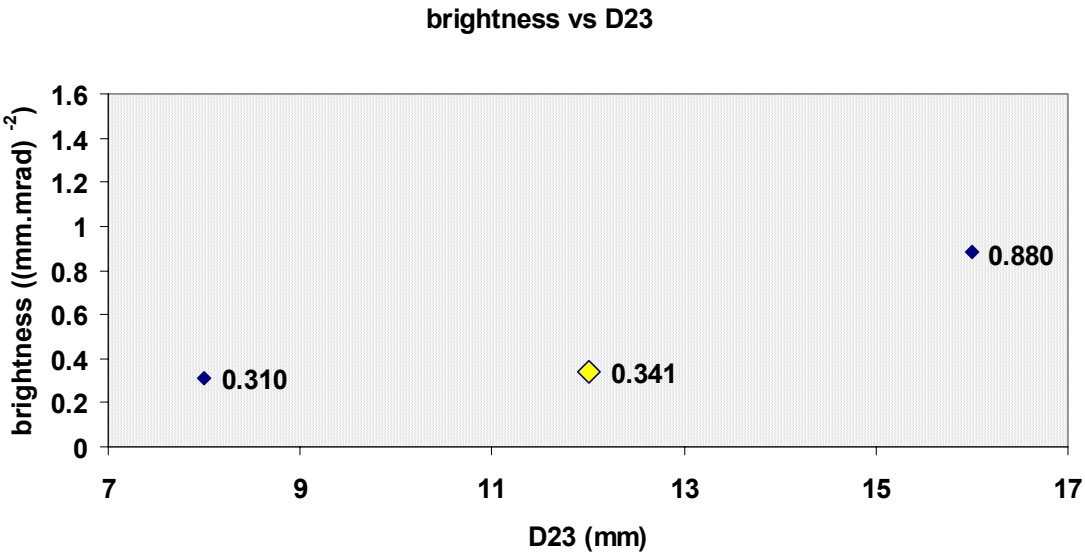

Figure 3.4 Plot of beam brightness versus D23. All other variables were held constant at the nominal values shown in Table 3.1. The observable trend is that increasing the value of D23 resulted in having a brighter beam at the beamstop, as it did with increasing D12, although less significantly here.

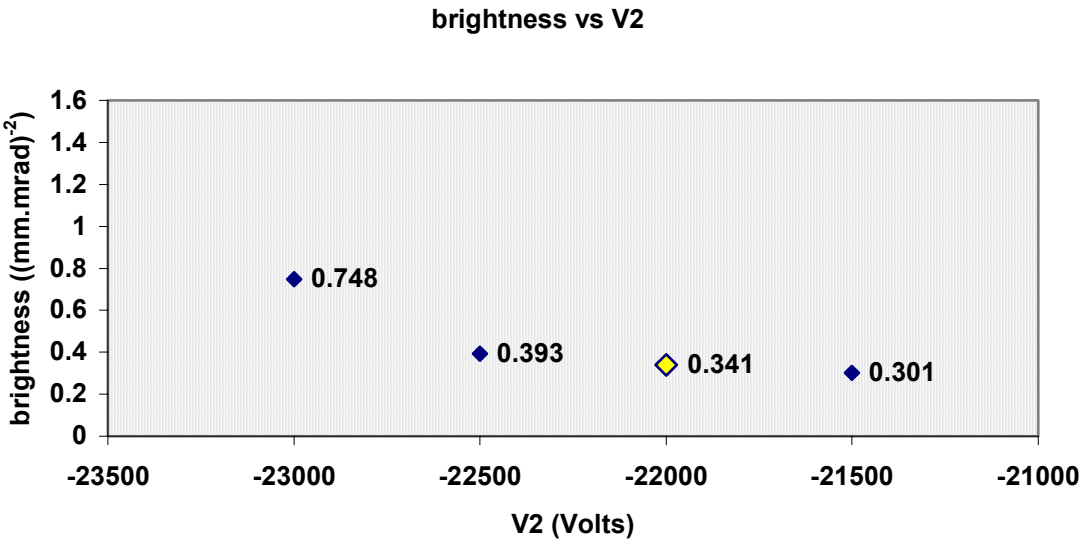

Figure 3.5 Plot of beam brightness versus V2. With the remaining parameter values held at the nominal values shown in Table 3.1, the observable trend from varying only the voltage potential on E2 is that smaller (more negative) values of V2 resulted in a brighter beam at the beamstop.

The variable that affected brightness the most was D12, the spacing between the first and second electrodes, more than quadrupling the brightness obtained in the nominal test case. The next most influential parameter was D23, the spacing between the second and third electrodes. In both of these cases, increasing the spacing between electrodes resulted in higher beam brightness at the beamstop. The effect of increasing D12 and D23 simultaneously will be explored in Chapter 4. Decreasing the value of V2, which effectively decreased the potential difference between electrodes E1 and E2, and increased the potential difference between electrodes E2 and E3, also noticeably increased beam brightness at the beamstop.

The trends of the above plots are summarized in Table 3.3. Listed in order of decreasing beam brightness, *b*, the test number and lens configuration that resulted in the brightest beam in each of the above plots is listed in the table. The values of the parameters that resulted in the highest brightness are highlighted. The nominal configuration, included

for reference, is also the configuration that resulted in the highest brightness for the range of values of A2 tested.

Table 3.3 Summary of observed trends for the study of variations on the nominal configuration to achieve the brightest beam. Increasing the value of D12 was the most effective change to the nominal configuration to achieve the brightest beam.

observed trend	**b** $(mm \cdot mrad)^{-2}$	**test #**	**V2 (V)**	**A2 (mm)**	**A3 (mm)**	**D12 (mm)**	**D23 (mm)**
increase D12	1.493	test 7	-22000	9.5	10	***10***	12
increase D23	0.880	test 3	-22000	9.5	10	4	***16***
decrease V2	0.748	test 109	***-23000***	9.5	10	4	12
A3 flat	0.346	test 10	-22000	9.5	***9***	4	12
A2 flat *(nominal)*	0.341	test 1	-22000	***9.5***	10	4	12

3.2 Low Normalized Beam Emittance

Normalized emittance at the beamstop was calculated, as per equation (1.12), for each of the test cases listed in Table 3.2. Normalized emittance is plotted against the five variable test parameters in the following figures, Figure 3.6 to Figure 3.10. In each plot, the nominal data point is enlarged and highlighted. The normalized emittance values are labelled at each data point.

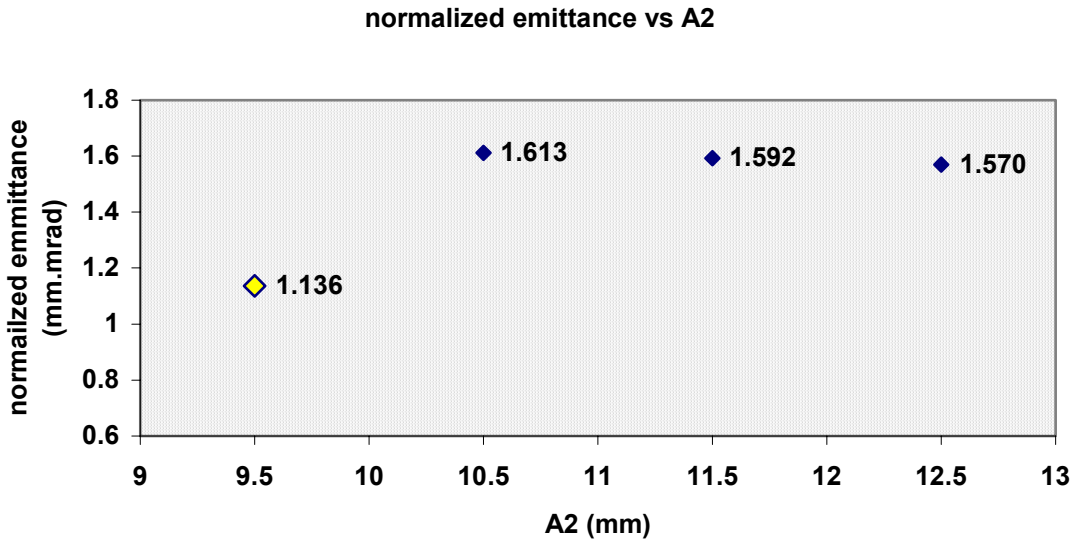

Figure 3.6 Plot of normalized beam emittance versus A2. With all other parameter values held constant at the nominal values shown in Table 3.1, the trend resulting from varying A2 only is that normalized emittance is lower for smaller values of A2.

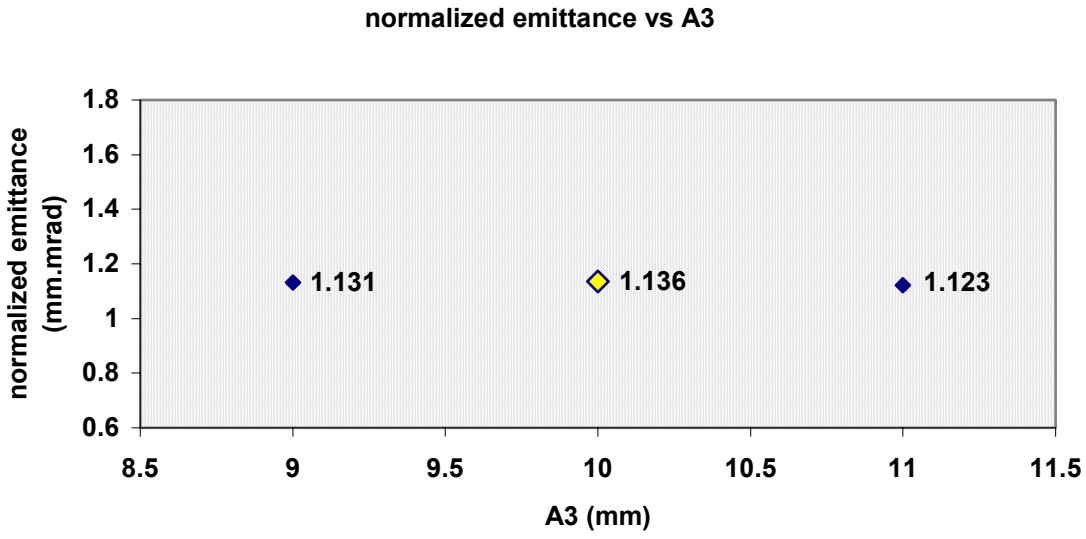

Figure 3.7 Plot of normalized beam emittance versus A3. The trend is flat, suggesting that the values of A3 tested in this study, with the remaining parameter values held at the nominal values shown in Table 3.1, did not have a significant effect on normalized emittance.

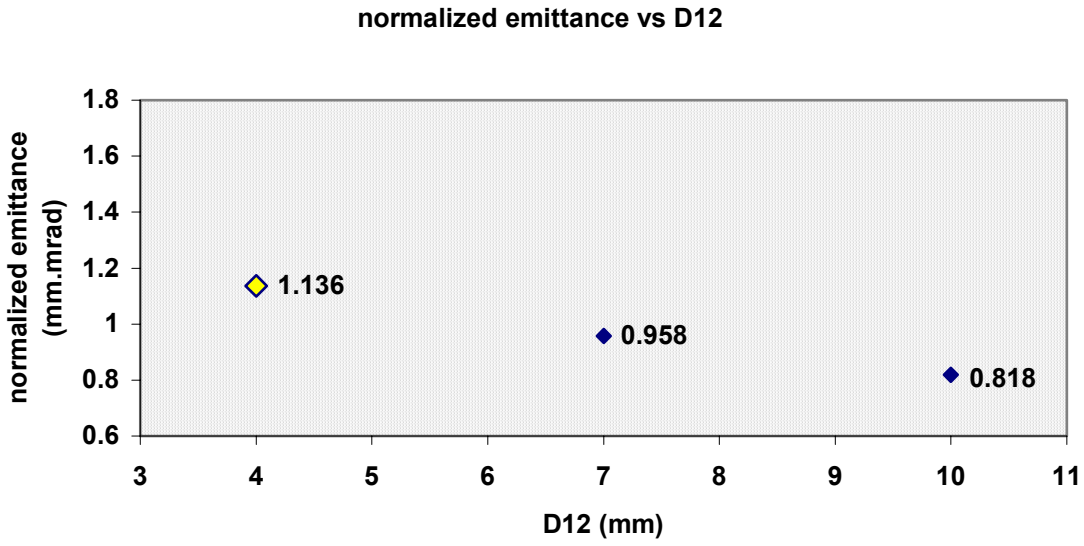

Figure 3.8 Plot of normalized beam emittance versus D12. The observable trend is that lower normalized emittance resulted when the value of D12 was increased, while the remaining parameter values were held constant at the nominal values shown in Table 3.1.

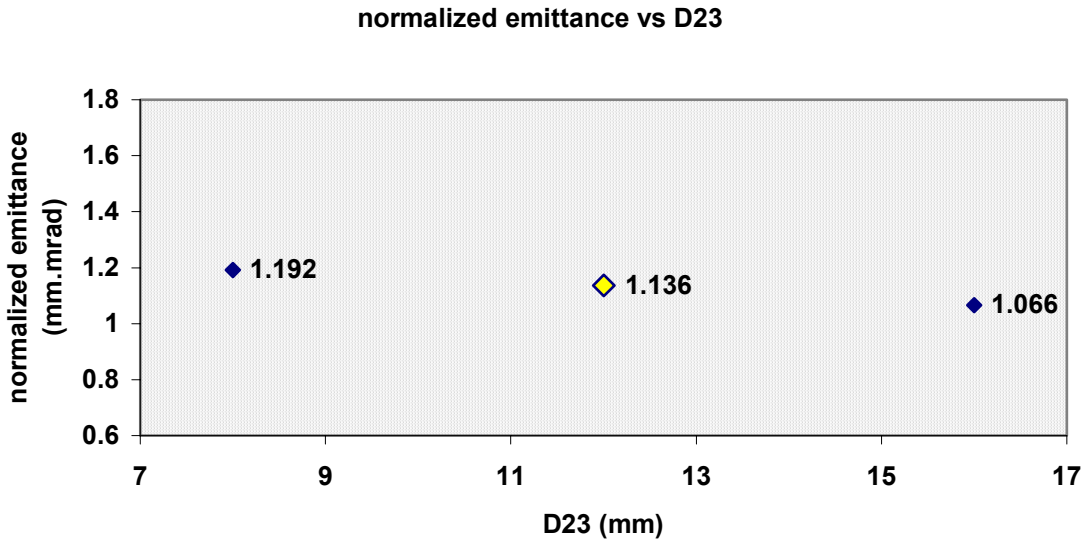

Figure 3.9 Plot of normalized beam emittance versus D23. Although the trend is slight, lower normalized emittance resulted when the value of D23 was increased, while the remaining parameter values were held constant at the nominal parameter values shown in Table 3.1.

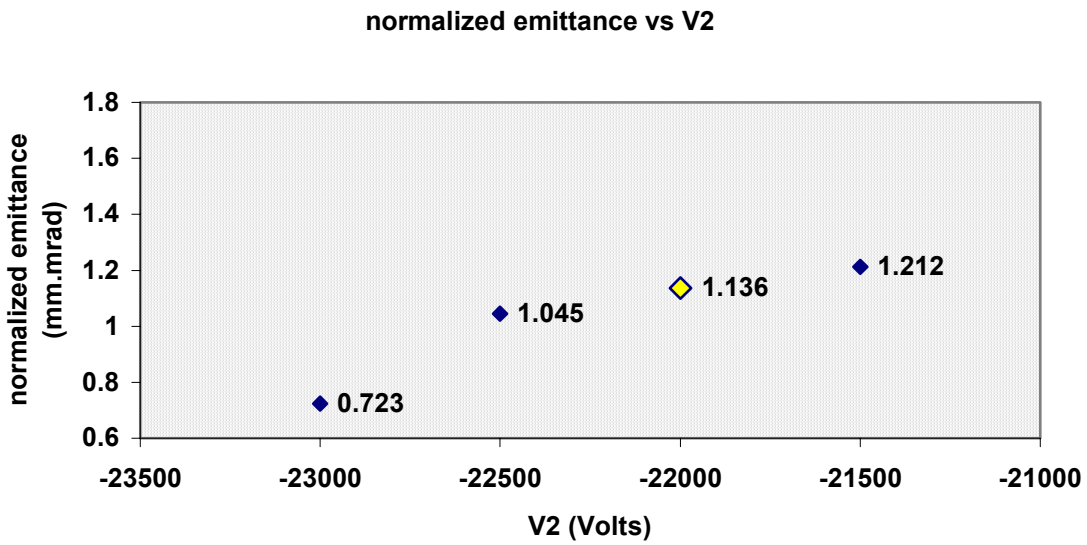

Figure 3.10 Plot of normalized beam emittance versus V2. With all other parameter values held constant at the nominal values shown in Table 3.1, the observable trend is that lower values of V2 resulted in lower normalized emittance values.

Varying test parameter V2 was the most effective way to achieve low normalized beam emittance. At its lowest test value, V2 = –23 kV, normalized beam emittance was reduced from its nominal value by over a third. Increasing D12 was the next most effective change from the nominal configuration to achieve low normalized emittance. Although less notably, increasing D23 also resulted in lowering normalized emittance. For the range of values of A2 tested, normalized emittance was lowest at the nominal value and increased as A2 was increased. Varying the value of A3 appeared to have no effect on normalized beam emittance at the beamstop.

The trends of the plots in Figure 3.6 to Figure 3.10 are summarized in Table 3.4. Listed in order of increasing normalized emittance, ε_N, the test number and lens configuration that resulted in the lowest normalized emittance in each of the above plots is listed in the table. The values of the parameters that resulted in the lowest emittance are highlighted. The nominal configuration, included for reference, is also the configuration that resulted in the lowest normalized emittance for the range of values of A2 tested.

Table 3.4 Summary of observed trends for the study of variations on the nominal configuration to achieve the lowest normalized beam emittance. Decreasing the value of V2 was the most effective change to the nominal configuration to achieve the lowest normalized emittance.

observed trend	ε_N (mm·mrad)	test #	V2 (V)	A2 (mm)	A3 (mm)	D12 (mm)	D23 (mm)
decrease V2	0.723	test 109	***-23000***	9.5	10	4	12
increase D12	0.818	test 7	-22000	9.5	10	***10***	12
increase D23	1.066	test 3	-22000	9.5	10	4	***16***
A3 flat	1.123	test 19	-22000	9.5	***11***	4	12
decrease A2 *(nominal)*	1.136	test 1	-22000	***9.5***	10	4	12

3.3 Percent of Beam Transmitted

The percentage of beam transmitted through the extraction lens system was measured for each of the test cases listed in Table 3.2. Percent of beam transmitted is plotted against the five variable test parameters in the following figures, Figure 3.11 to Figure 3.15. In each plot, the nominal data point is enlarged and highlighted. Gridlines are shown in these plots to alert the reader that the vertical axes do not have the same range in the following series of plots. The percentages are labelled at each data point. The terms beam current and percent of beam transmitted are used interchangeably herein.

Depending on the application of the extraction lens systems for H^- volume cusp ion sources, beam current may be required high or low. In either case, a brighter beam is optimal. Hence, for low current applications, high brightness is achieved by having a small emittance, while for high current applications, emittance may be compromised because the high beam current lends itself to higher beam brightness.

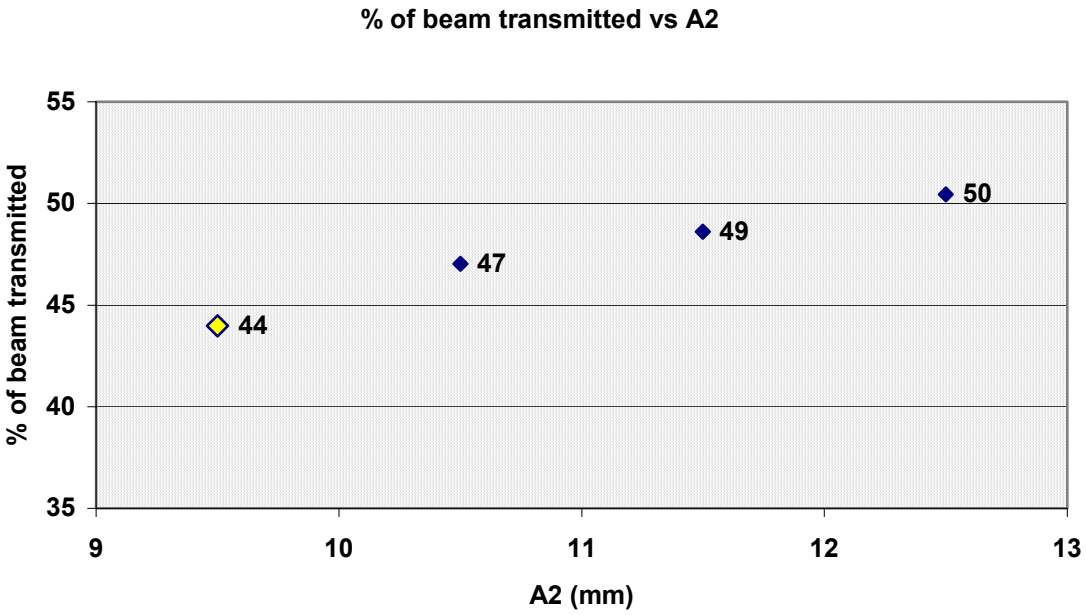

Figure 3.11 Plot of percent of beam transmitted versus A2. With the other parameter values fixed at the nominal values shown in Table 3.1, the observed trend is that increasing A2 resulted in increasing beam current.

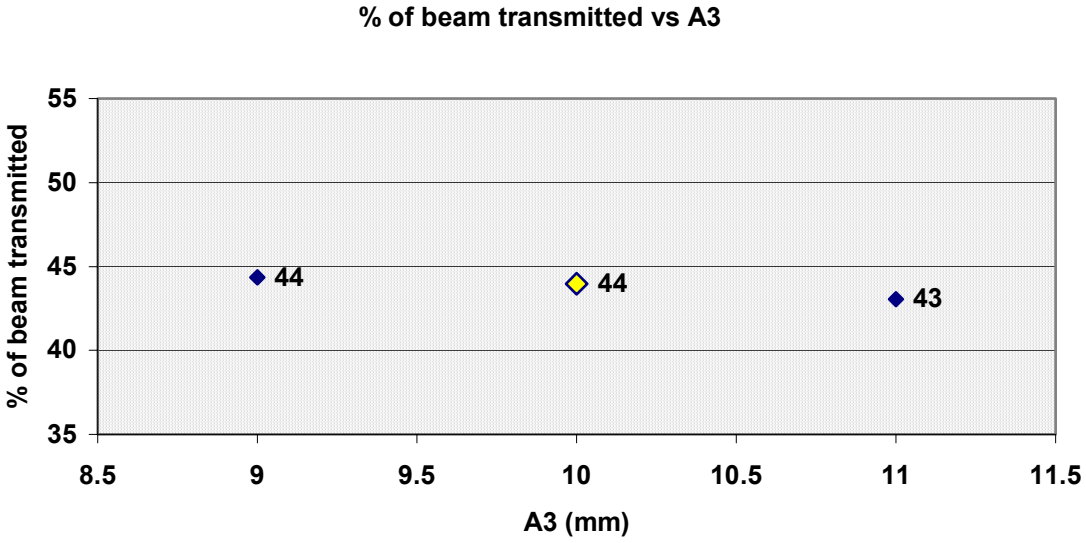

Figure 3.12 Plot of percent of beam transmitted versus A3. The trend is flat, suggesting that the values of A3 tested in this study, with the remaining parameter values held at the nominal values shown in Table 3.1, did not have a significant effect on beam current.

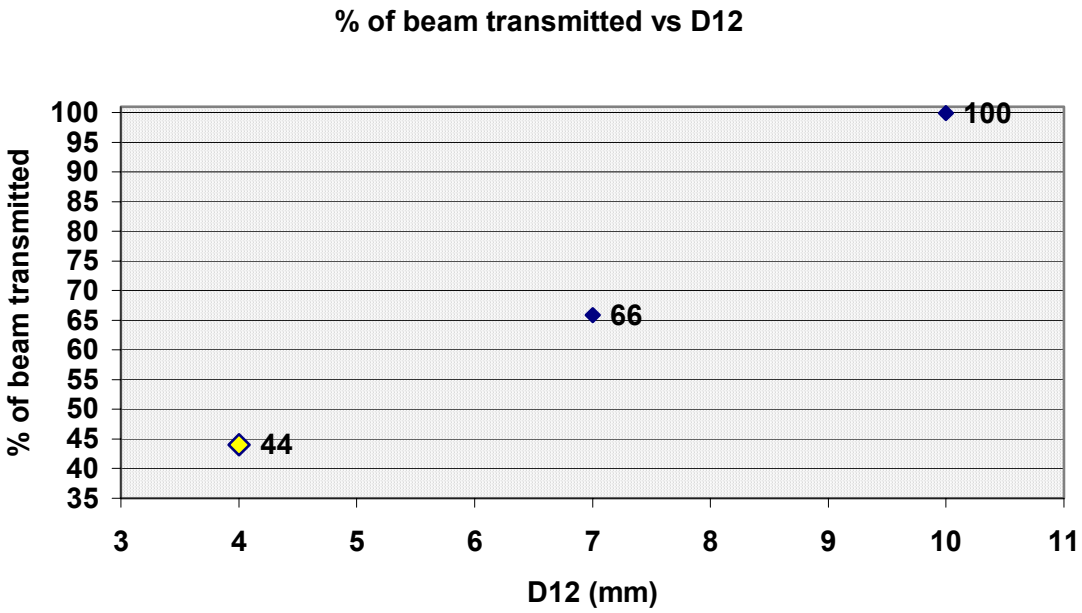

Figure 3.13 Plot of percent of beam transmitted versus D12. The observed trend clearly shows that beam current increased when D12 was increased from its nominal value, while the other test parameters remained constant at the nominal values shown in Table 3.1.

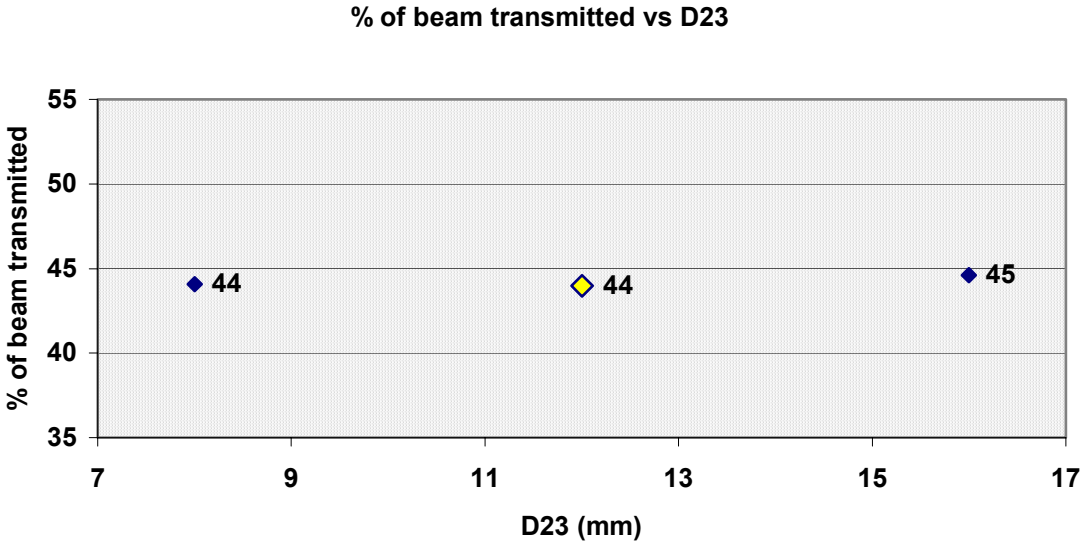

Figure 3.14 Plot of percent of beam transmitted versus D23. The trend is flat, suggesting that the values of D23 tested in this study, with the remaining parameter values held at the nominal values shown in Table 3.1, did not have a significant effect on beam current.

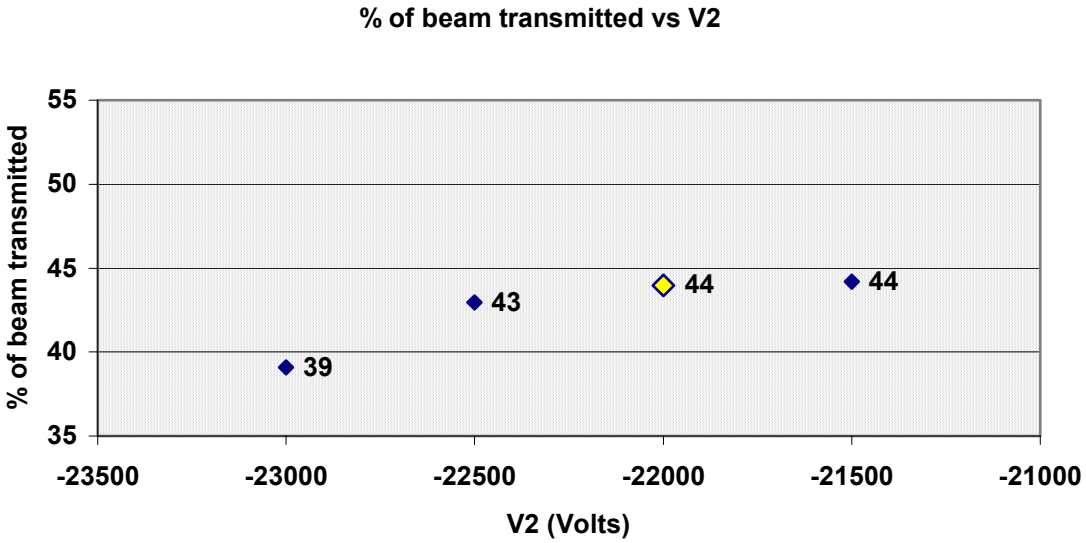

Figure 3.15 Plot of percent of beam transmitted versus V2. Although the trend is not very pronounced, beam current did increase when the value of V2 was increased and the remaining parameter values were held constant at the nominal values shown in Table 3.1.

The variable that affected beam transmission the most was D12. 100% beam transmission was measured for the largest value of D12 tested, with the other parameters held at the nominal values. Increasing the values of A2 and V2 also increased beam current, but to a much lesser extent than increasing D12.

The trends of the plots shown in Figure 3.11 to Figure 3.15 that resulted in the highest beam currents are listed in Table 3.5. Listed in order of decreasing percent of beam transmitted, the test number and lens configuration that resulted in the highest beam current in each of the above plots is listed in the table. The values of brightness corresponding to each test case in the table are also included, as these help to determine the usefulness of the high current beam. The values of the parameters that resulted in the highest percent of beam transmitted are highlighted. The nominal configuration is included in the last row for reference.

Table 3.5 Summary of observed trends for the study of variations on the nominal configuration to achieve the highest beam current. Increasing the value of D12 was the most effective change to the nominal configuration to achieve the highest beam current.

observed trend	% of beam transmitted	b $(mm \cdot mrad)^{-2}$	test #	V2 (V)	A2 (mm)	A3 (mm)	D12 (mm)	D23 (mm)
increase D12	100	1.493	test 7	-22000	9.5	10	***10***	12
increase A2	50	0.205	test 82	-22000	***12.5***	10	4	12
D23 flat	45	0.880	test 3	-22000	9.5	10	4	***16***
increase V2	44	0.301	test 325	***-21500***	9.5	10	4	12
A3 flat	44	0.346	test 10	-22000	9.5	***9***	4	12
nominal	44	0.341	test 1	-22000	9.5	10	4	12

While increasing the value of A2 resulted in increasing the beam current, the brightness decreased from the nominal value. Increasing D12 was the only useful change to the nominal lens configuration to achieve both high beam current and high brightness.

Table 3.6 is a listing of all of the test cases used to study variations on the nominal configuration that includes the values of brightness, normalized emittance, and percent of beam transmitted obtained for each test run. The table entries are listed in order of decreasing brightness to facilitate the comparison of beam brightness and beam current across the tested configurations. Again, the varied parameter value in each test configuration is highlighted.

Table 3.6 A summary of all of the test cases for the study of variations on the nominal system, including the values of brightness, normalized emittance, and percent of beam transmitted for each test. The table entries are listed in order of decreasing brightness.

test #	V2 (V)	A2 (mm)	A3 (mm)	D12 (mm)	D23 (mm)	b $(mm \cdot mrad)^{-2}$	ε_N (mm·mrad)	% of beam transmitted
test 7	-22000	9.5	10	***10***	12	1.493	0.818	100
test 3	-22000	9.5	10	4	***16***	0.880	1.066	45
test 109	***-23000***	9.5	10	4	12	0.748	0.723	39
test 4	-22000	9.5	10	***7***	12	0.717	0.958	66
test 217	***-22500***	9.5	10	4	12	0.393	1.045	43
test 10	-22000	9.5	***9***	4	12	0.346	1.131	44
test 1	-22000	9.5	10	4	12	0.341	1.136	44
test 19	-22000	9.5	***11***	4	12	0.341	1.123	43
test 2	-22000	9.5	10	4	***8***	0.310	1.192	44
test 325	***-21500***	9.5	10	4	12	0.301	1.212	44
test 82	-22000	***12.5***	10	4	12	0.205	1.570	50
test 55	-22000	***11.5***	10	4	12	0.192	1.592	49
test 28	-22000	***10.5***	10	4	12	0.181	1.613	47

The test configurations in the first four rows of Table 3.6 have distinctly higher brightness values than the remaining test configurations. Of these, tests 7 and 4, which correspond to increasing the value of D12, produced the highest beam currents, with 100% beam transmission obtained concurrently with the highest beam brightness and the second lowest normalized emittance (test 7, D12 = 10 mm). Tests 3 and 109, in the first four rows, have amongst the lowest beam currents while maintaining relatively high beam brightness and low normalized emittance. For some applications, the beam current obtained from the configuration of test 4 may be considered reasonably low (66% transmission) with relatively high beam brightness and low normalized emittance. Note

also that increasing A2 resulted in the three lowest observed brightness values and the three highest observed normalized emittance values (last three rows of Table 3.6).

3.4 Small Half Divergence and Half Width at the Beam Waist

Recall from section 1.2.2 that beam emittance is the product of half width and half divergence at the beam waist. As such, smaller half width and half divergence at the beam waist contribute to a lower beam emittance, which is considered to be a beam of higher quality. Four independent values of half width and half divergence were measured for each test run. From these, average values and measurement errors were calculated. The plots of half divergence and half width versus the five variable test parameter values are shown in Figure 3.16 to Figure 3.25. In each plot, the nominal data point is enlarged and highlighted. The values of half divergence and half width are labelled at each data point and the measurement errors are included as error bars.

The remainder of this page is intentionally left blank so that the plots of half divergence and half width versus each of the variable test parameters appear on the same page.

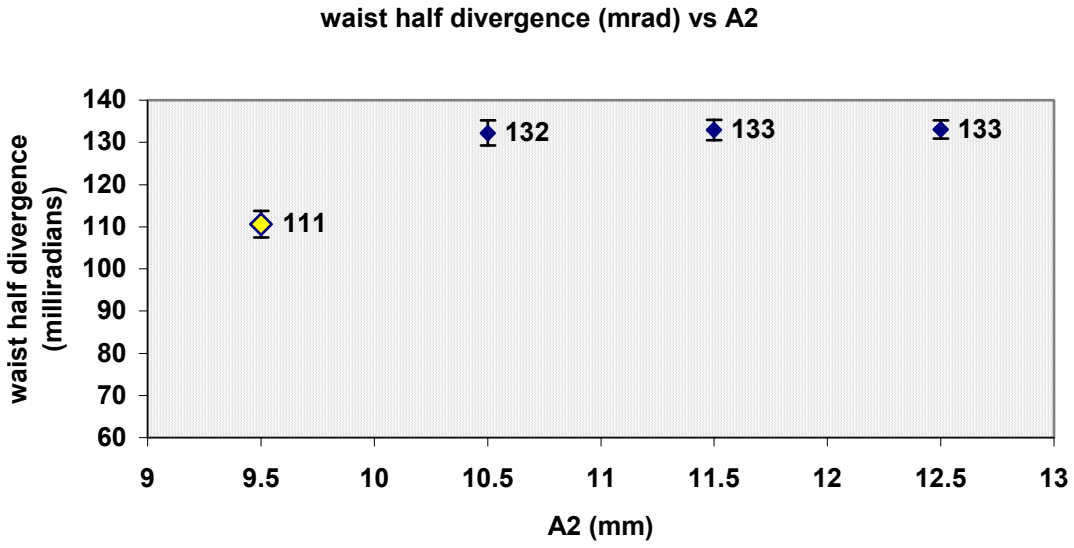

Figure 3.16 Plot of half divergence at the beam waist versus A2. With all other parameter values held constant at the nominal values shown in Table 3.1, the observed trend is that the half divergence at the waist decreased when the value of A2 was decreased.

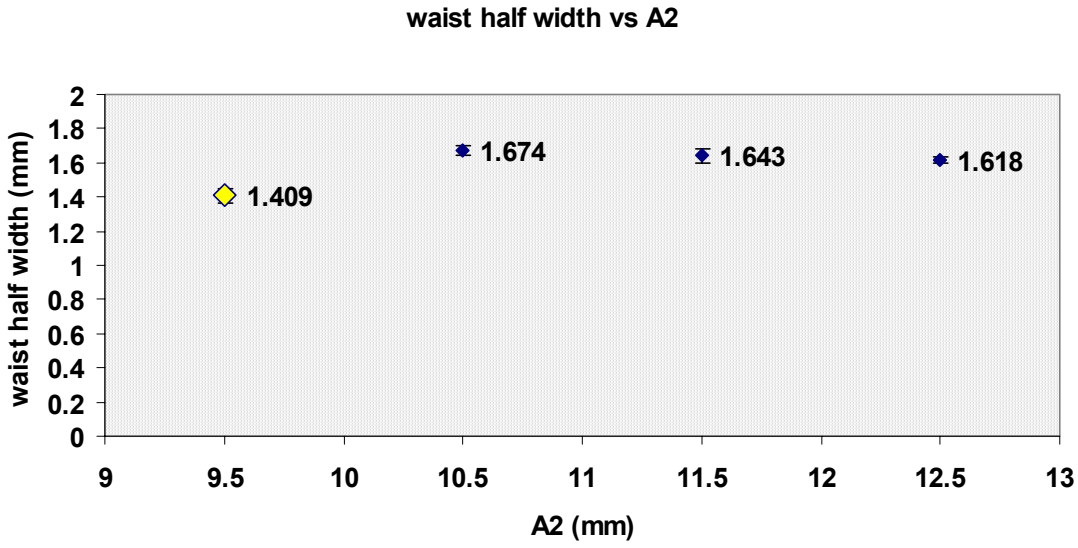

Figure 3.17 Plot of half width at the beam waist versus A2. With all other parameter values held constant at the nominal values shown in Table 3.1, the observed trend is vague, showing that the half width at the waist decreased when the value of A2 was decreased.

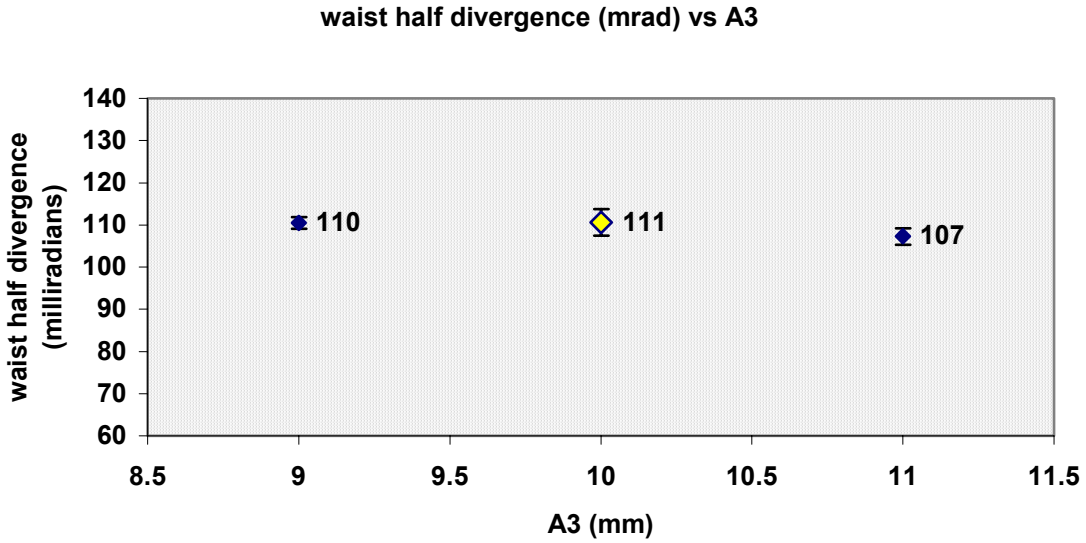

Figure 3.18 Plot of half divergence at the beam waist versus A3. The trend is flat, suggesting that the values of A3 tested in this study, with the remaining parameter values held at the nominal values shown in Table 3.1, did not have a significant effect on the half divergence of the beam waist.

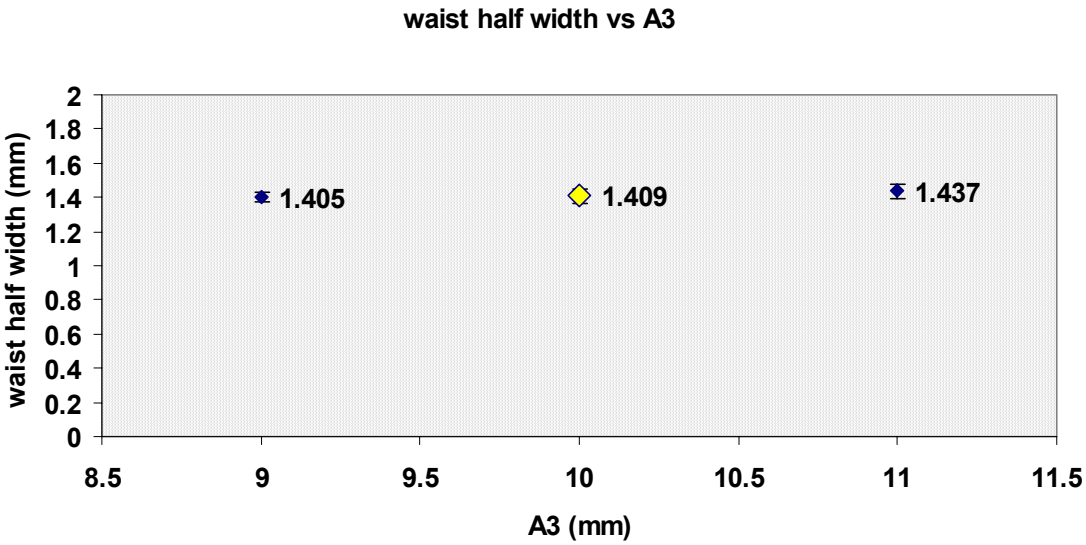

Figure 3.19 Plot of half width at the beam waist versus A3. The trend is flat, suggesting that the values of A3 tested in this study, with the remaining parameter values held at the nominal values shown in Table 3.1, did not have a significant effect on the half width of the beam waist.

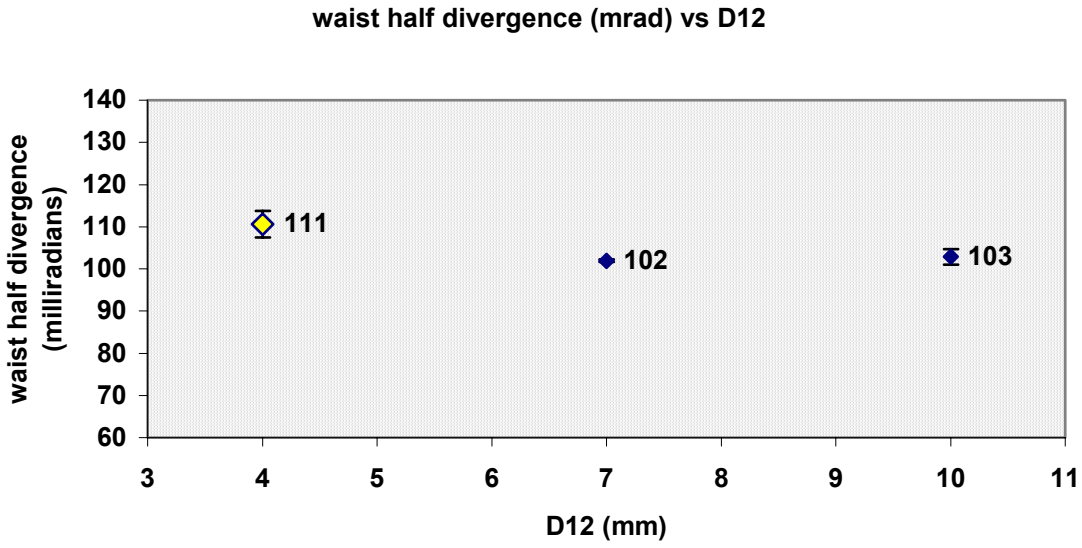

Figure 3.20 Plot of half divergence at the beam waist versus D12. The observed trend is that the half divergence of the beam waist decreased when the value of D12 was increased, while the remaining parameter values were held constant at the nominal values shown in Table 3.1.

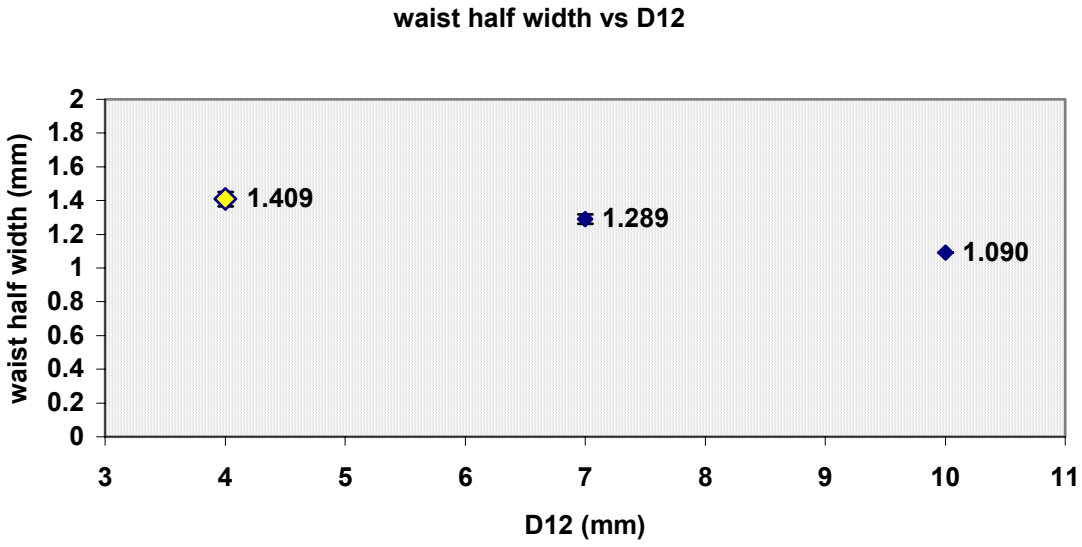

Figure 3.21 Plot of half width at the beam waist versus D12. The observed trend is that the half width of the beam waist decreased when the value of D12 was increased, while all other parameter values were held constant at the nominal values shown in Table 3.1.

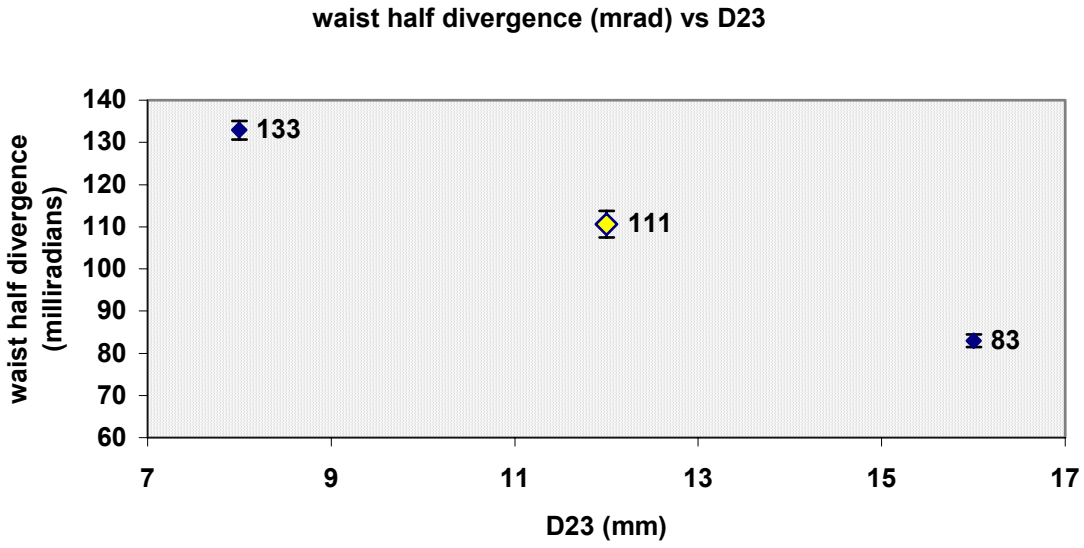

Figure 3.22 Plot of half divergence at the beam waist versus D23. The observed trend is that the half divergence of the beam waist decreased when the value of D23 was increased, while the remaining parameter values were held constant at the nominal values shown in Table 3.1.

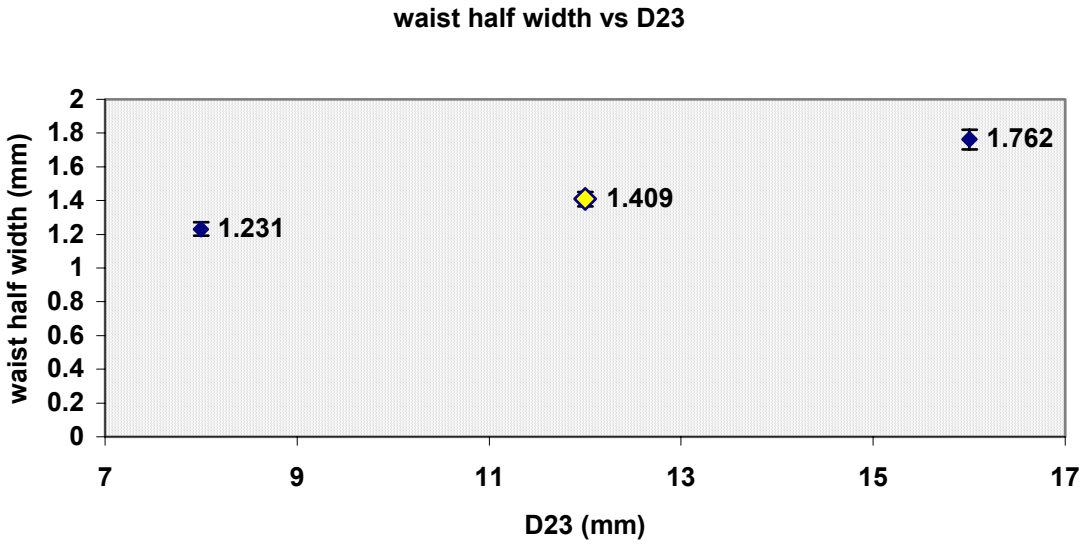

Figure 3.23 Plot of half width at the beam waist versus D23. The observed trend is that the half width of the beam waist decreased when the value of D23 was decreased, while all other parameter values were held constant at the nominal values shown in Table 3.1.

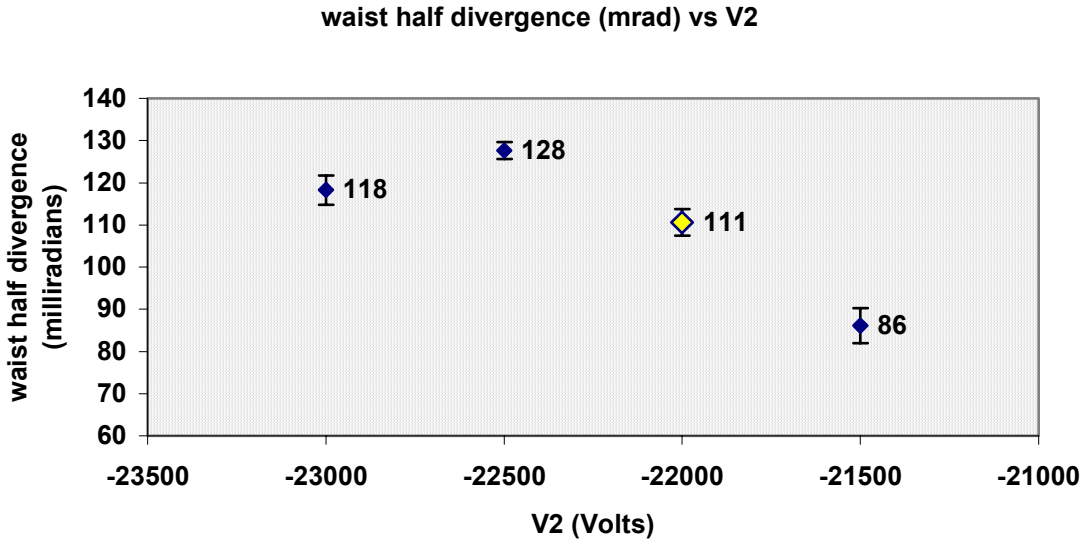

Figure 3.24 Plot of half divergence at the beam waist versus V2. The general trend observed is that the half divergence of the beam waist decreased when the value of V2 was increased, while the remaining parameter values were held constant at the nominal values shown in Table 3.1.

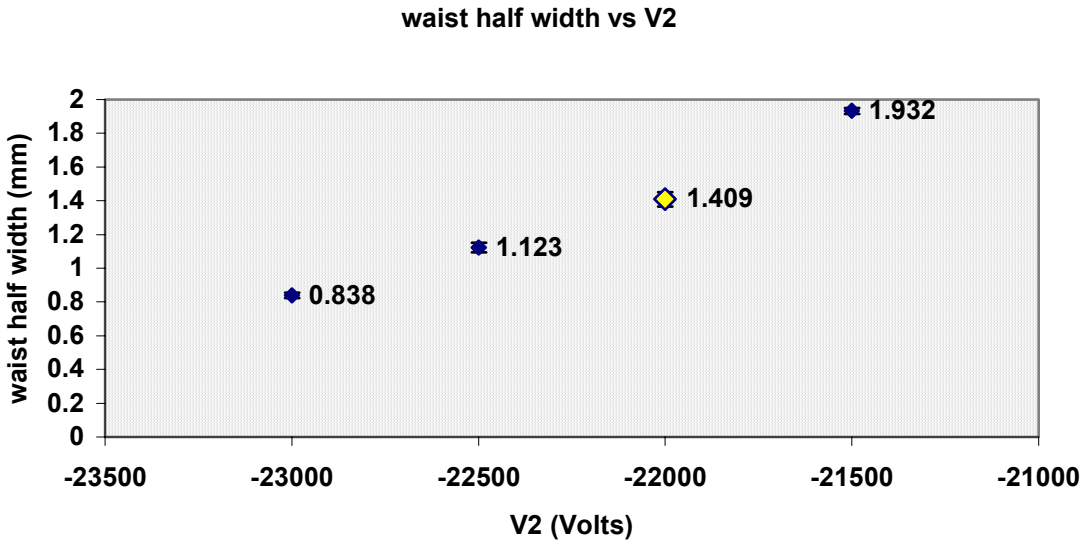

Figure 3.25 Plot of half width at the beam waist versus V2. The observed trend is that the half width of the beam waist decreased when the value of V2 was decreased, while all other parameter values were held constant at the nominal values shown in Table 3.1.

Arranged in order of increasing normalized emittance, Table 3.7 includes the values of half divergence (x') and half width (x) at the beam waist for all of the test cases used to study variations on the nominal configuration. The varied parameter value for each test configuration is highlighted. The values of beam brightness and percent of beam transmitted are included for the curious reader.

Table 3.7 A summary of all of the test cases for the study of variations on the nominal system, including the values of brightness, normalized emittance, and percent of beam transmitted for each test. The table entries are listed in order of decreasing brightness.

test #	V2 (V)	A2 (mm)	A3 (mm)	D12 (mm)	D23 (mm)	ε_N (mm·mrad)	x' (mrad)	x (mm)	b $(mm \cdot mrad)^{-2}$	% beam trans'd
test 109	***-23000***	9.5	10	4	12	0.723	118	0.838	0.748	39
test 7	-22000	9.5	10	***10***	12	0.818	103	1.090	1.493	100
test 4	-22000	9.5	10	***7***	12	0.958	102	1.289	0.717	66
test 217	***-22500***	9.5	10	4	12	1.045	128	1.123	0.393	43
test 3	-22000	9.5	10	4	***16***	1.066	83	1.762	0.880	45
test 19	-22000	9.5	***11***	4	12	1.123	107	1.437	0.341	43
test 10	-22000	9.5	***9***	4	12	1.131	110	1.405	0.346	44
test 1	-22000	9.5	10	4	12	1.136	111	1.409	0.341	44
test 2	-22000	9.5	10	4	***8***	1.192	133	1.231	0.310	44
test 325	***-21500***	9.5	10	4	12	1.212	86	1.932	0.301	44
test 82	-22000	***12.5***	10	4	12	1.570	133	1.618	0.205	50
test 55	-22000	***11.5***	10	4	12	1.592	133	1.643	0.192	49
test 28	-22000	***10.5***	10	4	12	1.613	132	1.674	0.181	47

Considering briefly the first four rows in Table 3.7, the values of x' that resulted in the four lowest normalized emittance values fall in the middle of the measured range of half divergence values. The corresponding values of x are amongst the lowest in the measured range of half width values. Reassuringly, the values of x' and x that give rise to the undesirable highest normalized emittance values are amongst the highest in their respective ranges of measured values.

3.5 Beam Waist Position Farthest Downstream from E3

The waist position is important in determining beam size at the next optical element. The beam size must be known in order to capture all the beam with the next lens. Waist position farthest downstream (i.e., closest to the beamstop) is typically favoured because the spot size will remain relatively small as the ions drift to the beamstop, undergoing less divergence over the shorter length of drift space.

Four independent values of waist position were measured for each of the test configurations listed in Table 3.2. From these, average values and measurement errors were calculated. The average waist positions are plotted against the five variable test parameters in the following figures, Figure 3.26 to Figure 3.30, including error bars to show the calculated measurement error for each data point. In each plot, the nominal data point is enlarged and highlighted. The positions, measured relative to the beamstop (i.e., from the beamstop back towards the origin), are labelled at each data point.

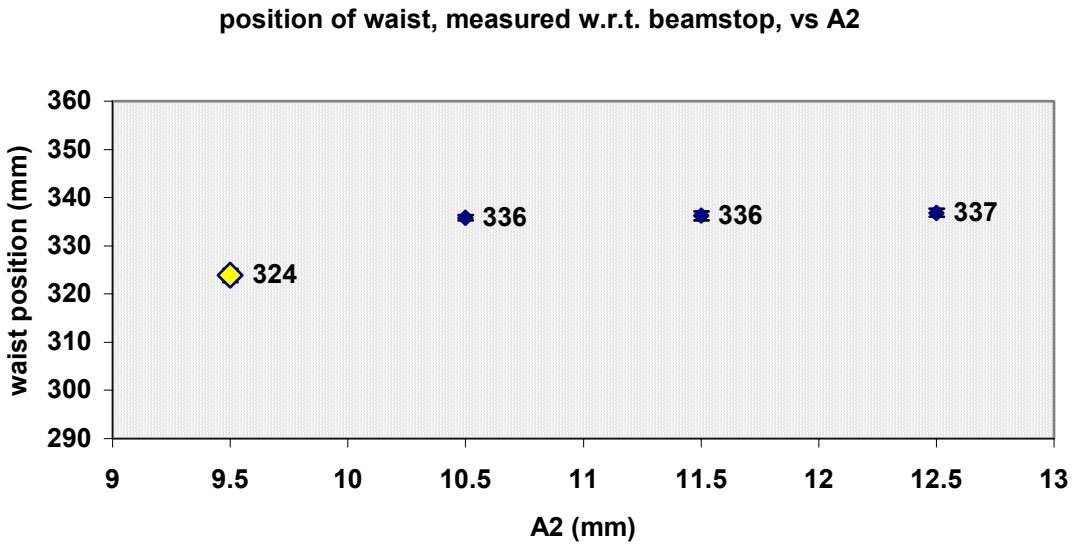

Figure 3.26 Plot of waist position versus A2. With all other parameters held constant at the nominal values shown in Table 3.1, the observed trend is that the waist position moved farther downstream as A2 was decreased.

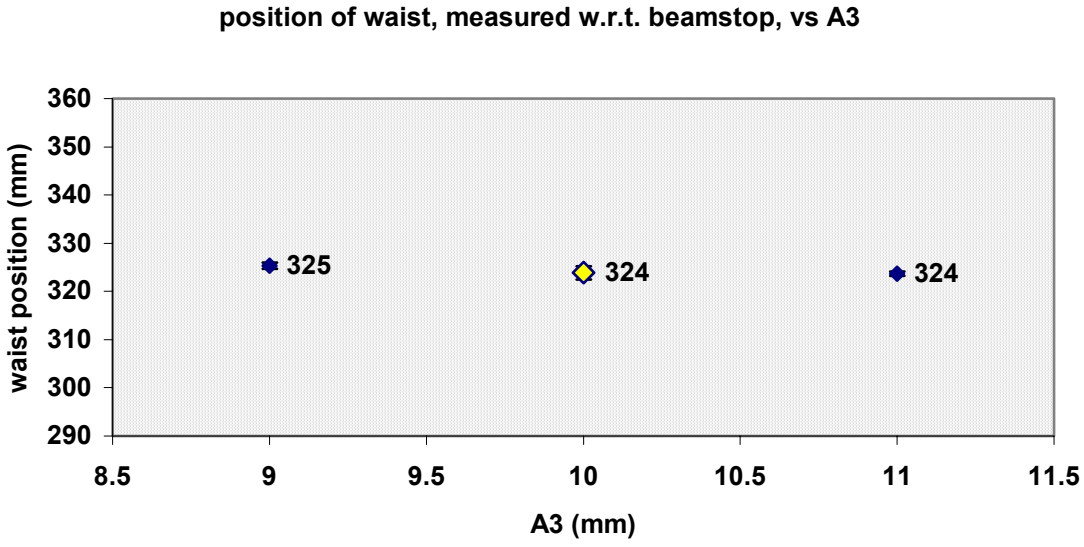

Figure 3.27 Plot of waist position versus A3. This flat trend suggests that for the values of A3 tested, and with the remaining parameter values held constant at the nominal values shown in Table 3.1, A3 had little effect on the waist position.

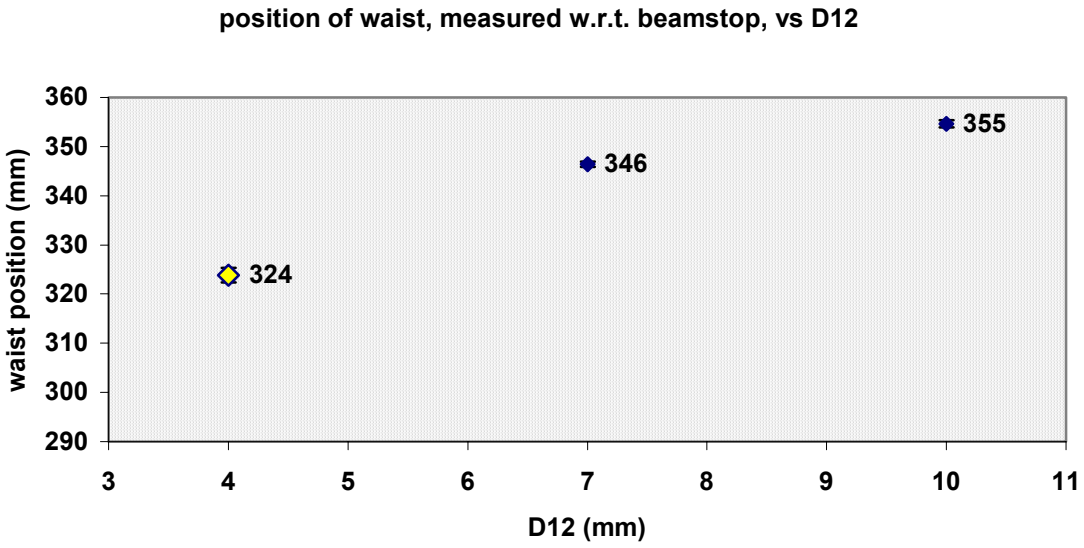

Figure 3.28 Plot of waist position versus D12. The observed trend is that, while holding all other parameters constant at the nominal values shown in Table 3.1, decreasing the value of D12 resulted in moving the waist farther downstream.

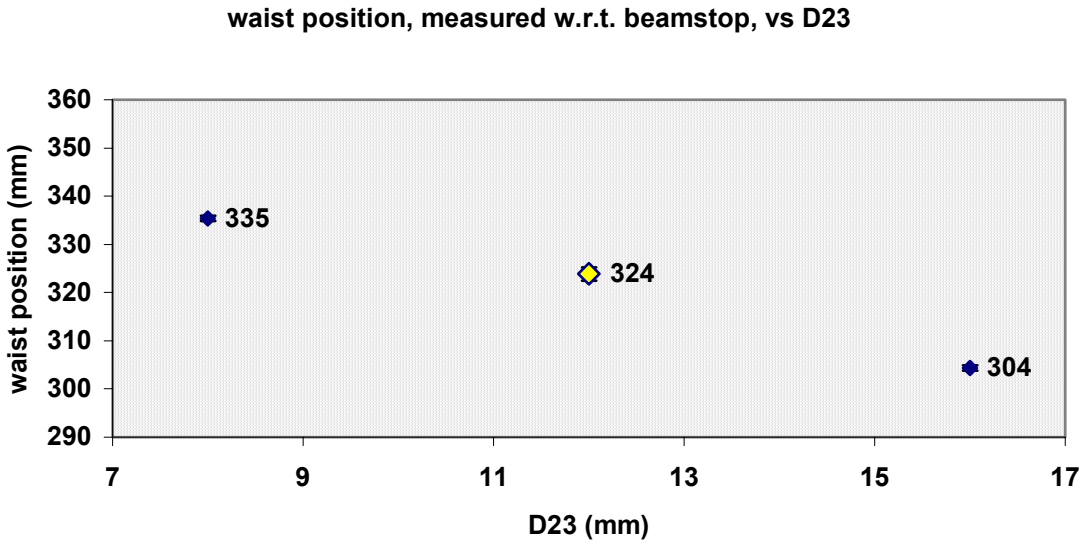

Figure 3.29 Plot of waist position versus D23. The observed trend is that the waist position was moved farther downstream when the value of D23 was increased, while all other parameters were held constant at the nominal values listed in Table 3.1.

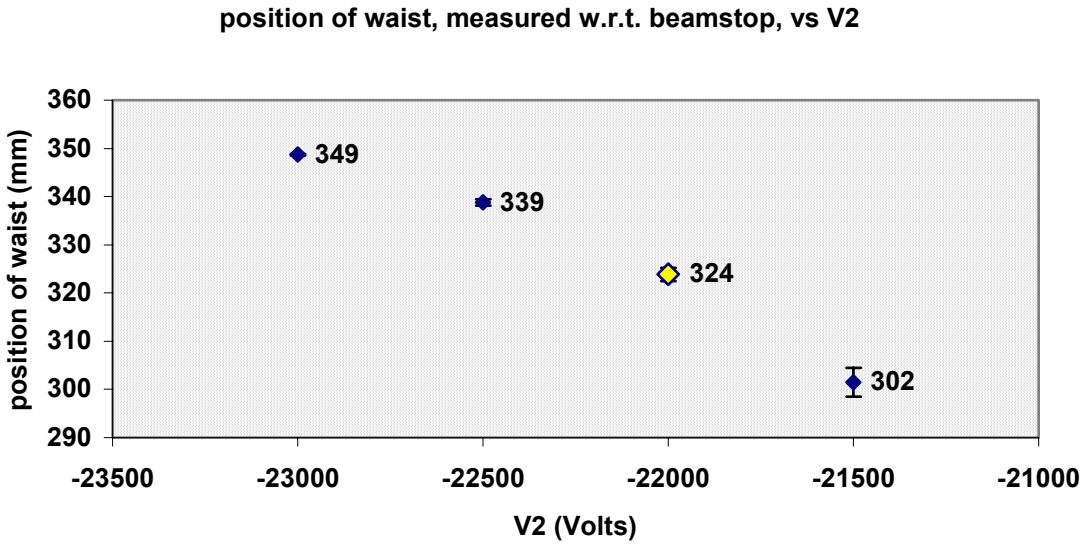

Figure 3.30 Plot of waist position versus V2. The observed trend is that the waist was moved farther downstream as the value of V2 was increased, with the remaining parameters held constant at the nominal values shown in Table 3.1.

The variable that affected position of the beam waist the most was V2. Increasing the value of V2 while the other parameter values were held constant resulted in decreasing the distance between the beam waist and the beamstop. The next most effective change of variable was to increase the value of D23 to move the beam waist farther downstream. A trend in the opposite direction was observed for increasing the value of D12: this change resulted in moving the waist position farther from the beamstop.

The trends of the plots shown in Figure 3.26 to Figure 3.30 that resulted in waist positions closest to the beamstop are listed in Table 3.8. Listed in order of increasing waist position, the test number and lens configuration that resulted in the beam waist closest to the beamstop in each of the above plots is listed in the table. The values of the tested parameters that resulted in the farthest downstream position of the beam waist are highlighted. The nominal configuration, included for reference, is also the configuration that resulted in the farthest downstream waist position for the ranges of D12 and A2 values tested.

Table 3.8 Summary of observed trends for the study of variations on the nominal configuration to achieve the farthest downstream waist positions. Increasing the value of V2 was the most effective change to the nominal configuration to achieve the farthest downstream waist position.

observed trend	waist position (mm)	test #	V2 (V)	A2 (mm)	A3 (mm)	D12 (mm)	D23 (mm)
increase V2	302	test 325	***-21500***	9.5	10	4	12
increase D23	304	test 3	-22000	9.5	10	4	***16***
decrease D12 *(nominal)*	324	test 1	-22000	9.5	10	4	12
decrease A2 *(nominal)*	324	test 1	-22000	9.5	10	4	12
A3 flat	324	test 19	-22000	9.5	***11***	4	12

For a waist that is not positioned nearest to the beamstop, the beam may still be readily useful, provided it has a small emittance. The emittance values of each test configuration are included in Table 3.9 to associate normalized emittance values (related to beam size) with the position of the waist for each of the tested lens configurations. The varied parameter in each test configuration is highlighted.

Table 3.9 List of all of the tested configurations for the study of variations on the nominal configuration, in order of increasing normalized emittance. There is no obvious trend relating the measured positions of beam waist to the calculated normalized emittance values.

test #	V2 (V)	A2 (mm)	A3 (mm)	D12 (mm)	D23 (mm)	ε_N (mm·mrad)	waist position (mm)
test 109	***-23000***	9.5	10	4	12	0.723	349
test 7	-22000	9.5	10	***10***	12	0.818	355
test 4	-22000	9.5	10	***7***	12	0.958	346
test 217	***-22500***	9.5	10	4	12	1.045	339
test 3	-22000	9.5	10	4	***16***	1.066	304
test 19	-22000	9.5	***11***	4	12	1.123	324
test 10	-22000	9.5	***9***	4	12	1.131	325
test 1	-22000	9.5	10	4	12	1.136	324
test 2	-22000	9.5	10	4	***8***	1.192	335
test 325	***-21500***	9.5	10	4	12	1.212	302
test 82	-22000	***12.5***	10	4	12	1.570	337
test 55	-22000	***11.5***	10	4	12	1.592	336
test 28	-22000	***10.5***	10	4	12	1.613	336

Note that the four lowest emittance values (first four rows of Table 3.9) occurred when the measured separations between beam waist and beamstop were greatest. Increasing the value of D12 and decreasing the value of V2 constitutes these top four test configurations.

3.6 Average Kinetic Energy of the H^- Ions at the Beamstop

The average kinetic energy of the H^- ions at the beamstop upon emerging from the nominal system was 24913 eV. Prior to doing this study, it had been assumed that the energy of the particles was 25000 eV upon reaching the beamstop in the actual extraction lens system. Downstream devices, such as the inflector, have been designed based on this assumption. If the ions had been accelerated away from a disk of uniform -25 kV voltage potential, then upon reaching the 0 V target, the system would have imparted 25 keV of energy to the H^- ions. But the ions are extracted from a plasma through the aperture of the plasma lens. The plasma electrode can be represented by a donut whose voltage potential is –25 kV, but the potential at the centre of the donut is slightly more positive than –25 kV. Rather than being parallel to the plasma lens' transversal surface, the electric field intensity planes are slightly bowed downstream from the lens. Thus, the ions nearer to the axial centre of the beam acquire less energy than 25 keV because they can only acquire an energy corresponding to the total potential change from the source to the beamstop. Having observed that the ions have less energy than the assumed 25 keV will allow DCL to adjust the power supplies controlling V1 and V3 such that the beam is coupled into downstream devices more efficiently.

Table 3.10 is a list of all of the test configurations for the study of variations on the nominal system, listed in order of decreasing average kinetic energy, measured at the beamstop. The varied parameter value in each test configuration is highlighted. While increasing the separation between the first and second electrodes (increasing the value of D12) resulted in the highest measured kinetic energies, the most significant trend observed here is the increase in average kinetic energy of the ions at the beamstop as V2 was decreased. In the region between E2 and E3, where the potential difference is greatest, the ions are most significantly accelerated. By decreasing the value of V2, the voltage potential between the second and third electrodes increased, resulting in a stronger electric field, and thus, a stronger accelerating force acting on the ions. As a result, more energy was imparted to the ions over the distance they were accelerated.

Table 3.10 Average kinetic energies of the H^- ions at the beamstop. A list of all of the test cases for the study of variations on the nominal system, ordered from highest to lowest average kinetic energy.

test #	V2 (V)	A2 (mm)	A3 (mm)	D12 (mm)	D23 (mm)	KE (eV)
test 7	-22000	9.5	10	***10***	12	24973
test 4	-22000	9.5	10	***7***	12	24952
test 109	***-23000***	9.5	10	4	12	24942
test 82	-22000	***12.5***	10	4	12	24928
test 217	***-22500***	9.5	10	4	12	24928
test 55	-22000	***11.5***	10	4	12	24923
test 28	-22000	***10.5***	10	4	12	24918
test 1	-22000	9.5	10	4	12	24913
test 2	-22000	9.5	10	4	***8***	24913
test 3	-22000	9.5	10	4	***16***	24913
test 10	-22000	9.5	***9***	4	12	24913
test 19	-22000	9.5	***11***	4	12	24913
test 325	***-21500***	9.5	10	4	12	24898

3.6.1 Summary of Trends for Variations on the Nominal System

As a summary of the observed trends and the data presented in this chapter, Table 3.11 is a list of all of the tested lens configurations used to study variations on the nominal lens configuration. Test 1, the nominal lens configuration, is shaded in the table. The table entries are in order of highest quality beam to lowest quality beam, based on the calculated beam brightness values. A comparison of the calculated beam brightness, *b*,

and normalized emittance, ε_N, values indicates that the lens configurations that resulted in the brightest beam were also those that resulted in the lowest normalized beam emittance, both equivalent measures of high beam quality. Similarly, the lowest quality beams had both the lowest brightness values and the highest normalized emittance values. The lowest quality beams resulted when the aperture of the extraction electrode, A2, was made larger.

From Table 3.11, the trends resulting from varying a single parameter through its range of test values can be observed by scanning down the column headed by each parameter ID tag. The trends are as follows: decreasing V2, decreasing A2, increasing D12, and increasing D23 independently resulted in increasing beam quality. For the range of values of A3 tested in this study, and with the remaining parameters held constant at the nominal values, varying A3 had no effect on beam quality.

Table 3.11 Summary of the data for the study of variations on the nominal lens configuration. The table entries are listed in order of decreasing beam quality, based on beam brightness. A scan of the boldfaced and italicized parameter values in the second to sixth columns reveals the trends observed from varying a single test parameter value while the other parameter values were held constant at the nominal values.

test #	V2 (V)	A2 (mm)	A3 (mm)	D12 (mm)	D23 (mm)	b $(mm \cdot mrad)^{-2}$	ε_N (mm·mrad)	% of beam transmitted	x' (mrad)	x (mm)	waist position (mm)	KE (eV)
test 7	-22000	9.5	10	***10***	12	1.493	0.818	100	103	1.090	355	24973
test 3	-22000	9.5	10	4	***16***	0.880	1.066	45	83	1.762	304	24913
test 109	***-23000***	9.5	10	4	12	0.748	0.723	39	118	0.838	349	24942
test 4	-22000	9.5	10	***7***	12	0.717	0.958	66	102	1.289	346	24952
test 217	***-22500***	9.5	10	4	12	0.393	1.045	43	128	1.123	339	24928
test 10	-22000	9.5	***9***	4	12	0.346	1.131	44	110	1.405	325	24913
test 1	-22000	9.5	10	4	12	0.341	1.136	44	111	1.409	324	24913
test 19	-22000	9.5	***11***	4	12	0.341	1.123	43	107	1.437	324	24913
test 2	-22000	9.5	10	4	***8***	0.310	1.192	44	133	1.231	335	24913
test 325	***-21500***	9.5	10	4	12	0.301	1.212	44	86	1.932	302	24898
test 82	-22000	***12.5***	10	4	12	0.205	1.570	50	133	1.618	337	24928
test 55	-22000	***11.5***	10	4	12	0.192	1.592	49	133	1.643	336	24923
test 28	-22000	***10.5***	10	4	12	0.181	1.613	47	132	1.674	336	24918

To further summarize the findings, high current applications would benefit from increasing the spacing between the first and second lenses (increasing D12), and low current applications would benefit from decreasing the voltage potential of the second lens (decreasing V2) or increasing the spacing between the second and third lenses (increasing D23). V2 is the most practical parameter value to adjust as it does not require mechanical disassembly of the system nor does it require manufacturing new components, as would the adjustment of any of the four other test parameters. A change in the aperture size of the second electrode (avoid increasing A2) should be avoided because this resulted in the lowest observed brightness values and the highest observed normalized emittance values. The large normalized emittance values were a result of having both the largest half widths and half divergences when the value of A2 was increased. These conclusions are, of course, based on variations around the nominal configuration resulting from the change of a single test parameter and the trends reported do not account for parameter values outside the tested ranges.

Chapter 4

Global Trends

While reading about the trends observed in studying the model extraction lens system, it is important to remember that the observed trends are limited to the range of values tested in this study. Outside of these ranges, the trends may differ. The values through which the five variable design parameters, V2, A2, A3, D12, and D23, were varied are listed in Table 3.1. The parameter values of the four hundred thirty two test configurations are listed in Appendix B. Seven characteristic measurements of the beam were made following each test run:

1) position of waist,
2) half width at waist,
3) half divergence at waist,
4) average kinetic energy of ions at beamstop,
5) normalized beam emittance,
6) percent of beam transmitted, and
7) beam brightness.

Average kinetic energy of the ions could have equivalently been measured at the waist, as the value did not change as the particles drifted from the waist position to the beamstop. However, it was more practical to measure the average kinetic energy at the beamstop, utilizing SIMION's data recording capabilities for predetermined event triggers. The

measured parameter values of all of the tests were graphically analysed, and any observed trends were explored to determine their cause. Of the seven measured beam characteristics, three were deemed most important in determining quality of beam: brightness, normalized emittance, and percent transmission.

In accelerator physics, a high quality beam is one with high brightness and low emittance. But when beam quality is subject to a given application, beam brightness, normalized emittance, and percent of beam transmitted are the key measurements that assess the usefulness of the beam. Beam brightness is the subject of section 4.1, where brightness is plotted against each of the five design parameters. The effects of each parameter on brightness are individually assessed. Sections 4.2 and 4.3 follow a format similar to that of section 4.1, with normalized beam emittance as the subject of section 4.2 and percent of beam transmitted as the subject of section 4.3. Section 4.4 reveals the correlations between the three key measurements, namely brightness, normalized emittance, and percent transmission. Trends in test parameter values are highlighted to provide insight to how the best beam is chosen, depending on the intended application. What to avoid is also pointed out. Section 4.5 presents the trends observed regarding how the position of waist changed as a result of varying the test parameters. Representative ion trajectories of the best and worst lens configurations are shown in a series of figures in section 4.6.

In the following series of plots, all of the collected data points are included. In a manner similar to the way in which the plots were presented in Chapter 3, each figure is a plot of a test parameter (e.g., V2, A2, etc) versus a beam characteristic (e.g., brightness, normalized emittance, etc). To produce each plot, the data (see Appendix B, Appendix C. and Appendix D for a complete listing of all of the data) was organized in order of increasing test parameter value and plotted against a given beam characteristic. Although the plots are admittedly overloaded with information, their intended purpose is to see if there are observable trends suggesting how each test parameter affects a given beam characteristic in a global manner. In some instances, patterns in the plotted data suggested that certain combinations of test parameter values affected a given beam characteristic. The results of this analysis provide insight for the engineer to design a lens configuration suited to a particular application.

4.1 Beam Brightness

The following subsections contain figures of each of the test parameters plotted against beam brightness. In each plot, the minimum and maximum values of brightness are labelled, as is the nominal test configuration.

4.1.1 V2 versus Beam Brightness

Figure 4.1 is a plot of V2 versus brightness, with brightness increasing from left to right.

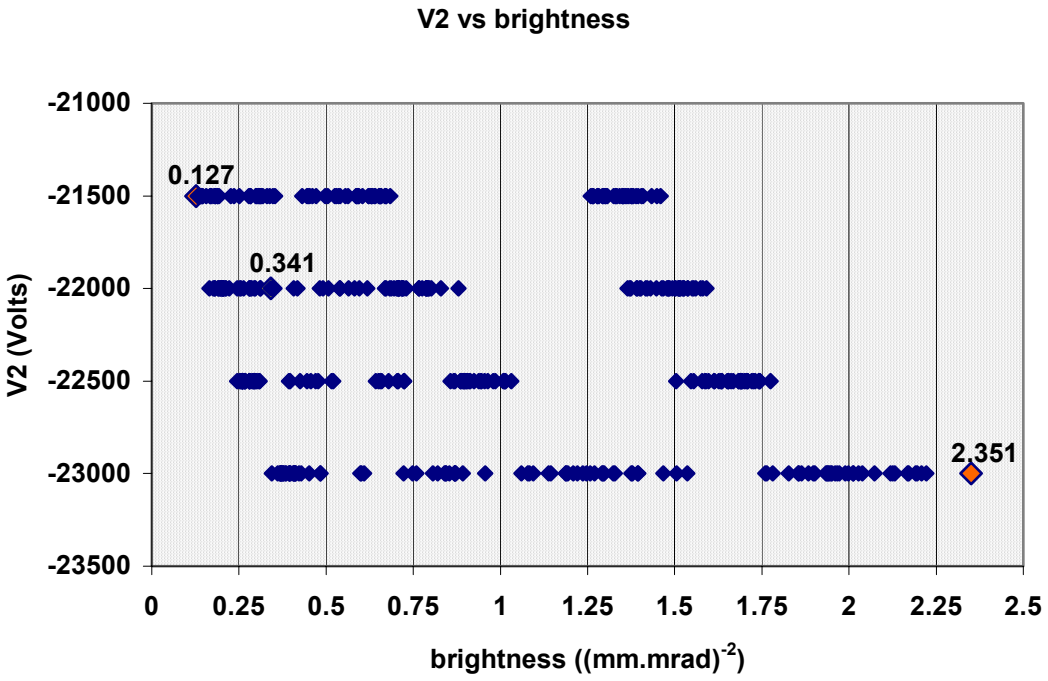

Figure 4.1 Plot of V2 versus beam brightness. The general trend suggested by this plot is that brightness increased as the value of V2 was decreased.

The distinct separation of data points on the right hand side of the plot in Figure 4.1 suggests that another trend exists, arising from a factor other than the value of V2. While the rightmost data points, for brightness greater than about 1.8 $(mm \cdot mrad)^{-2}$, occurred when V2 = -23 kV, the low values of brightness that also occurred when V2 = -23 kV suggest that it is not sufficient to decrease the value of V2 to obtain a brighter beam.

4.1.2 A2 versus Beam Brightness

Figure 4.2 is a plot of A2 versus brightness, with brightness increasing from left to right.

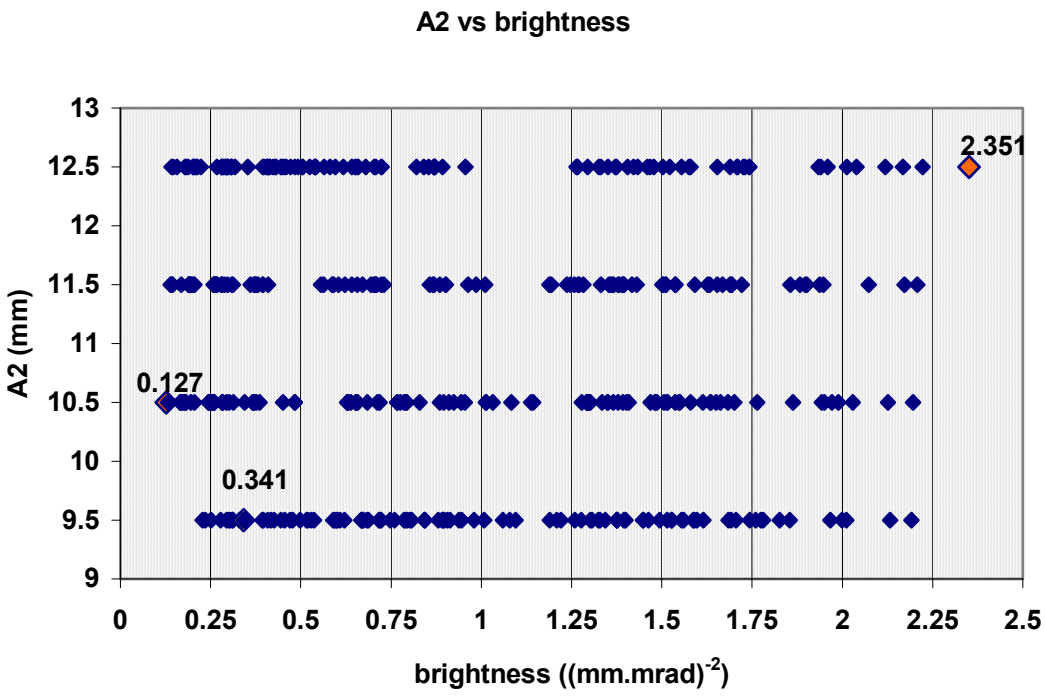

Figure 4.2 Plot of A2 versus beam brightness. This plot shows no trends governing the effects of varying A2 from 9.5 mm to 12.5 mm in diameter.

The overlap in data points in Figure 4.2 suggests no preferential value of A2 for achieving higher beam brightness. The conclusion is that the value of A2 does not affect beam brightness in a global manner.

It was recognized during the course of data analysis, however, that the second electrode effectively has two apertures that affect the beam characteristics. The label "A2" was assigned to the upstream aperture (closest to E1). While A2 took on four different values for testing, the downstream aperture remained fixed at its nominal value, 14 mm in diameter. Inspection of printouts of the ion trajectories for several tests in which A2 had larger than nominal values (> 9.5 mm in diameter) revealed that the more divergent H^-

ions were lost at the downstream aperture. Note, however, that the range of tested A2 parameter values remained smaller than 14 mm, the diameter of the downstream aperture of E2. The ion trajectories of two test configurations were chosen to illustrate the observed beam loss. Figure 4.3 is a close-up view of the ion trajectories of the nominal lens configuration (test 1), on the left, and of test 424, in which A2 = 12.5 mm, on the right (refer to Appendix B for a complete description of the lens configuration of test 424).

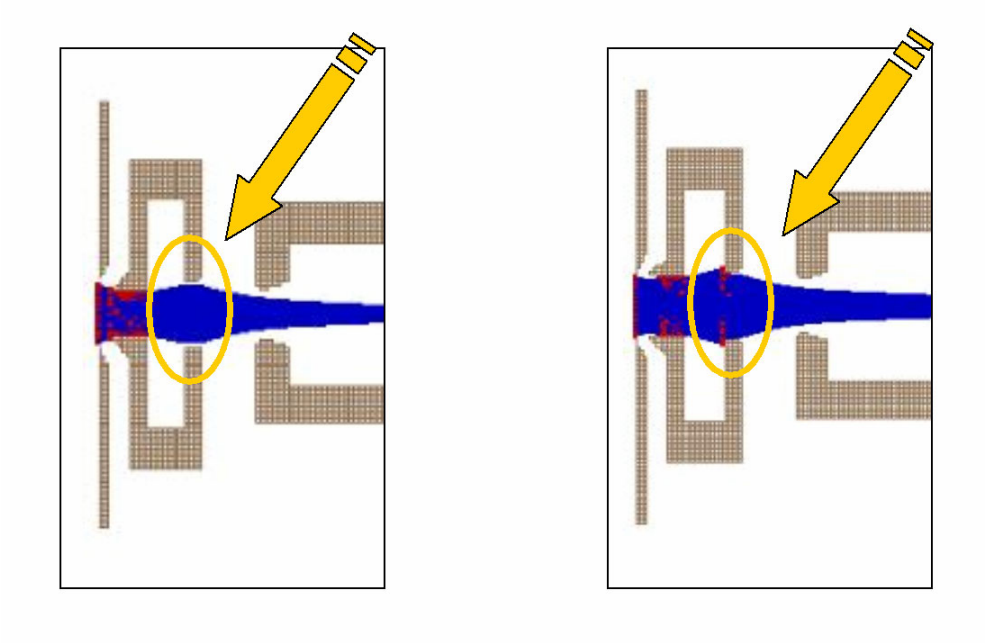

Figure 4.3 The beam trajectory through the nominal lens configuration is shown on the left. Note that no beam loss is evident at the downstream aperture of E2. The beam trajectory on the right passes through the lens configuration associated with test 424, in which A2 = 12.5 mm, and shows loss of beam at the downstream aperture of E2. The blue region is the beam. The red dots indicate ions hitting the electrode. The brown shapes in each frame are the electrodes, E1, E2, and E3. Only a part of E3 is shown to allow a close-up view of the downstream aperture of E2, circled in yellow and indicated by the arrows in each frame.

The beam trajectory for the nominal test case shows that the entire beam passes through the downstream aperture of E2, while the beam trajectory of test 424 shows that some ions are lost at the downstream aperture of E2, indicated by the encircled red points.

4.1.3 A3 versus Beam Brightness

Figure 4.4 is a plot of A3 versus beam brightness, with brightness increasing from left to right.

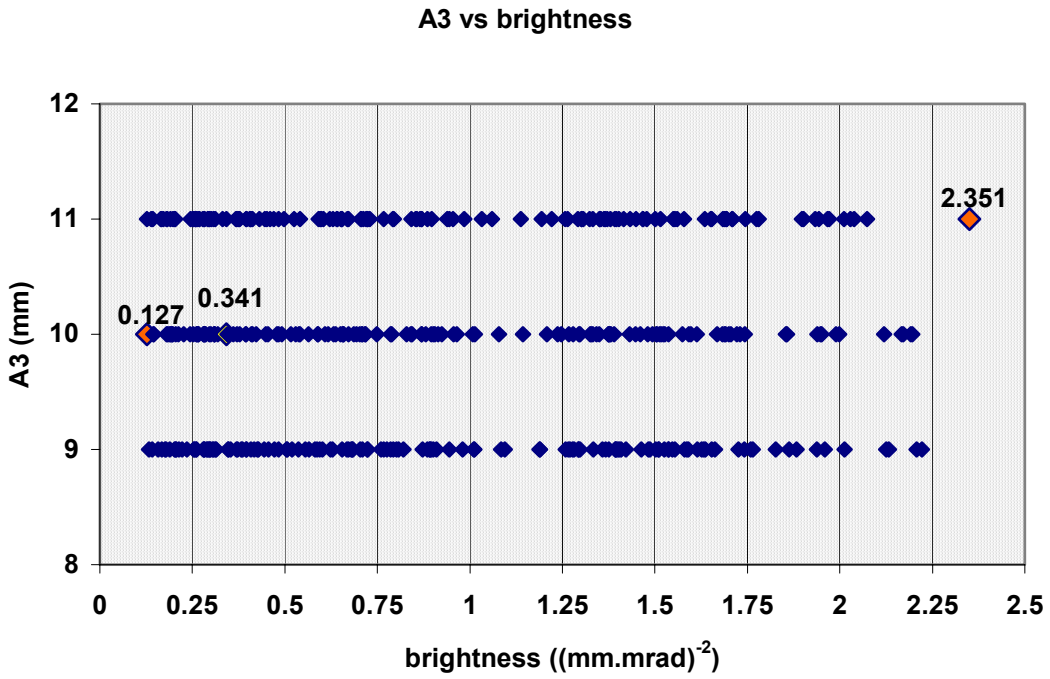

Figure 4.4 Plot of A3 versus beam brightness. There are no noticeable trends to report of the role A3 played in determining beam brightness.

Similarly to the variation of brightness with A2, Figure 4.4 shows that varying A3 from 9 mm to 11 mm in diameter has no global affect on beam brightness. The overlap of data points over the entire range of measured brightness shows no optimal value of A3 to achieve higher brightness. The lack of an observable trend may be a result of holding the diameter of the downstream aperture of E2 at a fixed value, rather than varying it proportionally with the values of A2 tested. The fixed value of the downstream aperture of E2 precluded ions with a half width greater than 7 mm, the radius of the downstream aperture of E2, from passing through the system. Thus, the role of A3 in changing beam characteristics was not effectively tested.

4.1.4 D12 versus Beam Brightness

Figure 4.5 is a plot of D12 versus beam brightness, with brightness increasing from left to right.

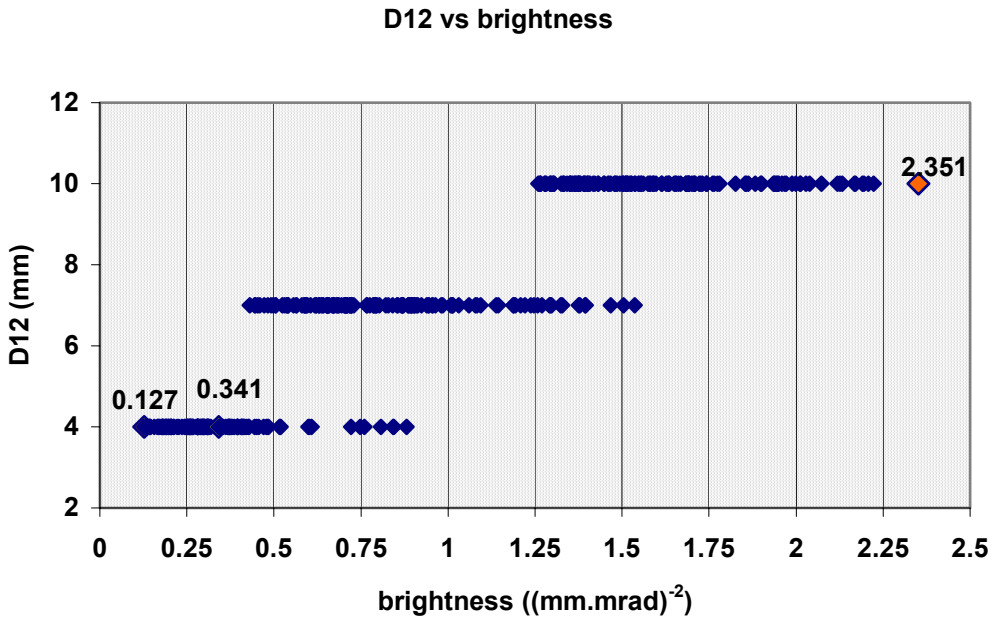

Figure 4.5 Plot of D12 versus beam brightness. The three distinct groups of data points in this plot of D12 versus beam brightness suggest that increases the spacing between the first two electrodes, i.e., increase the value of D12, will generally achieve a brighter beam.

The role D12 played in determining beam brightness was the most obvious. Minimal overlap of the data points over the range of calculated beam brightness values shows that increasing the value of D12 increased beam brightness, largely independent of the values of the other design parameters. This observation lead to the exploration of the distinct grouping of data points observed in Figure 4.1. The plot of V2 against beam brightness was modified to show the values of D12 for each data point. Figure 4.6 indicates that the data is isolated into three distinct groups, representing the three values of D12 tested. Within each of these groups, the trend in increasing brightness for decreasing values of

V2 is observable. A preliminary generalization at this point, regarding achieving high beam brightness, is that, of the values tested, the optimal value of D12 is 10 mm and of V2 is –23 kV.

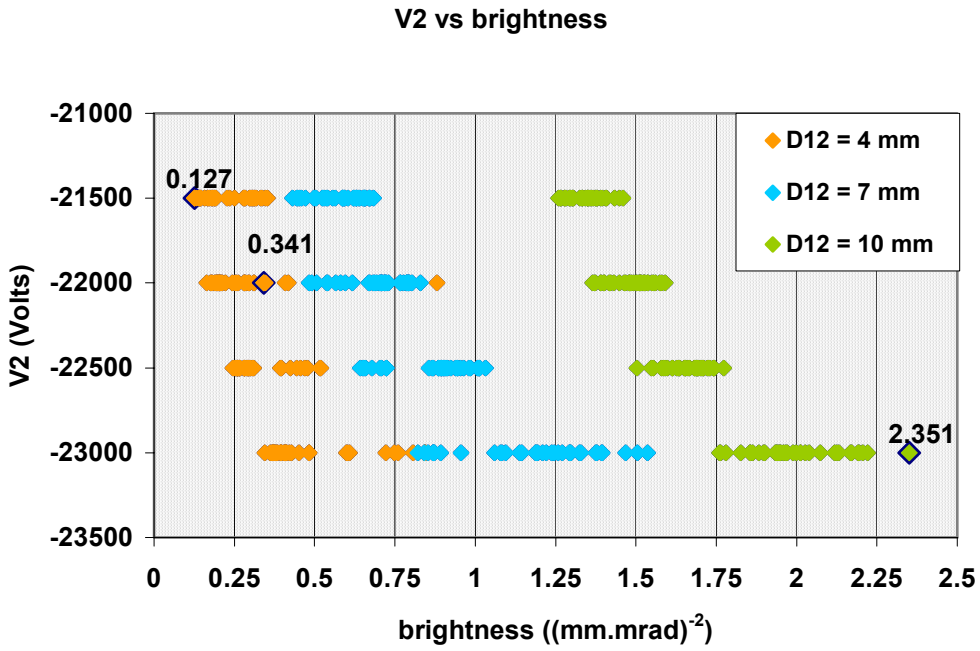

Figure 4.6 A modification of Figure 4.1, this plot of V2 versus beam brightness indicates the value of D12 for each data point. The distinct grouping of data points mentioned in section 4.1.1 is clearly a function of D12, the spacing between E1 and E2.

4.1.5 D23 versus Beam Brightness

Figure 4.7 is a plot of D23 versus brightness, with brightness increasing from left to right.

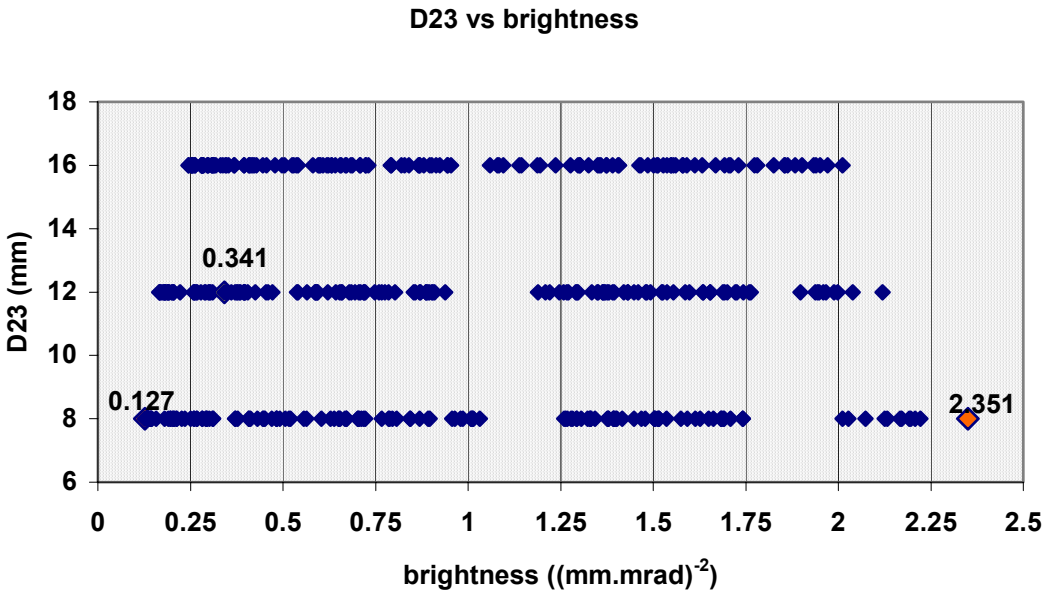

Figure 4.7 Plot of D23 versus beam brightness. This plot shows no trends governing the effects of varying D23 from 8 mm to 16 mm. The vague grouping of data points was explored but revealed no trends.

Although there are some indications of grouping of certain data points in the plot of D23 versus beam brightness in Figure 4.7, the effect of varying the values of D23 was largely arbitrary. An exploration into the source of the partial grouping of some data points proved to be unfruitful. Possibly the lack of an observable trend is due to having fixed the diameter of the downstream aperture of E2 at a constant value.

4.1.6 Summary of Trends Regarding Beam Brightness

Table 4.1 lists the top thirty five test configurations that resulted in the brightest beams. Several trends emerge from this table, ordered by decreasing brightness, namely that the listed configurations all have values of D12 = 10 mm and all but the last have values of V2 = -23 kV. The trend in D12 is significant: the 79 brightest beams had D12 = 10 mm, with a mix of other test parameter values. The tested values of A2, A3, and D23 show no particular trend. Maximum, minimum, and average values of brightness amongst these brightest observed beams are included at the bottom of the table.

The thirty five lens configurations that resulted in the lowest brightness values for the beam at the beamstop are listed in Table 4.2. High values of V2 and low values of D12 (4 mm only) predominate. The values of the other test parameters, A2, A3, and D23, appear to have no global effect on beam brightness, although all of the values of D23 are either 8 mm or 12 mm. The nine least bright beams resulted when D23 = 8 mm, but the nine brightest beams also resulted when D23 = 8 mm, indicating that the tested values of D23 did not effect beam brightness in a predictable manner. Maximum, minimum, and average values of brightness amongst these lowest brightness values are included at the bottom of the table.

Table 4.1 List of the test configurations that produced the brightest beam at the beamstop. The top thirty five configurations are shown to observe the trends in the test parameter values. D12 and V2 show particularly obvious trends.

test #	V2 (V)	A2 (mm)	A3 (mm)	D12 (mm)	D23 (mm)	brightness $(mm.mrad)^{-2}$
test 215	-23000	12.5	11	10	8	2.351
test 206	-23000	12.5	9	10	8	2.222
test 179	-23000	11.5	9	10	8	2.207
test 143	-23000	10.5	10	10	8	2.196
test 116	-23000	9.5	10	10	8	2.191
test 170	-23000	11.5	10	10	8	2.171
test 197	-23000	12.5	10	10	8	2.168
test 125	-23000	9.5	9	10	8	2.132
test 152	-23000	10.5	9	10	8	2.125
test 196	-23000	12.5	10	10	12	2.119
test 188	-23000	11.5	11	10	8	2.073
test 214	-23000	12.5	11	10	12	2.039
test 161	-23000	10.5	11	10	8	2.028
test 207	-23000	12.5	9	10	16	2.012
test 134	-23000	9.5	11	10	8	2.012
test 115	-23000	9.5	10	10	12	1.999
test 142	-23000	10.5	10	10	12	1.989
test 162	-23000	10.5	11	10	16	1.972
test 133	-23000	9.5	11	10	12	1.966
test 205	-23000	12.5	9	10	12	1.959
test 144	-23000	10.5	10	10	16	1.951
test 169	-23000	11.5	10	10	12	1.948
test 160	-23000	10.5	11	10	12	1.944
test 198	-23000	12.5	10	10	16	1.939
test 178	-23000	11.5	9	10	12	1.938
test 216	-23000	12.5	11	10	16	1.934
test 189	-23000	11.5	11	10	16	1.902
test 187	-23000	11.5	11	10	12	1.897
test 180	-23000	11.5	9	10	16	1.883
test 153	-23000	10.5	9	10	16	1.863
test 171	-23000	11.5	10	10	16	1.856
test 117	-23000	9.5	10	10	16	1.854
test 126	-23000	9.5	9	10	16	1.826
test 135	-23000	9.5	11	10	16	1.780
test 243	-22500	9.5	11	10	16	1.774
					max	2.351
					min	1.774
					average	2.006

Table 4.2 List of the test configurations that produced the lowest brightness values at the beamstop. These thirty five configurations are shown to observe the trends in the test parameter values. Again, D12 and V2 show particularly obvious trends.

test #	V2 (V)	A2 (mm)	A3 (mm)	D12 (mm)	D23 (mm)	brightness $(mm.mrad)^{-2}$
test 92	-22000	12.5	9	4	8	0.213
test 83	-22000	12.5	10	4	8	0.211
test 38	-22000	10.5	9	4	8	0.206
test 65	-22000	11.5	9	4	8	0.205
test 82	-22000	12.5	10	4	12	0.205
test 100	-22000	12.5	11	4	12	0.204
test 64	-22000	11.5	9	4	12	0.202
test 101	-22000	12.5	11	4	8	0.201
test 73	-22000	11.5	11	4	12	0.198
test 29	-22000	10.5	10	4	8	0.196
test 56	-22000	11.5	10	4	8	0.196
test 379	-21500	11.5	10	4	12	0.192
test 55	-22000	11.5	10	4	12	0.192
test 74	-22000	11.5	11	4	8	0.190
test 388	-21500	11.5	9	4	12	0.189
test 406	-21500	12.5	10	4	12	0.188
test 352	-21500	10.5	10	4	12	0.182
test 424	-21500	12.5	11	4	12	0.181
test 28	-22000	10.5	10	4	12	0.181
test 47	-22000	10.5	11	4	8	0.180
test 415	-21500	12.5	9	4	12	0.179
test 37	-22000	10.5	9	4	12	0.176
test 370	-21500	10.5	11	4	12	0.172
test 397	-21500	11.5	11	4	12	0.168
test 361	-21500	10.5	9	4	12	0.167
test 46	-22000	10.5	11	4	12	0.165
test 416	-21500	12.5	9	4	8	0.157
test 407	-21500	12.5	10	4	8	0.146
test 380	-21500	11.5	10	4	8	0.145
test 425	-21500	12.5	11	4	8	0.142
test 389	-21500	11.5	9	4	8	0.141
test 398	-21500	11.5	11	4	8	0.139
test 362	-21500	10.5	9	4	8	0.132
test 371	-21500	10.5	11	4	8	0.127
test 353	-21500	10.5	10	4	8	0.127
					max	0.213
					min	0.127
					average	0.177

4.2 Normalized Beam Emittance

The following subsections contain figures of each of the test parameters plotted against normalized beam emittance. In each plot, Figure 4.8 to Figure 4.13, the minimum and maximum values of normalized emittance are labelled, as is the nominal test configuration.

4.2.1 V2 versus Normalized Beam Emittance

Figure 4.8 is a plot of V2 versus normalized beam emittance, with normalized emittance values increasing from left to right. Recall that highest quality beams have low normalized emittance values; these are on the left hand side of the plot.

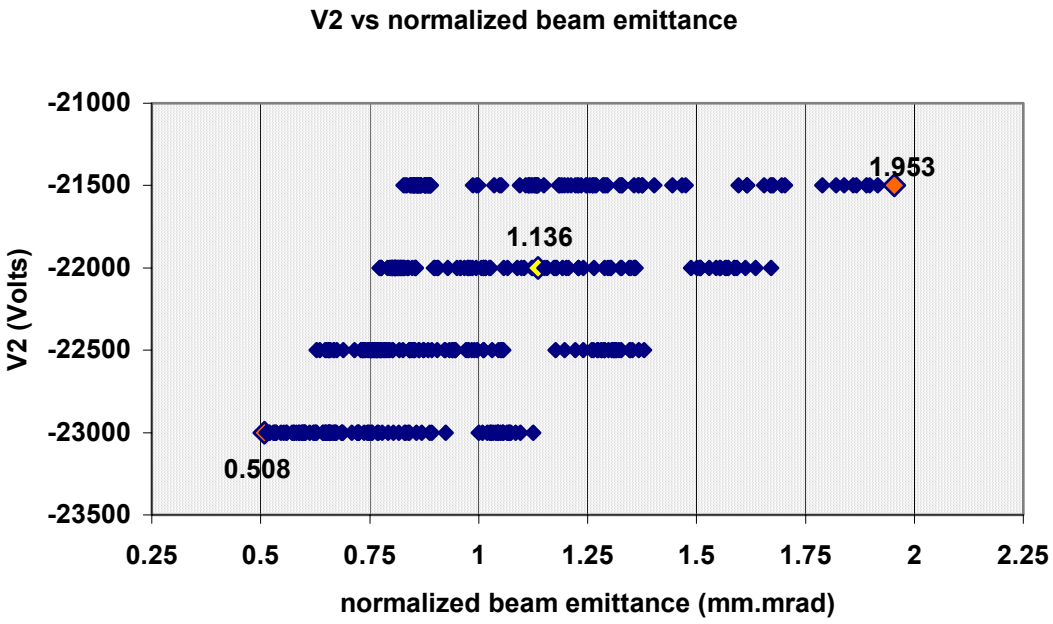

Figure 4.8 Plot of V2 versus normalized beam emittance. This plot suggests that decreasing the value of V2 tended to achieve lower normalized emittance values.

The plot of V2 versus normalized beam emittance in Figure 4.8 shows overlap of the data points over the range of calculated normalized emittance, values but a vague trend is noticeable. In general, lower values of V2 resulted in lower normalized emittance values,

although for some of the tested lens configurations, relatively low normalized emittance values were achieved with highest tested value of V2. Grouping of the rightmost data points for each of the tested values of V2 suggests that a test parameter other than V2 had global effects on normalized emittance values.

4.2.2 A2 versus Normalized Beam Emittance

Figure 4.9 is a plot of A2 versus normalized beam emittance, with normalized emittance values increasing from left to right. Recall that the highest quality beams have low normalized emittance values; these are on the left hand side of the plot.

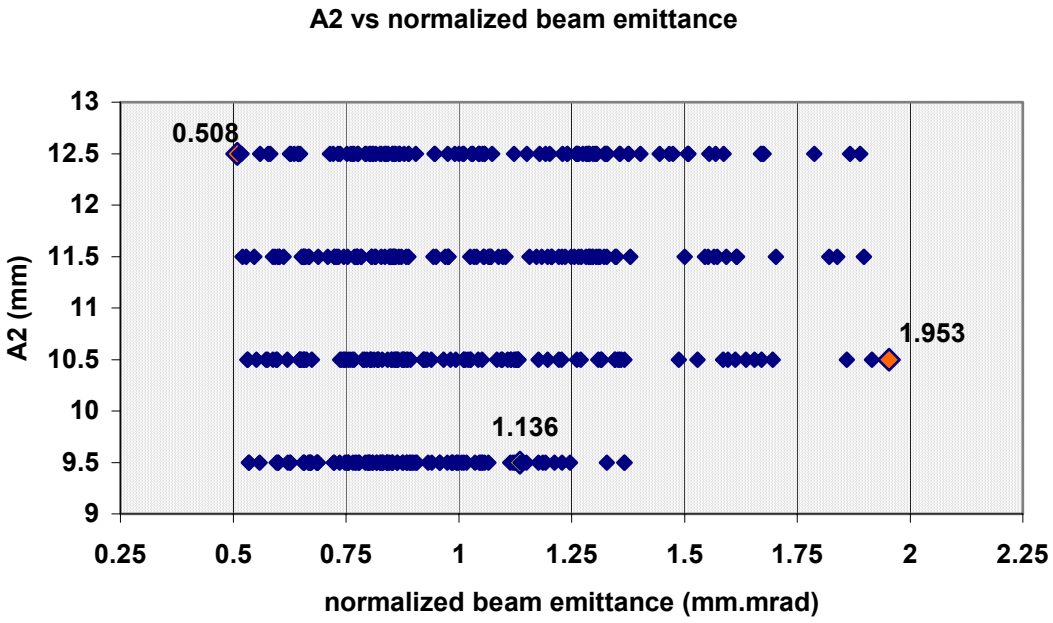

Figure 4.9 Plot of A2 versus normalized beam emittance. No obvious trend can be identified in this plot.

The effect of varying A2 cannot be predicted from the plot in Figure 4.9. Most of the range of recorded beam emittance values resulted from all values of A2. A slight advantage is observed for the nominal value of A2 since the rightmost data points, corresponding to high normalized emittance values, did not result when A2 = 9.5 mm.

4.2.3 A3 versus Normalized Beam Emittance

Figure 4.10 is a plot of A3 versus normalized beam emittance, with normalized emittance values increasing from left to right. Recall that the highest quality beams have low normalized emittance values; these are on the left hand side of the plot.

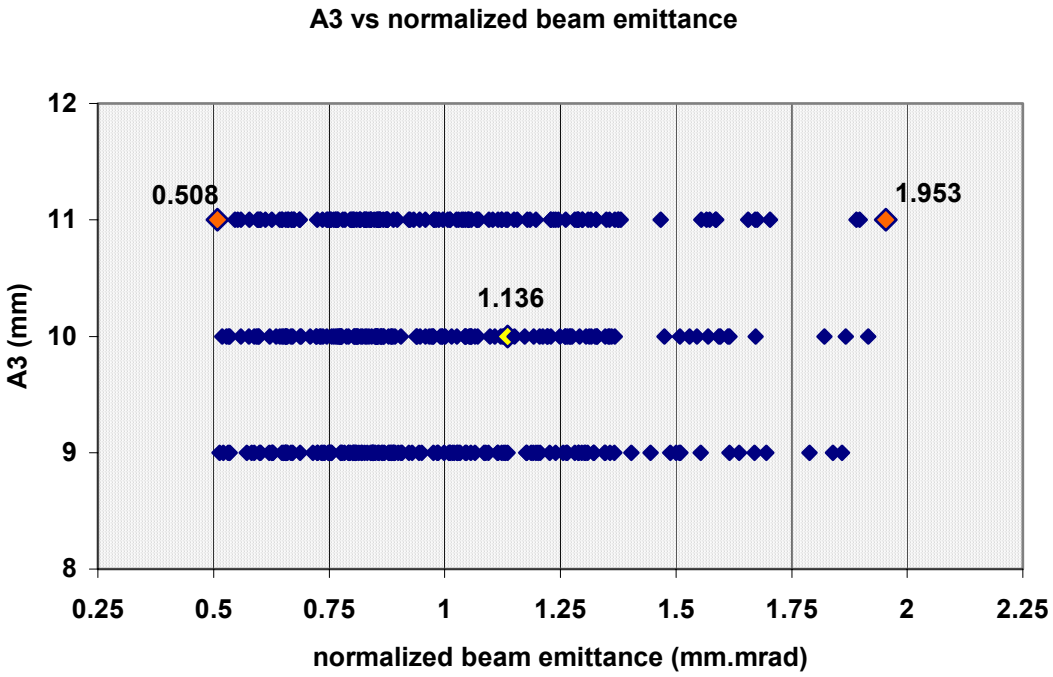

Figure 4.10 Plot of A3 versus normalized beam emittance. There is no observable trend governing the role of A3 in determining beam emittance.

As can be seen in Figure 4.10, there is overlap over the entire range of recorded normalized beam emittance values. Thus, no observable global trend governs how A3 affects the value of normalized beam emittance. As discussed in section 4.1.2, the lack of observable trend may be due having fixed the size of the downstream aperture diameter of E2 to its nominal value, 14 mm.

4.2.4 D12 versus Normalized Beam Emittance

Figure 4.11 is a plot of V2 versus normalized beam emittance, with normalized emittance values increasing from left to right. Recall that the highest quality beams have low normalized emittance values; these are on the left hand side of the plot.

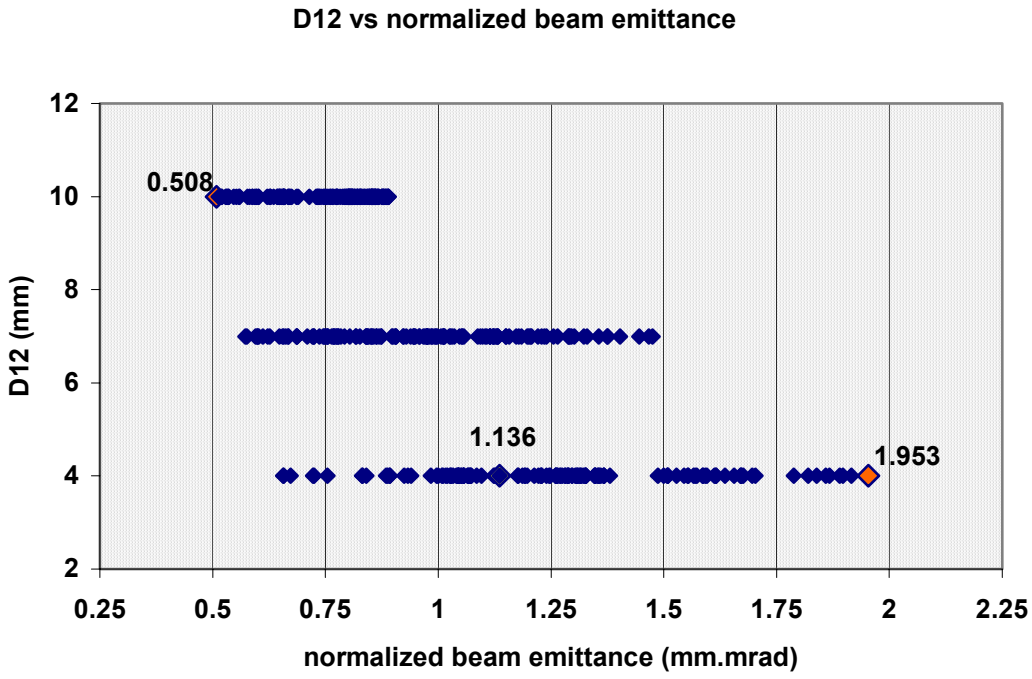

Figure 4.11 Plot of D12 versus normalized beam emittance. While certain lens configurations having D12 = 4 mm resulted in relatively low normalized emittance values, setting D12 = 10 mm consistently resulted in relatively low normalized beam emittance, regardless of the other test parameter values.

A global trend governing how D12 affected normalized beam emittance can be seen in Figure 4.11. Increasing the value of D12 had the effect of lowering the value of normalized beam emittance. Note, however, that relatively low normalized beam emittance values were obtained from lens configurations in which D12 was not maximal.

The observed global effect D12 had on normalized emittance values motivated further exploration of the grouping of data points mentioned in section 4.2.1.

Figure 4.12 is a modification of the plot in Figure 4.8, in which the three values of D12 tested are indicated by colour. Figure 4.12 indicates that the data is segregated into three groups, although not entirely distinct. Within each coloured grouping, lower emittance values resulted when the values of V2 were decreased. This trend parallels that observed for achieving higher beam brightness, as one would expect from the inverse mathematical relation between b and ε_N.

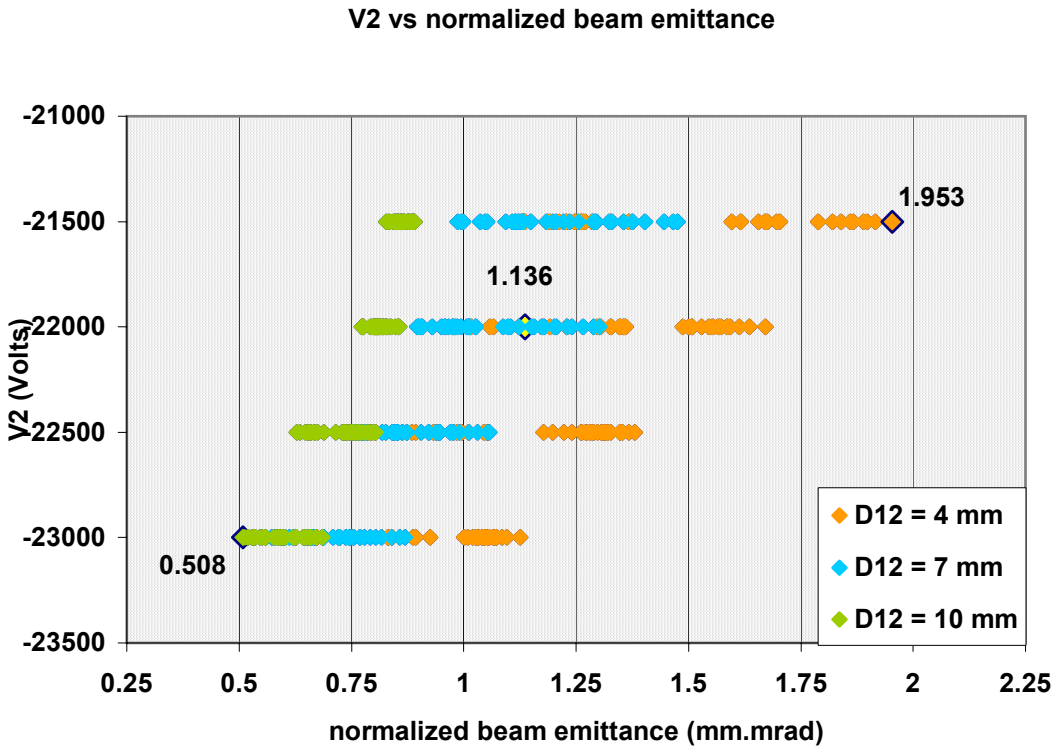

Figure 4.12 A modification of Figure 4.8, this plot of V2 versus normalized beam emittance distinguishes between the values of D12 by colour. The grouping of data points mentioned in section 4.2.1 is clearly a function of D12, the spacing between E1 and E2.

4.2.5 D23 versus Normalized Beam Emittance

Figure 4.13 is a plot of D23 versus normalized beam emittance, with normalized emittance values increasing from left to right. Recall that the highest quality beams have low normalized emittance values; these are on the left hand side of the plot.

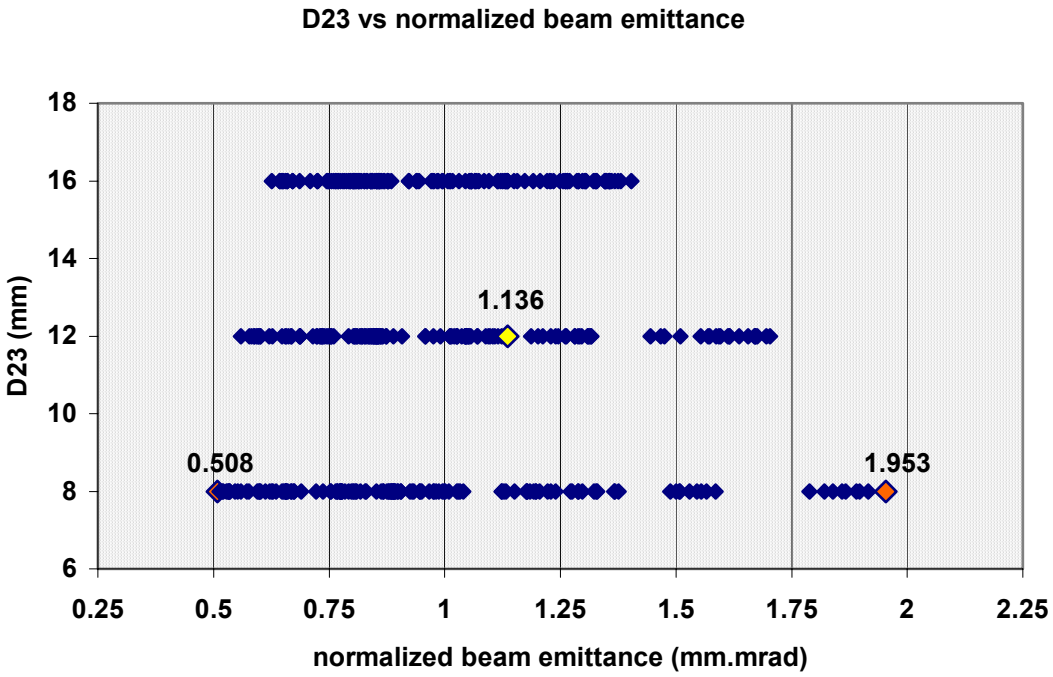

Figure 4.13 Plot of D23 versus normalize beam emittance, showing no significant global trend governed by the parameter D23.

The overlap over most of the range of calculated normalized beam emittance values indicates little to no trend about the values of D23 tested. While the smallest value of D23 tested (8 mm) was amongst the lens configurations that resulted in both the lowest and highest values of normalized beam emittance, the largest value of D23 tested (16 mm) resulted in a more concentrated range of relatively low normalized emittance values.

4.2.6 Summary of Trends Regarding Normalized Beam Emittance

Table 4.3 lists the top thirty five test configurations that resulted in the lowest normalized beam emittance values. The most significant trend in this table is that all but the last entry have values of V2 = -23 kV. The top twelve entries have the values D12 = 10 mm, while the remaining values of D12 are either 7 mm or 10 mm. The tested values of A2, A3, and D23 show no particular trend, although all but one value of D23 are either 8 mm or 12 mm. Maximum, minimum, and average values of normalized emittance of these overall lowest calculated normalized emittance values are included at the bottom of the table.

The thirty five lens configurations that resulted in the largest normalized beam emittance values are listed in Table 4.4. All of the lens configurations listed in this table have D12 = 4 mm and the last thirteen entries have V2 = -21.5 kV. All the values of D23 are either 8 mm or 12 mm, which is not much different than the lens configurations that resulted in the lowest normalized emittance values. The tested values of A2, A3, and D23 show no particular trend. Maximum, minimum, and average values of the overall highest normalized emittance values calculated are included at the bottom of the table.

Table 4.3 List of the tested lens configurations that resulted in the thirty five lowest normalized beam emittance values. The entries are in order of lowest to highest normalized emittance, ε_N .

test #	V2 (V)	A2 (mm)	A3 (mm)	D12 (mm)	D23 (mm)	ε_N (mm.mrad)
test 215	-23000	12.5	11	10	8	0.508
test 206	-23000	12.5	9	10	8	0.513
test 197	-23000	12.5	10	10	8	0.519
test 179	-23000	11.5	9	10	8	0.521
test 170	-23000	11.5	10	10	8	0.528
test 152	-23000	10.5	9	10	8	0.531
test 143	-23000	10.5	10	10	8	0.532
test 125	-23000	9.5	9	10	8	0.535
test 116	-23000	9.5	10	10	8	0.535
test 188	-23000	11.5	11	10	8	0.547
test 161	-23000	10.5	11	10	8	0.552
test 134	-23000	9.5	11	10	8	0.559
test 196	-23000	12.5	10	10	12	0.559
test 149	-23000	10.5	9	7	8	0.572
test 140	-23000	10.5	10	7	8	0.576
test 214	-23000	12.5	11	10	12	0.577
test 205	-23000	12.5	9	10	12	0.582
test 142	-23000	10.5	10	10	12	0.588
test 178	-23000	11.5	9	10	12	0.588
test 169	-23000	11.5	10	10	12	0.593
test 158	-23000	10.5	11	7	8	0.595
test 115	-23000	9.5	10	10	12	0.596
test 160	-23000	10.5	11	10	12	0.597
test 167	-23000	11.5	10	7	8	0.598
test 122	-23000	9.5	9	7	8	0.600
test 133	-23000	9.5	11	10	12	0.600
test 176	-23000	11.5	9	7	8	0.602
test 187	-23000	11.5	11	10	12	0.602
test 185	-23000	11.5	11	7	8	0.612
test 151	-23000	10.5	9	10	12	0.621
test 113	-23000	9.5	10	7	8	0.622
test 207	-23000	12.5	9	10	16	0.626
test 131	-23000	9.5	11	7	8	0.626
test 124	-23000	9.5	9	10	12	0.628
test 314	-22500	12.5	9	10	8	0.628
					max	0.628
					min	0.508
					average	0.576

Table 4.4 List of the tested lens configurations that resulted in the thirty five largest normalized beam emittance values. The entries are in order of increasing normalized emittance, ε_N.

test #	V2 (V)	A2 (mm)	A3 (mm)	D12 (mm)	D23 (mm)	ε_N (mm.mrad)
test 65	-22000	11.5	9	4	8	1.500
test 92	-22000	12.5	9	4	8	1.508
test 83	-22000	12.5	10	4	8	1.508
test 91	-22000	12.5	9	4	12	1.509
test 29	-22000	10.5	10	4	8	1.529
test 56	-22000	11.5	10	4	8	1.545
test 64	-22000	11.5	9	4	12	1.553
test 101	-22000	12.5	11	4	8	1.555
test 74	-22000	11.5	11	4	8	1.566
test 82	-22000	12.5	10	4	12	1.570
test 73	-22000	11.5	11	4	12	1.573
test 47	-22000	10.5	11	4	8	1.586
test 100	-22000	12.5	11	4	12	1.587
test 55	-22000	11.5	10	4	12	1.592
test 352	-21500	10.5	10	4	12	1.596
test 28	-22000	10.5	10	4	12	1.613
test 379	-21500	11.5	10	4	12	1.615
test 388	-21500	11.5	9	4	12	1.616
test 37	-22000	10.5	9	4	12	1.636
test 370	-21500	10.5	11	4	12	1.656
test 415	-21500	12.5	9	4	12	1.670
test 46	-22000	10.5	11	4	12	1.671
test 406	-21500	12.5	10	4	12	1.672
test 424	-21500	12.5	11	4	12	1.676
test 361	-21500	10.5	9	4	12	1.695
test 397	-21500	11.5	11	4	12	1.703
test 416	-21500	12.5	9	4	8	1.788
test 380	-21500	11.5	10	4	8	1.820
test 389	-21500	11.5	9	4	8	1.839
test 362	-21500	10.5	9	4	8	1.860
test 407	-21500	12.5	10	4	8	1.867
test 425	-21500	12.5	11	4	8	1.890
test 398	-21500	11.5	11	4	8	1.897
test 353	-21500	10.5	10	4	8	1.916
test 371	-21500	10.5	11	4	8	1.953
					max	1.953
					min	1.500
					average	1.667

4.3 Percent of Beam Transmitted

In this study, beam current is represented by percent of beam transmitted, a value utilized in calculating beam brightness. The terms beam current and percent of beam transmitted are used interchangeably herein. The highest beam current achievable is one hundred percent transmission. Five thousand ions populated the beam in each test run. The following subsections contain figures of each of the test parameters plotted against percent of beam transmitted. In each plot, the nominal test configuration is labelled. Recall that the usefulness of a quantitative measure of beam current depends on the intended application of the beam, as discussed in sections 2.4 and 3.3.

4.3.1 V2 versus Percent of Beam Transmitted

Figure 4.14 is a plot of V2 versus percent of beam transmitted.

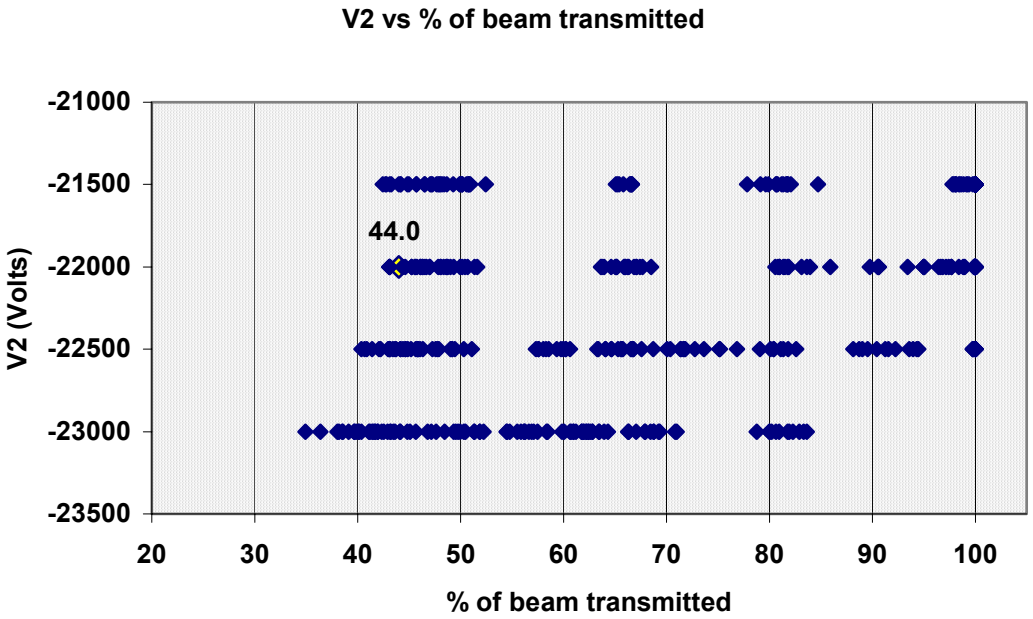

Figure 4.14 Plot of V2 versus percent of beam transmitted. All of the tested values of V2 resulted the full range of beam currents measured in this study. Slight preference is shown for higher values of V2 to achieve the highest beam currents.

Figure 4.14 shows minimal information relating the values of V2 to the resulting beam currents. The plot shows a slight preference for higher values of V2 in obtaining higher beam currents.

4.3.2 A2 versus Percent of Beam Transmitted

Figure 4.15 is a plot of A2 versus percent of beam transmitted.

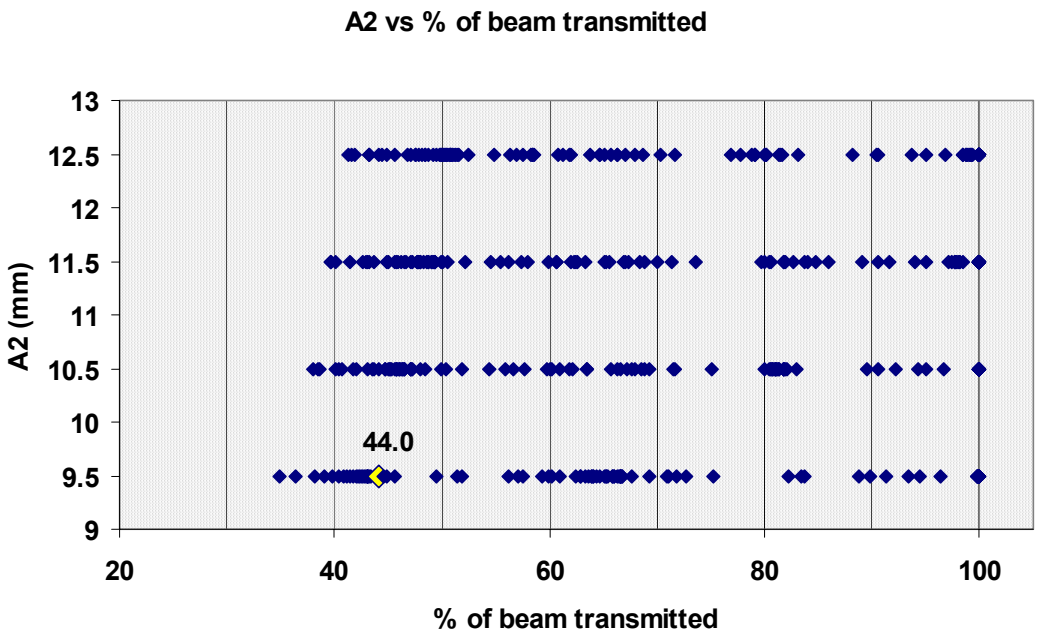

Figure 4.15 Plot of A2 versus percent of beam transmitted. This plot indicates that the values of A2 tested have no global effect on the beam current.

All of the data points overlap for the entire range of measured beam currents, indicating that the tested values of A2 had no global effect on the beam current. Recall from the discussion in section 4.1.2 that the absence of a global trend may be the result of having held the downstream aperture of E2 constant at its nominal value of 14 mm in diameter.

4.3.3 A3 versus Percent of Beam Transmitted

Figure 4.16 is a plot of A3 versus percent of beam transmitted.

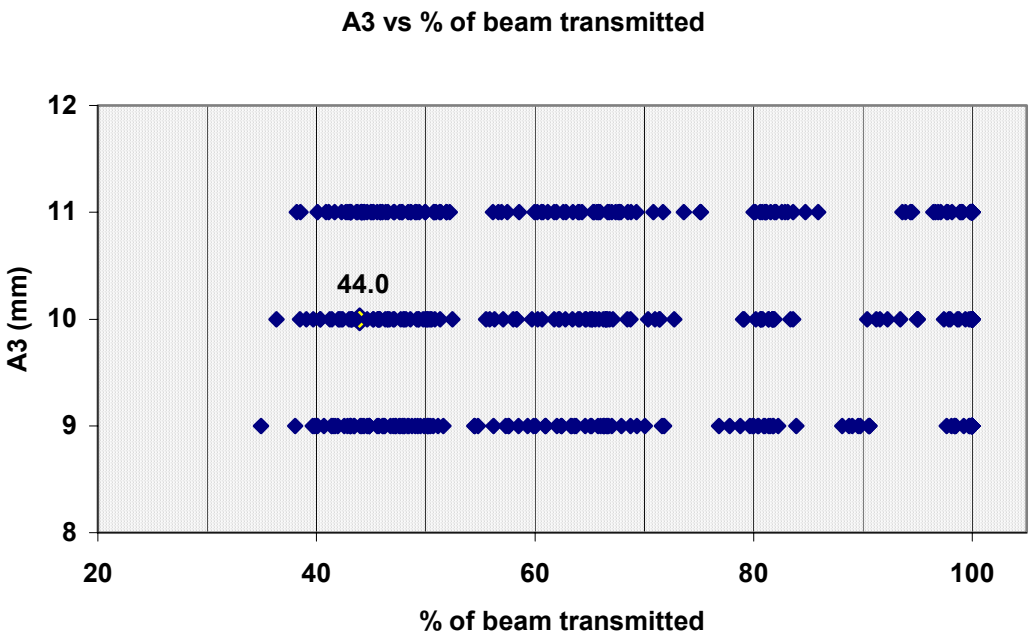

Figure 4.16 Plot of A3 versus percent of beam transmitted. The distribution of data points over the range of measured beam currents for all tested values of A3 indicates that varying A3 had no global effect on the beam current.

The plot shown in Figure 4.16 shows complete randomness in the beam current for the range of values of A3 tested.

4.3.4 D12 versus Percent of Beam Transmitted

Figure 4.17 is a plot of D12 versus percent of beam transmitted.

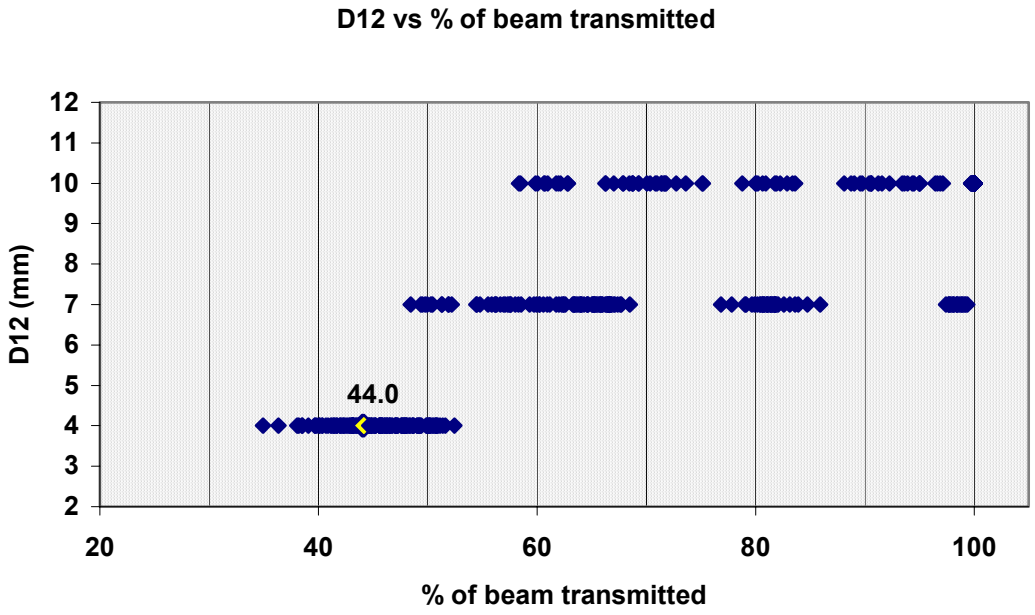

Figure 4.17 Plot of D12 versus percent of beam transmitted. The general trend suggested by this plot is that beam current increased as the value of D12 was increased.

The most obvious global trend governing beam current arose from varying D12 through the tested range of values, 4 mm to 10 mm. Increasing the value of D12 resulted in increasing the beam current, although for some of the tested lens configurations, high beam currents were achieved with D12 = 7 mm. The lowest beam currents measured resulted from lens configurations with D12 = 4 mm.

4.3.5 D23 versus Percent of Beam Transmitted

Figure 4.18 is a plot of D23 versus percent of beam transmitted.

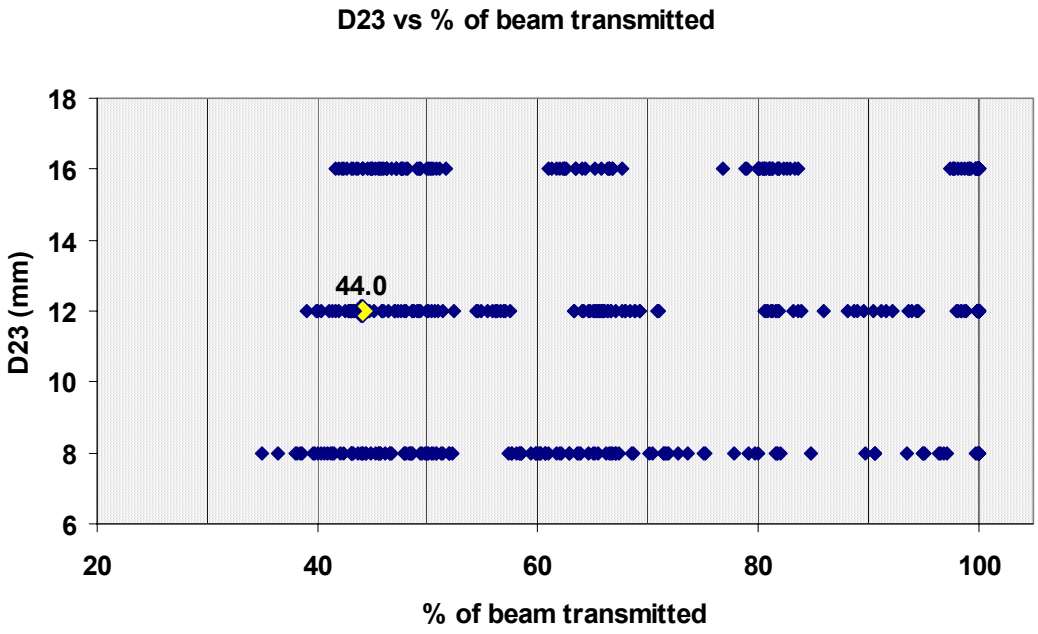

Figure 4.18 Plot of D23 versus percent of beam transmitted. There is no observable global trend relating the tested values of D23 to the measured beam currents.

As with A2 and A3, the range of values for which D23 was tested showed no global trend relating the beam current to the spacing between E2 and E3.

The summary of trends regarding the measured percents of beam transmitted are discussed in greater detail in the following section, in relation to beam brightness and normalized beam emittance.

4.4 Correlating Beam Brightness, Normalized Beam Emittance, and Percent of Beam Transmitted

Combining the global trends observed in sections 4.1 to 4.3, the three key measurements, namely brightness, normalized emittance, and beam current, are analyzed collectively in this section. Of the five test parameters, varying V2 and D12 produced global changes to the beam characteristics for the range of parameter values tested. The other three test parameters played no obvious role in determining the three key beam characteristics. The general trends observed in the three previous sections were the achievement of high beam quality (high brightness and low normalized emittance) by reducing the value of V2 and by increasing the value of D12.

Table 4.5 lists the thirty five lens configurations that resulted in the highest beam qualities overall. The table includes the calculated values of beam brightness, normalized beam emittance, and percent of beam transmitted. The table entries are listed in order of decreasing beam brightness, as this is the primary measure of beam quality for both high and low beam current applications (refer to section 2.4 for a discussion of beam quality for high and low beam current applications). Maximum, minimum, and average values of the listed configurations are included at the bottom of the table. While the uniform values of V2 = -23 kV and D12 = 10 mm for the first thirty four lens configurations in Table 4.5 are significant, a look at the percent of beam transmitted reveals an important clue about how to choose the optimum lens configuration.

Table 4.5 List of the thirty five lens configurations that resulted in the highest quality beam overall. The table entries are listed in order of decreasing brightness because beam brightness is the primary measurement of beam quality.

test #	V2 (V)	A2 (mm)	A3 (mm)	D12 (mm)	D23 (mm)	brightness $(mm.mrad)^{-2}$	normalized emittance (mm.mrad)	% of beam transmitted
test 215	-23000	12.5	11	10	8	2.351	0.508	60.7
test 206	-23000	12.5	9	10	8	2.222	0.513	58.5
test 179	-23000	11.5	9	10	8	2.207	0.521	59.9
test 143	-23000	10.5	10	10	8	2.196	0.532	62.2
test 116	-23000	9.5	10	10	8	2.191	0.535	62.8
test 170	-23000	11.5	10	10	8	2.171	0.528	60.6
test 197	-23000	12.5	10	10	8	2.168	0.519	58.4
test 125	-23000	9.5	9	10	8	2.132	0.535	61.0
test 152	-23000	10.5	9	10	8	2.125	0.531	60.0
test 196	-23000	12.5	10	10	12	2.119	0.559	66.3
test 188	-23000	11.5	11	10	8	2.073	0.547	61.9
test 214	-23000	12.5	11	10	12	2.039	0.577	67.9
test 161	-23000	10.5	11	10	8	2.028	0.552	61.8
test 207	-23000	12.5	9	10	16	2.012	0.626	78.8
test 134	-23000	9.5	11	10	8	2.012	0.559	62.8
test 115	-23000	9.5	10	10	12	1.999	0.596	71.0
test 142	-23000	10.5	10	10	12	1.989	0.588	68.8
test 162	-23000	10.5	11	10	16	1.972	0.648	82.9
test 133	-23000	9.5	11	10	12	1.966	0.600	70.9
test 205	-23000	12.5	9	10	12	1.959	0.582	66.3
test 144	-23000	10.5	10	10	16	1.951	0.647	81.8
test 169	-23000	11.5	10	10	12	1.948	0.593	68.4
test 160	-23000	10.5	11	10	12	1.944	0.597	69.3
test 198	-23000	12.5	10	10	16	1.939	0.643	80.2
test 178	-23000	11.5	9	10	12	1.938	0.588	67.0
test 216	-23000	12.5	11	10	16	1.934	0.643	80.0
test 189	-23000	11.5	11	10	16	1.902	0.656	81.9
test 187	-23000	11.5	11	10	12	1.897	0.602	68.8
test 180	-23000	11.5	9	10	16	1.883	0.652	80.0
test 153	-23000	10.5	9	10	16	1.863	0.659	81.0
test 171	-23000	11.5	10	10	16	1.856	0.659	80.7
test 117	-23000	9.5	10	10	16	1.854	0.671	83.4
test 126	-23000	9.5	9	10	16	1.826	0.671	82.3
test 135	-23000	9.5	11	10	16	1.780	0.685	83.6
test 243	-22500	9.5	11	10	16	1.774	0.750	99.8
					max	2.351	0.750	99.8
					min	1.774	0.508	58.4
					average	2.006	0.596	71.2

For high beam current applications, the lens configurations that resulted in the brightest beams would not be suitable. The top half of the entries in Table 4.5 has beam currents of less than 80%. Depending on the low beam current application, these lens configurations may be very suitable, resulting in both the highest beam brightness values and lowest normalized beam emittance values overall.

Figure 4.19 is a plot of normalized beam emittance versus beam brightness for all of the test configurations. Each data point has a distinctive shape, colour, and marker. The shapes of the data points represent the values of D12: D12 = 4 mm is a square, D12 = 7 mm is a triangle, and D12 = 10 mm is a circle. The colours represent ranges of beam current, grouped in ranges of 10% of beam transmitted, with the exception that 100% transmission is represented by its own group. The markers of the data points represent the values of V2: V2 = -23 kV is a cross, V2 = -22 kV is a bar, V2 = -22.5 kV is a point, and V2 = -21.5 kV is a plus. These codes are included in the legend. (The shapes of the colour samples in the legend do not mean anything.)

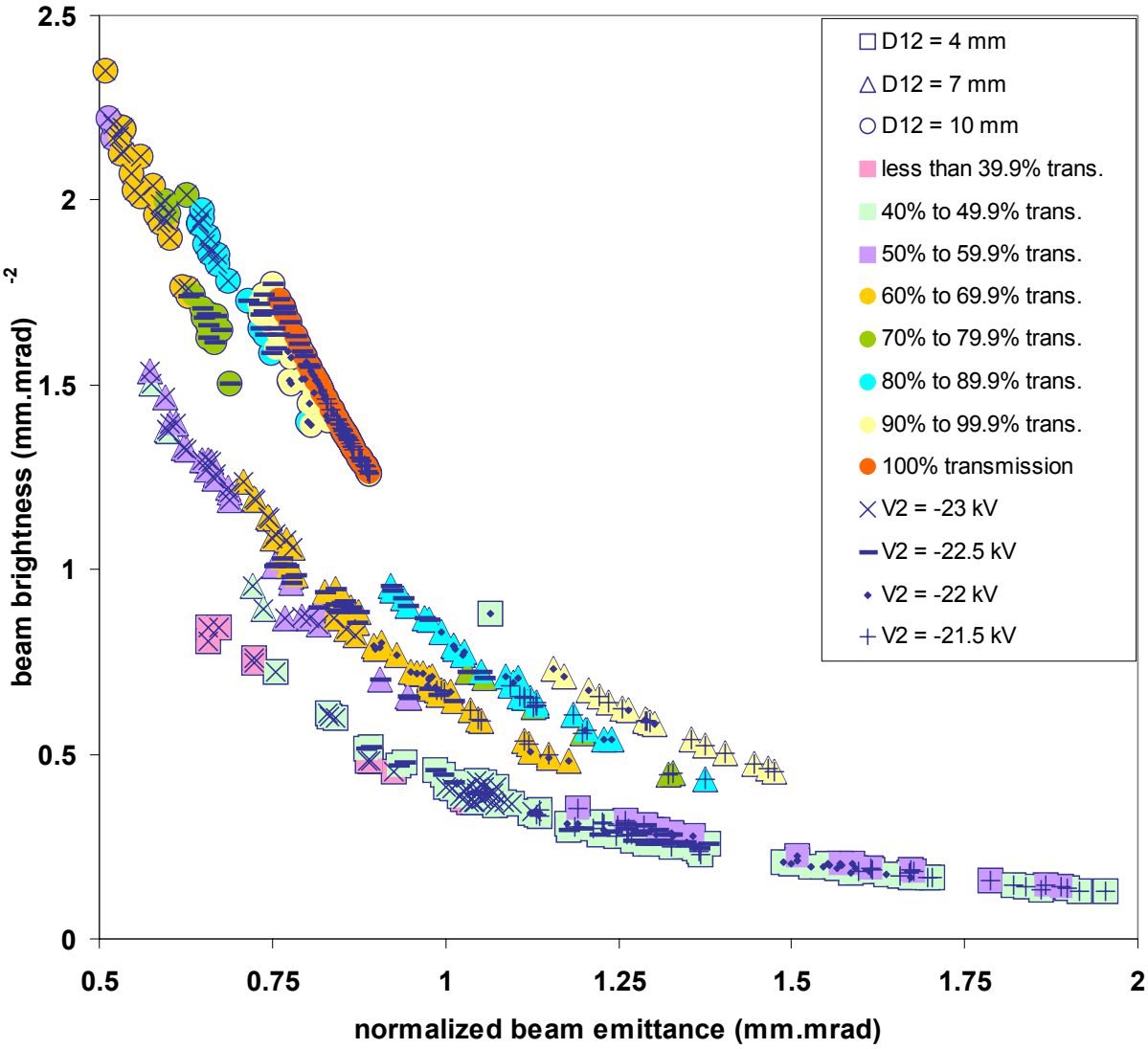

Figure 4.19 Plot of normalized beam emittance versus beam brightness. Each data point contains three additional pieces of information, based on their shape, colour, and marker. The legend shows the three shapes that are associated with the three values of D12 tested, the colours associated with ranges of percent of beam transmitted, and the markers the four values of V2 tested.

The cluster of data points in the top left corner of the plot are associated with the lens configurations that resulted in the brightest beam and lowest normalized beam emittance. With the exception of three data points, this cluster of points falls in the range of 60% to 69.9% beam transmission (a look at Table 4.5 shows that the three purple points have

almost 60% beam transmission). This cluster of data points is explored in more detail in the following plot, Figure 4.20.

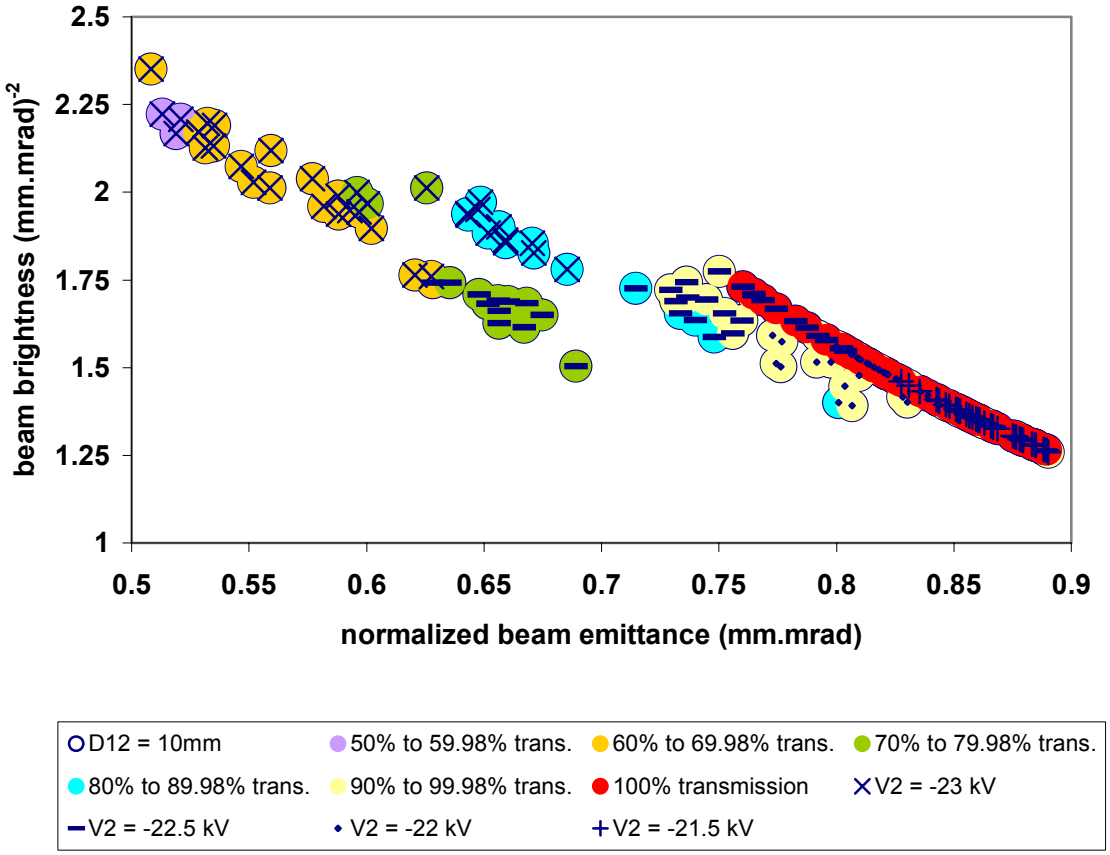

Figure 4.20 A subplot of normalized beam emittance versus beam brightness, highlighting the cluster of data points that resulted in the highest brightness values and lowest normalized emittance values. The data points have the same shape, colour, and marker code utilized in the previous figure.

Aside from including only those test configurations for which D12 = 10 mm, the most striking feature of Figure 4.20 is that all of the lens configurations that resulted in 100% beam transmission are grouped together (coloured in red). The data points showing 90% to 99.9% beam transmission (in pale yellow) are the nearest to the 100% transmission data points. It is difficult to tell from the plot, but the red data points overlap many of the pale yellow ones. A list of the test configurations that resulted in the highest beam currents is included in Table 4.6.

Table 4.6 List of the test configurations that resulted in the highest beam currents.

test #	V2 (V)	A2 (mm)	A3 (mm)	D12 (mm)	D23 (mm)	brightness $(mm.mrad)^{-2}$	normalized emittance (mm.mrad)	% of beam transmitted
test 306	-22500	12.5	10	10	16	1.731	0.760	100.0
test 324	-22500	12.5	11	10	16	1.710	0.765	100.0
test 297	-22500	11.5	11	10	16	1.693	0.769	100.0
test 279	-22500	11.5	10	10	16	1.668	0.774	100.0
test 288	-22500	11.5	9	10	16	1.632	0.783	100.0
test 252	-22500	10.5	10	10	16	1.613	0.787	100.0
test 99	-22000	12.5	9	10	16	1.580	0.796	100.0
test 270	-22500	10.5	11	10	16	1.579	0.796	100.0
test 315	-22500	12.5	9	10	16	1.555	0.802	100.0
test 25	-22000	9.5	11	10	12	1.554	0.802	100.0
test 54	-22000	10.5	11	10	16	1.549	0.803	100.0
test 261	-22500	10.5	9	10	16	1.548	0.804	100.0
test 70	-22000	11.5	9	10	12	1.538	0.806	100.0
test 63	-22000	11.5	10	10	16	1.537	0.807	100.0
test 88	-22000	12.5	10	10	12	1.522	0.810	100.0
test 36	-22000	10.5	10	10	16	1.513	0.813	100.0
test 72	-22000	11.5	9	10	16	1.510	0.814	100.0
test 81	-22000	11.5	11	10	16	1.501	0.816	100.0
test 45	-22000	10.5	9	10	16	1.486	0.820	100.0
test 43	-22000	10.5	9	10	12	1.482	0.821	100.0
test 34	-22000	10.5	10	10	12	1.480	0.822	100.0
test 108	-22000	12.5	11	10	16	1.468	0.825	100.0
test 412	-21500	12.5	10	10	12	1.460	0.828	100.0
test 430	-21500	12.5	11	10	12	1.433	0.835	100.0
test 61	-22000	11.5	10	10	12	1.431	0.836	100.0
test 97	-22000	12.5	9	10	12	1.421	0.839	100.0
test 369	-21500	10.5	9	10	16	1.408	0.843	100.0
test 423	-21500	12.5	9	10	16	1.404	0.844	100.0
test 79	-22000	11.5	11	10	12	1.391	0.848	100.0
test 387	-21500	11.5	10	10	16	1.390	0.848	100.0
test 385	-21500	11.5	10	10	12	1.381	0.851	100.0
test 377	-21500	10.5	11	10	8	1.379	0.852	100.0
test 333	-21500	9.5	10	10	16	1.375	0.853	100.0
test 90	-22000	12.5	10	10	16	1.374	0.853	100.0
test 106	-22000	12.5	11	10	12	1.371	0.854	100.0
					max	1.731	0.854	100.0
					min	1.371	0.760	100.0
					average	1.505	0.817	100.0

Optimal values of D12 and V2 for high and low beam current applications can be determined from the data in Figure 4.19 and Figure 4.20. The general observations are listed in Table 4.7. The adjective "relatively" implies a higher quality than "reasonably".

Table 4.7 List of the general trends for choosing the optimal values of D12 and V2 based on the intended application of the extraction lens system.

beam current **(range of beam transmitted)**	**D12 (mm)**	**V2 (V)**	**beam brightness**	**normalized emittance**
relatively low (50% to 59.9%)	7	-23000	reasonably high	low
moderately low (60% to 69.9%)	10	-23000	high	low
High (90% to 100%)	10	-22500 to -21500	relatively high	relatively low

The values of D12 and V2 listed in Table 4.7 are based on the range of values tested in this study.

As informative as it is to know of the trends that were observed to improve beam quality, one should be aware of lens configurations that tended to degrade the quality of the beam. A list of the thirty five lens configurations that resulted in the lowest values of beam brightness is shown in Table 4.8. The table includes the calculated values of normalized emittance and percent of beam transmitted. Maximum, minimum, and average values of the overall lowest beam brightness values, highest normalized emittance values, and percentages of beam transmitted are included at the bottom of the table.

The most significant trend from Table 4.8 is the value of D12 = 4 mm for all of the lens configurations. Of the four values of V2 tested, the values V2 = -21.5 kV and V2 = -22 kV appear in this table. The values A2 = 9.5 mm and D23 = 16 mm do not appear in the table.

Table 4.8 List of the tested lens configurations that resulted in the thirty five lowest quality beams. The entries are listed in order of decreasing beam brightness.

test #	V2 (V)	A2 (mm)	A3 (mm)	D12 (mm)	D23 (mm)	brightness $(mm.mrad)^{-2}$	ε_N (mm.mrad)	% of beam transmitted
test 92	-22000	12.5	9	4	8	0.213	1.508	48.4
test 83	-22000	12.5	10	4	8	0.211	1.508	48.1
test 38	-22000	10.5	9	4	8	0.206	1.487	45.6
test 65	-22000	11.5	9	4	8	0.205	1.500	46.1
test 82	-22000	12.5	10	4	12	0.205	1.570	50.4
test 100	-22000	12.5	11	4	12	0.204	1.587	51.4
test 64	-22000	11.5	9	4	12	0.202	1.553	48.8
test 101	-22000	12.5	11	4	8	0.201	1.555	48.7
test 73	-22000	11.5	11	4	12	0.198	1.573	49.0
test 29	-22000	10.5	10	4	8	0.196	1.529	45.7
test 56	-22000	11.5	10	4	8	0.196	1.545	46.7
test 379	-21500	11.5	10	4	12	0.192	1.615	50.1
test 55	-22000	11.5	10	4	12	0.192	1.592	48.6
test 74	-22000	11.5	11	4	8	0.190	1.566	46.5
test 388	-21500	11.5	9	4	12	0.189	1.616	49.3
test 406	-21500	12.5	10	4	12	0.188	1.672	52.5
test 352	-21500	10.5	10	4	12	0.182	1.596	46.5
test 424	-21500	12.5	11	4	12	0.181	1.676	50.9
test 28	-22000	10.5	10	4	12	0.181	1.613	47.0
test 47	-22000	10.5	11	4	8	0.180	1.586	45.2
test 415	-21500	12.5	9	4	12	0.179	1.670	49.9
test 37	-22000	10.5	9	4	12	0.176	1.636	47.0
test 370	-21500	10.5	11	4	12	0.172	1.656	47.1
test 397	-21500	11.5	11	4	12	0.168	1.703	48.7
test 361	-21500	10.5	9	4	12	0.167	1.695	48.0
test 46	-22000	10.5	11	4	12	0.165	1.671	46.1
test 416	-21500	12.5	9	4	8	0.157	1.788	50.1
test 407	-21500	12.5	10	4	8	0.146	1.867	50.8
test 380	-21500	11.5	10	4	8	0.145	1.820	47.9
test 425	-21500	12.5	11	4	8	0.142	1.890	50.8
test 389	-21500	11.5	9	4	8	0.141	1.839	47.8
test 398	-21500	11.5	11	4	8	0.139	1.897	49.9
test 362	-21500	10.5	9	4	8	0.132	1.860	45.7
test 371	-21500	10.5	11	4	8	0.127	1.953	48.4
test 353	-21500	10.5	10	4	8	0.127	1.916	46.6
					max	0.213	1.953	52.5
					min	0.127	1.487	45.2
					average	0.177	1.666	48.3

4.5 Position of Waist

The position of the waist, measured in millimeters relative to the beamstop (i.e., measured backwards from beamstop to source), is plotted against beam brightness in Figure 4.21, against normalized beam emittance in Figure 4.22, and against percent of beam transmitted in Figure 4.23. The beams of highest quality are those whose waist positions are relatively far from the beamstop, compared with all of the test configurations. Although waist positions farthest downstream are preferred by rule of thumb because the beam, of known size at the waist, drifts over a shorter distance, it is the beam size that dictates the usefulness of the beam. A beam with smaller normalized emittance and whose waist is farther from a downstream transport system is preferred to a beam of large normalized emittance with a waist located farther downstream, closer to the next transport system. Refer to Table 4.5 for the tested parameter values that gave rise to the highest quality beams.

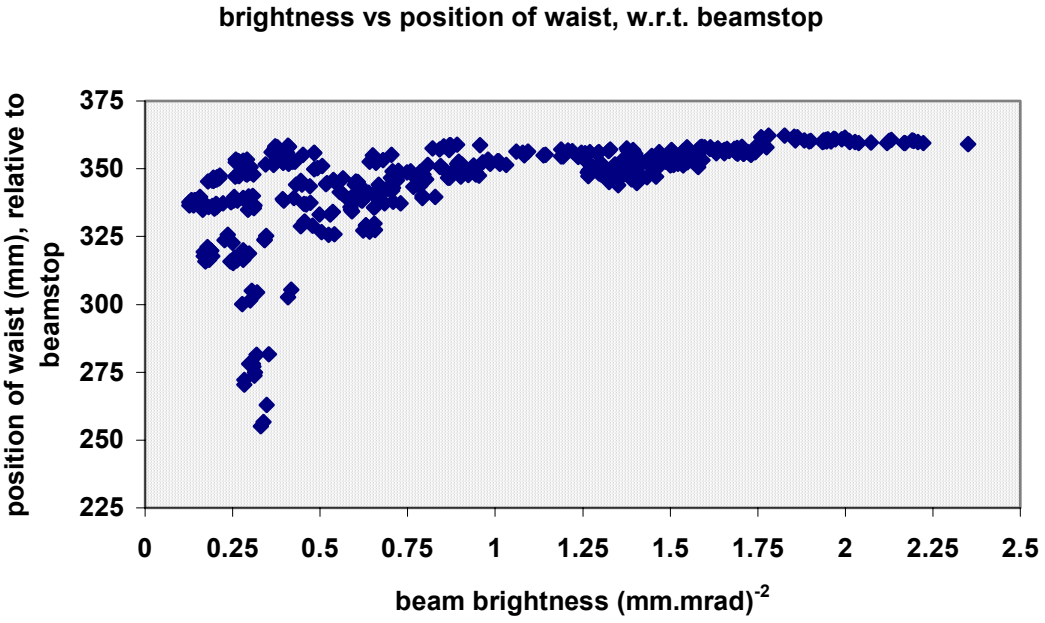

Figure 4.21 Plot of beam brightness versus position of beam waist. The test configurations that resulted in the brighter beams had beam waists located farther from the beamstop.

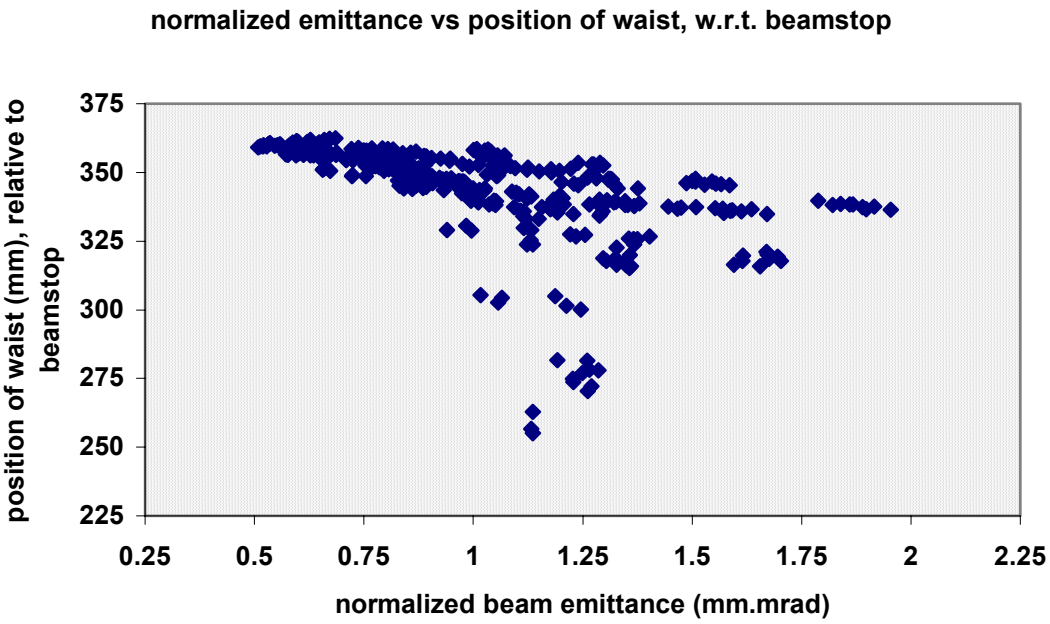

Figure 4.22 Plot of normalized beam emittance versus position of beam waist. The lens configurations that resulted in the lowest normalized emittance values had beam waists located farther away from the downstream beamstop.

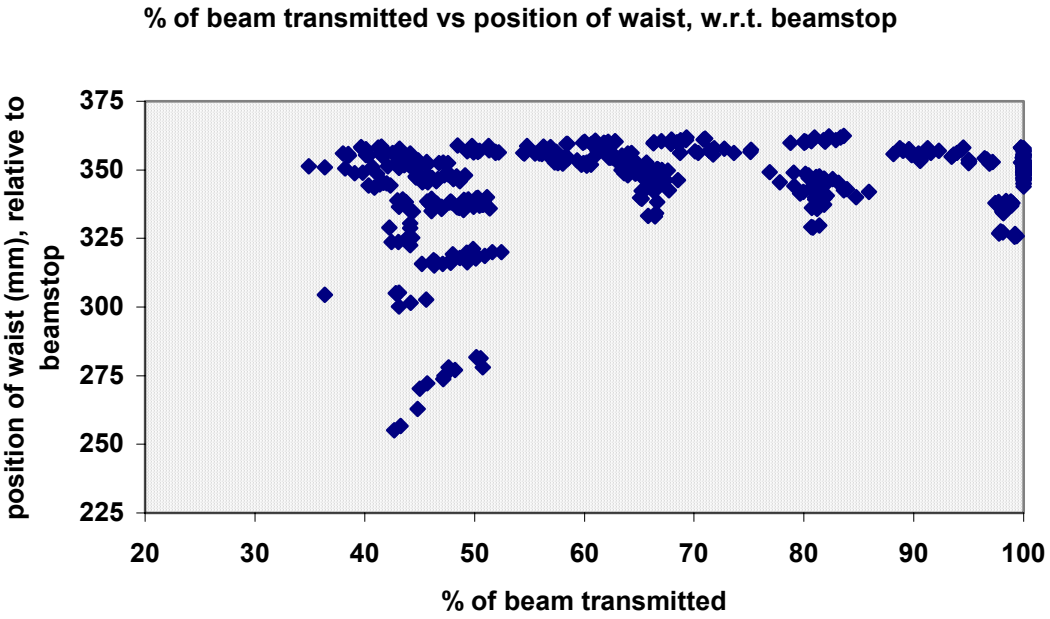

Figure 4.23 Plot of percent of beam transmitted versus position of beam waist. The lens configurations that resulted in all but the lowest percentages of beam transmitted had beam waists located farther away from the downstream beamstop.

4.6 Summary of Observations

To impart a visual sense of the beam characteristics, selected ion trajectories are presented here. Ion trajectories for each test run were calculated by SIMION and displayed on the computer monitor while the simulations were underway.

The lens configurations and values of brightness, normalized emittance, and beam current that resulted in the brightest beams are reiterated in Table 4.9. These configurations are suited to moderately low beam current applications. The ion trajectories of these five test configurations have similar beam characteristics. Notably, the waist position and the amount of beam lost as it leaves the shoulder electrode are characteristic of these lens configurations. The ion trajectory of test 215, representative of the lens configurations resulting in the highest observed beam brightness values, is shown in Figure 4.24.

Table 4.9 The five lens configurations that resulted in the brightest beams.

test #	V2 (V)	A2 (mm)	A3 (mm)	D12 (mm)	D23 (mm)	brightness $(mm.mrad)^{-2}$	normalized emittance (mm.mrad)	% of beam transmitted
test 215	-23000	12.5	11	10	8	2.351	0.508	60.7
test 206	-23000	12.5	9	10	8	2.222	0.513	58.5
test 179	-23000	11.5	9	10	8	2.207	0.521	59.9
test 143	-23000	10.5	10	10	8	2.196	0.532	62.2
test 116	-23000	9.5	10	10	8	2.191	0.535	62.8

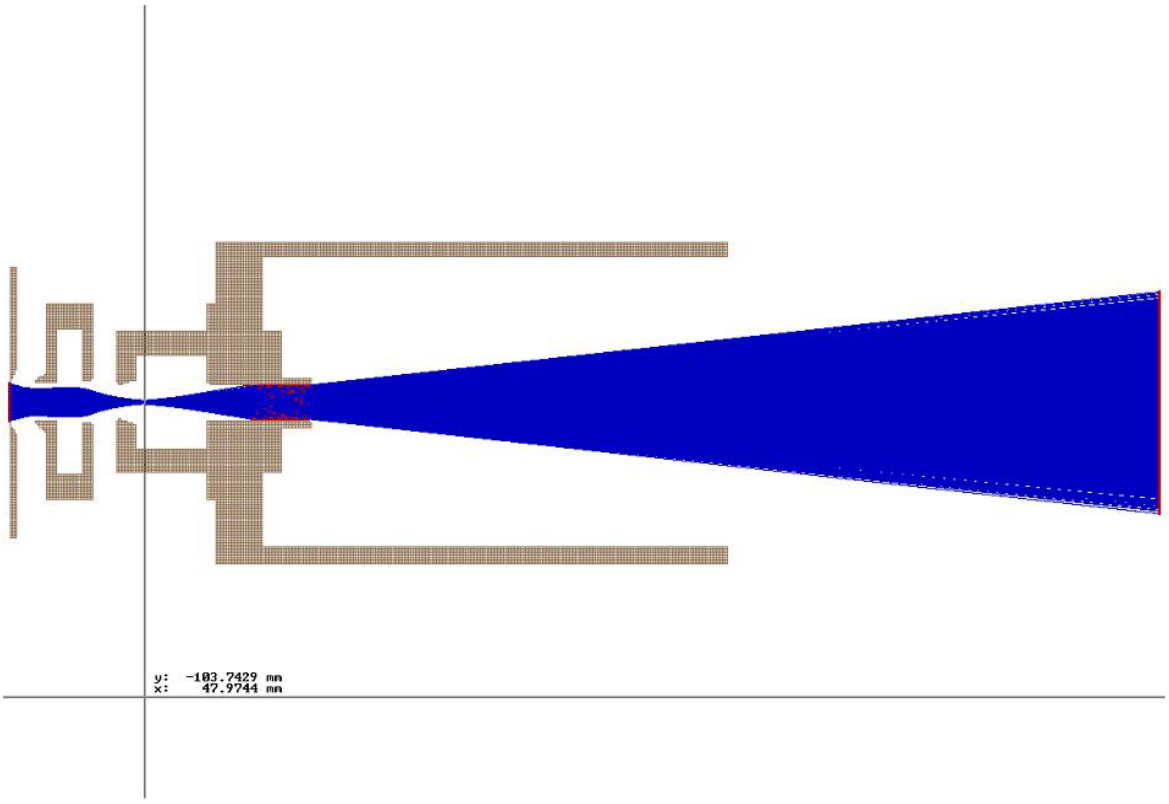

Figure 4.24 Ion trajectory of test 215, representative of the lens configurations that resulted in the highest beam brightness and lowest normalized beam emittance, and moderate beam current (~60%).

The lens configurations and values of brightness, normalized emittance, and beam current that resulted in the highest beam currents are reiterated in Table 4.10.

Table 4.10 The five lens configurations that resulted in the highest beam currents.

test #	V2 (V)	A2 (mm)	A3 (mm)	D12 (mm)	D23 (mm)	brightness $(mm.mrad)^{-2}$	normalized emittance (mm.mrad)	% of beam transmitted
test 306	-22500	12.5	10	10	16	1.731	0.760	100.0
test 324	-22500	12.5	11	10	16	1.710	0.765	100.0
test 297	-22500	11.5	11	10	16	1.693	0.769	100.0
test 279	-22500	11.5	10	10	16	1.668	0.774	100.0
test 288	-22500	11.5	9	10	16	1.632	0.783	100.0

While the waist position of this set of lens configurations is similar to that of the previous set, no beam is lost as it leaves the shoulder electrode, giving rise to 100% beam transmission, the common factor of the lens configurations listed in Table 4.10. The ion trajectory of test 306, representative of the beam characteristics of these five test configurations, is shown in Figure 4.25.

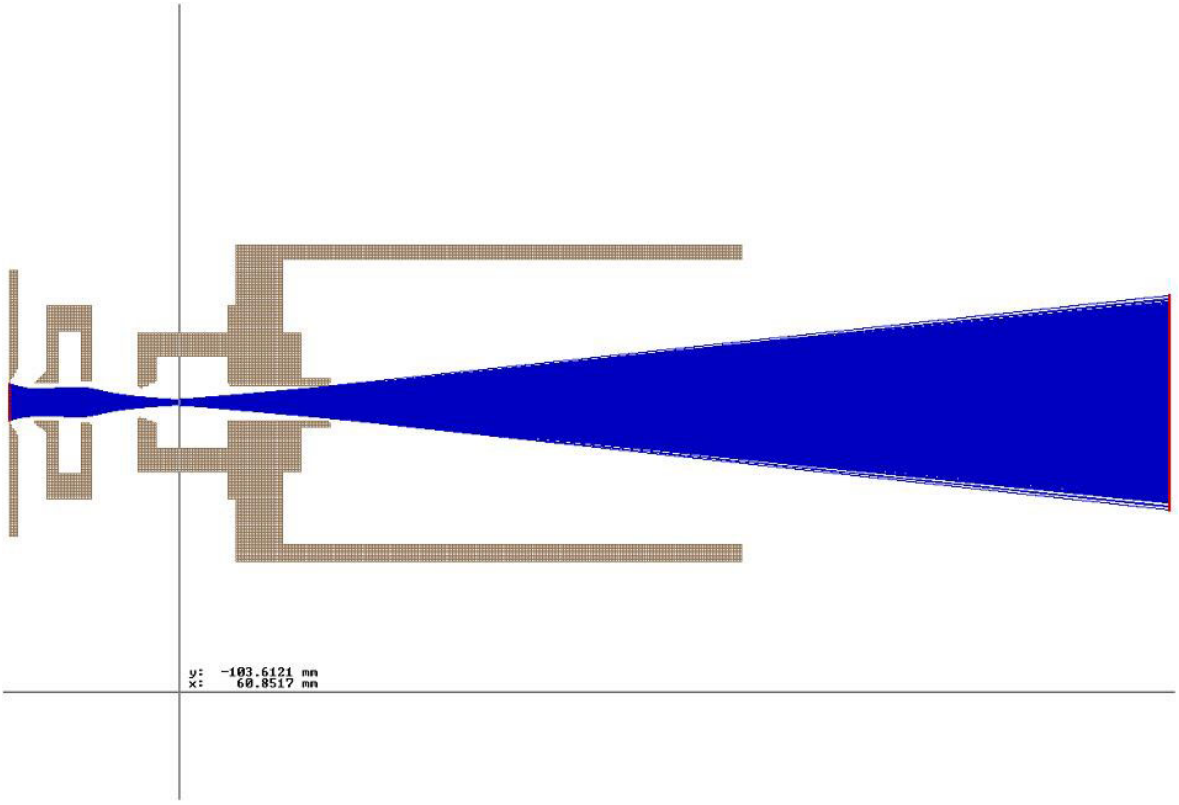

Figure 4.25 Ion trajectory of test 306, representative of the lens configurations that resulted in the highest beam brightness and lowest normalized beam emittance for a beam current of 100% transmission.

The lens configurations and values of brightness, normalized emittance, and beam current that resulted in the lowest quality beams are reiterated in Table 4.11. The ion trajectory of test 353, shown in Figure 4.26, is characteristic of the lens configurations listed in the

table below. In particular, the waist position is farther downstream, and the beam is more divergent and sparser than those shown in Figure 4.24 and Figure 4.25. Beam loss occurs at both the extraction and shoulder electrodes.

Table 4.11 The five lens configurations that resulted in the lowest quality beams.

test #	V2 (V)	A2 (mm)	A3 (mm)	D12 (mm)	D23 (mm)	brightness $(mm.mrad)^{-2}$	normalized emittance (mm.mrad)	% of beam transmitted
test 353	-21500	10.5	10	4	8	0.127	1.916	46.6
test 371	-21500	10.5	11	4	8	0.127	1.953	48.4
test 362	-21500	10.5	9	4	8	0.132	1.860	45.7
test 398	-21500	11.5	11	4	8	0.139	1.897	49.9
test 389	-21500	11.5	9	4	8	0.141	1.839	47.8

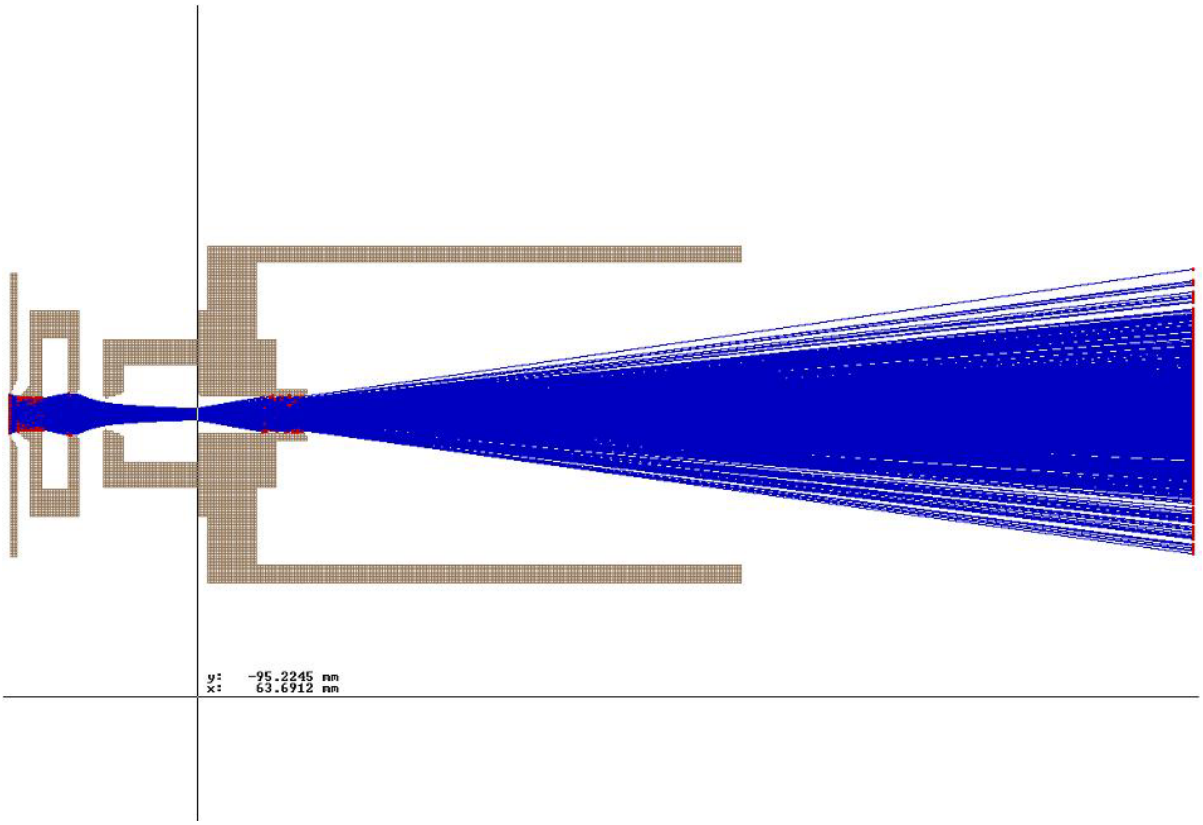

Figure 4.26 Ion trajectory of test 353, representative of the ion trajectories of lens configurations that resulted in the lowest quality beam. Beam quality was based on the value of beam brightness.

Note that the lens configurations listed in Table 4.9 all used the same parameter values V2, D12, and D23. The same is true of the lens configurations listed in Table 4.10 and Table 4.11.

[This page intentionally left blank.]

Chapter 5

Conclusions and Future Work

A simulation model of the extraction lens systems for H^- volume cusp ion sources was designed using a software program called SIMION [1]. At every stage in the design process, considerations were made to ensure that the simulation model resembled the actual system as closely as possible. Nominal dimensions were utilized as much as possible: for instance, nominal dimensions were used for the outer diameters of the model lenses.

The study of variations on the nominal lens configuration, the topic of Chapter 3, showed that beam quality could be improved from that obtained from the nominal configuration by changing a single test parameter value. The highest beam brightness values were measured of test configurations with the following independent values: smaller V2, larger D12, and larger D23. Of these three parameters, varying V2 would be the most practical change to make to the nominal system. Varying the value of A3, while holding the other parameter values constant at the nominal values, had no effect on beam quality. The nominal value of A2 was preferable over the other, larger values of A2 tested. In fact, these larger values of A2 degraded the beam quality the most.

Test parameters V2 and D12 affected beam quality in a global manner (i.e., largely independent of other parameter values). For the range of test parameter values tested, increasing D12 had the effect of increasing beam brightness, decreasing normalized beam emittance, and generally increasing beam current, regardless of the values of the other test parameters. For high beam currents, larger, more positive values of V2 resulted in relatively high beam brightness and relatively low normalized emittance. For low beam

currents, smaller, more negative values of V2 resulted in high beam brightness and low normalized emittance.

Prior to working on this study, it had been assumed that the energy of the particles was 25 keV upon reaching the beamstop in the actual extraction lens system. The results of this study indicate that ion energy decreases as they are transported through the system.

This study was limited by the ranges of parameter values tested. While informative trends were observed, both locally to the nominal system and globally, the ranges over which these trends hold are not known. Future work might include testing the parameters over a wider range of values.

Several assumptions and approximations were made, and discussed in Chapter 2, when the model of the extraction lens system was formulated. Future work might entail studying the effects of varying the curvature of the plasma meniscus; modeling the magnetic filter designed to strip electrons out of the extracted particle beam; modeling the steering magnets used to realign the beam of H^- ions downstream of the magnetic filter. Space charge repulsion between the like-charged particles in the beam was ignored. The assumption that ion-ion interaction could be ignored will not be discussed. SIMION claims to have the ability to account for space charge repulsion but this aspect of the problem was beyond the scope of this study.

The only apparent short coming of this study was that the downstream aperture of E2 was not varied, causing loss of beam for many of the lens configurations that used A2 > 9.5 mm. The downstream aperture was held at its nominal value of 14 mm in diameter. A prudent approach would have been to increase this downstream aperture by the same amount as A2, the upstream aperture of E2. Possibly the lack of trends observed upon varying the test parameter A3 were a direct result of holding the downstream aperture size of E2 constant while the size of the upstream aperture was increased. Should this study be developed in the future, varying the sizes of the downstream apertures of both E2 and E3 ought to be a priority.

Appendix A

A Quick Guide to SIMION 3D, Version 7.0

A product of Idaho National Engineering and Environmental Laboratory (INEEL), SIMION 3D, Version 7.0 is software developed to simulate electrostatic and static magnetic devices used to accelerate, transport, and otherwise manipulate beams of charged particles. This section is intended to provide general guidance in developing a system of cylindrically symmetric electrostatic lenses and simulating a user defined beam of ions interacting with the system. Refer to [1] for the complete user manual provided by INEEL. You should work through the demos included in the SIMION package because these were designed to sequentially introduce you to the basic steps involved in modeling an electromagnetic transport system. It is assumed that you have read section 2.2 and are familiar with SIMION terminology.

A.1 An Introduction to SIMION

The custom graphical user interface of SIMION is unique to its purpose and requires little time to become familiar with it. The software is constructed such that the graphical user interface (GUI) interacts with what is referred to as a potential array. A potential array (PA) is a three dimensional array of points used to define the geometry of electrostatic devices. The buttons in the main window act on a PA, allowing new ones to be created, and existing ones to be modified, refined, and viewed, to name a few actions.

SIMION uses its own file manager GUI to access the file directory. SIMION expects to find all of the files associated with a PA in the same directory as the parent PA file (the parent file is the one that defines the geometric and electric boundaries of the modeled

electrodes). Proceeding otherwise is not recommended; the consequences are unknown. Creating project directories to which one or several related PAs are saved is very important. In addition to pleasing SIMION, it helps to maintain order in project development. A view of Windows File Manager (not the SIMION file manager GUI) is shown in Figure A1. The "Sim7" folder is created when SIMION is installed. The SIMION demonstration files are in this folder (the demo subfolders, prefixed by an underscore, can be seen in Figure A1). Project files should also be kept in subfolders in this directory. For example, the files associated with this study were kept in the subfolder named "test lenses" and contained all of the SIMION files associated with the parent file, "lenses.PA#".

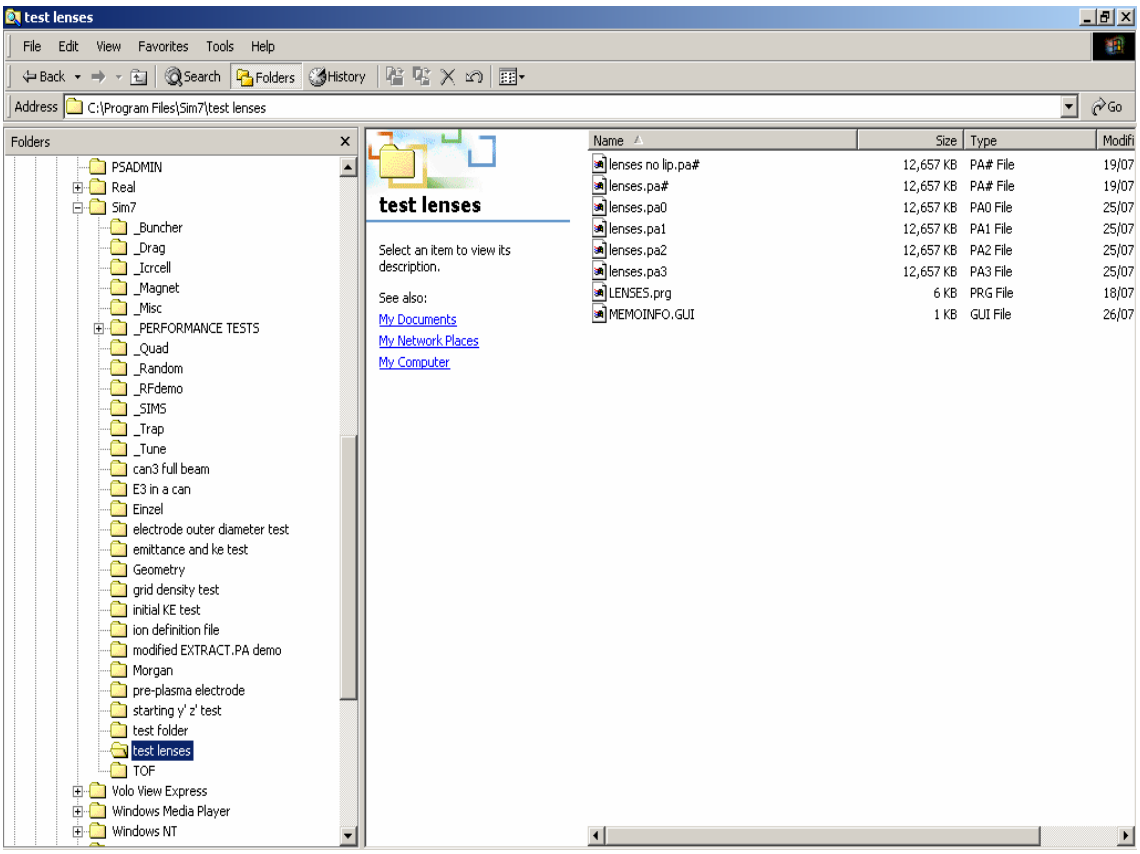

Figure A1 Directory for SIMION files. It is good practice to keep all of the files associated with a project in a single file. SIMION expects this and it helps to keep projects organized.

A project folder contains:

- the .PA# file that defines the electrode geometry;
- the .PA(?) files where (?) = 0 to 30, depending on how many electrostatic devices are in the PA; SIMION creates these when it refines the .PA# file;
- the .FLY or .ION file which contains information about the ions: their mass, charge, kinetic energy, starting position, and direction;
- the .PRG file, if a user defined program is used in the project.

Here is a brief overview of the steps involved in creating a PA and simulating a test run. Details of how to implement these steps are the topics of the remaining sections. From SIMION's main screen, potential arrays are created or modified. Once a PA is created or modified, the PA is loaded into the ion optics simulation workbench. In the workbench view, the electrodes defined in the PA are shown in two dimensions, with the option of three dimensional viewing. From within the simulation workbench, you can assign voltage potentials to the electrodes in the PA and defined ions. More specifically, details of ion mass, charge, kinetic energy, and starting position and direction can be defined, as it is unlikely that the default values accurately represent the ion beam intended for the system being modeled. When prompted to do so, SIMION simulates ion transport in the model system and draws the ion trajectories on the screen.

The following sections contain figures of different views you see when using SIMION. These figures are printed in greyscale, although the accompanying text will make reference to the colours of various buttons and regions in the figures. It is assumed that you are concurrently working with SIMION and correlating the material enclosed herein to the software.

A.2 Creating a New PA

The main SIMION screen is a menu that lists all of the actions that can be invoked on a PA. The main menu is shown in Figure A2.

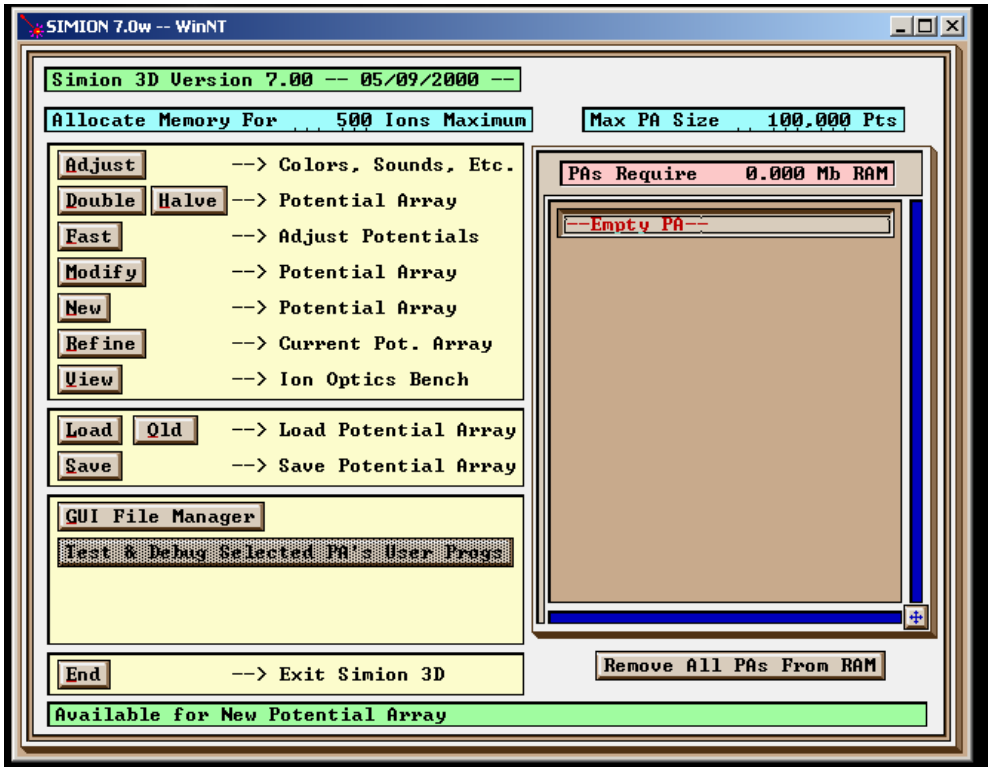

Figure A2 Main menu. The buttons on the left are all of the possible actions that can be invoked on a PA. The text to the immediate right of the buttons describes each button's action. The brown panel on the right is a list of the PAs loaded into RAM. In this figure, the list is empty.

The brown panel that is the right half of the main menu screen contains the list of PAs loaded into RAM. To invoke an action listed in the buttons on the left side of the main menu screen, the desired PA must be selected from the list on the right (the PA is selected when the letters are red). The list shown in Figure A2 is empty. To remove the PAs from the list (all or nothing), select the button under the PA list. As the button says, selecting it will "Remove All PAs From RAM" (i.e., you can not selectively remove PAs

from RAM). To access these PAs again, they must be reloaded via the "Load" button in the main menu. Remember to ensure that the "Empty PA" button is depressed to load a PA into a new section of RAM. If an existing PA is selected (letters in red) in the list, it will be overwritten in the RAM. (The PA will still exist on the hard drive but will need to be reloaded to access it.)

The blue dialog box in the upper right hand corner of the main menu screen contains the number of points that will be allocated to a new PA. If the expected size of the array is large, this number should be increased before clicking on the "New" or "Modify" buttons in the main menu.

To create a new PA, make sure that the "Empty PA" button is depressed (letters in red) in the PA list on the right, and select the "New" button from the main menu. The Modify view will appear on the screen with a blank PA (white area with green points representing each of the points in the array). These green points are non-electrode points. They will become black points once they have been defined as electrode points. The Modify view shown in Figure A3 is of a PA with electrodes already defined.

A.3 Drawing Potential Arrays

The Modify view is shown in Figure A3. The rightmost group of buttons in the top panel should be set first, as these define the size of the PA (upper limit set by the amount of RAM reserved for the PA from the main menu view), the type of points that make up the array (electrode points or magnets), and the symmetry (spherical, cylindrical, etc). A caveat of changing these settings is that the cursor must stay in the box enclosing these buttons until the “Set” button is pressed. If the cursor moves out of the enclosing box, the changes will not be made.

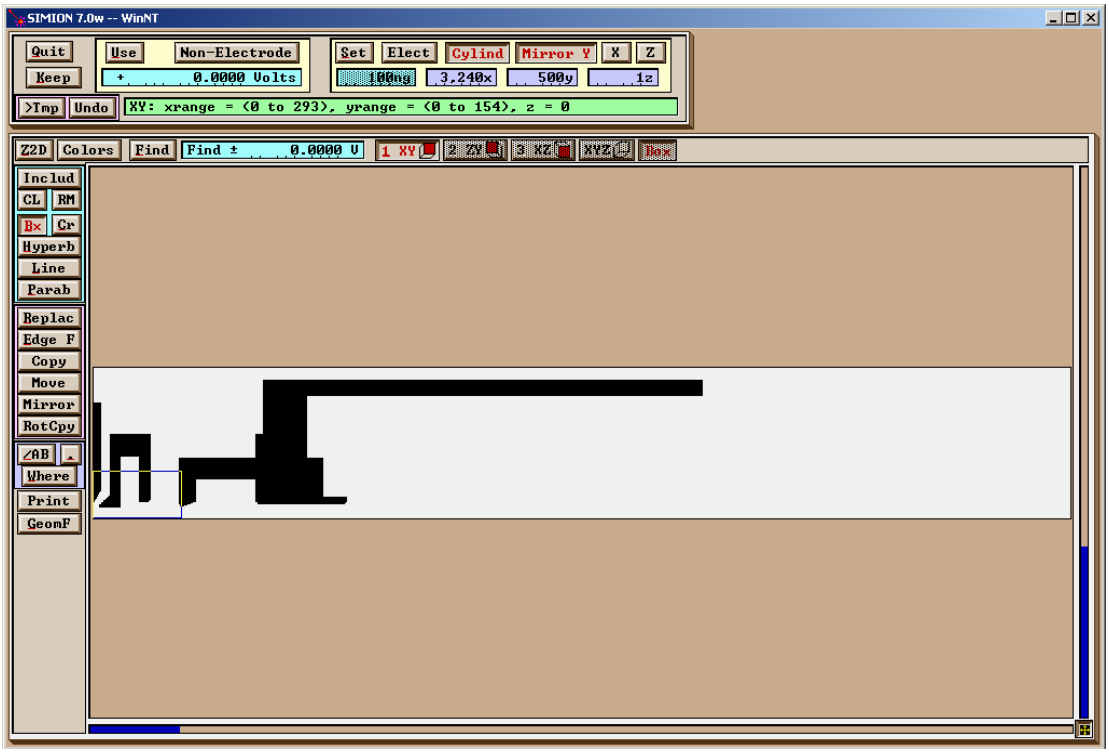

Figure A3 Modify view. This is where PAs are created and modified. This view is accessed from the "New" or "Modify" buttons in main menu.

The five buttons in the rightmost group of buttons in the top panel of the Modify view are shown in Figure A3. To create electrodes with cylindrical symmetry, toggle the second button from the left to “Elect” to select electrode points, toggle the third button from the right to select “Cylind” and select “Mirror Y” with the fourth button for cylindrical symmetry mirrored about the y axis. With these settings, y and z are the transverse directions, and x is the longitudinal direction. Note that in accelerator physics, z is the longitudinal direction, by convention. You are responsible for keeping the axis directions in mind if you utilise the latter convention. The size of the PA in the x and y directions can be varied, but the size in the z direction must be set at one. A 3D volume is created by SIMION when an instance of the PA is loaded into the simulation workbench. In the simulation workbench view, SIMION will rotate the geometric profile of the electrodes, drawn in two dimensions, about the x axis to produce a three dimensional cylindrical model.

To create a .PA# file with several electrodes, in which the voltage potential of each electrode can be modified after the .PA# file is created, toggle the "Non-Electrode" button in the top, central panel to "Electrode" and set the voltage in the dialog box below it to 0 V. Use the buttons down the left side of the Modify view (Figure A3) to select the basic geometrical shape of the first electrode. Then place the mouse cursor on the PA and draw an outline of the electrode by clicking the left mouse button on a starting point and dragging the cursor to an end point.

The buttons "Bx", "Cr", "Hyperb", "Line", and "Parab" define basic geometric shapes: box, circle, hyperbola, line, and parabola, respectively. If the basic shapes provided do not represent the geometry of the electrode, select the "Line" button to draw the electrode. To join several line segments, draw the first line by clicking the left mouse button on a point and dragging the mouse to an end point (diagonal lines are acceptable). To draw the next line, the cursor must be placed on the end point of the existing line and the new line drawn in by clicking the left mouse button at the said end point and dragging in a new direction. (Clicking a mouse button on a point that is not the end point of an existing line will cause the existing line to be erased.) The lines must enclose a group of points in order to be considered an electrode. Once the electrode shape is drawn, and the "Electrode" button and 0 V are selected, select the "Replace" button to fill the shape with electrode points of 0 V. The first button of the group of buttons on the left can be toggled between "Includ" and "Exclud" to select whether to replace the points either inside (included in) or outside (excluded from) the shape drawn in the PA.

To create a second electrode, change the voltage potential in the dialog box under the "Electrode" button to 1 V and draw the shape of the new electrode using the mouse and the buttons on the left. Replace the points inside this shape by 1 V electrode points by selecting "Replace" from the buttons on the left. If a third electrode is desired, change the voltage potential to 2 V, draw the shape and replace the points, and so on for up to thirty electrodes. The important thing to remember is that the electrode points that make up an electrode must all have the same voltage potential.

To get rid of electrode points that were drawn in error, toggle the "Electrode" back to "Non-Electrode" and set the voltage potential back to 0 V. Then draw a shape around the points that you wish to convert back to non-electrode points and select the "Replace" button. The points will turn green to indicate that they are again non-electrode points.

To be able to change the voltage potentials of the electrodes from within the simulation workbench, the electrode points in the first electrode must have zero volts, those in the second electrode 1 V, those in the third electrode 2 V, and so on. This preliminary chronological voltage assignment is how SIMION knows which points in the PA belong to a given electrode when the PA is refined. Up to thirty electrodes can be included in a PA in this manner. The voltage potentials must have integer values starting with zero volts and must increase sequentially to n – 1, where n is the number of electrodes in the PA. Once the PA is refined and an instance of the PA is loaded into the simulation workbench, the electrodes can be assigned their actual voltage potentials, which will be discussed momentarily.

Press “Keep” to exit the Modify view and keep the newly defined electrode geometries, or to keep modifications made to existing ones, and return to the Main menu. (If “Quit” is selected, SIMION exits the Modify view without keeping any changes made to the PA.) The name of the PA in the PA list will be outlined in a red box to indicate that the PA has been changed and the changes have not yet been saved. To save the creation or modifications, press “Save” in the Main menu. In the “Save PA” dialog box, enter a new name or confirm the existing name. The file extension must be .PA# in order for SIMION to refine the PA and to be able to change the voltage potentials of the electrodes after they are created.

A.3.1 Modifying an Existing PA

An existing PA is modified by loading the PA into RAM and accessing the PA electrode and non-electrode points in the Modify view. To load an existing PA into RAM, depress the "Empty PA" button and select the "Load" button from the main menu. This action will open the Modify view. The geometry of electrodes in the existing PA will appear in the PA area, and will look similar to the view shown in Figure A3. Modifications can

now be made to the existing PA, such as shape, voltage potential, symmetry, etc. Remember to press "Keep" to keep the changes and, once in the Main menu, to save these changes. Normally, only a small region of a large PA can be seen at a time. To see the entire PA, as shown in Figure A3, place the mouse on the blue square in the bottom right corner of the window. Press and hold either button and move the mouse around to see what this does.

A.4 Refining a PA

Refining is an iterative numerical process in which the electric field intensity between electrodes is solved by the Runge-Kutta method [1]. By calculating the electric field intensity at every point in the potential array that is not defined as an electrode point, SIMION can simulate ion trajectories through a system of electrostatic devices. Saving the potential array as a .PA# file, and then refining it, allows you to set the voltage potential of each electrode in the PA to any value. Hence, the voltage potentials are not fixed, meaning that you can change their values at any time during simulation runs.

With the .PA# file saved and the PA name selected in the PA list in the main menu view, select the “Refine” button from the buttons in the main menu. The Refine view, shown in Figure A4, will appear on the screen. The two blue text boxes site the file name to be refined and describe the symmetry and size of the PA. The four green text boxes define parameters of the numerical method used to refine the PA that govern quality of the refining process. The default values are adequate for refining most PAs. Refer to [1] for details about these parameters and “Skipped Point Refining”. Once the refining is completed, SIMION returns to the main menu.

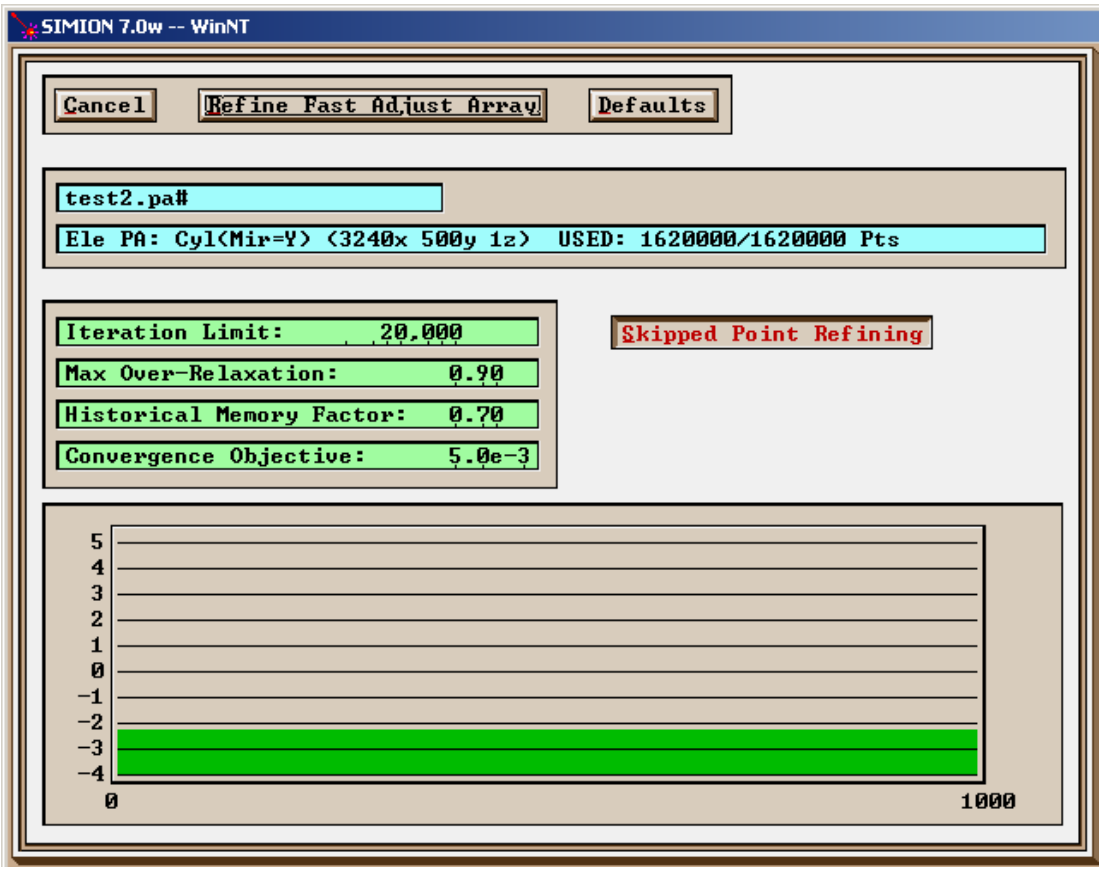

Figure A4 Refine view. The default settings are adequate for refining most PAs. Select the "Refine Fast Adjust Array" button, the middle button at the top of the screen.

Select the "Refine Fast Adjust Array" button, the middle button at the top of the screen, to start the refining process. Red bars will appear in the bottom portion of the screen to indicate the progress of the iteration process. The term "fast adjust" refers to being able to change the voltage potentials of the electrodes from within the simulation workbench. The alternative is to set the voltage potentials of the electrodes at the time these are created, forfeiting the ability to change the potentials from within the simulation workbench.

A.5 Simulating the Ion Trajectories

With the PA selected in the list of PAs in RAM (letters in red), select the “View” button from the main menu. The ion optics workbench, also referred to as the simulation workbench, is accessed, with an instance of the PA loaded into the viewing area of the workbench. The workbench view is shown in Figure A5.

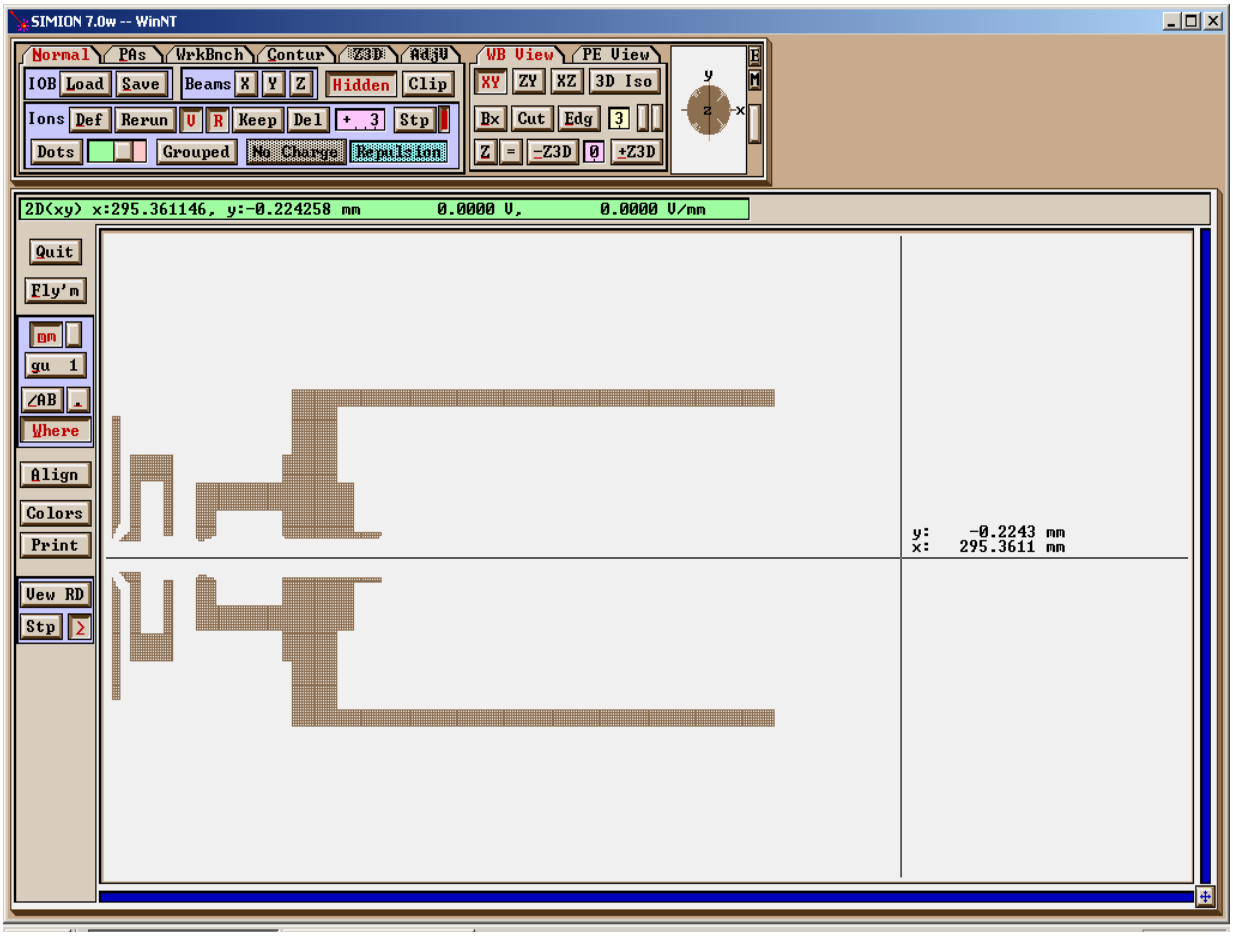

Figure A5 Workbench view. Aspects of a simulation run can be defined by accessing the control buttons associated with each of the tabs at the top of the screen. The “Normal” tab provides access to defining the ions and the “PAs” tab provides access to setting the voltage potentials of the electrodes in the PA.

The tabs at the top of the workbench view provide access to different groups of controls that set up different aspects of the simulation workbench. Some of the tabs are greyed, indicating that they cannot be accessed with the current settings. The first two tabs, which are always accessible, are the most important. The "Normal" tab provides access to defining the ions. The "PAs" tab provides access to setting the voltage potentials of the electrodes in the PA. In Figure A5, the "Normal" tab is selected: the tab label has red lettering. Recall from the discussion in section 2.3.1.1, the grid density of the PA that best models a system typically differs from one-to-one scaling. The scale at which the PA is created needs to be defined in the simulation workbench. Define the scale factor by selecting the "WrkBnch" tab (third tab from left at top of workbench view) and change the scale factor in the appropriate text box. For example, the PA created in this study had one-to-eight scaling, so the scale factor was set to 0.125 mm/gu (gu = grid unit).

A.5.1 Fast Adjusting the Electrode Potentials

The voltage potentials of the electrodes can be fast adjusted because the PA was saved as a .PA# file as opposed to a .PA file. In the latter, the voltage potentials of electrodes are fixed.

Select the "PAs" tab (second tab from left at top of workbench view) to access a different set of control buttons. From these, select the "Fadj" button. The fast adjust view will appear, as shown in Figure A6. The fast adjust view has three buttons and as many text boxes as there are electrodes in the PA (up to thirty).

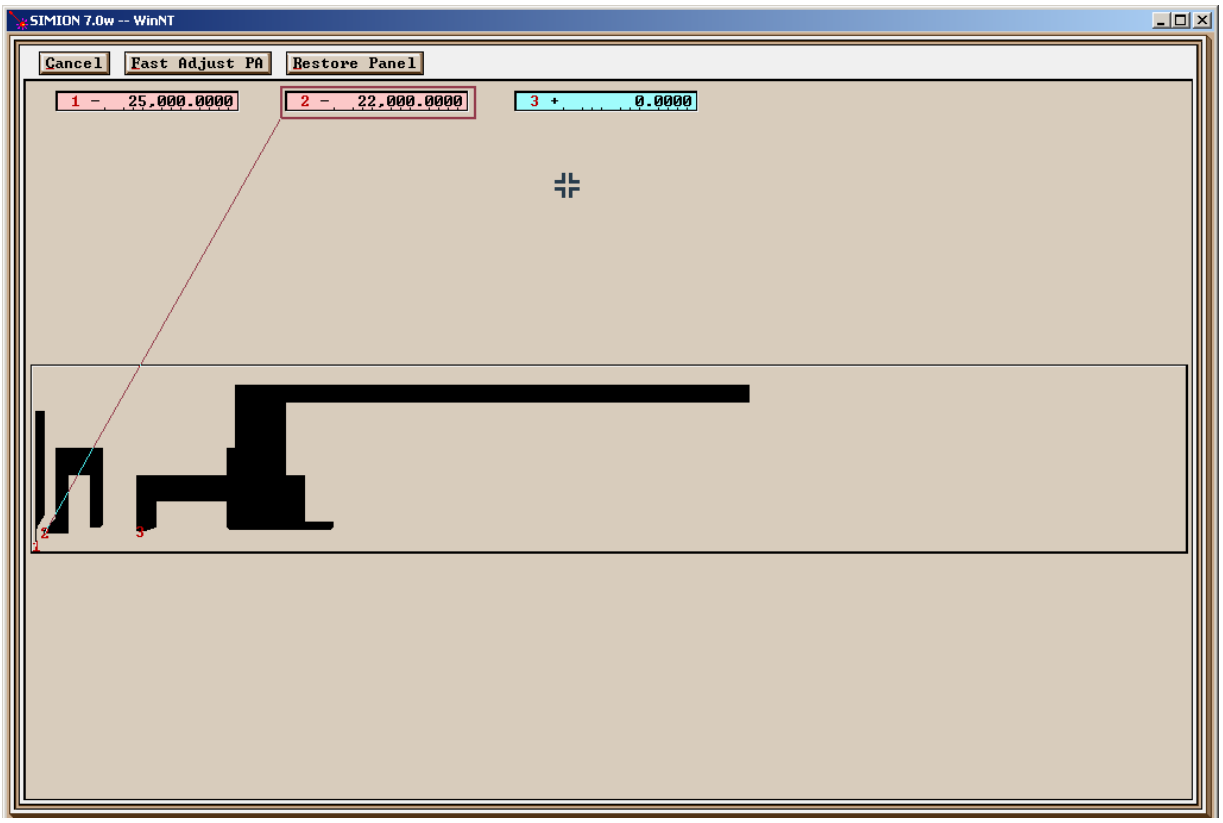

Figure A6 Fast adjust view. The electrodes and their corresponding voltage potentials are associated by the numbers in red. To edit the potential voltage of an electrode, place the cursor in the appropriate text box and use the arrow keys and number pad on the keyboard to change the value. The selected text box and its associated electrode will be joined by a red line and the text box lined in red.

To adjust an electrode's voltage potential, click on the appropriate text box (electrode and text box associated by numbers). The text box will be outlined in a red box and a line will join the electrode and text box. In Figure A6, the second electrode is selected. Use the arrow keys and number pad of the keyboard to change the value of the voltage potential. The values will be highlighted in blue when the fast adjust view is first accessed. An edited value will then be highlighted in red. Press on the "Restore Panel" button to restore the original values. To accept the changes made to the values, press on the "Fast Adjust PA" button. To exit this view without making any changes, press on the "Cancel" button. Pressing on the first or second button will cause SIMION to return to the workbench view, Figure A5.

A.5.2 Defining the Ions

From the workbench view, select the "Normal" tab, if it is not already selected, then select the "Def" button in the Ions group of control buttons. The Ion Definition panel will appear on the screen, as shown in Figure A7. This panel has two tabs: one for defining ions by group and the other for defining the ions individually. The "Define Ions by Groups" tab is selected in Figure A7, as was done in this study. Two common particles, electrons and protons, are predefined and can be selected to populate the beam by pressing on either the "Use Electrons" or "Use Protons" button found near the top of the panel.

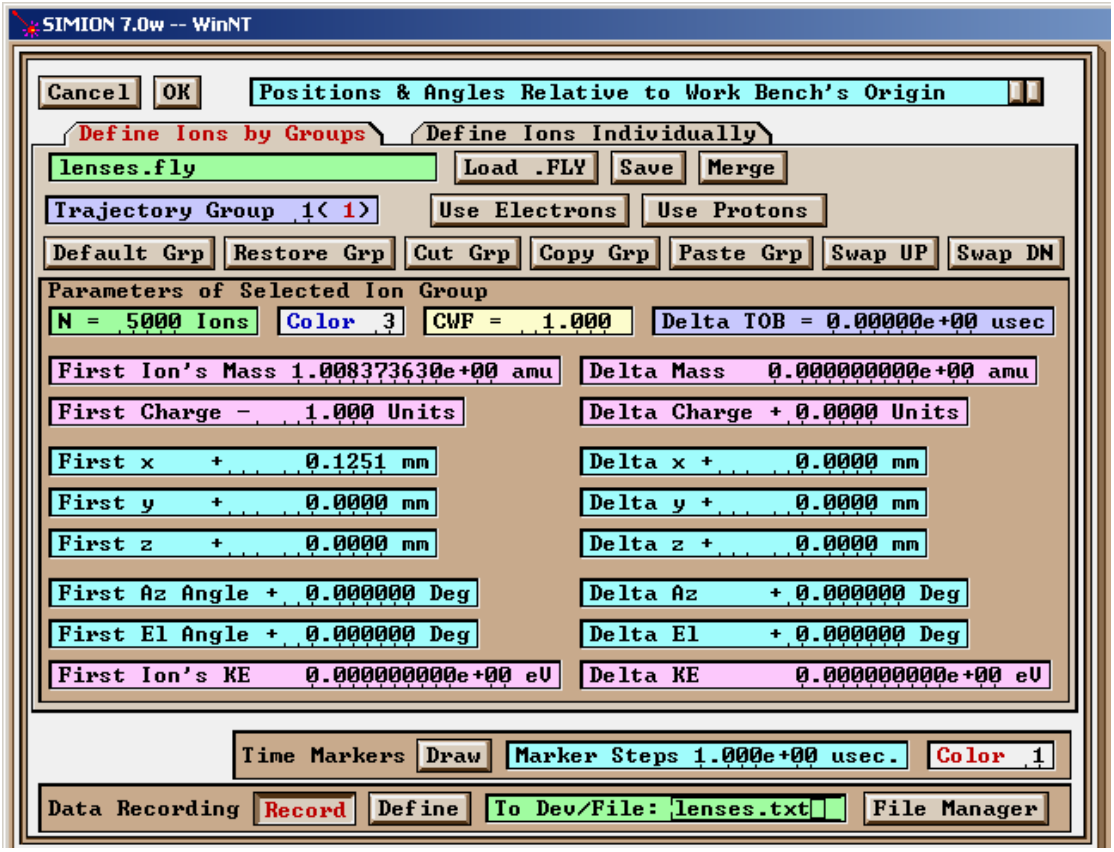

Figure A7 Ion definition panel. The number of ions, ion mass, charge, starting position and direction, and initial kinetic energy are some of the parameters that can be defined in this panel.

Of great practical use is the ability to save ion definitions and load these again in subsequent simulation sessions. If an ion file is loaded, the file name appears in the green text box in the upper left corner of the ion definition panel (in Figure A7, the file name is "lenses.fly"). An ion file has the extension .FLY if the ions are defined in a group or .ION if the ions are defined individually. Press the “Load .FLY” button to the right of the ion file name to load an existing ion definition file into the workbench. Press the “Save” button to the right of the “Load .FLY” button to save the current ion definition. The file manager GUI is accessed by pressing on “Save”, from which you should select the project directory (if this is not already done) and enter the file name.

In the “Parameters of Selected Ion Group” panel in the Ion Definition panel (Figure A7), such parameters as the number of ions, colour of the ions, ion’s mass, charge, initial kinetic energy, and starting position and direction can be defined. The maximum number of ions is limited by the value set in the main menu view, which must be set before entering the workbench view. To change the maximum number of ions once one is already in the workbench view, any changes made to the workbench settings (voltage potentials of PAs, ion definitions, scaling of workbench view, etc) should be saved before exiting the workbench view to return to the main menu. Saving the workbench settings will be discussed shortly. From the main menu view (Figure A2), edit the value in the “Allocated Memory For…” text box at the top of the main menu view. Now return to the workbench view by selecting the appropriate PA (if it is not already selected) and pressing “View”. Return to the Ion Definition panel, Figure A7, accessed from the “Normal” tab and by pressing “Def” in the Ions group of control buttons. The maximum number of ions, N, can now be increased to the new maximum if desired.

The Charge Weighting Factor (CWF) and Time of Birth (Delta TOB) text boxes were not used in this study. Note that the remaining sixteen text boxes in the “Parameters of Selected Ion Group” panel are arranged in two columns. The text box entries in the first column all begin with the word “First” while the text box entries in the second column all begin with the word “Delta”. This structure allows you to define the parameters of the first ion in the group and to create the subsequent ions that differ by an amount delta from the previous ion. If the delta value of a particular parameter is set to zero, the subsequent

ions will have the same parameter value as the first. The starting positions x, y, and z can be given in mm or grid units (gu), by toggling the buttons in the very top right corner of the Ion Definition panel. While it may not be obvious from the words entered in the text box directly to the left of the buttons, pressing on these buttons toggles the units of the x, y, and z text boxes between mm and gu.

The starting direction of the ions is specified in terms of azimuth ("Az") and elevation ("El") angles. With x being the longitudinal direction, and y and z the transverse directions, the elevation angle represents y', divergence in the y direction, and the azimuth angle represents z', divergence in the z direction.

The last group of controls, at the bottom of the Ion Definition panel, labelled "Data Recording", allow you to turn data recording on and off (by toggling the "Record" button) and to define what output parameters to record (by pressing "Define"). Specify the location where the output is to be written in the green text box to the right of the "Define" button, either to a device or to a file. A .txt file is a practical file format to output to, as these can be opened by several mathematical software packages for data analysis. The "File Manager" button provides access to the File Manager GUI to select in what directory to save the output file.

You should save the ion definitions for future use; otherwise, you will be required to re-enter the definitions the next time SIMION is started, rather than simply re-load the .FLY file. To exit the Ion Definition panel and return to the workbench view, press "OK", located in the top left corner of the Ion Definition panel.

A.5.2.1 Data Recording

The Data record view is shown in Figure A8. The settings can be saved by selecting "Save", the top, rightmost button in the data record view. An existing .REC file can be loaded by selecting "Load". Broken up into three sections, the data record panel is used to select what data elements to record, when to record these data elements, and what format to use when recording the data.

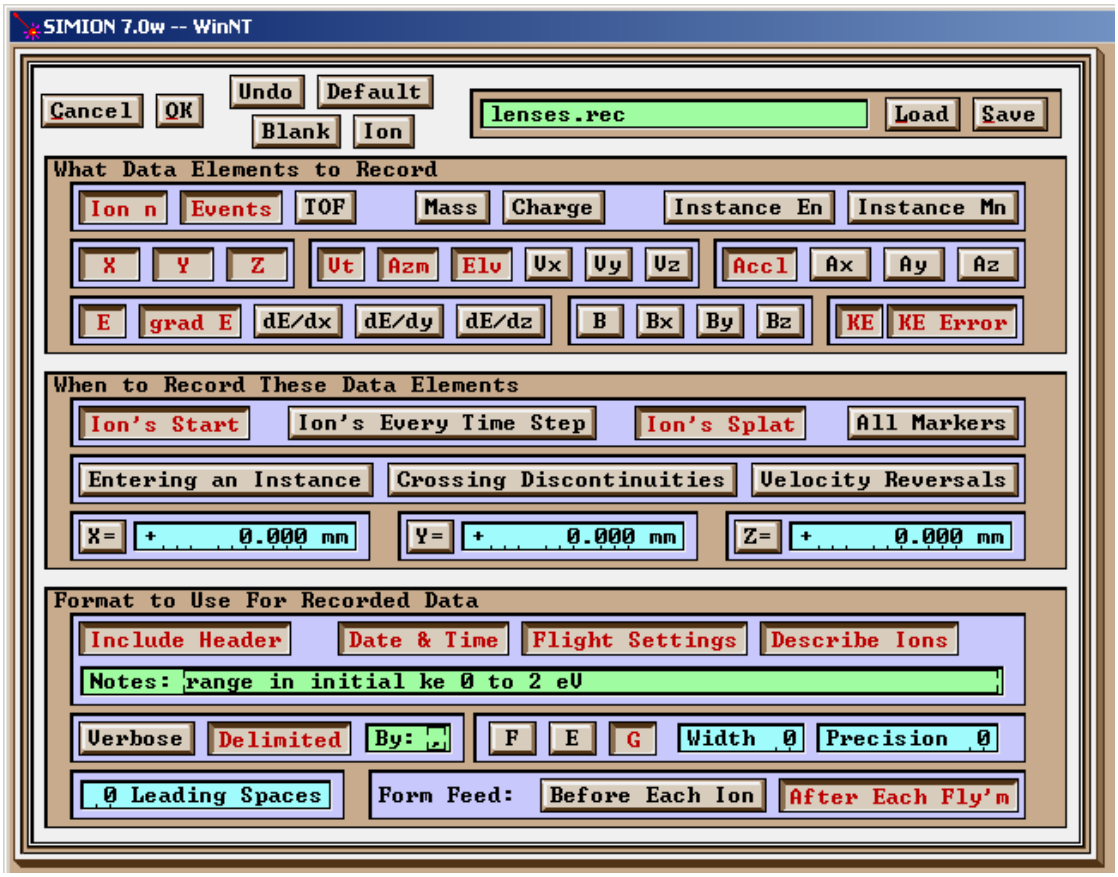

Figure A8 Data record view. The data elements to record, when these data elements should be recorded, and the format used to record the data are specified from this panel.

The button names clearly indicate what data elements can be recorded. A few of these are position (x, y, z), acceleration ($|\vec{a}|, a_x, a_y, a_z$), velocity ($|\vec{v}|, v_x, v_y, v_z$), electric field intensity ($|\vec{E}|, E_x, E_y, E_z$), and kinetic energy (KE). Ten events can be utilised to trigger when the selected data elements are to be recorded. Two of these are selected in Figure A8. The data elements selected in the top group of buttons (selected data elements are labelled in red) will be recorded when the ions are created, "Ion's Start", and when an ion either hits an electrode or reaches the end of the PA, "Ion's Splat". The x, y, and z buttons and text boxes in this group of buttons are used to trigger data recording when an ion crosses the specified x, y, or z plane (value specified in the text box).

The last group of buttons defines the output format. A header and details of the output settings can be included, but more practical is the panel that allows you to specify if the output is to be delimited and what character to delimit the output with, and the number format: E = exponential, F = floating point, G = chosen automatically.

You should elect to save the record data definitions in the same directory as the rest of the project (select “Save” and give the .REC file a name). Otherwise, the definitions will have to be re-entered the next time a simulation session is started (i.e., when SIMION is exited and restarted). To exit the data record view, press “OK”. SIMION will return to the Ion Definition panel. Make sure that the “Record” button is depressed (letters in red) to turn data recording on and that an output file name is specified and the proper directory selected. To exit the Ion Definition panel and return to the workbench view, press “OK”, located in the top left corner of the Ion Definition panel. Remember to save the ion definitions before exiting the Ion Definition panel.

A.5.3 Starting the Simulation Run

Now that the electrode potentials are assigned, the ions are defined, and the output data to record is defined, a simulation of the model system can commence. Press “Fly’m”, located on the left hand side of the workbench view. The ions will start to travel through the system. Depending on the state of the “Grouped” button, located in the Ions group of control buttons (accessed via the "Normal" tab), the ions will fly one at a time or in a group. The more ions there are, the longer it takes for the group of ions to be drawn. To stop the ions from flying, press on “Fly’m” again. To keep the ion trajectories on the screen while a new simulation is started (by pressing “Fly’m”), press “Keep”. In this manner, the effects of changes made to the ion beam or to the electrode potentials can be compared from one simulation run to another by comparing the resulting ion trajectories. Changing the colour of the ions in a subsequent run proves to be further useful in comparing the ion trajectories of different simulations (change the colour of the ions by accessing the ion definition panel). To remove the drawn trajectories from the screen, press “Del”. To turn the cursor into a crosshair with coordinate labels, press on “Where”, located on the left side of the workbench (see Figure A5).

The workbench settings, ion definitions, and record data settings can be saved for future use, and you should do so. In the spirit of project management, all of the workbench settings are saved in a common directory as an .IOB file (**I**on **O**ptics **B**ench). Rather than accessing the workbench view by selecting to view a PA from the main menu, an .IOB file can be loaded into the simulation workbench, by selecting the "Load" button (Figure A2). When the .IOB file is loaded into the workbench, an instance of the PA is loaded, the associated .FLY (or .ION) and .REC files are loaded, and the workbench settings, such as electrode voltage potentials and PA scaling, are restored. The project can be developed from how it was left, and these new developments can be saved for the next development session.

A.6 SIMION Extras

SIMION is capable of many other control functions than those discussed herein. Please refer to the user manual for instructions on how to utilise these and for clarification of the guidelines presented in this appendix. A couple of other useful SIMION features not indispensable to creating and simulating an electrostatic model are introduced in this section.

Once the PA has been fast adjusted, a potential energy view of the PA can be accessed. The two tabs in the top right group of control buttons in Figure A5 allow the user to switch between workbench view (“WB View”) and potential energy view (“PE view”). Select the “PE view” tab to access the screen view shown in Figure A9.

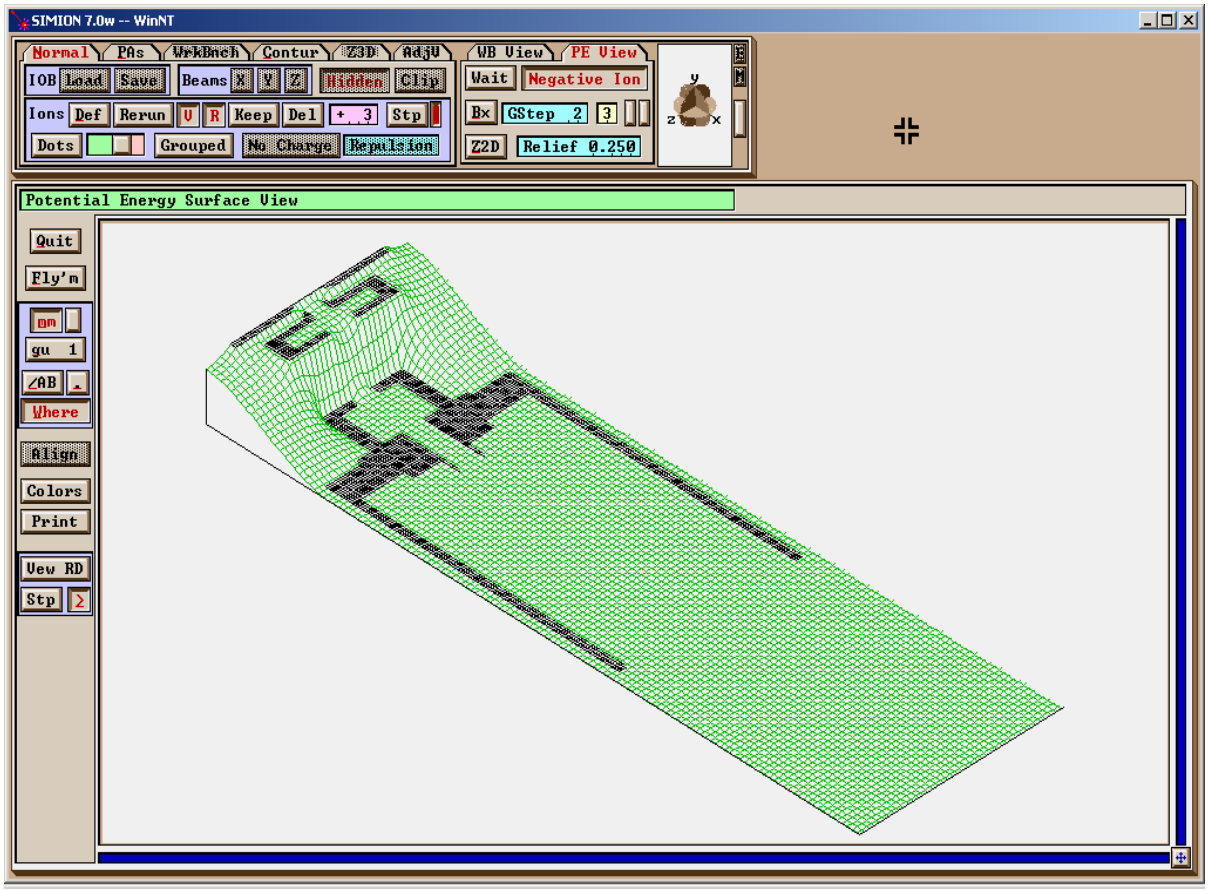

Figure A9 Potential energy view. SIMION calculates the potential energy at every point in the PA. The idea was to have the potential energy view look and act like a mini golf course.

From the data SIMION generates when it refines a PA, the potential energy at every point in the PA can be calculated. The idea behind the potential energy view is to represent the potential energy of the system much like the gravitational potential energy of a miniature golf course. Ions created in the regions of higher potential energy will accelerate towards regions of lower potential energy. The density of the potential energy grid can be adjusted using the buttons provided in the upper right panel when "PE View" is selected. Also, you need to specify if the ions are negative or positive, so that the golf course-like potential energy view is drawn accordingly.

From either the workbench view or the potential energy view, SIMION can be made to draw potential contours around the electrodes. Returning to the workbench view (select the "WB View" tab) and selecting the "Contur" tab brings the view shown in Figure A10 onto the screen. Setting the appropriate buttons accessed by selecting the "Contur" tab allows you to see the specified number of contours and contour values. Press the "Draw" button to have the contours drawn on the screen.

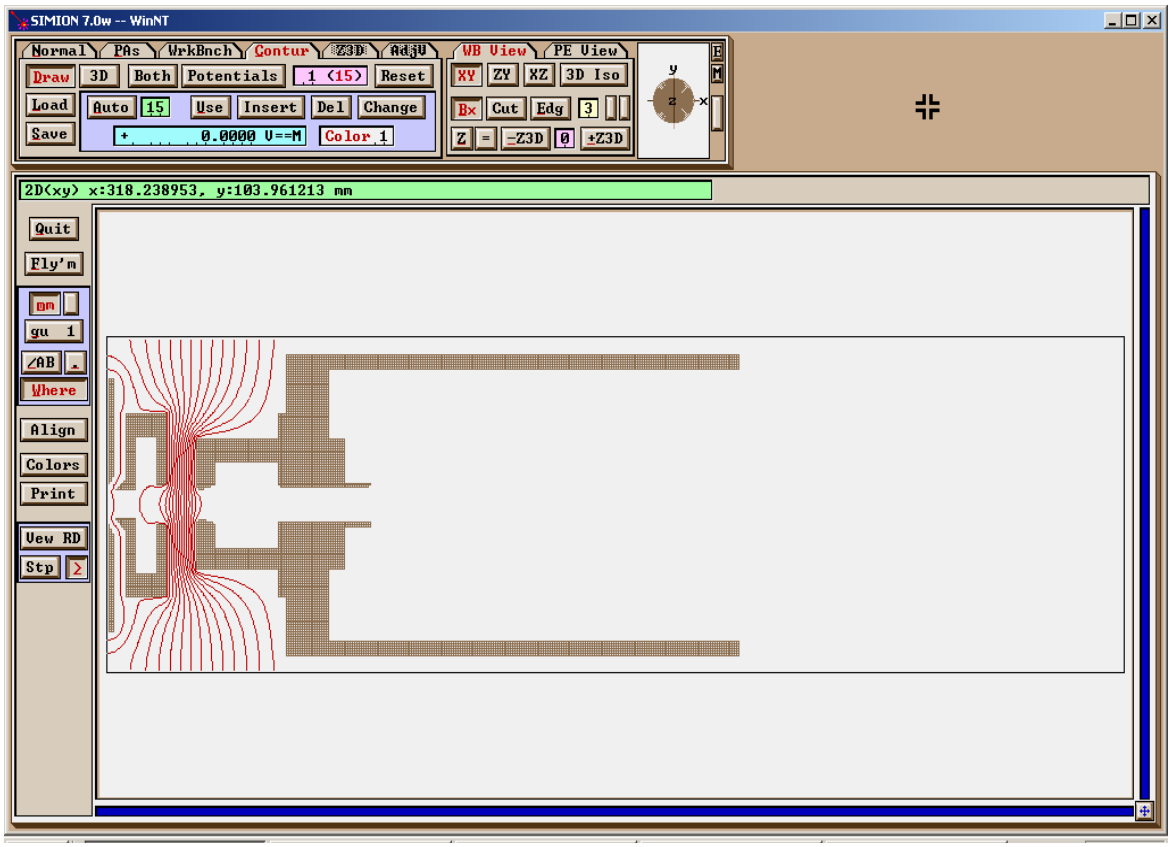

Figure A10 Contour view. The number of contours and the values of each contour can be specified and drawn to view select voltage potentials in a contour plot.

While only the minimum steps required to create a PA and simulate ion transport through a cylindrical electrostatic model were discussed in this appendix, it should be apparent

that SIMION is a powerful tool for simulating electromagnetic charged particle transport systems. Manipulating the two and three dimensional views and zooming into and out of regions of the PA in both the modify and workbench views are very useful skills for a SIMION user to have. These topics will not be discussed in this thesis; working through the first two demos that SIMION provides is the most useful and efficient means by which you can become familiar with these skills. As stated at the beginning of this appendix, the information presented here is only intended to provide basic guidance for using SIMION. The manual [1] is a very thorough document that provides excellent examples and instruction for using SIMION.

Appendix B

List of the Test Parameter Values for Each Lens Configurations Tested

test #	V2 (V)	A2 (mm)	A3 (mm)	D12 (mm)	D23 (mm)	test #	V2 (V)	A2 (mm)	A3 (mm)	D12 (mm)	D23 (mm)
test 1	-22000	9.5	10	4	12	**test 25**	-22000	9.5	11	10	12
test 2	-22000	9.5	10	4	8	**test 26**	-22000	9.5	11	10	8
test 3	-22000	9.5	10	4	16	**test 27**	-22000	9.5	11	10	16
test 4	-22000	9.5	10	7	12	**test 28**	-22000	10.5	10	4	12
test 5	-22000	9.5	10	7	8	**test 29**	-22000	10.5	10	4	8
test 6	-22000	9.5	10	7	16	**test 30**	-22000	10.5	10	4	16
test 7	-22000	9.5	10	10	12	**test 31**	-22000	10.5	10	7	12
test 8	-22000	9.5	10	10	8	**test 32**	-22000	10.5	10	7	8
test 9	-22000	9.5	10	10	16	**test 33**	-22000	10.5	10	7	16
test 10	-22000	9.5	9	4	12	**test 34**	-22000	10.5	10	10	12
test 11	-22000	9.5	9	4	8	**test 35**	-22000	10.5	10	10	8
test 12	-22000	9.5	9	4	16	**test 36**	-22000	10.5	10	10	16
test 13	-22000	9.5	9	7	12	**test 37**	-22000	10.5	9	4	12
test 14	-22000	9.5	9	7	8	**test 38**	-22000	10.5	9	4	8
test 15	-22000	9.5	9	7	16	**test 39**	-22000	10.5	9	4	16
test 16	-22000	9.5	9	10	12	**test 40**	-22000	10.5	9	7	12
test 17	-22000	9.5	9	10	8	**test 41**	-22000	10.5	9	7	8
test 18	-22000	9.5	9	10	16	**test 42**	-22000	10.5	9	7	16
test 19	-22000	9.5	11	4	12	**test 43**	-22000	10.5	9	10	12
test 20	-22000	9.5	11	4	8	**test 44**	-22000	10.5	9	10	8
test 21	-22000	9.5	11	4	16	**test 45**	-22000	10.5	9	10	16
test 22	-22000	9.5	11	7	12	**test 46**	-22000	10.5	11	4	12
test 23	-22000	9.5	11	7	8	**test 47**	-22000	10.5	11	4	8
test 24	-22000	9.5	11	7	16	**test 48**	-22000	10.5	11	4	16

test #	V2 (V)	A2 (mm)	A3 (mm)	D12 (mm)	D23 (mm)	test #	V2 (V)	A2 (mm)	A3 (mm)	D12 (mm)	D23 (mm)
test 49	-22000	10.5	11	7	12	**test 78**	-22000	11.5	11	7	16
test 50	-22000	10.5	11	7	8	**test 79**	-22000	11.5	11	10	12
test 51	-22000	10.5	11	7	16	**test 80**	-22000	11.5	11	10	8
test 52	-22000	10.5	11	10	12	**test 81**	-22000	11.5	11	10	16
test 53	-22000	10.5	11	10	8	**test 82**	-22000	12.5	10	4	12
test 54	-22000	10.5	11	10	16	**test 83**	-22000	12.5	10	4	8
test 55	-22000	11.5	10	4	12	**test 84**	-22000	12.5	10	4	16
test 56	-22000	11.5	10	4	8	**test 85**	-22000	12.5	10	7	12
test 57	-22000	11.5	10	4	16	**test 86**	-22000	12.5	10	7	8
test 58	-22000	11.5	10	7	12	**test 87**	-22000	12.5	10	7	16
test 59	-22000	11.5	10	7	8	**test 88**	-22000	12.5	10	10	12
test 60	-22000	11.5	10	7	16	**test 89**	-22000	12.5	10	10	8
test 61	-22000	11.5	10	10	12	**test 90**	-22000	12.5	10	10	16
test 62	-22000	11.5	10	10	8	**test 91**	-22000	12.5	9	4	12
test 63	-22000	11.5	10	10	16	**test 92**	-22000	12.5	9	4	8
test 64	-22000	11.5	9	4	12	**test 93**	-22000	12.5	9	4	16
test 65	-22000	11.5	9	4	8	**test 94**	-22000	12.5	9	7	12
test 66	-22000	11.5	9	4	16	**test 95**	-22000	12.5	9	7	8
test 67	-22000	11.5	9	7	12	**test 96**	-22000	12.5	9	7	16
test 68	-22000	11.5	9	7	8	**test 97**	-22000	12.5	9	10	12
test 69	-22000	11.5	9	7	16	**test 98**	-22000	12.5	9	10	8
test 70	-22000	11.5	9	10	12	**test 99**	-22000	12.5	9	10	16
test 71	-22000	11.5	9	10	8	**test 100**	-22000	12.5	11	4	12
test 72	-22000	11.5	9	10	16	**test 101**	-22000	12.5	11	4	8
test 73	-22000	11.5	11	4	12	**test 102**	-22000	12.5	11	4	16
test 74	-22000	11.5	11	4	8	**test 103**	-22000	12.5	11	7	12
test 75	-22000	11.5	11	4	16	**test 104**	-22000	12.5	11	7	8
test 76	-22000	11.5	11	7	12	**test 105**	-22000	12.5	11	7	16
test 77	-22000	11.5	11	7	8	**test 106**	-22000	12.5	11	10	12

test #	V2 (V)	A2 (mm)	A3 (mm)	D12 (mm)	D23 (mm)	test #	V2 (V)	A2 (mm)	A3 (mm)	D12 (mm)	D23 (mm)
test 107	-22000	12.5	11	10	8	**test 136**	-23000	10.5	10	4	12
test 108	-22000	12.5	11	10	16	**test 137**	-23000	10.5	10	4	8
test 109	-23000	9.5	10	4	12	**test 138**	-23000	10.5	10	4	16
test 110	-23000	9.5	10	4	8	**test 139**	-23000	10.5	10	7	12
test 111	-23000	9.5	10	4	16	**test 140**	-23000	10.5	10	7	8
test 112	-23000	9.5	10	7	12	**test 141**	-23000	10.5	10	7	16
test 113	-23000	9.5	10	7	8	**test 142**	-23000	10.5	10	10	12
test 114	-23000	9.5	10	7	16	**test 143**	-23000	10.5	10	10	8
test 115	-23000	9.5	10	10	12	**test 144**	-23000	10.5	10	10	16
test 116	-23000	9.5	10	10	8	**test 145**	-23000	10.5	9	4	12
test 117	-23000	9.5	10	10	16	**test 146**	-23000	10.5	9	4	8
test 118	-23000	9.5	9	4	12	**test 147**	-23000	10.5	9	4	16
test 119	-23000	9.5	9	4	8	**test 148**	-23000	10.5	9	7	12
test 120	-23000	9.5	9	4	16	**test 149**	-23000	10.5	9	7	8
test 121	-23000	9.5	9	7	12	**test 150**	-23000	10.5	9	7	16
test 122	-23000	9.5	9	7	8	**test 151**	-23000	10.5	9	10	12
test 123	-23000	9.5	9	7	16	**test 152**	-23000	10.5	9	10	8
test 124	-23000	9.5	9	10	12	**test 153**	-23000	10.5	9	10	16
test 125	-23000	9.5	9	10	8	**test 154**	-23000	10.5	11	4	12
test 126	-23000	9.5	9	10	16	**test 155**	-23000	10.5	11	4	8
test 127	-23000	9.5	11	4	12	**test 156**	-23000	10.5	11	4	16
test 128	-23000	9.5	11	4	8	**test 157**	-23000	10.5	11	7	12
test 129	-23000	9.5	11	4	16	**test 158**	-23000	10.5	11	7	8
test 130	-23000	9.5	11	7	12	**test 159**	-23000	10.5	11	7	16
test 131	-23000	9.5	11	7	8	**test 160**	-23000	10.5	11	10	12
test 132	-23000	9.5	11	7	16	**test 161**	-23000	10.5	11	10	8
test 133	-23000	9.5	11	10	12	**test 162**	-23000	10.5	11	10	16
test 134	-23000	9.5	11	10	8	**test 163**	-23000	11.5	10	4	12
test 135	-23000	9.5	11	10	16	**test 164**	-23000	11.5	10	4	8

test #	V2 (V)	A2 (mm)	A3 (mm)	D12 (mm)	D23 (mm)	test #	V2 (V)	A2 (mm)	A3 (mm)	D12 (mm)	D23 (mm)
test 165	-23000	11.5	10	4	16	**test 194**	-23000	12.5	10	7	8
test 166	-23000	11.5	10	7	12	**test 195**	-23000	12.5	10	7	16
test 167	-23000	11.5	10	7	8	**test 196**	-23000	12.5	10	10	12
test 168	-23000	11.5	10	7	16	**test 197**	-23000	12.5	10	10	8
test 169	-23000	11.5	10	10	12	**test 198**	-23000	12.5	10	10	16
test 170	-23000	11.5	10	10	8	**test 199**	-23000	12.5	9	4	12
test 171	-23000	11.5	10	10	16	**test 200**	-23000	12.5	9	4	8
test 172	-23000	11.5	9	4	12	**test 201**	-23000	12.5	9	4	16
test 173	-23000	11.5	9	4	8	**test 202**	-23000	12.5	9	7	12
test 174	-23000	11.5	9	4	16	**test 203**	-23000	12.5	9	7	8
test 175	-23000	11.5	9	7	12	**test 204**	-23000	12.5	9	7	16
test 176	-23000	11.5	9	7	8	**test 205**	-23000	12.5	9	10	12
test 177	-23000	11.5	9	7	16	**test 206**	-23000	12.5	9	10	8
test 178	-23000	11.5	9	10	12	**test 207**	-23000	12.5	9	10	16
test 179	-23000	11.5	9	10	8	**test 208**	-23000	12.5	11	4	12
test 180	-23000	11.5	9	10	16	**test 209**	-23000	12.5	11	4	8
test 181	-23000	11.5	11	4	12	**test 210**	-23000	12.5	11	4	16
test 182	-23000	11.5	11	4	8	**test 211**	-23000	12.5	11	7	12
test 183	-23000	11.5	11	4	16	**test 212**	-23000	12.5	11	7	8
test 184	-23000	11.5	11	7	12	**test 213**	-23000	12.5	11	7	16
test 185	-23000	11.5	11	7	8	**test 214**	-23000	12.5	11	10	12
test 186	-23000	11.5	11	7	16	**test 215**	-23000	12.5	11	10	8
test 187	-23000	11.5	11	10	12	**test 216**	-23000	12.5	11	10	16
test 188	-23000	11.5	11	10	8	**test 217**	-22500	9.5	10	4	12
test 189	-23000	11.5	11	10	16	**test 218**	-22500	9.5	10	4	8
test 190	-23000	12.5	10	4	12	**test 219**	-22500	9.5	10	4	16
test 191	-23000	12.5	10	4	8	**test 220**	-22500	9.5	10	7	12
test 192	-23000	12.5	10	4	16	**test 221**	-22500	9.5	10	7	8
test 193	-23000	12.5	10	7	12	**test 222**	-22500	9.5	10	7	16

test #	V2 (V)	A2 (mm)	A3 (mm)	D12 (mm)	D23 (mm)	test #	V2 (V)	A2 (mm)	A3 (mm)	D12 (mm)	D23 (mm)
test 223	-22500	9.5	10	10	12	**test 252**	-22500	10.5	10	10	16
test 224	-22500	9.5	10	10	8	**test 253**	-22500	10.5	9	4	12
test 225	-22500	9.5	10	10	16	**test 254**	-22500	10.5	9	4	8
test 226	-22500	9.5	9	4	12	**test 255**	-22500	10.5	9	4	16
test 227	-22500	9.5	9	4	8	**test 256**	-22500	10.5	9	7	12
test 228	-22500	9.5	9	4	16	**test 257**	-22500	10.5	9	7	8
test 229	-22500	9.5	9	7	12	**test 258**	-22500	10.5	9	7	16
test 230	-22500	9.5	9	7	8	**test 259**	-22500	10.5	9	10	12
test 231	-22500	9.5	9	7	16	**test 260**	-22500	10.5	9	10	8
test 232	-22500	9.5	9	10	12	**test 261**	-22500	10.5	9	10	16
test 233	-22500	9.5	9	10	8	**test 262**	-22500	10.5	11	4	12
test 234	-22500	9.5	9	10	16	**test 263**	-22500	10.5	11	4	8
test 235	-22500	9.5	11	4	12	**test 264**	-22500	10.5	11	4	16
test 236	-22500	9.5	11	4	8	**test 265**	-22500	10.5	11	7	12
test 237	-22500	9.5	11	4	16	**test 266**	-22500	10.5	11	7	8
test 238	-22500	9.5	11	7	12	**test 267**	-22500	10.5	11	7	16
test 239	-22500	9.5	11	7	8	**test 268**	-22500	10.5	11	10	12
test 240	-22500	9.5	11	7	16	**test 269**	-22500	10.5	11	10	8
test 241	-22500	9.5	11	10	12	**test 270**	-22500	10.5	11	10	16
test 242	-22500	9.5	11	10	8	**test 271**	-22500	11.5	10	4	12
test 243	-22500	9.5	11	10	16	**test 272**	-22500	11.5	10	4	8
test 244	-22500	10.5	10	4	12	**test 273**	-22500	11.5	10	4	16
test 245	-22500	10.5	10	4	8	**test 274**	-22500	11.5	10	7	12
test 246	-22500	10.5	10	4	16	**test 275**	-22500	11.5	10	7	8
test 247	-22500	10.5	10	7	12	**test 276**	-22500	11.5	10	7	16
test 248	-22500	10.5	10	7	8	**test 277**	-22500	11.5	10	10	12
test 249	-22500	10.5	10	7	16	**test 278**	-22500	11.5	10	10	8
test 250	-22500	10.5	10	10	12	**test 279**	-22500	11.5	10	10	16
test 251	-22500	10.5	10	10	8	**test 280**	-22500	11.5	9	4	12

test #	V2 (V)	A2 (mm)	A3 (mm)	D12 (mm)	D23 (mm)	test #	V2 (V)	A2 (mm)	A3 (mm)	D12 (mm)	D23 (mm)
test 281	-22500	11.5	9	4	8	**test 310**	-22500	12.5	9	7	12
test 282	-22500	11.5	9	4	16	**test 311**	-22500	12.5	9	7	8
test 283	-22500	11.5	9	7	12	**test 312**	-22500	12.5	9	7	16
test 284	-22500	11.5	9	7	8	**test 313**	-22500	12.5	9	10	12
test 285	-22500	11.5	9	7	16	**test 314**	-22500	12.5	9	10	8
test 286	-22500	11.5	9	10	12	**test 315**	-22500	12.5	9	10	16
test 287	-22500	11.5	9	10	8	**test 316**	-22500	12.5	11	4	12
test 288	-22500	11.5	9	10	16	**test 317**	-22500	12.5	11	4	8
test 289	-22500	11.5	11	4	12	**test 318**	-22500	12.5	11	4	16
test 290	-22500	11.5	11	4	8	**test 319**	-22500	12.5	11	7	12
test 291	-22500	11.5	11	4	16	**test 320**	-22500	12.5	11	7	8
test 292	-22500	11.5	11	7	12	**test 321**	-22500	12.5	11	7	16
test 293	-22500	11.5	11	7	8	**test 322**	-22500	12.5	11	10	12
test 294	-22500	11.5	11	7	16	**test 323**	-22500	12.5	11	10	8
test 295	-22500	11.5	11	10	12	**test 324**	-22500	12.5	11	10	16
test 296	-22500	11.5	11	10	8	**test 325**	-21500	9.5	10	4	12
test 297	-22500	11.5	11	10	16	**test 326**	-21500	9.5	10	4	8
test 298	-22500	12.5	10	4	12	**test 327**	-21500	9.5	10	4	16
test 299	-22500	12.5	10	4	8	**test 328**	-21500	9.5	10	7	12
test 300	-22500	12.5	10	4	16	**test 329**	-21500	9.5	10	7	8
test 301	-22500	12.5	10	7	12	**test 330**	-21500	9.5	10	7	16
test 302	-22500	12.5	10	7	8	**test 331**	-21500	9.5	10	10	12
test 303	-22500	12.5	10	7	16	**test 332**	-21500	9.5	10	10	8
test 304	-22500	12.5	10	10	12	**test 333**	-21500	9.5	10	10	16
test 305	-22500	12.5	10	10	8	**test 334**	-21500	9.5	9	4	12
test 306	-22500	12.5	10	10	16	**test 335**	-21500	9.5	9	4	8
test 307	-22500	12.5	9	4	12	**test 336**	-21500	9.5	9	4	16
test 308	-22500	12.5	9	4	8	**test 337**	-21500	9.5	9	7	12
test 309	-22500	12.5	9	4	16	**test 338**	-21500	9.5	9	7	8

test #	V2 (V)	A2 (mm)	A3 (mm)	D12 (mm)	D23 (mm)	test #	V2 (V)	A2 (mm)	A3 (mm)	D12 (mm)	D23 (mm)
test 339	-21500	9.5	9	7	16	**test 368**	-21500	10.5	9	10	8
test 340	-21500	9.5	9	10	12	**test 369**	-21500	10.5	9	10	16
test 341	-21500	9.5	9	10	8	**test 370**	-21500	10.5	11	4	12
test 342	-21500	9.5	9	10	16	**test 371**	-21500	10.5	11	4	8
test 343	-21500	9.5	11	4	12	**test 372**	-21500	10.5	11	4	16
test 344	-21500	9.5	11	4	8	**test 373**	-21500	10.5	11	7	12
test 345	-21500	9.5	11	4	16	**test 374**	-21500	10.5	11	7	8
test 346	-21500	9.5	11	7	12	**test 375**	-21500	10.5	11	7	16
test 347	-21500	9.5	11	7	8	**test 376**	-21500	10.5	11	10	12
test 348	-21500	9.5	11	7	16	**test 377**	-21500	10.5	11	10	8
test 349	-21500	9.5	11	10	12	**test 378**	-21500	10.5	11	10	16
test 350	-21500	9.5	11	10	8	**test 379**	-21500	11.5	10	4	12
test 351	-21500	9.5	11	10	16	**test 380**	-21500	11.5	10	4	8
test 352	-21500	10.5	10	4	12	**test 381**	-21500	11.5	10	4	16
test 353	-21500	10.5	10	4	8	**test 382**	-21500	11.5	10	7	12
test 354	-21500	10.5	10	4	16	**test 383**	-21500	11.5	10	7	8
test 355	-21500	10.5	10	7	12	**test 384**	-21500	11.5	10	7	16
test 356	-21500	10.5	10	7	8	**test 385**	-21500	11.5	10	10	12
test 357	-21500	10.5	10	7	16	**test 386**	-21500	11.5	10	10	8
test 358	-21500	10.5	10	10	12	**test 387**	-21500	11.5	10	10	16
test 359	-21500	10.5	10	10	8	**test 388**	-21500	11.5	9	4	12
test 360	-21500	10.5	10	10	16	**test 389**	-21500	11.5	9	4	8
test 361	-21500	10.5	9	4	12	**test 390**	-21500	11.5	9	4	16
test 362	-21500	10.5	9	4	8	**test 391**	-21500	11.5	9	7	12
test 363	-21500	10.5	9	4	16	**test 392**	-21500	11.5	9	7	8
test 364	-21500	10.5	9	7	12	**test 393**	-21500	11.5	9	7	16
test 365	-21500	10.5	9	7	8	**test 394**	-21500	11.5	9	10	12
test 366	-21500	10.5	9	7	16	**test 395**	-21500	11.5	9	10	8
test 367	-21500	10.5	9	10	12	**test 396**	-21500	11.5	9	10	16

test #	V2 (V)	A2 (mm)	A3 (mm)	D12 (mm)	D23 (mm)	test #	V2 (V)	A2 (mm)	A3 (mm)	D12 (mm)	D23 (mm)
test 397	-21500	11.5	11	4	12	**test 416**	-21500	12.5	9	4	8
test 398	-21500	11.5	11	4	8	**test 417**	-21500	12.5	9	4	16
test 399	-21500	11.5	11	4	16	**test 418**	-21500	12.5	9	7	12
test 400	-21500	11.5	11	7	12	**test 417**	-21500	12.5	9	4	16
test 401	-21500	11.5	11	7	8	**test 418**	-21500	12.5	9	7	12
test 402	-21500	11.5	11	7	16	**test 409**	-21500	12.5	10	7	12
test 403	-21500	11.5	11	10	12	**test 410**	-21500	12.5	10	7	8
test 404	-21500	11.5	11	10	8	**test 411**	-21500	12.5	10	7	16
test 405	-21500	11.5	11	10	16	**test 412**	-21500	12.5	10	10	12
test 406	-21500	12.5	10	4	12	**test 413**	-21500	12.5	10	10	8
test 407	-21500	12.5	10	4	8	**test 414**	-21500	12.5	10	10	16
test 408	-21500	12.5	10	4	16	**test 415**	-21500	12.5	9	4	12
test 409	-21500	12.5	10	7	12	**test 416**	-21500	12.5	9	4	8
test 410	-21500	12.5	10	7	8	**test 417**	-21500	12.5	9	4	16
test 411	-21500	12.5	10	7	16	**test 418**	-21500	12.5	9	7	12
test 412	-21500	12.5	10	10	12	**test 417**	-21500	12.5	9	4	16
test 413	-21500	12.5	10	10	8	**test 418**	-21500	12.5	9	7	12
test 414	-21500	12.5	10	10	16	**test 417**	-21500	12.5	9	4	16
test 415	-21500	12.5	9	4	12	**test 418**	-21500	12.5	9	7	12
test 416	-21500	12.5	9	4	8	**test 409**	-21500	12.5	10	7	12
test 417	-21500	12.5	9	4	16	**test 410**	-21500	12.5	10	7	8
test 418	-21500	12.5	9	7	12	**test 411**	-21500	12.5	10	7	16
test 409	-21500	12.5	10	7	12	**test 412**	-21500	12.5	10	10	12
test 410	-21500	12.5	10	7	8	**test 413**	-21500	12.5	10	10	8
test 411	-21500	12.5	10	7	16	**test 414**	-21500	12.5	10	10	16
test 412	-21500	12.5	10	10	12	**test 415**	-21500	12.5	9	4	12
test 413	-21500	12.5	10	10	8	**test 416**	-21500	12.5	9	4	8
test 414	-21500	12.5	10	10	16	**test 417**	-21500	12.5	9	4	16
test 415	-21500	12.5	9	4	12	**test 418**	-21500	12.5	9	7	12

test #	V2 (V)	A2 (mm)	A3 (mm)	D12 (mm)	D23 (mm)
test 419	-21500	12.5	9	7	8
test 420	-21500	12.5	9	7	16
test 421	-21500	12.5	9	10	12
test 422	-21500	12.5	9	10	8
test 423	-21500	12.5	9	10	16
test 424	-21500	12.5	11	4	12
test 425	-21500	12.5	11	4	8
test 426	-21500	12.5	11	4	16
test 427	-21500	12.5	11	7	12
test 428	-21500	12.5	11	7	8
test 429	-21500	12.5	11	7	16
test 430	-21500	12.5	11	10	12
test 431	-21500	12.5	11	10	8
test 432	-21500	12.5	11	10	16

[This page intentionally left blank.]

Appendix C

Measured Data: position of beam waist, half width and half divergence at waist

	waist info:						
test #	**z**	**stdev z**	**y max**	**stdev y**	**y' max (mrad)**	**beamstop**	**z from bs**
10k ions	80.07362575	0.475387381	1.48922925	0.021865925	109.8730579	405	324.9263743
test 1	81.1574965	1.428028906	1.40874375	0.043260596	110.6144301	405	323.8425035
test 2	65.59492375	0.575240518	1.23101475	0.039635903	132.887973	401	335.4050763
test 3	104.624336	0.575558667	1.762278	0.059217769	82.9887915	409	304.375664
test 4	61.6075745	0.488370405	1.289448	0.028974443	101.913222	408	346.3924255
test 5	55.36810475	0.650325735	1.082639	0.019527285	114.6658629	404	348.6318953
test 6	69.58923825	0.45132978	1.48013475	0.031769948	90.25913503	412	342.4107618
test 7	56.3697285	0.734974945	1.09020175	6.07587E-06	102.8564416	411	354.6302715
test 8	52.16985725	0.462985316	0.962186	0.02575373	114.4565107	407	354.8301428
test 9	61.483949	0.915846413	1.2432295	0.046062357	89.18331408	415	353.516051
test 10	79.64615	0.670398033	1.4053005	0.027506789	110.4680843	405	325.35385
test 11	64.45921575	0.235985488	1.2059425	0.033331443	133.8481659	401	336.5407843
test 12	103.669193	1.038607665	1.69469825	0.033414736	82.32094126	409	305.330807
test 13	61.892998	0.39637083	1.21799025	0.046667336	102.1169456	408	346.107002
test 14	55.2160935	0.102281719	1.05400475	0.01089812	117.0378963	404	348.7839065
test 15	69.82519575	0.217378439	1.50034725	0.047531845	90.1024481	412	342.1748043
test 16	56.7879085	0.48886379	1.08269075	0.03831481	102.4440639	411	354.2120915
test 17	51.55316325	0.150599758	0.959926	0.036556469	114.354758	407	355.4468368
test 18	60.59578975	0.828715871	1.26898625	0.021201623	89.25618158	415	354.4042103
test 19	81.31642625	0.460631595	1.43651275	0.03961622	107.2768806	405	323.6835738
test 20	66.15796775	0.509944876	1.26436275	0.011618707	133.3945112	401	334.8420323
test 21	106.3750933	1.551101204	1.785948	0.047960807	81.23809536	409	302.6249068
test 22	62.34082125	0.442653895	1.2960345	0.024357097	101.3202028	408	345.6591788
test 23	56.0638745	0.646522052	1.08917975	0.029548511	112.9089709	404	347.9361255

test #	z	stdev z	y max	stdev y	y' max (mrad)	beamstop	z from bs
test 24	69.48600775	0.776843848	1.52372725	0.046735554	90.55208855	412	342.5139923
test 25	56.550183	0.772807739	1.0837585	0.059768483	101.4415032	411	354.449817
test 26	52.82287075	0.373157231	0.9603375	0.002797954	113.861048	407	354.1771293
test 27	61.8318025	0.416626407	1.23911675	0.016411724	88.4932109	415	353.1681975
test 28	69.18461725	0.509485499	1.673521	0.030425202	132.2051565	405	335.8153828
test 29	55.5644175	0.568410732	1.58217425	0.024120532	132.5704103	401	345.4355825
test 30	93.2051245	0.745942688	1.8561455	0.043414681	100.5644316	409	315.7948755
test 31	64.345126	0.215113326	1.189528	0.021113261	116.9237081	408	343.654874
test 32	57.22407025	0.071206689	1.034603	0.015820344	128.1127085	404	346.7759298
test 33	72.35953225	0.924125449	1.3889185	0.054753868	98.1265557	412	339.6404678
test 34	57.5081265	0.596477765	1.0690265	0.031673428	105.3744281	411	353.4918735
test 35	53.322241	0.347088	0.931759	0.050540916	116.4402083	407	353.677759
test 36	62.6592965	0.57202517	1.24440125	0.034380774	89.53726686	415	352.3407035
test 37	68.50890925	0.383627076	1.6857415	0.051469117	133.1643459	405	336.4910908
test 38	54.97444275	0.54446668	1.5547555	0.013304814	131.253254	401	346.0255573
test 39	91.87942	1.002009067	1.813121	0.038770212	101.844587	409	317.12058
test 40	63.8354095	0.326971389	1.19156075	0.013615523	118.1392427	408	344.1645905
test 41	56.61366525	0.131632136	1.00094	0.02380136	127.3361243	404	347.3863348
test 42	71.9361745	0.371566738	1.4014645	0.021249838	98.90039106	412	340.0638255
test 43	57.73487925	0.713023279	1.06936775	0.029555698	105.2709301	411	353.2651208
test 44	52.63891425	0.232334976	0.93502625	0.032695297	118.2512055	407	354.3610858
test 45	62.4191935	0.563775523	1.23360225	0.035320123	91.13350136	415	352.5808065
test 46	70.0719995	0.954260999	1.7289055	0.038695894	132.6273517	405	334.9280005
test 47	55.61980675	0.374821392	1.634236	0.031800473	133.1574955	401	345.3801933
test 48	93.7634125	0.705047239	1.8962245	0.052200105	98.12585757	409	315.2365875
test 49	64.7117425	0.256969344	1.216974	0.029267132	115.5041446	408	343.2882575
test 50	57.67004	0.147715156	1.04678425	0.019164505	128.5389616	404	346.32996
test 51	72.837294	0.471945861	1.41207125	0.021190101	98.22734847	412	339.162706
test 52	57.64840925	0.764165477	1.12432075	0.028911856	104.2865208	411	353.3515908
test 53	53.2557675	0.458074029	0.96533375	0.018886599	117.8630443	407	353.7442325

test #	z	stdev z	y max	stdev y	y' max (mrad)	beamstop	z from bs
test 54	62.64447625	1.240949732	1.23004075	0.052490706	89.51531934	415	352.3555238
test 55	68.78706025	0.944072562	1.642914	0.040342416	132.9689999	405	336.2129398
test 56	54.390376	0.261999959	1.59099575	0.039233104	133.2422312	401	346.609624
test 57	92.605277	1.079624174	1.81334775	0.021424092	100.4627662	409	316.394723
test 58	65.42961575	0.278837361	1.17495825	0.028640113	128.0994876	408	342.5703843
test 59	57.23916825	0.089501448	1.04064175	0.018325132	128.5607782	404	346.7608318
test 60	74.182871	0.877660641	1.37933825	0.009901807	116.5295255	412	337.817129
test 61	58.3696255	0.557300452	1.078925	0.010970985	106.191504	411	352.6303745
test 62	53.90664625	0.453032433	0.89300125	0.029235817	118.6090853	407	353.0933538
test 63	63.79111275	0.682987702	1.2264795	0.017600524	90.13696199	415	351.2088873
test 64	68.0259225	0.535757408	1.637196	0.049556462	130.1338434	405	336.9740775
test 65	54.04902875	0.641769758	1.54811075	0.0349548	132.9576553	401	346.9509713
test 66	91.2080195	1.046222706	1.762171	0.049587543	101.5320421	409	317.7919805
test 67	65.0759345	0.088525068	1.15957925	0.021570334	128.6463866	408	342.9240655
test 68	56.18547575	0.169267921	1.0118015	0.058943667	128.6826458	404	347.8145243
test 69	73.706557	0.453458723	1.393845	0.034285116	118.6726589	412	338.293443
test 70	58.30609125	0.942317835	1.03380275	0.034748832	106.9137649	411	352.6939088
test 71	53.40104825	0.307449996	0.8995365	0.02760681	117.988708	407	353.5989518
test 72	63.58754175	0.968271923	1.2025845	0.032544016	92.74749458	415	351.4124583
test 73	69.687753	0.224468799	1.65440225	0.035050601	130.4284986	405	335.312247
test 74	55.24173525	0.590301952	1.6209985	0.042406652	132.5259917	401	345.7582648
test 75	92.82182625	0.57610955	1.8425165	0.033437819	100.4619808	409	316.1781738
test 76	66.0314665	0.349577745	1.1728825	0.036929402	129.0216324	408	341.9685335
test 77	57.80227375	0.276420867	1.03682275	0.016416454	129.1915838	404	346.1977263
test 78	74.67267225	0.307480471	1.35106625	0.028410038	117.3913691	412	337.3273278
test 79	58.432362	0.742522225	1.09256575	0.021595163	106.362939	411	352.567638
test 80	54.1267475	0.366178932	0.9600605	0.005812119	118.2396864	407	352.8732525
test 81	63.76178425	0.36861179	1.238778	0.038070123	90.29517608	415	351.2382158
test 82	68.1329345	0.863622324	1.61803825	0.016968611	133.0743741	405	336.8670655
test 83	54.41632375	0.221934811	1.56567825	0.0254381	132.1076363	401	346.5836763

test #	z	stdev z	y max	stdev y	y' max (mrad)	beamstop	z from bs
test 84	90.231642	0.875896576	1.763861	0.048100711	103.0860833	409	318.768358
test 85	62.18304975	0.234564192	1.311254	0.020537392	128.5550622	408	345.8169503
test 86	53.67732125	0.529165248	1.23157725	0.031150875	128.0579488	404	350.3226788
test 87	73.6218595	0.483559169	1.3810955	0.035080409	125.5570665	412	338.3781405
test 88	59.2687875	0.353512819	1.02738575	0.042991276	108.1142023	411	351.7312125
test 89	54.63152675	0.50669624	0.89832125	0.033452781	118.5092961	407	352.3684733
test 90	63.9674885	0.536967166	1.250402	0.017566584	93.52050091	415	351.0325115
test 91	67.66037775	0.993086594	1.5776845	0.018918877	131.2022904	405	337.3396223
test 92	53.432831	0.090451288	1.557592	0.021263937	132.7752683	401	347.567169
test 93	89.0618105	0.769591842	1.78686525	0.052167181	104.1982071	409	319.9381895
test 94	61.5717315	0.843999308	1.3013585	0.04261771	126.5743317	408	346.4282685
test 95	53.07649925	0.251901302	1.209088	0.046865207	127.3006941	404	350.9235008
test 96	73.325422	0.828310218	1.40796225	0.019159481	126.7493882	412	338.674578
test 97	58.87561125	0.718098011	1.050075	0.040499773	109.493667	411	352.1243888
test 98	53.7015305	0.212446963	0.9003105	0.037954617	118.1929115	407	353.2984695
test 99	64.40558625	1.109125271	1.1808965	0.03018941	92.32639027	415	350.5944138
test 100	69.0783035	0.648936918	1.627255	0.04863625	133.8022637	405	335.9216965
test 101	55.123276	0.065210547	1.6008245	0.023717702	133.2198473	401	345.876724
test 102	90.222317	0.231250413	1.742131	0.073364836	102.1327845	409	318.777683
test 103	62.645022	0.373636585	1.313503	0.026480789	129.4238871	408	345.354978
test 104	54.121912	0.156513318	1.248007	0.037449565	129.4878534	404	349.878088
test 105	74.02803475	0.487043742	1.4138805	0.030089899	125.0137019	412	337.9719653
test 106	59.29284275	0.710480453	1.077438	0.004920181	108.6504548	411	351.7071573
test 107	54.65065225	0.623423482	0.9303005	0.03754837	119.2801644	407	352.3493478
test 108	64.26565375	0.786417097	1.24823825	0.030639221	90.63656249	415	350.7343463
test 109	56.31036325	0.194896904	0.83820425	0.015552313	118.2761638	405	348.6896368
test 110	50.0654105	0.106288094	0.75609625	0.013696412	119.0503045	401	350.9345895
test 111	63.91321825	0.586650561	0.97324225	0.017575247	117.0619818	409	345.0867818
test 112	51.24983625	0.358490395	0.8281425	0.005992698	113.7580736	408	356.7501638
test 113	46.8343695	0.200028342	0.74746425	0.020854226	113.9969219	404	357.1656305

test #	z	stdev z	y max	stdev y	y' max (mrad)	beamstop	z from bs
test 114	56.0454015	0.140167126	0.948962	0.017679792	111.2102419	412	355.9545985
test 115	49.659091	0.217170327	0.76813825	0.015886233	106.3305195	411	361.340909
test 116	46.604069	0.239334913	0.68104275	0.02318534	107.7237722	407	360.395931
test 117	53.20883375	0.636254464	0.88340175	0.043869783	104.0181328	415	361.7911663
test 118	55.95973975	0.320417465	0.82921475	0.031188764	119.7953856	405	349.0402603
test 119	49.673701	0.385305383	0.7434765	0.032222395	121.3463288	401	351.326299
test 120	63.778286	0.333973695	0.9472505	0.017218204	120.5678247	409	345.221714
test 121	50.92127475	0.39809438	0.83104325	0.031493613	113.4083968	408	357.0787253
test 122	46.4894185	0.442424953	0.72515075	0.016164592	113.408615	404	357.5105815
test 123	55.72354625	0.488305778	0.93944225	0.030808021	110.2054559	412	356.2764538
test 124	49.288916	0.494388087	0.81414725	0.031442834	105.6443433	411	361.711084
test 125	46.36863025	0.330362969	0.6898605	0.023815751	106.2530705	407	360.6313698
test 126	52.852299	0.261612318	0.88534925	0.042314452	103.8888475	415	362.147701
test 127	56.363979	0.31897664	0.862827	0.024891531	119.933572	405	348.636021
test 128	50.47158325	0.178801568	0.76453775	0.022058067	120.7692793	401	350.5284168
test 129	64.78922475	0.113507519	0.96700625	0.02924994	119.2509301	409	344.2107753
test 130	51.540911	0.246080127	0.8247105	0.022158535	114.0269852	408	356.459089
test 131	47.46798975	0.215110807	0.7516555	0.023145752	114.2099393	404	356.5320103
test 132	55.76677225	0.769789048	0.97228875	0.03842766	109.8376277	412	356.2332278
test 133	49.9770175	0.16701471	0.780494	0.015807327	105.4027025	411	361.0229825
test 134	46.81696625	0.158050103	0.6985155	0.015685119	109.6335987	407	360.1830338
test 135	52.6927245	0.108125885	0.8995255	0.020289952	104.4185986	415	362.3072755
test 136	49.79187975	0.219487635	1.1908715	0.014493888	120.1595485	405	355.2081203
test 137	45.2854555	0.151231438	1.025588	0.025665323	119.3292954	401	355.7145445
test 138	57.30300775	0.760527378	1.27803875	0.039139755	120.7799258	409	351.6969923
test 139	52.09442375	0.072037663	0.78835075	0.01537917	114.2536598	408	355.9055763
test 140	47.57488325	0.165506589	0.6857105	0.008774086	115.1495373	404	356.4251168
test 141	56.855391	0.04037513	0.8987255	0.018359346	113.5760357	412	355.144609
test 142	50.2005005	0.285468718	0.76149375	0.020980926	105.8068771	411	360.7994995
test 143	46.79666825	0.46235281	0.68006025	0.018457037	107.2372617	407	360.2033318

test #	z	stdev z	y max	stdev y	y' max (mrad)	beamstop	z from bs
test 144	54.206637	0.32402289	0.85162	0.019415665	104.1862952	415	360.793363
test 145	49.67371325	0.587298521	1.1700185	0.034276389	119.587866	405	355.3262868
test 146	45.029697	0.119055232	1.0133775	0.030613601	120.1040907	401	355.970303
test 147	56.691389	0.358883995	1.253583	0.028260451	118.6916394	409	352.308611
test 148	51.91459875	0.164110104	0.78545675	0.008216221	113.0802313	408	356.0854013
test 149	47.435781	0.117322831	0.689586	0.006146341	113.7197636	404	356.564219
test 150	57.02247625	0.329895149	0.90488425	0.007752747	113.5876858	412	354.9775238
test 151	49.99195225	0.318142374	0.78675175	0.02038769	108.0800812	411	361.0080478
test 152	46.82596175	0.253501236	0.67848275	0.019730674	107.3469992	407	360.1740383
test 153	53.286663	0.379047939	0.86977125	0.02986335	103.8487486	415	361.713337
test 154	50.172058	0.370723566	1.19120825	0.019514063	120.9917215	405	354.827942
test 155	45.91179425	0.309379494	1.0420825	0.034795089	121.6813448	401	355.0882058
test 156	57.5419035	0.551508687	1.25460225	0.007590639	119.7664568	409	351.4580965
test 157	52.476626	0.125461827	0.799306	0.011624056	113.5639493	408	355.523374
test 158	47.83839275	0.078076381	0.71150613	0.01795266	114.5479223	404	356.1616073
test 159	57.1364135	0.273782226	0.89872575	0.029424253	113.9037213	412	354.8635865
test 160	50.27069975	0.557691322	0.76001475	0.0386912	107.6314879	411	360.7293003
test 161	47.09051075	0.28372898	0.697804	0.031086164	108.3736019	407	359.9094893
test 162	54.12995725	0.64195819	0.853885	0.045470117	104.0642967	415	360.8700428
test 163	48.90853775	0.250224622	1.2224875	0.01837006	120.1341976	405	356.0914623
test 164	43.07687425	0.078039382	1.1717835	0.01869069	120.0546979	401	357.9231258
test 165	57.2457165	0.503108607	1.2225605	0.04070755	118.3465005	409	351.7542835
test 166	52.068561	0.339600077	0.7985155	0.014700956	114.5345705	408	355.931439
test 167	47.262434	0.110392309	0.7225785	0.011943978	113.5101059	404	356.737566
test 168	57.595699	0.212164249	0.859264	0.013740302	113.1513535	412	354.404301
test 169	50.88536125	0.249981579	0.75314575	0.010022534	107.8612169	411	360.1146388
test 170	47.48146025	0.26374853	0.669244	0.030687798	108.2096719	407	359.5185398
test 171	54.632734	0.453085116	0.865176	0.028526187	104.4029342	415	360.367266
test 172	48.9126855	0.32911723	1.217891	0.018011847	118.8604127	405	356.0873145
test 173	42.6614875	0.098800297	1.1869915	0.019849194	119.349454	401	358.3385125

test #	z	stdev z	y max	stdev y	y' max (mrad)	beamstop	z from bs
test 174	56.8458205	0.207330436	1.2354675	0.027197571	118.2102339	409	352.1541795
test 175	51.95983525	0.134982062	0.7900385	0.024107257	113.6463288	408	356.0401648
test 176	47.132638	0.170748873	0.7300505	0.019803543	112.9810093	404	356.867362
test 177	57.5373505	0.256451402	0.86927475	0.019122929	114.3133501	412	354.4626495
test 178	50.57086425	0.3616216	0.75095375	0.022245622	107.3394071	411	360.4291358
test 179	47.209995	0.157585496	0.655668	0.020646973	108.8608542	407	359.790005
test 180	54.55518925	0.540016765	0.833124	0.034225633	107.22199	415	360.4448108
test 181	49.29805725	0.217834095	1.23140125	0.016038844	119.1955159	405	355.7019428
test 182	43.404812	0.207985957	1.20771625	0.035429298	118.0818213	401	357.595188
test 183	56.6783255	0.346134263	1.2340705	0.013732943	118.7226626	409	352.3216745
test 184	52.328246	0.316165074	0.7963515	0.013838158	115.0275388	408	355.671754
test 185	47.60914425	0.099369846	0.73586825	0.027073816	113.962408	404	356.3908558
test 186	57.5376885	0.19612783	0.87433025	0.024065462	113.5025137	412	354.4623115
test 187	50.89977775	0.229327971	0.76028475	0.02364794	108.5223912	411	360.1002223
test 188	47.40350375	0.370089804	0.68808525	0.015760947	108.8659157	407	359.5964963
test 189	54.79820275	0.660273425	0.853493	0.017319429	105.393234	415	360.2017973
test 190	48.95447625	0.502922348	1.1965475	0.030283168	119.8442985	405	356.0455238
test 191	42.9769055	0.230569586	1.1501	0.034238428	119.2687325	401	358.0230945
test 192	56.324604	0.210892638	1.2318105	0.004517669	117.6483688	409	352.675396
test 193	49.453564	0.277895367	0.967585	0.043890498	113.9632806	408	358.546436
test 194	45.40812675	0.222727834	0.870717	0.031374665	113.5614186	404	358.5918733
test 195	54.8065845	0.262073739	1.036619	0.029579353	113.3370565	412	357.1934155
test 196	51.436174	0.201892758	0.71315775	0.030813167	107.466118	411	359.563826
test 197	47.5104575	0.321481118	0.66069675	0.040568583	107.6238085	407	359.4895425
test 198	54.85553875	0.263043873	0.831495	0.01307759	105.9762176	415	360.1444613
test 199	48.67746225	0.104715016	1.18674475	0.022661665	118.7350544	405	356.3225378
test 200	42.454613	0.231812558	1.15757575	0.02474586	119.4719325	401	358.545387
test 201	56.487421	0.425411791	1.21410275	0.045627635	117.9983946	409	352.512579
test 202	49.232869	0.272543789	0.955953	0.032982441	113.6506922	408	358.767131
test 203	45.13062675	0.228605691	0.8861965	0.020120466	113.9934312	404	358.8693733

test #	z	stdev z	y max	stdev y	y' max (mrad)	beamstop	z from bs
test 204	54.4781675	0.144973745	1.038249	0.013805929	114.7560965	412	357.5218325
test 205	50.88602775	0.57938652	0.73618125	0.029932645	108.2951494	411	360.1139723
test 206	47.521012	0.408497044	0.6487625	0.019172766	108.3599011	407	359.478988
test 207	55.07926575	0.413589378	0.8061425	0.030932998	106.3642043	415	359.9207343
test 208	49.04088675	0.295440155	1.185036	0.017211163	120.808811	405	355.9591133
test 209	43.29037475	0.267748549	1.1758515	0.022895789	120.0945787	401	357.7096253
test 210	56.6205775	0.362650799	1.2334785	0.017576151	119.3309099	409	352.3794225
test 211	49.6755515	0.362811498	0.97613075	0.005194134	114.6812655	408	358.3244485
test 212	45.291219	0.249478654	0.9131215	0.033709658	115.2868947	404	358.708781
test 213	55.00147575	0.434771827	1.00633675	0.0455349	114.2958968	412	356.9985243
test 214	51.623747	0.293325958	0.7331685	0.020324127	107.8515739	411	359.376253
test 215	47.928637	0.381001845	0.6382615	0.023638063	109.1357872	407	359.071363
test 216	55.14674075	0.458497009	0.828142	0.040976429	106.4470638	415	359.8532593
test 217	66.22729475	0.676753771	1.12315125	0.028131229	127.6355791	405	338.7727053
test 218	56.63373625	0.17847652	0.96728	0.020285777	125.4468926	401	344.3662638
test 219	80.0153185	1.062390955	1.240398	0.039419968	103.9652493	409	328.9846815
test 220	56.49149825	0.343810555	1.03579775	0.0166246	111.3774008	408	351.5085018
test 221	51.28855925	0.379047034	0.88164275	0.036208974	120.2295363	404	352.7114408
test 222	62.26798275	0.264393496	1.197814	0.004418553	97.67233377	412	349.7320173
test 223	53.022717	0.192304618	0.94804325	0.038854146	109.2462665	411	357.977283
test 224	49.33637825	0.241969778	0.798895	0.016946752	112.509945	407	357.6636218
test 225	56.9946865	0.367487847	1.05127575	0.007925485	99.70140992	415	358.0053135
test 226	65.73886	0.460800792	1.093087	0.027856001	126.8421088	405	339.26114
test 227	56.23649925	0.211157374	0.9652865	0.014369475	126.8265754	401	344.7635008
test 228	78.456232	1.336058723	1.248084	0.028701237	108.1681767	409	330.543768
test 229	56.1269795	0.221507432	1.0347945	0.020346129	111.6787755	408	351.8730205
test 230	50.61147375	0.379897524	0.8869935	0.026362459	120.2544508	404	353.3885263
test 231	61.82073075	0.647111669	1.21248175	0.02640767	97.59807001	412	350.1792693
test 232	53.03030225	0.454136204	0.93306575	0.020644415	109.8490596	411	357.9696978
test 233	49.0165495	0.408797428	0.814585	0.035341005	112.2210493	407	357.9834505

test #	z	stdev z	y max	stdev y	y' max (mrad)	beamstop	z from bs
test 234	56.907011	0.450720123	1.0940805	0.041116084	99.20137309	415	358.092989
test 235	66.8052885	0.38598924	1.1310015	0.021027621	127.461788	405	338.1947115
test 236	57.393245	0.372312867	1.00105575	0.029407801	127.7842376	401	343.606755
test 237	80.268504	0.752274849	1.29241775	0.035242179	105.7315225	409	328.731496
test 238	56.72490575	0.351782226	1.03727925	0.015512359	109.1900669	408	351.2750943
test 239	51.47565975	0.435413107	0.91929925	0.021101344	121.9607283	404	352.5243403
test 240	63.2569045	0.112190439	1.17463575	0.023867994	98.1294355	412	348.7430955
test 241	52.81105775	0.380368819	0.93249725	0.020179119	108.1821829	411	358.1889423
test 242	49.68230025	0.524124494	0.82258425	0.020799641	111.3213321	407	357.3176998
test 243	57.06960875	0.222895979	1.0505955	0.035220882	97.84224157	415	357.9303913
test 244	57.53298675	0.216522501	1.40321525	0.0369876	128.7004918	405	347.4670133
test 245	49.74113725	0.311720436	1.31653625	0.047826671	127.3380441	401	351.2588628
test 246	70.82293875	0.619298298	1.480478	0.04572633	125.3893404	409	338.1770613
test 247	57.683574	0.315584617	0.98012925	0.035121883	120.7139088	408	350.316426
test 248	52.148358	0.121610122	0.85778875	0.022847999	122.6825965	404	351.851642
test 249	64.32598225	0.31897157	1.13732125	0.027711701	113.1291878	412	347.6740178
test 250	54.09432075	0.799485316	0.910197	0.038334585	110.9220008	411	356.9056793
test 251	50.119675	0.399301795	0.79655825	0.020875171	112.1018434	407	356.880325
test 252	57.75625625	0.425558759	1.04542575	0.038454275	103.2168957	415	357.2437438
test 253	57.4406065	0.426027919	1.395255	0.036138756	128.6648871	405	347.5593935
test 254	49.80996125	0.362360164	1.258368	0.025389162	128.3084908	401	351.1900388
test 255	69.46610025	0.703094045	1.47391075	0.063626127	125.3779521	409	339.5338998
test 256	57.575261	0.075974212	0.9602515	0.018570962	121.3868204	408	350.424739
test 257	51.62742275	0.15592631	0.84951325	0.031585362	121.7344028	404	352.3725773
test 258	64.036341	0.220168019	1.11258125	0.007205033	113.7229924	412	347.963659
test 259	53.54956825	0.306313088	0.917024	0.014227255	110.5860249	411	357.4504318
test 260	49.6257415	0.26130203	0.78878425	0.034443787	114.0520743	407	357.3742585
test 261	57.06524025	0.395703508	1.066564	0.031844332	103.2869271	415	357.9347598
test 262	57.87504475	0.496133728	1.421826	0.018675046	126.8931597	405	347.1249553
test 263	50.376206	0.609502528	1.299441	0.040042925	126.3893268	401	350.623794

test #	z	stdev z	y max	stdev y	y' max (mrad)	beamstop	z from bs
test 264	71.3089945	0.300073128	1.50606525	0.007511966	124.5317292	409	337.6910055
test 265	58.165393	0.204789084	0.98656775	0.011210336	121.4084625	408	349.834607
test 266	52.52218575	0.070700326	0.85291025	0.017316773	122.7850037	404	351.4778143
test 267	64.552716	0.356824154	1.12990775	0.015521818	111.8478107	412	347.447284
test 268	53.73509425	0.583607536	0.95014275	0.043739567	109.5838568	411	357.2649058
test 269	50.44392975	0.455993146	0.8158025	0.027197386	113.3580005	407	356.5560703
test 270	58.1625935	0.616748411	1.0590965	0.044464802	102.9741641	415	356.8374065
test 271	57.30101425	0.310667749	1.4117175	0.030249396	127.548269	405	347.6989858
test 272	48.1779465	0.365567723	1.35882925	0.023812124	128.3620288	401	352.8220535
test 273	70.8533775	1.278133807	1.45451425	0.025656477	127.0516356	409	338.1466225
test 274	58.35152525	0.131353238	0.9635265	0.025120037	121.3115968	408	349.6484748
test 275	51.679875	0.265572097	0.87568275	0.02388041	121.4607351	404	352.320125
test 276	65.238621	0.16842961	1.09478025	0.006172665	121.5004414	412	346.761379
test 277	54.81986125	0.293114747	0.89278975	0.032421028	111.9560211	411	356.1801388
test 278	50.14310925	0.261686926	0.817965	0.010546808	115.4405273	407	356.8568908
test 279	58.434173	1.172628784	1.0289975	0.04730865	103.1219935	415	356.565827
test 280	56.9347495	0.150764204	1.397161	0.024823575	125.803987	405	348.0652505
test 281	47.5695215	0.101405463	1.3809195	0.027078442	128.0665446	401	353.4304785
test 282	69.88060075	0.227697473	1.444247	0.033912383	125.5155277	409	339.1193993
test 283	58.12388225	0.163233889	0.94831675	0.039359128	122.2667282	408	349.8761178
test 284	51.25842275	0.135186605	0.85552125	0.031516086	120.6760787	404	352.7415773
test 285	64.9776265	0.326047596	1.06621625	0.036759473	121.4207235	412	347.0223735
test 286	54.13892025	0.458555723	0.89904025	0.033990202	111.8322773	411	356.8610798
test 287	50.2526745	0.157022236	0.78867875	0.035951545	114.0428677	407	356.7473255
test 288	59.1853865	0.242164812	1.01509725	0.014426441	105.6727485	415	355.8146135
test 289	57.6801605	0.416626454	1.42342975	0.031012081	126.1917991	405	347.3198395
test 290	48.52086875	0.198304189	1.40228	0.002047291	126.8695978	401	352.4791313
test 291	70.26392475	0.487604222	1.5023565	0.045887476	125.9937915	409	338.7360753
test 292	58.49657875	0.33423744	0.97311825	0.008170756	123.0117656	408	349.5034213
test 293	52.155803	0.17552037	0.88364975	0.022566845	121.7009797	404	351.844197

test #	z	stdev z	y max	stdev y	y' max (mrad)	beamstop	z from bs
test 294	65.2744575	0.329514443	1.10885425	0.0452698	120.7828056	412	346.7255425
test 295	54.77899225	0.497493899	0.908077	0.034803439	112.4019527	411	356.2210078
test 296	50.920275	0.146750794	0.78761875	0.023270864	114.9084201	407	356.079725
test 297	59.52809975	0.596128423	1.007717	0.01613638	104.528118	415	355.4719003
test 298	57.06918625	0.386044898	1.37599625	0.02854738	125.6070702	405	347.9308138
test 299	48.06791875	0.293330951	1.3646085	0.046600729	128.1440372	401	352.9320813
test 300	69.18241875	0.458680517	1.45195425	0.022821766	123.3214307	409	339.8175813
test 301	55.81084875	0.586583509	1.110846	0.061054573	122.2484022	408	352.1891513
test 302	49.0772655	0.314380231	1.06650425	0.043024399	121.7093137	404	354.9227345
test 303	63.03219725	0.551331074	1.199691	0.034822991	120.7826747	412	348.9678028
test 304	54.99152675	0.55953226	0.88621325	0.014019114	113.1545387	411	356.0084733
test 305	50.8501985	0.311771916	0.7608415	0.028151198	114.4551144	407	356.1498015
test 306	59.7752315	0.106756185	0.974719	0.020484818	106.8742768	415	355.2247685
test 307	56.60383625	0.491396785	1.3632055	0.050477267	127.0652055	405	348.3961638
test 308	47.56774475	0.24676616	1.35039425	0.003348451	125.9410826	401	353.4322553
test 309	68.91289525	0.517230848	1.4272165	0.024503526	123.8609556	409	340.0871048
test 310	54.9150245	0.584202282	1.100631	0.009301684	121.508819	408	353.0849755
test 311	48.85359525	0.315240279	1.023019	0.036090056	121.2379875	404	355.1464048
test 312	62.7799505	0.284292661	1.16136275	0.035871359	121.6671203	412	349.2200495
test 313	55.305574	0.576992971	0.862032	0.051051899	113.599554	411	355.694426
test 314	50.87894975	0.279960124	0.7570935	0.021573216	113.7203308	407	356.1210503
test 315	59.9239145	0.412450354	1.0212135	0.026617916	107.6255102	415	355.0760855
test 316	57.21016275	0.082092039	1.39369625	0.027824043	126.1203279	405	347.7898373
test 317	48.44591475	0.237774586	1.38591575	0.016140276	127.4125261	401	352.5540853
test 318	69.72775175	0.448871305	1.456702	0.044745279	124.9112947	409	339.2722483
test 319	55.397375	0.51246107	1.12682375	0.052649008	123.0568387	408	352.602625
test 320	49.74697525	0.462747384	1.05154075	0.040187389	123.3121804	404	354.2530248
test 321	63.342214	0.320492211	1.188479	0.02409133	121.4287083	412	348.657786
test 322	55.334392	0.566813333	0.91232675	0.026311497	113.0129052	411	355.665608
test 323	51.4760825	0.263827814	0.774078	0.020506918	114.7061364	407	355.5239175

test #	z	stdev z	y max	stdev y	y' max (mrad)	beamstop	z from bs
test 324	59.5121865	0.693108373	1.0155955	0.045649908	103.2031949	415	355.4878135
test 325	103.4994543	2.951201182	1.93245	0.017742288	86.11537432	405	301.5005458
test 326	77.29521775	0.534428645	1.6043775	0.029479717	116.9931286	401	323.7047823
test 327	152.4094978	2.540698965	2.59243875	0.05584862	59.94040973	409	256.5905023
test 328	68.4987505	0.937629929	1.520778	0.011076848	94.88652648	408	339.5012495
test 329	60.87587275	0.535996403	1.272342	0.031676253	107.2558494	404	343.1241273
test 330	78.9283425	0.179224164	1.861495	0.016961468	82.53819112	412	333.0716575
test 331	59.71981925	0.529698876	1.26372575	0.030281027	92.44494176	411	351.2801808
test 332	55.41221875	0.249533035	1.1072565	0.01931865	106.8237059	407	351.5877813
test 333	65.28862375	0.859369338	1.43151375	0.053323932	81.65143296	415	349.7113763
test 334	100.0118973	1.271765306	1.8227055	0.053815979	89.36181763	405	304.9881028
test 335	75.2939955	0.948921289	1.5456545	0.039262009	121.3833734	401	325.7060045
test 336	146.1426005	1.040856467	2.48283025	0.030810516	62.81069095	409	262.8573995
test 337	68.241019	0.716753595	1.510515	0.049632152	95.0936098	408	339.758981
test 338	59.76802075	0.780665505	1.26599325	0.02559966	108.2194893	404	344.2319793
test 339	77.872766	0.949334182	1.81947875	0.042516701	83.98013852	412	334.127234
test 340	60.1445085	0.501729472	1.25311425	0.043322143	92.59870526	411	350.8554915
test 341	54.2482525	0.233541035	1.130617	0.054187643	107.9171547	407	352.7517475
test 342	65.7596295	0.507224697	1.45722375	0.037293192	83.23575559	415	349.2403705
test 343	104.8070278	1.031827589	1.9874365	0.024814454	86.04652109	405	300.1929723
test 344	78.37952075	0.194551687	1.58630575	0.067340813	114.8650486	401	322.6204793
test 345	153.9643163	0.652507541	2.61449825	0.035174793	59.61512399	409	255.0356838
test 346	69.68037	0.850233338	1.52772775	0.034808819	93.00335985	408	338.31963
test 347	61.73097975	0.602237114	1.29070975	0.018560429	104.8176245	404	342.2690203
test 348	78.831603	0.980093781	1.892798	0.026656812	83.29553312	412	333.168397
test 349	60.384119	0.182377234	1.25209025	0.053236623	90.95054722	411	350.615881
test 350	55.47927675	0.310560975	1.1372455	0.025370802	105.4707267	407	351.5207233
test 351	65.22173525	0.610108346	1.453946	0.034250935	82.61856354	415	349.7782648
test 352	88.50907525	0.931256521	2.008517	0.059564813	109.0605199	405	316.4909248
test 353	63.36693625	0.369685684	1.897876	0.0493382	138.5575442	401	337.6330638

test #	z	stdev z	y max	stdev y	y' max (mrad)	beamstop	z from bs
test 354	136.8002548	1.893355788	2.56241725	0.045294524	68.01569912	409	272.1997453
test 355	71.91655725	0.269769676	1.472679	0.058723587	103.1453372	408	336.0834428
test 356	62.844761	0.118961331	1.244073	0.015192645	124.7642943	404	341.155239
test 357	82.8083455	0.471679403	1.774755	0.013612458	87.34443518	412	329.1916545
test 358	61.1955575	0.710662392	1.2704075	0.057242188	92.89946913	411	349.8044425
test 359	56.09475575	0.27027054	1.1127025	0.041390492	108.9494733	407	350.9052443
test 360	66.807728	1.020347211	1.471178	0.045522837	81.8062873	415	348.192272
test 361	85.72394775	0.797117357	2.0221945	0.043753567	115.0710847	405	319.2760523
test 362	62.607542	0.284979008	1.828719	0.036257469	139.5589705	401	338.392458
test 363	134.0517088	2.883602869	2.4239485	0.015174841	69.48906244	409	274.9482913
test 364	70.73143625	0.202213384	1.4289695	0.033998188	104.9788929	408	337.2685638
test 365	62.037077	0.284609129	1.216785	0.02618576	127.1051736	404	341.962923
test 366	82.29169375	0.733200852	1.75114625	0.044286479	87.2966568	412	329.7083063
test 367	61.41480175	0.507219436	1.26562925	0.033795264	93.76297077	411	349.5851983
test 368	55.996849	0.366117711	1.0731565	0.032364065	112.3324014	407	351.003151
test 369	66.59733225	0.715756978	1.40764875	0.041291384	82.04858263	415	348.4026678
test 370	89.1760395	0.907525058	2.07219775	0.051093446	109.6612622	405	315.8239605
test 371	64.62264375	0.234407584	1.91819125	0.047866286	139.7685409	401	336.3773563
test 372	138.652779	2.136292094	2.553926	0.070759439	67.8067832	409	270.347221
test 373	72.2472295	0.511998563	1.492394	0.008876943	102.4269597	408	335.7527705
test 374	63.46176475	0.334497708	1.2625265	0.024579159	121.9437986	404	340.5382353
test 375	83.0751135	0.613341006	1.79688125	0.056045523	86.39144178	412	328.9248865
test 376	61.663058	0.590998292	1.288384	0.040104091	91.529822	411	349.336942
test 377	56.96263125	0.309420088	1.0952395	0.028621056	106.5681897	407	350.0373688
test 378	67.070727	1.455407239	1.474969	0.047306364	81.42807445	415	347.929273
test 379	87.22223675	0.732963694	2.012441	0.044476306	110.1515252	405	317.7777633
test 380	62.95110675	0.344141209	1.84204	0.022818569	135.6179297	401	338.0488933
test 381	131.9370783	1.358738213	2.42394775	0.035914678	70.69905557	409	277.0629218
test 382	73.13895025	0.454558391	1.43326125	0.031544646	123.5496325	408	334.8610498
test 383	63.28181975	0.391020947	1.23344875	0.021214018	133.9151429	404	340.7181803

test #	z	stdev z	y max	stdev y	y' max (mrad)	beamstop	z from bs
test 384	84.49425375	1.041817568	1.73917075	0.047010035	96.28593147	412	327.5057463
test 385	62.4928145	0.549520361	1.2437845	0.025780134	93.78251846	411	348.5071855
test 386	57.4686195	0.564490405	1.09411275	0.030204156	111.2822367	407	349.5313805
test 387	68.9059965	0.456253254	1.418562	0.024153776	81.95616745	415	346.0940035
test 388	85.21136475	0.871363113	1.9581775	0.046550633	113.2590839	405	319.7886353
test 389	62.46812275	0.866443281	1.83116175	0.045359576	137.8282147	401	338.5318773
test 390	130.8609183	1.728194234	2.4197595	0.007038721	71.75681237	409	278.1390818
test 391	72.214451	0.279486694	1.38392	0.017879033	128.3679629	408	335.785549
test 392	62.60656025	0.171467721	1.22679775	0.035979366	133.8364722	404	341.3934398
test 393	84.744364	0.852967712	1.760635	0.029918054	97.77186117	412	327.255636
test 394	62.36447725	0.382489262	1.2393475	0.022219338	94.58545718	411	348.6355228
test 395	56.84977575	0.414584933	1.0835195	0.02702032	111.7178709	407	350.1502243
test 396	68.090336	0.581669662	1.44130925	0.068845914	81.59606239	415	346.909664
test 397	87.19971675	1.278150907	2.05233375	0.058226146	113.8662403	405	317.8002833
test 398	64.497923	0.530392265	1.874952	0.027833859	138.854861	401	336.502077
test 399	135.2073175	2.189136963	2.445989	0.026092791	68.95171919	409	273.7926825
test 400	73.73455075	0.366316149	1.43307175	0.019170716	123.2345569	408	334.2654493
test 401	63.93606525	0.465516156	1.2139895	0.008950579	133.7493802	404	340.0639348
test 402	85.2518975	0.75354936	1.752857	0.028605116	96.63770259	412	326.7481025
test 403	62.99571175	1.056806603	1.24414375	0.023628565	94.3781557	411	348.0042883
test 404	57.820746	0.37095202	1.08835975	0.025842936	109.1376198	407	349.179254
test 405	68.53801075	0.626924035	1.451586	0.047757423	81.14441482	415	346.4619893
test 406	85.01165075	0.263766216	1.994096	0.023554672	115.0772807	405	319.9883493
test 407	62.6442475	0.733827122	1.822211	0.042113453	140.6013683	401	338.3557525
test 408	127.610341	2.349676517	2.375924	0.038614684	72.80619158	409	281.389659
test 409	70.91378625	0.742057717	1.50873025	0.056775621	134.0599179	408	337.0862138
test 410	59.8052725	0.179857105	1.3637315	0.050890835	133.6673061	404	344.1947275
test 411	86.18920925	0.650002472	1.68026375	0.018125003	110.6526528	412	325.8107908
test 412	63.84877775	1.13156284	1.1918415	0.029279032	95.17197508	411	347.1512223
test 413	57.92429625	0.487005895	1.05171325	0.015898116	112.9399068	407	349.0757038

test #	z	stdev z	y max	stdev y	y' max (mrad)	beamstop	z from bs
test 414	69.96612175	0.899628692	1.452678	0.050871256	81.96406507	415	345.0338783
test 415	83.8706455	0.258991656	1.9428115	0.047114242	117.9274906	405	321.1293545
test 416	61.34184825	0.172765829	1.77699125	0.020867862	138.0759206	401	339.6581518
test 417	127.2938423	3.798207148	2.26759	0.040746185	72.09950777	409	281.7061578
test 418	70.52827575	0.711183495	1.480391	0.049324944	133.8561944	408	337.4717243
test 419	58.48052875	0.777696719	1.36028475	0.0496224	133.3606954	404	345.5194713
test 420	85.38505375	0.348151256	1.6975685	0.052784081	113.3231811	412	326.6149463
test 421	63.77144675	0.506874764	1.25573225	0.02055198	97.00875958	411	347.2285533
test 422	57.677259	0.479590312	1.04781225	0.039627328	115.004675	407	349.322741
test 423	70.202722	0.355655213	1.40719925	0.04190904	82.18986704	415	344.797278
test 424	86.399209	0.961676966	2.0123175	0.039351805	114.2558851	405	318.600791
test 425	63.70337325	0.159700662	1.866779	0.035378016	138.8850116	401	337.2966268
test 426	130.9576053	0.263521449	2.450215	0.081084644	71.98933386	409	278.0423948
test 427	71.15758775	0.18610567	1.5114285	0.016424192	133.0369805	408	336.8424123
test 428	59.76762875	0.757131061	1.4109845	0.051040951	133.7455405	404	344.2323713
test 429	86.36884225	0.694987916	1.74515225	0.036509295	108.0251906	412	325.6311578
test 430	64.12342725	0.718541945	1.2320925	0.042411697	92.93271765	411	346.8765728
test 431	58.3027475	0.500657932	1.08613575	0.044108458	112.2477965	407	348.6972525
test 432	71.00363725	0.503257355	1.45635975	0.012015331	80.98113926	415	343.9963628

[This page intentionally left blank.]

Appendix D

Calculated Data: brightness, normalized emittance, % of beam lost

test #	emittance	average ke	gamma	beta gamma	norm. emittance	# ions lost	% losses	new brightness
10k ions	163.62617	24912.6449	1.00002655E+00	0.007287525	1.19242989	5593	0.5593	0.309939795
test 1	155.82739	24912.6803	1.00002655E+00	0.007287531	1.13559686	2801	0.5602	0.34104121
test 2	163.58705	24912.5613	1.00002655E+00	0.007287513	1.19214283	2796	0.5592	0.31015944
test 3	146.24932	24912.7935	1.00002655E+00	0.007287547	1.06579883	2769	0.6364	0.320090948
test 4	131.4118	24952.2526	1.00002660E+00	0.007293316	0.95842783	1707	0.3414	0.716973156
test 5	124.14174	24950.6612	1.00002659E+00	0.007293084	0.90537607	1769	0.3538	0.78833159
test 6	133.59568	24952.3239	1.00002660E+00	0.007293327	0.97435696	1739	0.3478	0.686980816
test 7	112.13427	24973.1528	1.00002662E+00	0.00729637	0.81817317	2	0.0004	1.493261213
test 8	110.12845	24972.0034	1.00002662E+00	0.007296202	0.80351947	327	0.0654	1.447547997
test 9	110.87533	24973.0549	1.00002662E+00	0.007296356	0.80898585	3	0.0006	1.527064913
test 10	155.24085	24912.6456	1.00002655E+00	0.007287526	1.13132169	2783	0.5566	0.346436354
test 11	161.41319	24912.7326	1.00002655E+00	0.007287538	1.17630482	2843	0.5686	0.311774355
test 12	139.50916	24912.7406	1.00002655E+00	0.007287539	1.01667847	2843	0.5686	0.41736198
test 13	124.37744	24951.9145	1.00002660E+00	0.007293267	0.9071179	1699	0.3398	0.802320793
test 14	123.3585	24950.6607	1.00002659E+00	0.007293084	0.89966385	1819	0.3638	0.786019143
test 15	135.18496	24951.9992	1.00002660E+00	0.007293279	0.98594167	1683	0.3366	0.682453432
test 16	110.91524	24972.9362	1.00002662E+00	0.007296339	0.80927514	3	0.0006	1.525973323
test 17	109.77211	24971.3419	1.00002662E+00	0.007296106	0.80090888	511	0.1022	1.399630458
test 18	113.26487	24972.7282	1.00002662E+00	0.007296308	0.82641538	4	0.0008	1.463038139
test 19	154.10461	24912.5532	1.00002655E+00	0.007287512	1.12303918	2847	0.5694	0.341416267
test 20	168.65905	24912.6853	1.00002655E+00	0.007287531	1.22910813	2782	0.5564	0.293637391
test 21	145.08701	24912.6542	1.00002655E+00	0.007287527	1.05732551	2721	0.5442	0.4077152
test 22	131.31448	24952.3323	1.00002660E+00	0.007293328	0.95771956	1701	0.3402	0.719342296
test 23	122.97816	24950.6555	1.00002659E+00	0.007293083	0.89688995	1803	0.3606	0.794866724
test 24	137.97668	24952.2895	1.00002660E+00	0.007293322	1.00630835	1615	0.323	0.66853864

test #	emittance	average ke	gamma	beta gamma	norm. emittance	# ions lost	% losses	new brightness
test 25	109.93809	24973.0797	1.00002662E+00	0.00729636	0.80214784	0	0	1.554143672
test 26	109.34503	24972.3246	1.00002662E+00	0.007296249	0.79780862	178	0.0356	1.515164391
test 27	109.65342	24972.9735	1.00002662E+00	0.007296344	0.80006907	5	0.001	1.560667987
test 28	221.24811	24918.0996	1.00002656E+00	0.007288323	1.61252771	2649	0.5298	0.180829071
test 29	209.74949	24918.3589	1.00002656E+00	0.007288361	1.52873003	2713	0.5426	0.195719711
test 30	186.66222	24918.0564	1.00002656E+00	0.007288317	1.3604534	2739	0.5478	0.244322362
test 31	139.08402	24955.1155	1.00002660E+00	0.007293735	1.01444198	957	0.1914	0.785740812
test 32	132.54579	24951.6874	1.00002660E+00	0.007293234	0.96668744	1644	0.3288	0.718256875
test 33	136.28979	24955.3111	1.00002660E+00	0.007293763	0.99406546	905	0.181	0.828808001
test 34	112.64806	24972.9415	1.00002662E+00	0.007296339	0.82191844	0	0	1.480275494
test 35	108.49421	24972.1577	1.00002662E+00	0.007296225	0.79159816	250	0.05	1.51605183
test 36	111.42029	24972.6594	1.00002662E+00	0.007296298	0.81295563	0	0	1.513095413
test 37	224.48066	24917.9103	1.00002656E+00	0.007288296	1.63608143	2649	0.5298	0.175659966
test 38	204.06672	24918.3997	1.00002656E+00	0.007288367	1.48731317	2722	0.5444	0.205958097
test 39	184.65656	24918.1284	1.00002656E+00	0.007288327	1.34583747	2687	0.5374	0.255399708
test 40	140.77008	24955.1449	1.00002660E+00	0.007293739	1.02674026	911	0.1822	0.775757396
test 41	127.45582	24951.5858	1.00002660E+00	0.007293219	0.92956319	1688	0.3376	0.766588827
test 42	138.60539	24955.1558	1.00002660E+00	0.007293741	1.01095174	949	0.1898	0.792741129
test 43	112.57334	24972.8614	1.00002662E+00	0.007296328	0.82137195	0	0	1.482245914
test 44	110.56798	24971.7369	1.00002662E+00	0.007296163	0.80672205	470	0.094	1.392131752
test 45	112.42249	24972.827	1.00002662E+00	0.007296323	0.82027077	0	0	1.486228296
test 46	229.30016	24917.9521	1.00002656E+00	0.007288302	1.67120872	2696	0.5392	0.164987515
test 47	217.61077	24918.3099	1.00002656E+00	0.007288354	1.58602435	2738	0.5476	0.179846875
test 48	186.06866	24918.109	1.00002656E+00	0.007288325	1.35612876	2683	0.5366	0.251973099
test 49	140.56554	24954.9341	1.00002660E+00	0.007293708	1.02524404	970	0.194	0.766797231
test 50	134.55256	24951.8473	1.00002660E+00	0.007293257	0.98132642	1574	0.3148	0.711525347
test 51	138.70401	24955.1926	1.00002660E+00	0.007293746	1.01167185	949	0.1898	0.79161298
test 52	117.2515	25002.3	1.00002665E+00	0.007300627	0.85600946	0	0	1.36471786
test 53	113.77717	24972.3316	1.00002662E+00	0.00729625	0.83014674	168	0.0336	1.402320205
test 54	110.10749	24972.9767	1.00002662E+00	0.007296344	0.80338218	0	0	1.549371674

test #	emittance	average ke	gamma	beta gamma	norm. emittance	# ions lost	% losses	new brightness
test 55	218.45663	24923.2489	1.00002656E+00	0.007289076	1.59234705	2570	0.514	0.191672944
test 56	211.98782	24923.7223	1.00002657E+00	0.007289146	1.54521009	2666	0.5332	0.195504058
test 57	182.17393	24923.4334	1.00002657E+00	0.007289103	1.3278846	2533	0.5066	0.279819824
test 58	150.51155	24955.9099	1.00002660E+00	0.007293851	1.09780879	818	0.1636	0.694001831
test 59	133.78571	24952.6862	1.00002660E+00	0.00729338	0.97575	1658	0.3316	0.702035895
test 60	160.73363	24956.9593	1.00002660E+00	0.007294004	1.17239178	129	0.0258	0.708765542
test 61	114.57267	24972.973	1.00002662E+00	0.007296344	0.83596159	0	0	1.43095952
test 62	105.91806	24972.1873	1.00002662E+00	0.007296229	0.77280245	247	0.0494	1.591698591
test 63	110.55114	24973.0503	1.00002662E+00	0.007296355	0.80662036	0	0	1.536956732
test 64	213.05461	24923.4194	1.00002657E+00	0.007289101	1.5529766	2562	0.5124	0.202177989
test 65	205.83318	24923.7638	1.00002657E+00	0.007289152	1.50034921	2693	0.5386	0.204971217
test 66	178.91682	24923.2323	1.00002656E+00	0.007289074	1.30413792	2599	0.5198	0.282341756
test 67	149.17568	24955.8021	1.00002660E+00	0.007293835	1.08806281	803	0.1606	0.70902416
test 68	130.20129	24952.6775	1.00002660E+00	0.007293378	0.94960731	1742	0.3484	0.722591717
test 69	165.41129	24956.9882	1.00002660E+00	0.007294008	1.20651135	115	0.023	0.671168764
test 70	110.52774	24973.0515	1.00002662E+00	0.007296355	0.8064497	0	0	1.537607283
test 71	106.13515	24971.8141	1.00002662E+00	0.007296175	0.77438058	469	0.0938	1.511176343
test 72	111.5367	24973.062	1.00002662E+00	0.007296357	0.81381157	0	0	1.509914239
test 73	215.7812	24923.2863	1.00002657E+00	0.007289082	1.57284682	2549	0.5098	0.198152909
test 74	214.82443	24923.7019	1.00002657E+00	0.007289143	1.56588591	2674	0.5348	0.189722776
test 75	185.10286	24923.3325	1.00002657E+00	0.007289089	1.34923111	2609	0.5218	0.262685971
test 76	151.32721	24956.4591	1.00002660E+00	0.007293931	1.10377027	704	0.1408	0.705239911
test 77	133.94877	24953.1215	1.00002660E+00	0.007293443	0.97694778	1630	0.326	0.706182892
test 78	158.60352	24956.94	1.00002660E+00	0.007294001	1.15685427	116	0.0232	0.729874762
test 79	116.2085	24973.1446	1.00002662E+00	0.007296369	0.84790013	0	0	1.390947056
test 80	113.51725	24969.5	1.00002661E+00	0.007295837	0.82820332	142	0.0284	1.416490194
test 81	111.85568	24972.8906	1.00002662E+00	0.007296332	0.81613615	0	0	1.501325192
test 82	215.31943	24928.4186	1.00002657E+00	0.007289832	1.5696425	2478	0.4956	0.204726273
test 83	206.83805	24928.6966	1.00002657E+00	0.007289873	1.50782311	2596	0.5192	0.211477257
test 84	181.82952	24928.3694	1.00002657E+00	0.007289825	1.3255054	2493	0.4986	0.285378551

test #	emittance	average ke	gamma	beta gamma	norm. emittance	# ions lost	% losses	new brightness
test 85	168.56834	24957.0337	1.00002660E+00	0.007294015	1.22954	932	0.1864	0.538177596
test 86	157.71326	24954.097	1.00002660E+00	0.007293586	1.15029518	1747	0.3494	0.491694624
test 87	173.4063	24957.7361	1.00002660E+00	0.007294118	1.26484596	59	0.0118	0.617688587
test 88	111.07499	24973.0708	1.00002662E+00	0.007296358	0.81044292	0	0	1.522492397
test 89	106.45942	24972.392	1.00002662E+00	0.007296259	0.7767555	250	0.05	1.574544473
test 90	116.93822	24973.2539	1.00002662E+00	0.007296385	0.85322628	0	0	1.373635645
test 91	206.99582	24928.3361	1.00002657E+00	0.00728982	1.5089623	2466	0.4932	0.222576765
test 92	206.8097	24928.6976	1.00002657E+00	0.007289873	1.50761642	2582	0.5164	0.212767149
test 93	186.18816	24928.4447	1.00002657E+00	0.007289836	1.35728112	2419	0.4838	0.280206613
test 94	164.71858	24956.7499	1.00002660E+00	0.007293974	1.20145299	923	0.1846	0.564881231
test 95	153.91774	24953.916	1.00002660E+00	0.007293559	1.12260819	1812	0.3624	0.5059317
test 96	178.45835	24958.1183	1.00002660E+00	0.007294174	1.3017062	79	0.0158	0.580841199
test 97	114.97656	24973.2998	1.00002662E+00	0.007296392	0.83891403	0	0	1.420905131
test 98	106.41032	24972.1609	1.00002662E+00	0.007296225	0.77639366	472	0.0944	1.502354598
test 99	109.02791	24973.0519	1.00002662E+00	0.007296355	0.79550639	0	0	1.580202156
test 100	217.7304	24928.2855	1.00002657E+00	0.007289813	1.58721387	2431	0.4862	0.203949762
test 101	213.2616	24928.6863	1.00002657E+00	0.007289871	1.5546496	2567	0.5134	0.201329339
test 102	177.92869	24928.3542	1.00002657E+00	0.007289823	1.29706862	2503	0.5006	0.296840143
test 103	169.99866	24957.1672	1.00002660E+00	0.007294035	1.23997613	843	0.1686	0.540733618
test 104	161.60175	24954.2586	1.00002660E+00	0.007293609	1.17866004	1647	0.3294	0.482710149
test 105	176.75444	24958.0746	1.00002660E+00	0.007294167	1.2892764	51	0.0102	0.595463829
test 106	117.06413	24973.1764	1.00002662E+00	0.007296374	0.85414362	0	0	1.370686685
test 107	110.9664	24972.7167	1.00002662E+00	0.007296306	0.80964484	156	0.0312	1.47789992
test 108	113.13602	24973.1672	1.00002662E+00	0.007296372	0.82548255	0	0	1.467520591
test 109	99.139583	24942.4972	1.00002659E+00	0.00729189	0.72291498	3045	0.609	0.748173476
test 110	90.013489	24942.6685	1.00002659E+00	0.007291915	0.65637075	3182	0.6364	0.843966932
test 111	113.92967	24942.098	1.00002659E+00	0.007291832	0.830756	2900	0.58	0.608558477
test 112	94.207895	24967.1302	1.00002661E+00	0.00729549	0.68729279	2145	0.429	1.208794658
test 113	85.208624	24966.9839	1.00002661E+00	0.007295469	0.62163687	2433	0.4866	1.328563559
test 114	105.53429	24967.3461	1.00002661E+00	0.007295522	0.76992775	1802	0.3604	1.078967873

test #	emittance	average ke	gamma	beta gamma	norm. emittance	# ions lost	% losses	new brightness
test 115	81.676539	24980.1256	1.00002663E+00	0.007297389	0.59602546	1450	0.29	1.998613088
test 116	73.364494	24979.8687	1.00002663E+00	0.007297351	0.53536648	1860	0.372	2.191075232
test 117	91.889801	24980.8559	1.00002663E+00	0.007297495	0.6705654	832	0.1664	1.853853564
test 118	99.336101	24942.4288	1.00002659E+00	0.00729188	0.72434697	3008	0.6016	0.759322085
test 119	90.218144	24942.7364	1.00002659E+00	0.007291925	0.65786398	3254	0.6508	0.80686713
test 120	114.20793	24942.1243	1.00002659E+00	0.007291836	0.83278551	2914	0.5828	0.60155866
test 121	94.247283	24967.1491	1.00002661E+00	0.007295493	0.6875804	2190	0.438	1.188746742
test 122	82.238342	24966.9797	1.00002661E+00	0.007295468	0.59996722	2524	0.5048	1.375705863
test 123	103.53166	24967.3019	1.00002661E+00	0.007295515	0.75531683	1878	0.3756	1.094471785
test 124	86.010052	24980.1287	1.00002663E+00	0.007297389	0.62764882	1534	0.3068	1.759645234
test 125	73.299796	24979.8737	1.00002663E+00	0.007297352	0.53489441	1950	0.39	2.13203197
test 126	91.977913	24980.8193	1.00002663E+00	0.00729749	0.67120791	886	0.1772	1.826333777
test 127	103.48192	24942.3899	1.00002659E+00	0.007291875	0.75457723	2944	0.5888	0.722180422
test 128	92.332673	24942.6596	1.00002659E+00	0.007291914	0.67328193	3090	0.618	0.842693115
test 129	115.31639	24942.1006	1.00002659E+00	0.007291832	0.84086783	2884	0.5768	0.598535866
test 130	94.039252	24967.1583	1.00002661E+00	0.007295494	0.68606284	2127	0.4254	1.220781192
test 131	85.846529	24967.0218	1.00002661E+00	0.007295474	0.62629116	2405	0.481	1.323167394
test 132	106.79389	24967.3112	1.00002661E+00	0.007295517	0.77911661	1784	0.3568	1.059597942
test 133	82.266177	24980.1841	1.00002663E+00	0.007297397	0.60032898	1457	0.2914	1.966176657
test 134	76.580768	24979.9418	1.00002663E+00	0.007297362	0.55883758	1859	0.3718	2.011530979
test 135	93.927192	24980.8751	1.00002663E+00	0.007297498	0.68543352	818	0.1636	1.780259649
test 136	143.09458	24946.2407	1.00002659E+00	0.007292438	1.04350832	2982	0.5964	0.370646009
test 137	122.38269	24946.4862	1.00002659E+00	0.007292474	0.89247255	3075	0.615	0.483360317
test 138	154.36143	24945.9342	1.00002659E+00	0.007292393	1.12566416	2819	0.5638	0.344245274
test 139	90.071958	24967.7164	1.00002661E+00	0.007295576	0.65712681	2206	0.4412	1.294070744
test 140	78.959247	24967.6521	1.00002661E+00	0.007295567	0.57605244	2503	0.5006	1.504958398
test 141	102.07368	24967.8662	1.00002661E+00	0.007295598	0.74468852	1828	0.3656	1.143967958
test 142	80.571276	24980.0965	1.00002663E+00	0.007297385	0.58795958	1562	0.3124	1.989028145
test 143	72.927799	24979.885	1.00002663E+00	0.007297354	0.53217994	1891	0.3782	2.195501418
test 144	88.727133	24980.882	1.00002663E+00	0.007297499	0.64748618	911	0.1822	1.950680283

test #	emittance	average ke	gamma	beta gamma	norm. emittance	# ions lost	% losses	new brightness
test 145	139.92002	24946.1381	1.00002659E+00	0.007292423	1.02035589	2994	0.5988	0.385351959
test 146	121.71078	24946.49	1.00002659E+00	0.007292474	0.88757273	3098	0.6196	0.482872647
test 147	148.78982	24945.9805	1.00002659E+00	0.0072924	1.08503484	2826	0.5652	0.369319443
test 148	88.819631	24967.7301	1.00002661E+00	0.007295578	0.64799054	2277	0.4554	1.297000971
test 149	78.419557	24967.6475	1.00002661E+00	0.007295566	0.57211505	2485	0.497	1.536743014
test 150	102.78371	24967.8606	1.00002661E+00	0.007295597	0.74986851	1953	0.3906	1.083757739
test 151	85.032193	24980.0898	1.00002663E+00	0.007297384	0.62051252	1604	0.3208	1.763991847
test 152	72.833087	24979.8443	1.00002663E+00	0.007297348	0.53148836	1998	0.3996	2.125461138
test 153	90.324656	24980.8152	1.00002663E+00	0.007297489	0.65914323	952	0.1904	1.863420692
test 154	144.12634	24946.2154	1.00002659E+00	0.007292434	1.05103179	2917	0.5834	0.377126942
test 155	126.802	24946.3752	1.00002659E+00	0.007292457	0.92469817	3072	0.6144	0.450958968
test 156	150.25927	24945.8573	1.00002659E+00	0.007292382	1.09574791	2796	0.5592	0.367130347
test 157	90.772346	24967.7385	1.00002661E+00	0.007295579	0.66223684	2168	0.4336	1.291506427
test 158	81.501548	24967.6694	1.00002661E+00	0.007295569	0.59460018	2405	0.481	1.467970367
test 159	102.36821	24967.8772	1.00002661E+00	0.007295599	0.74683744	1826	0.3652	1.138111357
test 160	81.801518	24980.1536	1.00002663E+00	0.007297393	0.59693781	1537	0.3074	1.943677933
test 161	75.623533	24979.8967	1.00002663E+00	0.007297355	0.55185179	1912	0.3824	2.02797397
test 162	88.858942	24980.9478	1.00002663E+00	0.007297509	0.64844892	855	0.171	1.971528198
test 163	146.86255	24949.7083	1.00002659E+00	0.007292944	1.07106046	2930	0.586	0.36088794
test 164	140.67811	24949.9764	1.00002659E+00	0.007292984	1.02596319	3014	0.6028	0.377351155
test 165	144.68576	24949.4779	1.00002659E+00	0.007292911	1.05518032	2718	0.5436	0.409913547
test 166	91.45763	24968.5335	1.00002661E+00	0.007295695	0.667247	2225	0.445	1.246578745
test 167	82.019962	24968.4372	1.00002661E+00	0.007295681	0.5983915	2532	0.5064	1.378492212
test 168	97.226885	24968.5771	1.00002661E+00	0.007295702	0.70933835	1888	0.3776	1.236980074
test 169	81.235217	24980.1608	1.00002663E+00	0.007297394	0.59280538	1578	0.3156	1.947537062
test 170	72.418674	24979.952	1.00002663E+00	0.007297363	0.52846538	1968	0.3936	2.171331394
test 171	90.326913	24980.9358	1.00002663E+00	0.007297507	0.65916129	967	0.1934	1.856413978
test 172	144.75903	24949.7649	1.00002659E+00	0.007292953	1.05572074	2872	0.5744	0.381859421
test 173	141.66679	24949.9744	1.00002659E+00	0.007292983	1.03317352	3017	0.6034	0.37154051
test 174	146.0449	24949.5197	1.00002659E+00	0.007292917	1.06509334	2759	0.5518	0.395090436

test #	emittance	average ke	gamma	beta gamma	norm. emittance	# ions lost	% losses	new brightness
test 175	89.784975	24968.4871	1.00002661E+00	0.007295689	0.65504322	2274	0.4548	1.270620739
test 176	82.481842	24968.4133	1.00002661E+00	0.007295678	0.60176095	2477	0.4954	1.393475218
test 177	99.369709	24968.5723	1.00002661E+00	0.007295701	0.72497169	1879	0.3758	1.187631405
test 178	80.60693	24980.1778	1.00002663E+00	0.007297396	0.58822072	1648	0.3296	1.937551998
test 179	71.376579	24979.9296	1.00002663E+00	0.00729736	0.5208606	2006	0.4012	2.20718523
test 180	89.329213	24980.8187	1.00002663E+00	0.00729749	0.65187904	999	0.1998	1.88306154
test 181	146.77751	24949.7108	1.00002659E+00	0.007292945	1.07044026	2855	0.571	0.374397051
test 182	142.60933	24949.9195	1.00002659E+00	0.007292975	1.04004636	2995	0.599	0.370713991
test 183	146.51214	24949.5119	1.00002659E+00	0.007292916	1.06850066	2747	0.5494	0.394676797
test 184	91.602353	24968.4838	1.00002661E+00	0.007295688	0.6683022	2192	0.4384	1.257422778
test 185	83.861318	24968.4697	1.00002661E+00	0.007295686	0.61182584	2389	0.4778	1.395022561
test 186	99.238681	24968.5833	1.00002661E+00	0.007295703	0.72401591	1871	0.3742	1.193821352
test 187	82.507919	24980.2317	1.00002663E+00	0.007297404	0.60209364	1561	0.3122	1.897291636
test 188	74.909031	24979.9681	1.00002663E+00	0.007297366	0.5466386	1903	0.3806	2.072863083
test 189	89.952388	24981.0051	1.00002663E+00	0.007297517	0.6564291	903	0.1806	1.901605009
test 190	143.3994	24953.0174	1.00002660E+00	0.007293428	1.04587318	2840	0.568	0.394935063
test 191	137.17097	24953.1893	1.00002660E+00	0.007293453	1.00045005	2939	0.5878	0.411829231
test 192	144.9205	24952.7851	1.00002660E+00	0.007293394	1.0569623	2643	0.5286	0.421959322
test 193	110.26916	24969.4055	1.00002661E+00	0.007295823	0.80450425	2186	0.4372	0.86955569
test 194	98.879858	24969.3498	1.00002661E+00	0.007295815	0.72140911	2512	0.5024	0.9561304
test 195	117.48735	24969.4799	1.00002661E+00	0.007295834	0.85716813	1912	0.3824	0.840572655
test 196	76.640295	24980.3081	1.00002663E+00	0.007297415	0.55927607	1686	0.3372	2.118995464
test 197	71.1067	24980.1109	1.00002663E+00	0.007297387	0.51889308	2082	0.4164	2.167502063
test 198	88.118695	24981.1235	1.00002663E+00	0.007297535	0.64304922	990	0.198	1.939482823
test 199	140.9082	24953.0137	1.00002660E+00	0.007293428	1.02770377	2903	0.5806	0.397093272
test 200	138.29781	24953.1722	1.00002660E+00	0.007293451	1.00866827	2924	0.5848	0.408094388
test 201	143.26218	24952.8205	1.00002660E+00	0.007293399	1.04486825	2661	0.5322	0.428486506
test 202	108.64472	24969.4048	1.00002661E+00	0.007295823	0.79265261	2260	0.452	0.872197366
test 203	101.02058	24969.3498	1.00002661E+00	0.007295815	0.73702742	2578	0.5156	0.891737111
test 204	119.1454	24969.4828	1.00002661E+00	0.007295834	0.86926508	1900	0.38	0.820516312

test #	emittance	average ke	gamma	beta gamma	norm. emittance	# ions lost	% losses	new brightness
test 205	79.724858	24980.3039	1.00002663E+00	0.007297415	0.58178536	1684	0.3368	1.959381204
test 206	70.29984	24980.1117	1.00002663E+00	0.007297387	0.51300512	2076	0.4152	2.222101859
test 207	85.744706	24981.0196	1.00002663E+00	0.007297519	0.62572365	1061	0.2122	2.012105927
test 208	143.16279	24953.0265	1.00002660E+00	0.007293429	1.04414771	2792	0.5584	0.405046782
test 209	141.21339	24953.1692	1.00002660E+00	0.00729345	1.02993284	2841	0.5682	0.407065993
test 210	147.19211	24952.8499	1.00002660E+00	0.007293404	1.07353148	2620	0.524	0.413025994
test 211	111.94391	24969.3963	1.00002661E+00	0.007295821	0.81672277	2154	0.4308	0.853327147
test 212	105.27094	24969.3664	1.00002661E+00	0.007295817	0.76803753	2436	0.4872	0.869326918
test 213	115.02016	24969.48	1.00002661E+00	0.007295834	0.83916796	1940	0.388	0.869067749
test 214	79.073377	24980.3303	1.00002663E+00	0.007297419	0.57703153	1606	0.3212	2.038650313
test 215	69.657171	24980.1053	1.00002663E+00	0.007297386	0.50831525	1963	0.3926	2.350761156
test 216	88.153284	24981.0897	1.00002663E+00	0.00729753	0.6433012	998	0.1996	1.934097475
test 217	143.35406	24927.5176	1.00002657E+00	0.0072897	1.04500816	2852	0.5704	0.393391443
test 218	121.34227	24927.8204	1.00002657E+00	0.007289745	0.88455418	2982	0.5964	0.515824875
test 219	128.95829	24927.2678	1.00002657E+00	0.007289664	0.94006258	2888	0.5776	0.477980722
test 220	115.36446	24958.976	1.00002660E+00	0.007294299	0.84150286	1794	0.3588	0.905487213
test 221	105.9995	24958.8194	1.00002660E+00	0.007294276	0.7731896	1988	0.3976	1.007657532
test 222	116.99329	24960.0642	1.00002660E+00	0.007294458	0.85340262	1674	0.3348	0.913364862
test 223	103.57019	24976.5814	1.00002662E+00	0.007296871	0.75573829	437	0.0874	1.597855907
test 224	89.883632	24975.1236	1.00002662E+00	0.007296658	0.65585013	1363	0.2726	1.691079687
test 225	104.81367	24977.4785	1.00002662E+00	0.007297002	0.7648256	13	0.0026	1.705079089
test 226	138.64946	24927.4023	1.00002657E+00	0.007289684	1.0107107	2828	0.5656	0.425241941
test 227	122.42398	24927.8003	1.00002657E+00	0.007289742	0.89243921	2931	0.5862	0.519556996
test 228	135.00297	24927.2885	1.00002657E+00	0.007289667	0.9841267	2793	0.5586	0.455753805
test 229	115.56458	24958.9752	1.00002660E+00	0.007294299	0.84296259	1836	0.3672	0.890532692
test 230	106.66492	24958.7739	1.00002660E+00	0.007294269	0.77804263	2034	0.4068	0.97992843
test 231	118.33588	24960.1213	1.00002660E+00	0.007294466	0.86319707	1663	0.3326	0.895707657
test 232	102.4964	24976.2668	1.00002662E+00	0.007296825	0.74789827	563	0.1126	1.586479152
test 233	91.413583	24975.0341	1.00002662E+00	0.007296645	0.66701247	1409	0.2818	1.614274906
test 234	108.53429	24977.6659	1.00002662E+00	0.007297029	0.7919779	13	0.0026	1.590168848

test #	emittance	average ke	gamma	beta gamma	norm. emittance	# ions lost	% losses	new brightness
test 235	144.15947	24927.2238	1.00002657E+00	0.007289658	1.05087319	2812	0.5624	0.396256766
test 236	127.91915	24927.6523	1.00002657E+00	0.00728972	0.93249478	2956	0.5912	0.470130115
test 237	136.6493	24927.328	1.00002657E+00	0.007289673	0.99612865	2793	0.5586	0.444837576
test 238	113.26059	24959.0023	1.00002660E+00	0.007294303	0.82615703	1797	0.3594	0.938559315
test 239	112.11841	24958.8884	1.00002660E+00	0.007294286	0.81782373	2003	0.4006	0.896184287
test 240	115.26634	24960.0433	1.00002660E+00	0.007294455	0.84080513	1660	0.332	0.944899793
test 241	100.87959	24976.7183	1.00002662E+00	0.007296891	0.73610736	275	0.055	1.744012064
test 242	91.571174	24975.2336	1.00002662E+00	0.007296674	0.66816502	1241	0.2482	1.683971922
test 243	102.79262	24977.6007	1.00002662E+00	0.00729702	0.75007979	9	0.0018	1.774200259
test 244	180.59449	24932.1714	1.00002657E+00	0.007290381	1.31660264	2740	0.548	0.260752805
test 245	167.64515	24932.4656	1.00002657E+00	0.007290424	1.22220422	2895	0.579	0.281834748
test 246	185.63616	24931.8027	1.00002657E+00	0.007290327	1.35334831	2684	0.5368	0.25290032
test 247	118.31523	24959.793	1.00002660E+00	0.007294418	0.86304079	1668	0.3336	0.894689497
test 248	105.23575	24959.5302	1.00002660E+00	0.00729438	0.76762954	2013	0.4026	1.01382234
test 249	128.66423	24962.487	1.00002661E+00	0.007294812	0.93858135	931	0.1862	0.923791247
test 250	100.96087	24976.5918	1.00002662E+00	0.007296873	0.73669862	387	0.0774	1.699940563
test 251	89.295648	24975.0501	1.00002662E+00	0.007296647	0.65155886	1428	0.2856	1.68280635
test 252	107.9056	24977.5015	1.00002662E+00	0.007297005	0.78738776	0	0	1.612956613
test 253	179.52033	24932.0197	1.00002657E+00	0.007290359	1.30876758	2768	0.5536	0.260614831
test 254	161.4593	24932.5019	1.00002657E+00	0.007290429	1.17710759	2965	0.593	0.293739321
test 255	184.79591	24931.7257	1.00002657E+00	0.007290316	1.34722054	2696	0.5392	0.253883851
test 256	116.56188	24959.783	1.00002660E+00	0.007294417	0.85025091	1712	0.3424	0.909635908
test 257	103.41499	24959.5595	1.00002660E+00	0.007294384	0.75434865	2120	0.424	1.012227774
test 258	126.52607	24962.2671	1.00002661E+00	0.00729478	0.92297981	978	0.1956	0.94425145
test 259	101.41004	24976.4641	1.00002662E+00	0.007296854	0.73997424	521	0.1042	1.635979494
test 260	89.96248	24975.0193	1.00002662E+00	0.007296643	0.65642409	1419	0.2838	1.662131194
test 261	110.16212	24977.5897	1.00002662E+00	0.007297018	0.803855	0	0	1.547549572
test 262	180.41999	24932.1078	1.00002657E+00	0.007290372	1.3153288	2767	0.5534	0.258136881
test 263	164.23547	24932.3732	1.00002657E+00	0.00729041	1.19734401	2843	0.5686	0.300913902
test 264	187.55291	24931.7838	1.00002657E+00	0.007290324	1.36732153	2706	0.5412	0.245404265

test #	emittance	average ke	gamma	beta gamma	norm. emittance	# ions lost	% losses	new brightness
test 265	119.77767	24959.8386	1.00002660E+00	0.007294425	0.87370925	1620	0.324	0.885549479
test 266	104.72459	24959.5586	1.00002660E+00	0.007294384	0.76390136	1990	0.398	1.031625157
test 267	126.37771	24962.4957	1.00002661E+00	0.007294813	0.92190177	945	0.189	0.954226682
test 268	104.12031	24976.898	1.00002662E+00	0.007296917	0.75975727	283	0.0566	1.634354047
test 269	92.47774	24975.2009	1.00002662E+00	0.007296669	0.6747795	1243	0.2486	1.65024124
test 270	109.05958	24977.5121	1.00002662E+00	0.007297007	0.7958085	0	0	1.579002648
test 271	180.06212	24936.5845	1.00002658E+00	0.007291026	1.31283764	2710	0.542	0.265731743
test 272	174.42208	24936.9223	1.00002658E+00	0.007291075	1.27172455	2842	0.5684	0.266867278
test 273	184.79841	24936.2486	1.00002658E+00	0.007290977	1.34736099	2614	0.5228	0.262864838
test 274	116.88694	24960.6918	1.00002660E+00	0.00729455	0.85263757	1723	0.3446	0.901524449
test 275	106.36107	24960.5039	1.00002660E+00	0.007294522	0.77585318	2099	0.4198	0.963870374
test 276	133.01628	24963.1281	1.00002661E+00	0.007294906	0.97034123	908	0.1816	0.869193864
test 277	99.953188	24976.7622	1.00002662E+00	0.007296897	0.72934816	422	0.0844	1.721218461
test 278	94.426311	24975.189	1.00002662E+00	0.007296668	0.68899741	1431	0.2862	1.50363133
test 279	106.11227	24977.5708	1.00002662E+00	0.007297016	0.77430291	0	0	1.667931517
test 280	175.76842	24936.5971	1.00002658E+00	0.007291028	1.2815325	2637	0.5274	0.287762681
test 281	176.84959	24936.9434	1.00002658E+00	0.007291079	1.28942425	2846	0.5692	0.259109913
test 282	181.27542	24936.2949	1.00002658E+00	0.007290984	1.32167618	2548	0.5096	0.280737441
test 283	115.94759	24960.6553	1.00002660E+00	0.007294544	0.8457848	1832	0.3664	0.885717891
test 284	103.24095	24960.4839	1.00002660E+00	0.007294519	0.75309309	2134	0.4268	1.01066879
test 285	129.46075	24962.9884	1.00002661E+00	0.007294885	0.94440129	979	0.1958	0.901676857
test 286	100.54172	24976.6195	1.00002662E+00	0.007296877	0.73364052	549	0.1098	1.653944664
test 287	89.943186	24975.116	1.00002662E+00	0.007296657	0.65628458	1497	0.2994	1.626618601
test 288	107.26812	24977.5045	1.00002662E+00	0.007297006	0.78273608	0	0	1.632184675
test 289	179.62516	24936.483	1.00002658E+00	0.007291011	1.30964907	2706	0.5412	0.267493682
test 290	177.9067	24936.7296	1.00002658E+00	0.007291047	1.29712617	2817	0.5634	0.259489202
test 291	189.28759	24936.317	1.00002658E+00	0.007290987	1.38009337	2542	0.5084	0.258104118
test 292	119.70499	24960.7242	1.00002660E+00	0.007294554	0.87319458	1734	0.3468	0.856690814
test 293	107.54104	24960.4994	1.00002660E+00	0.007294521	0.78446043	1969	0.3938	0.98508533
test 294	133.93053	24963.4534	1.00002661E+00	0.007294953	0.97701692	870	0.174	0.865318285

test #	emittance	average ke	gamma	beta gamma	norm. emittance	# ions lost	% losses	new brightness
test 295	102.06963	24976.9998	1.00002662E+00	0.007296932	0.74479515	303	0.0606	1.693467528
test 296	90.504026	24975.1612	1.00002662E+00	0.007296664	0.66037743	1318	0.2636	1.688609907
test 297	105.33476	24977.4889	1.00002662E+00	0.007297004	0.76862813	0	0	1.692651092
test 298	172.83486	24940.7356	1.00002658E+00	0.007291633	1.26024834	2542	0.5084	0.309527759
test 299	174.86644	24940.9782	1.00002658E+00	0.007291668	1.27506812	2718	0.5436	0.280723561
test 300	179.05708	24940.4025	1.00002658E+00	0.007291584	1.30560975	2485	0.497	0.295080978
test 301	135.79915	24961.7688	1.00002661E+00	0.007294707	0.990615	1765	0.353	0.65931732
test 302	129.8035	24961.6051	1.00002661E+00	0.007294683	0.94687539	2084	0.4168	0.650476864
test 303	144.90189	24963.6953	1.00002661E+00	0.007294988	1.0570576	1047	0.2094	0.707553861
test 304	100.27905	24976.8551	1.00002662E+00	0.007296911	0.73172732	479	0.0958	1.688752347
test 305	87.082201	24975.3382	1.00002662E+00	0.007296689	0.63541178	1482	0.2964	1.742670626
test 306	104.17239	24977.7826	1.00002662E+00	0.007297047	0.76015076	0	0	1.730615261
test 307	173.21599	24940.7251	1.00002658E+00	0.007291631	1.26302713	2621	0.5242	0.29826279
test 308	170.07011	24941.0876	1.00002658E+00	0.007291684	1.2400976	2757	0.5514	0.291707461
test 309	176.7764	24940.4607	1.00002658E+00	0.007291593	1.28898152	2444	0.4888	0.307678724
test 310	133.73637	24961.7004	1.00002661E+00	0.007294697	0.97556631	1769	0.3538	0.67897434
test 311	124.02876	24961.5701	1.00002661E+00	0.007294678	0.90474989	2121	0.4242	0.703419787
test 312	141.29966	24963.5225	1.00002661E+00	0.007294963	1.03077583	1157	0.2314	0.723389041
test 313	97.926451	24976.559	1.00002662E+00	0.007296868	0.71455636	593	0.1186	1.726235582
test 314	86.096923	24975.2662	1.00002662E+00	0.007296679	0.62822161	1563	0.3126	1.741741864
test 315	109.90862	24977.7038	1.00002662E+00	0.007297035	0.80200708	0	0	1.554689265
test 316	175.77343	24940.5746	1.00002658E+00	0.007291609	1.28167118	2607	0.5214	0.291352974
test 317	176.58303	24940.9464	1.00002658E+00	0.007291664	1.28758406	2780	0.556	0.267813083
test 318	181.95853	24940.4689	1.00002658E+00	0.007291594	1.32676774	2529	0.5058	0.280745584
test 319	138.66337	24961.7802	1.00002661E+00	0.007294709	1.01150887	1716	0.3432	0.641938988
test 320	129.66778	24961.619	1.00002661E+00	0.007294685	0.94588564	2073	0.4146	0.654297791
test 321	144.31547	24964.0735	1.00002661E+00	0.007295044	1.05278766	993	0.1986	0.723049058
test 322	103.1047	24977.2545	1.00002662E+00	0.007296969	0.75235181	319	0.0638	1.65396644
test 323	88.791497	24975.3848	1.00002662E+00	0.007296696	0.64788458	1414	0.2828	1.708618057
test 324	104.8127	24977.7682	1.00002662E+00	0.007297044	0.76482293	0	0	1.709535804

test #	emittance	average ke	gamma	beta gamma	norm. emittance	# ions lost	% losses	new brightness
test 325	166.41366	24897.9661	1.00002654E+00	0.007285378	1.21238641	2791	0.5582	0.300568588
test 326	187.70114	24897.9573	1.00002654E+00	0.007285377	1.36747357	2879	0.5758	0.226846865
test 327	155.39184	24898.0742	1.00002654E+00	0.007285394	1.13209079	2837	0.5674	0.337539035
test 328	144.30134	24943.8066	1.00002659E+00	0.007292082	1.0522572	1738	0.3476	0.589210045
test 329	136.46612	24944.1034	1.00002659E+00	0.007292125	0.99512805	1674	0.3348	0.671729315
test 330	153.64443	24943.9851	1.00002659E+00	0.007292108	1.12039177	1678	0.3356	0.529285265
test 331	116.82505	24968.399	1.00002661E+00	0.007295676	0.8523177	2	0.0004	1.376015195
test 332	118.28124	24968.3273	1.00002661E+00	0.007295665	0.86294035	2	0.0004	1.342346688
test 333	116.88515	24968.19	1.00002661E+00	0.007295645	0.85275257	0	0	1.375162192
test 334	162.88028	24898.1561	1.00002654E+00	0.007285406	1.18664894	2859	0.5718	0.304090009
test 335	187.61676	24898.0733	1.00002654E+00	0.007285394	1.36686197	2800	0.56	0.235506747
test 336	155.94828	24898.054	1.00002654E+00	0.007285391	1.13614423	2758	0.5516	0.34737509
test 337	143.64032	24944.3291	1.00002659E+00	0.007292158	1.04744797	1745	0.349	0.593356997
test 338	137.00514	24943.7472	1.00002659E+00	0.007292073	0.99905153	1667	0.3334	0.667866304
test 339	152.80008	24943.7644	1.00002659E+00	0.007292076	1.11422973	1673	0.3346	0.535961151
test 340	116.03676	24968.2059	1.00002661E+00	0.007295647	0.84656328	1	0.0002	1.395064487
test 341	122.01297	24968.3794	1.00002661E+00	0.007295673	0.89016671	11	0.0022	1.259217656
test 342	121.29312	24968.278	1.00002661E+00	0.007295658	0.88491312	0	0	1.27702303
test 343	171.012	24898.0398	1.00002654E+00	0.007285389	1.24588891	2843	0.5686	0.277921087
test 344	182.21109	24898.0984	1.00002654E+00	0.007285398	1.3274802	2793	0.5586	0.250481827
test 345	155.86364	24898.0506	1.00002654E+00	0.007285391	1.13552747	2865	0.573	0.331155968
test 346	142.08381	24943.6918	1.00002659E+00	0.007292065	1.03608442	1668	0.3336	0.62078999
test 347	135.28913	24943.8507	1.00002659E+00	0.007292088	0.98654028	1729	0.3458	0.672172736
test 348	157.66162	24943.8199	1.00002659E+00	0.007292084	1.14968173	1710	0.342	0.49781804
test 349	113.87829	24968.4119	1.00002661E+00	0.007295678	0.83081931	1	0.0002	1.448438184
test 350	119.94611	24968.2034	1.00002661E+00	0.007295647	0.87508449	0	0	1.305870255
test 351	120.12293	24968.3396	1.00002661E+00	0.007295667	0.8763769	1	0.0002	1.301761101
test 352	219.04991	24904.2685	1.00002654E+00	0.0072863	1.59606339	2676	0.5352	0.182459234
test 353	262.96504	24904.3628	1.00002654E+00	0.007286314	1.91604583	2672	0.5344	0.126823923
test 354	174.2846	24904.5279	1.00002655E+00	0.007286338	1.26989653	2715	0.543	0.283386739

test #	emittance	average ke	gamma	beta gamma	norm. emittance	# ions lost	% losses	new brightness
test 355	151.89997	24947.0913	1.00002659E+00	0.007292562	1.10773996	965	0.193	0.65765464
test 356	155.21589	24947.7747	1.00002659E+00	0.007292662	1.131937	914	0.1828	0.637799015
test 357	155.01497	24947.7808	1.00002659E+00	0.007292663	1.13047192	967	0.1934	0.631158824
test 358	118.02018	24968.3916	1.00002661E+00	0.007295675	0.86103685	0	0	1.348827852
test 359	121.22835	24968.352	1.00002661E+00	0.007295669	0.8844419	0	0	1.278384153
test 360	120.35161	24968.3761	1.00002661E+00	0.007295672	0.87804591	0	0	1.29707637
test 361	232.69611	24904.3327	1.00002654E+00	0.00728631	1.69549593	2598	0.5196	0.167112715
test 362	255.21414	24904.2747	1.00002654E+00	0.007286301	1.85956708	2715	0.543	0.13215771
test 363	168.43791	24904.4803	1.00002654E+00	0.007286331	1.22729439	2638	0.5276	0.313626242
test 364	150.01164	24947.8596	1.00002659E+00	0.007292674	1.093986	908	0.1816	0.683820463
test 365	154.65967	24947.3084	1.00002659E+00	0.007292594	1.12787013	1003	0.2006	0.628414152
test 366	152.86921	24947.5326	1.00002659E+00	0.007292626	1.11481807	931	0.1862	0.654801529
test 367	118.66916	24968.3058	1.00002661E+00	0.007295662	0.86577008	0	0	1.334119878
test 368	120.55025	24968.2993	1.00002661E+00	0.007295661	0.87949375	0	0	1.292809353
test 369	115.49558	24968.3428	1.00002661E+00	0.007295667	0.84261738	0	0	1.40844266
test 370	227.23982	24904.2862	1.00002654E+00	0.007286303	1.65573814	2646	0.5292	0.171732759
test 371	268.10279	24904.2644	1.00002654E+00	0.0072863	1.95347727	2579	0.5158	0.126884351
test 372	173.17351	24904.4341	1.00002654E+00	0.007286324	1.26179835	2750	0.55	0.282639335
test 373	152.86138	24947.5799	1.00002659E+00	0.007292633	1.11476201	940	0.188	0.653418932
test 374	153.95728	24947.7013	1.00002659E+00	0.007292651	1.12275671	896	0.1792	0.651127483
test 375	155.23516	24947.6359	1.00002659E+00	0.007292642	1.1320744	960	0.192	0.630465642
test 376	117.92556	24968.3454	1.00002661E+00	0.007295668	0.86034571	0	0	1.350995833
test 377	116.71769	24968.1439	1.00002661E+00	0.007295638	0.85153007	0	0	1.379113537
test 378	120.10389	24968.3348	1.00002661E+00	0.007295666	0.87623787	0	0	1.302434703
test 379	221.67345	24910.4806	1.00002655E+00	0.007287209	1.6153807	2494	0.4988	0.192070771
test 380	249.81365	24910.5078	1.00002655E+00	0.007287213	1.82044526	2603	0.5206	0.144658109
test 381	171.37082	24910.5642	1.00002655E+00	0.007287221	1.24881704	2589	0.5178	0.309192945
test 382	177.0789	24949.5351	1.00002659E+00	0.007292919	1.29142211	98	0.0196	0.58785047
test 383	165.17747	24948.5213	1.00002659E+00	0.007292771	1.20460143	913	0.1826	0.56331055
test 384	167.45768	24949.586	1.00002659E+00	0.007292927	1.22125654	105	0.021	0.656400478

test #	emittance	average ke	gamma	beta gamma	norm. emittance	# ions lost	% losses	new brightness
test 385	116.64524	24968.3548	1.00002661E+00	0.007295669	0.85100511	0	0	1.380815535
test 386	121.75531	24968.3697	1.00002661E+00	0.007295671	0.88828676	0	0	1.267341386
test 387	116.2599	24968.5934	1.00002661E+00	0.007295704	0.84819787	0	0	1.389970714
test 388	221.78139	24910.4316	1.00002655E+00	0.007287202	1.61616573	2536	0.5072	0.18866829
test 389	252.38575	24910.6105	1.00002655E+00	0.007287228	1.83919251	2608	0.5216	0.141428453
test 390	173.63423	24910.6559	1.00002655E+00	0.007287235	1.26531335	2617	0.5234	0.297685622
test 391	177.65099	24950.0329	1.00002659E+00	0.007292992	1.29560724	80	0.016	0.586203442
test 392	164.19028	24948.1995	1.00002659E+00	0.007292724	1.19739441	1017	0.2034	0.555604621
test 393	172.14056	24949.4547	1.00002659E+00	0.007292907	1.25540517	95	0.019	0.622445284
test 394	117.22425	24968.2806	1.00002661E+00	0.007295658	0.85522808	0	0	1.367212728
test 395	121.04849	24968.2876	1.00002661E+00	0.007295659	0.88312857	0	0	1.282189248
test 396	117.60516	24968.3676	1.00002661E+00	0.007295671	0.85800856	0	0	1.35836585
test 397	233.69153	24910.4352	1.00002655E+00	0.007287202	1.70295743	2567	0.5134	0.1677894
test 398	260.3462	24910.3702	1.00002655E+00	0.007287193	1.89719294	2503	0.5006	0.138747619
test 399	168.65515	24910.7563	1.00002655E+00	0.007287249	1.22903209	2643	0.5286	0.312077986
test 400	176.60396	24949.7686	1.00002659E+00	0.007292953	1.28796445	92	0.0184	0.591734377
test 401	162.37034	24948.6341	1.00002659E+00	0.007292787	1.1841324	763	0.1526	0.604349166
test 402	169.39207	24949.6907	1.00002659E+00	0.007292942	1.23536655	111	0.0222	0.64070536
test 403	117.41999	24968.3952	1.00002661E+00	0.007295675	0.85665812	0	0	1.362651904
test 404	118.78099	24968.5226	1.00002661E+00	0.007295694	0.86658975	0	0	1.331597307
test 405	117.7881	24968.3437	1.00002661E+00	0.007295668	0.8593428	0	0	1.354151056
test 406	229.47515	24916.354	1.00002656E+00	0.007288068	1.67243045	2377	0.4754	0.187556514
test 407	256.20536	24916.336	1.00002656E+00	0.007288065	1.8672414	2459	0.4918	0.145758445
test 408	172.98198	24916.4243	1.00002656E+00	0.007288078	1.26070619	2472	0.4944	0.318111446
test 409	202.26025	24950.7383	1.00002659E+00	0.007293095	1.47510325	66	0.0132	0.453507321
test 410	182.28632	24949.2907	1.00002659E+00	0.007292883	1.32939286	1044	0.2088	0.447692272
test 411	185.92564	24950.8471	1.00002659E+00	0.007293111	1.35597633	31	0.0062	0.540498855
test 412	113.42991	24968.6131	1.00002661E+00	0.007295707	0.82755138	0	0	1.460192328
test 413	118.7804	24968.7707	1.00002661E+00	0.00729573	0.8665897	0	0	1.331597439
test 414	119.06739	24968.5229	1.00002661E+00	0.007295694	0.86867925	0	0	1.325199018

test #	emittance	average ke	gamma	beta gamma	norm. emittance	# ions lost	% losses	new brightness
test 415	229.11088	24916.2936	1.00002656E+00	0.007288059	1.66977367	2506	0.5012	0.178900365
test 416	245.3597	24916.3983	1.00002656E+00	0.007288074	1.78819977	2493	0.4986	0.156802238
test 417	163.49212	24916.5354	1.00002656E+00	0.007288094	1.19154604	2491	0.4982	0.353434552
test 418	198.15951	24950.9441	1.00002659E+00	0.007293125	1.44520206	75	0.015	0.471605744
test 419	181.40852	24949.152	1.00002659E+00	0.007292863	1.32298751	1109	0.2218	0.444610521
test 420	192.37386	24950.4879	1.00002659E+00	0.007293058	1.40299382	38	0.0076	0.504167957
test 421	121.81703	24968.4492	1.00002661E+00	0.007295683	0.88873842	0	0	1.266053583
test 422	120.50331	24968.6884	1.00002661E+00	0.007295718	0.87915814	0	0	1.293796561
test 423	115.65752	24968.5131	1.00002661E+00	0.007295692	0.84380168	0	0	1.404491867
test 424	229.91912	24916.3066	1.00002656E+00	0.007288061	1.67566455	2454	0.4908	0.181348609
test 425	259.26762	24916.4599	1.00002656E+00	0.007288083	1.88956407	2460	0.492	0.14227889
test 426	176.38935	24916.4712	1.00002656E+00	0.007288085	1.28554056	2462	0.4924	0.307149665
test 427	201.07588	24950.6934	1.00002659E+00	0.007293088	1.46646421	56	0.0112	0.459796355
test 428	188.71288	24949.8291	1.00002659E+00	0.007292962	1.37627592	920	0.184	0.430803413
test 429	188.5204	24950.9987	1.00002659E+00	0.007293133	1.3749044	42	0.0084	0.524555587
test 430	114.5017	24968.6681	1.00002661E+00	0.007295715	0.8353718	0	0	1.432980812
test 431	121.91634	24968.4034	1.00002661E+00	0.007295676	0.88946219	0	0	1.263994012
test 432	117.93767	24968.6402	1.00002661E+00	0.007295711	0.86043916	0	0	1.350702376

[This page intentionally left blank.]

Appendix E

Code Used to Generate Randomly Energized, Positioned, and Oriented Ions

```
;-----------------------------------------------------------------------
; I modified existing code from a SIMION demo "RANDOM.PRG"
; The code now randomizes starting (y, z) and (y', z') coordinates
; within a radius of 6.5mm.  The range in (y', z') is +-90 degrees.
; Code for randomizing initial kinetic energy is included. The range
; of ke is 0 to 2 eV.
; Original SIMION code left intact but unused portions are commented out.
;
;-----------------------------------------------------------------------
; this user program randomly changes the initial ke and direction of ions
; energy is randomly changed +- Percent_Energy_Variation * ke
; ions are emitted randomly within a cone of revolution around the
; ion's defined velocity direction axis
; the full angle of the cone is +- Cone_Angle_Off_Vel_Axis
; (e.g. 90.0 is full hemisphere, 180 is a full sphere)
;-----------------------------------------------------------------------

;--------- you can use it with your own lenses without modification --------
;               (just rename user program file using your pa's name)
;------ Note: you can also modify the emission distributions as desired ----
;defa Percent_Energy_Variation  50    ; (+- 50%) random energy variation
defa Velocity_Variation     19.5637  ; (0 to 2eV) random ke
defa Cone_Angle_Off_Vel_Axis    90    ; (+- 90 deg) cone angle hemisphere
defa _Radius   6.5   ; (+- 6.5 mm) radius
defa Theta          360   ; polar coordinate random theta variation
defa temp1          0.0   ; stores temporary values

seg initialize                  ; initialize ion's velocity and direction
;------------------- get ion's initial velocity components -------------
rcl ion_vz_mm                   ; get ion's specified velocity components
rcl ion_vy_mm
rcl ion_vx_mm

;------------------- convert to 3d polar coords -------------
```

```
>p3d                          ; convert to polar 3d

;------------------- save polar coord values ----------------
sto speed rlup                ; store ion's speed
sto az_angle rlup             ; store ion's az angle
sto el_angle                  ; store ion's el angle

;------------------- make sure Percent_Energy_Variation is legal -----------
                              ; force 0 <= Percent_Energy_Variation <= 100
; rcl Percent_Energy_Variation abs
; 100 x>y rlup sto Percent_Energy_Variation

;------------------- make sure Velocity_Variation is legal
                              ; force 0 <= Velocity_Variation <= 19.5637
rcl Velocity_Variation abs
19.5637 x>y rlup sto Velocity_Variation

;------------------- make sure Radius is legal
                              ; force -6.5 <= Radius <= 6.5
rcl _Radius abs
6.5 x>y rlup sto _Radius

;------------------- make sure Theta is legal
                              ; force 0 <= Theta <= 360
rcl Theta abs
360 x>y rlup sto Theta

;------------------- make sure Cone_Angle_Off_Vel_Axis is legal ------------
                              ; force 0 <= Cone_Angle_Off_Vel_Axis <= 180
rcl Cone_Angle_Off_Vel_Axis abs
180 x>y rlup sto Cone_Angle_Off_Vel_Axis

; ---------------------- calculate randomized initial ke
rcl Velocity_Variation rand *   ; (Velocity_Variation * rand)
sto speed                     ; save random speed

; ---------------------- calculate ion's defined ke -------------
; rcl ion_mass                  ; get ion's mass
; rcl speed                     ; recall its total speed
; >ke                                ; convert speed to kinetic energy
; sto kinetic_energy                 ; save ion's defined kinetic energy

; ---------------------- compute new randomized ke -------------
                              ; convert from percent to fraction
; rcl Percent_Energy_Variation 100 /
; sto del_energy 2 * rand *          ; fac = 2 * del_energy * rand
; rcl del_energy - 1 +          ; fac += 1 - del_energy
; rcl kinetic_energy *          ; new ke = fac * ke

; ---------------------- convert new ke to new speed -----------
; rcl ion_mass                  ; recall ion mass
; x><y                          ; swap x any y
```

```
; >spd                          ; convert to speed
; sto speed                     ; save new speed

;----------------------- compute randomized radius change ------
2 rcl _Radius * rand *          ; (2 * Radius * rand)
rcl _Radius -                   ; - Radius
sto temp1

rand rcl Theta *                      ; (rand * Theta)
rcl temp1                       ; convert random Theta and
>R                              ; random Radius to polar coordinates
sto ion_py_mm                   ; store new y position
rlup
sto ion_pz_mm                   ; store new z position

;-- compute randomized el angle change 90 +- Cone_Angle_Off_Vel_Axis -------
;-------- we assume elevation of 90 degrees for mean ----------
;-------- so cone can be generated via rotating az +- 90 -------
                                ; (2 * Cone_Angle_Off_Vel_Axis * rand)
2 rcl Cone_Angle_Off_Vel_Axis * rand *
                                ; - Cone_Angle_Off_Vel_Axis + 90
rcl Cone_Angle_Off_Vel_Axis - 90 +

;-------------- compute randomized az angle change ------------
;--------- this gives 360 effective because of +- elevation angels ---
180 rand * 90 -                       ; +- 90 randomized az

;---------------------- recall new ion speed -----------------
rcl speed                       ; recall new speed

;--------- at this point x = speed, y = az, z = el --------------
;------------- convert to rectangular velocity components ---------
>r3d                            ; convert polar 3d to rect 3d

;------------- el rotate back to from 90 vertical -------------
-90 >elr

;------------- el rotate back to starting elevation -------------
rcl el_angle >elr

;------------- az rotate back to starting azimuth -------------
rcl az_angle >azr

;------------- update ion's velocity components with new values --------
sto ion_vx_mm                   ; return vx
rlup
sto ion_vy_mm                   ; return vy
rlup
sto ion_vz_mm                   ; return vz

;---------------------- done ----------------------------------------
```

[This page intentionally left blank.]

References

[1] Idaho National Engineering and Environmental Laboratory (INEEL), Idaho Falls, ID 83415.

[2] http://quarknet.fnal.gov/toolkits/ati/whatgevs.html

[3] M.P. Dehnel, "The development of an injection system for a compact H^- cyclotron, the concomitant measurement of injected beam and the experimental characterization of the spiral inflector", Thesis, Doctor of Philosophy, 1995.

[4] A.P. Banford, TRANSPORT OF CHARGED PARTICLE BEAMS, London: E. & F. N. Spon Ltd., 1966.

[5] J. Peters, "Review of negative hydrogen ion sources high brightness/high current", Deutsches Elektronen-Synchrotron, DESY, Hamburg, Germany.

[6] http://hyperphysics.phy-astr.gsu.edu/hbase/relativ/releng.html

[7] M.P. Dehnel, Private Communication, Dehnel Consulting Ltd., Nelson, BC, Canada, August 1, 2002.

[8] K.S. Golovanivsky, K. Jayamanna and P.W. Schmor, "Physical Fundamentals of H^- Ion Sources", TRIUMF design note TRI-DN-25, 1993.

[9] M.P. Dehnel, The TRIUMF Microcusp Source, Internal UBC Ph.D. Report, pp. 8, February 7, 1992.